

# Electromagnetic Shielding Potential of Polyaniline Nanopowders

A Dissertation

Presented in Partial Fulfillment of the Requirements for the

Degree of Doctorate of Philosophy

with a

Major in Chemical Engineering

in the

College of Graduate Studies

University of Idaho

by

Hesham Ramzy Tantawy

April 2014

Major Professor: D. Eric Aston, Ph.D.

## AUTHORIZATION TO SUBMIT DISSERTATION

This dissertation of Hesham Ramzy Gad Elkarim Tantawy, submitted for the degree of Doctorate of Philosophy with a Major in Chemical Engineering and titled "Electromagnetic Shielding Potential of Polyaniline Nanopowders," has been reviewed in final form. Permission, as indicated by the signatures and dates given below, is now granted to submit final copies to the College of Graduate Studies for approval.

Major Professor: \_\_\_\_\_ Date \_\_\_\_\_  
D. Eric Aston

Committee Members: \_\_\_\_\_ Date \_\_\_\_\_  
Armando G. McDonald

\_\_\_\_\_ Date \_\_\_\_\_  
Wudneh Admassu

\_\_\_\_\_ Date \_\_\_\_\_  
Daniel S. Choi

\_\_\_\_\_ Date \_\_\_\_\_  
Aicha Elshabini

Department Administrator: \_\_\_\_\_ Date \_\_\_\_\_  
Wudneh Admassu

Discipline's College Dean: \_\_\_\_\_ Date \_\_\_\_\_  
Larry A. Stauffer

Final Approval and Acceptance by the College of Graduate Studies:  
\_\_\_\_\_ Date \_\_\_\_\_  
Jie Chen

## ABSTRACT

Electromagnetic (EM) shielding in the microwave range using conducting polymers is a unique contribution beyond the more typical synthesis and physicochemical characterization work of many others on polyaniline (PAN) and other well-characterized polymers. This is why a well-studied polymer base system with two different dopant candidates was selected for expanding knowledge beyond materials characterization into an application area of EM shielding. This work is significant due to the new and uncommon use of exceedingly-limited solvent during oxidative polymerization, which has demonstrated as an apparent optimum in conductivity and EM shielding for (somewhat surprisingly) moderate polymer crystallinity compared to conventional solvent-rich synthesis. Furthermore, it describes a rather simple and inexpensive solvent-free and solvent-limited methods capable of producing relatively large amounts of nanoparticles (<50 nm) in a fashion easily scaled for practical uses in composite materials for a variety of electrical and electronic applications. To the best of our knowledge, this is the first time electromagnetic shielding with polyaniline has been considered as a function of synthesis conditions comparing the so-called solvent-free/solvent-limited approach. Moreover, the most favorable synthesis approach to achieve the highest possible conductivity is a primary target for practical considerations in fine-tuning production on large scales. Therefore, the long-term goal of this research is the development of new light-weight and affordable high-frequency EM shielding materials from an eco-friendly fabrication method.

Experimental work demonstrates the chemical/electronic/conformational, structural, morphological and electrical characteristics of doped PAN nanoparticles from different chemical synthesis conditions. Detailed x-ray photoelectron spectroscopy (XPS), Raman,

Fourier Transform-Infrared (FTIR), and ultraviolet (UV) spectroscopies were carried out for chemical analysis while transmission electron microscopy (TEM) and x-ray diffraction (XRD) were used for morphological and crystallinity characterization, respectively; a two-point probe technique was utilized for AC/DC electrical measurements, and EM shielding measurements used two different guided-transmission line techniques in the megahertz and gigahertz ranges. Results show that the nanopowders produced exhibit a range of EM shielding efficiencies for microwave radiation dependent on the average extent of oxidation, chemical/electronic/conformational structures, and electrical conductivity. Moreover, the effect of the synthesis approach and dopant type (species and organic/inorganic nature) on different physicochemical properties of the obtained PAN is elucidated. Collective data analysis demonstrates the importance of conductivity over crystallinity for enhanced shielding efficiency (SE) in nanoPANs doped with hydrochloric acid (HCl) and p-toluenesulphonic acid (PTSA). Furthermore, optimizing this new and unconventional approach for the best particular solvent-limited conditions (e.g., what is the optimum amount of solvent to maximize SE for a given dopant species) to well-defined polymer needs for conductivity and conformational structures shows inherent promise for future improvements toward various technological applications for made-to-order conducting polymeric materials.

## ACKNOWLEDGEMENTS

First and above all, all praise and thanks be to ALLAH the Almighty, the Most Beneficent, the Most Merciful, for granting me health, patience, determination, and capability to proceed successfully and accomplish this research.

Working towards a Ph.D. is not a path taken by one person but a hard and tough journey involving many contributors and collaborators. Therefore, I would like to acknowledge and express my deepest gratitude to all those who through their various assistance, inputs and contributions, made this research work possible.

First my sincere appreciation goes to my advisor, Professor Eric Aston for his innumerable support, encouragement, understanding, and generosity during the whole period of the study, and especially for his kind patience and guidance during the writing process.

My sincere gratitude also goes to my committee members: Prof. Armando McDonald, Prof. Daniel Choi, Prof. Wudneh Admassu, and Prof. Aicha Elshabini for their time, constructive criticisms and valuable suggestions.

My deep gratitude goes to Prof. Fred Barlow for the useful and interesting discussions regarding practical aspects for microwave measurements. I would like to thank him for the experience he has given me at every stage of this research.

Special appreciation and thanks goes to Prof. Thomas Williams. Through his deep knowledge and enthusiasm, he taught me the art of electron microscopy and how to work on the SEM, TEM and XRD. Thanks to him, I have received professional experience working on these instruments.

My sincere thanks go to Professor Aston's research group: Dr. Dennis Oriero, Andrew Weakley and Weston Corporon, for all their support both inside and outside the research lab.

Also, my deep appreciation goes to Professor McDonald's research group members, Dr. Noridah Osman, Hui Li, and Liqing Wei, for all their support, for introducing me to the laboratory equipment and showing me how to use them.

I wish to express my deepest gratitude to Prof. David McIlroy and his research assistant Blaise-Alexis for all their helpful assistance during the XPS characterization. Also, my sincere thanks goes to Prof. You Qiang and his research assistant Jennifer Sund for all their support and for helping me to do the low-frequency EM shielding measurements (1 MHz-1.5 GHz).

My sincere thanks goes to Prof. Deuk Heo at Washington State University and his postdoctoral group member Dr. Tai Nguyen for all their support and invaluable effort in helping me to do the broad frequency EM shielding measurements (2-14 GHz). I also wish to thank Prof. Jeffrey Young and his research assistant Jacob Smith for all their support and helping me to do the EM shielding measurements (8-12 GHz).

My truthful appreciation goes to Prof. Ray von Wandruszka for his tutelage, advice, and guidance during the UV-vis measurements.

I do appreciate all the effort of Russ Porter, who helped me to design sample holder and sample filling setup for the EM shielding measurements. He was so patient and helpful until we got the final setup working perfectly after many trials.

Truthful gratitude also goes to Gail Bergman and Margaret Baker; I'm really grateful for assisting me in many different ways and handling the paperwork and ordering the materials and chemicals used for this work. Thanks for Dr. Dave MacPherson for his priceless advice and assistance.

Special appreciation and thanks go to the chair (Professor Wudneh Admassu) and faculty of the Chemical and Materials Engineering Department, University of Idaho for providing the opportunity to learn in a wonderful environment and for all their support both inside and outside the research lab

I owe a lot to my dear friend Bennett Rieck, who has given me a lot of inspiration, hope and encouragement in the difficult times. He supported me through all the hard times I had from my first days in the USA till I left.

Of course I cannot forget my professors and colleagues in the Chemical Engineering Department at the MTC. I would like to thank all of them for their kind support before I came to the USA, during my study in the USA and after I came back to Egypt.

This work would not have been done without the support I had of my family. I owe a lot to my family; they suffered too much while I was working in this research. Actually, they spent almost all the time during our stay in the USA without me. I am very grateful and I can hardly express my gratitude to all of my family, especially my wife for her encouragement and support through all this work. She took full responsibility of the kids and the house all the time without complaint. Special appreciation is due to my son Ahmed and my daughter Rawan for enduring the little attention I gave to them during this research.

Finally, I'll never forget anyone who taught me any single word; anyone who tried to help in any way and for all those who remembered me in their prayers to accomplish this work successfully.

## TABLE OF CONTENTS

Authorization to Submit Dissertation .....	ii
Abstract .....	iii
Acknowledgements .....	v
Table of Contents .....	viii
List of Figures .....	xii
List of Tables .....	xiii
<b>Chapter 1: Introduction to Conducting Polymers for EMI Shielding</b> .....	<b>1</b>
1.1. Background and Significance .....	1
1.2. Theory on Shielding of Electromagnetic Interference .....	4
1.3. ICPs Nanostructures .....	6
1.4. Electromagnetic Potential Applications of ICPs Nanostructures .....	8
1.5. Characterization of ICPs Nanostructures .....	11
1.5.1. Morphological and Chemical Characterization .....	11
1.5.2. Thermal, Electrical and Magnetic Characterization .....	12
1.5.3. Electromagnetic Characterization Techniques .....	12
1.6. Perspective and Future Trends .....	14
1.7. Road Map of the Work Plan and Dissertation Outline .....	17
1.8. References .....	22
<b>Chapter 2: A Comparison of Electromagnetic Shielding with Polyaniline Nanopowders Produced in Solvent-limited Conditions</b> .....	<b>29</b>
2.1 Introduction .....	29
2.2 Theory of Electromagnetic Interference Shielding .....	31
2.3 Materials and Methods .....	34
2.3.1. Solvent-free (SF) Synthesis .....	36
2.3.2. Conventional Chemical Synthesis: Fast (CF) and Slow (CS) .....	37
Oxidations .....	
2.4. Characterization Methods .....	38
2.4.1. Chemical: FTIR .....	38
2.4.2. Morphological: TEM .....	38
2.4.3. Crystallinity: XRD .....	38
2.4.4. Electrical Conductivity .....	39
2.4.5. Electromagnetic Shielding .....	40
2.5. Results and Discussion .....	42
2.5.1. Morphology .....	42
2.5.2. Current-Voltage (I-V) Characterization .....	43
2.5.3. Fourier Transform Infrared (FTIR) Spectroscopy Analysis .....	44
2.5.4. XRD Characterization .....	47
2.5.5. Electromagnetic (EM) Measurements .....	51
2.6. Conclusions .....	56
2.7. References .....	58
<b>Chapter 3: Chemical Effects of a Solvent-Limited Approach to HCl-Doped Polyaniline Nanopowder Synthesis</b> .....	<b>69</b>
3.1. Introduction .....	69
3.2. Materials and Methods .....	71

3.2.1. Solvent-free (SF) Synthesis. ....	71
3.2.2. Conventional Chemical Synthesis: Fast (CF) and Slow (CS) Oxidations. ....	72
3.3. Characterization Methods ....	73
3.3.1. Micro-Raman Spectral Analysis of Polyaniline Samples. ....	73
3.3.2. UV-Vis Characterization. ....	74
3.4. Results and Discussion ....	74
3.4.1. Polymorphism, Chemical, and Electronic Structure. ....	74
3.4.1.1. Evidence of Various Polyaniline Forms. ....	75
3.4.1.2. Cross-linked Polyaniline Structures ....	78
3.4.1.3. Electronic Structure of Polyaniline ....	79
3.4.1.4. Average Oxidation Level from C-H Bending ....	79
3.4.1.5. Organization of Charge and Oxidation on the Chain ...	81
3.4.2. Conformation: Electronic Band Structure Dependence on Synthesis Approach (UV-vis Interpretation). ....	87
3.5. Conclusions ....	94
3.6. References ....	96
<b>Chapter 4: Broad-band EM Shielding Effects from Solvent-limited Synthesis of HCl-doped Polyaniline Nanopowders</b> .....	114
4.1. Introduction ....	114
4.2. Materials and Methods ....	115
4.2.1. XPS Instrumentation ....	116
4.2.2. Electromagnetic Shielding (SE) ....	117
4.3. Results and Discussion ....	119
4.3.1. XPS data interpretation: Evaluation of doping level dependence on synthesis approach ....	119
4.3.2. Electromagnetic Measurements ....	132
4.4. Conclusions ....	137
4.5. References ....	140
<b>Chapter 5: Dielectric Behavior and Conductivity HCl-Doped Polyaniline by Solvent-Limited Synthesis</b> .....	152
5.1. Introduction ....	152
5.2. Materials and Methods ....	154
5.2.1. Chemical Characterization ....	155
5.2.2. DC/AC Conductivity and Dielectric Permittivity Measurements ..	155
5.3. Results and Discussions ....	156
5.3.1. FTIR Interpretation ....	156
5.3.2. DC Electrical Conductivity ( $\sigma_{DC}$ ) ....	163
5.3.3. AC Conductivity ( $\sigma_{AC}$ ) ....	164
5.3.4. Dielectric Permittivity ....	170
5.3.5. Electric Modulus ....	174
5.4. Conclusions ....	178
5.5. References ....	181

<b>Chapter 6: Solvent-Limited versus Solvent-Free Unconventional Approaches for Synthesizing Nano-PTSA-Doped PAN for Broadband EM Shielding</b>	193
6.1. Introduction	193
6.2. Materials and Methods	196
6.2.1. Solvent-Limited (SL)/Solvent-Free (SF) Synthesis	196
6.2.2. Conventional Chemical Synthesis: Fast (CF) and Slow (CS) Oxidation	197
6.3. Characterization	198
6.3.1. DC Conductivity Measurements	198
6.3.2. Morphology: TEM	199
6.3.3. Crystallinity: XRD	199
6.3.4. UV–Visible Spectra	200
6.3.5. Electromagnetic Shielding Efficiency (SE)	200
6.4. Results and Discussions	201
6.4.1. DC Electrical Conductivity ( $\sigma_{DC}$ )	201
6.4.2. Morphology	202
6.4.3. XRD Characterization	205
6.4.4. UV-Vis Interpretation	211
6.4.5. Electromagnetic Measurements	216
6.5. Conclusions	219
6.6. References	222
<b>Chapter 7: Conclusions and Future Work</b>	235
7.1. Summary and Concluding Remarks	235
7.2. Future Work	246
<b>Appendix: Copyright Clearance</b>	252
Appendix A Copyright Form for Paper Published from Chapter 2 of Dissertation in the Journal Applied Materials	253
Appendix B Copyright Form for Paper Published from Chapter 3 of Dissertation in the Journal of Physical Chemistry C	255

## LIST OF FIGURES

<b>Figure 1.1:</b>	Simple schematic diagram for the three mechanisms contributing to the attenuation of an electromagnetic wave by a shield	5
<b>Figure 1.1:</b>	Classification of electromagnetic characterization methods .....	13
<b>Figure 1.1:</b>	Transmission/reflection characterization methods. ....	14
<b>Figure 2.1:</b>	Attenuation schematic of an electromagnetic wave by shielding material. ..	33
<b>Figure 2.2:</b>	Waveguide sample holder for X-band measurements performed. ....	41
<b>Figure 2.3:</b>	EMI waveguide measurement setup .....	41
<b>Figure 2.4:</b>	The TEM images of HCl-doped polyaniline: (a) fast oxidation, (b) slow oxidation, (c) solvent-free formulation. Note scale bars of 50 nm in (a-b) but 20 nm for (c).	42
<b>Figure 2.5:</b>	I-V curves from two-point probe measurements on three polyaniline sample types doped with HCl.	43
<b>Figure 2.6:</b>	FTIR spectra (in wavenumbers of $\text{cm}^{-1}$ ) of HCl-doped polyaniline prepared with different synthesis conditions: SF (top), CF (middle), CS (bottom).	45
<b>Figure 2.7:</b>	The XRD patterns of HCl-doped polyaniline nanoparticles from different synthesis	49
<b>Figure 2.8:</b>	Shielding effectiveness (SE) averaged over the tested X-band range of 8–12 GHz: (a) total ( $\text{SE}_T$ ), (b) absorbance component ( $\text{SE}_A$ ), and (c) reflectance component ( $\text{SE}_R$ ), identifying linear trends for CF, CS and SF type HCl-doped PAN nanopowders. Error bars represent standard deviations	53
<b>Figure 3.1:</b>	Raman spectra (in relative wavenumbers) of polyaniline samples (SF, CF, and CS).	76
<b>Figure 3.2:</b>	Gaussian-Lorentzian curve fitting for the C-H band ( $1100\text{-}1220 \text{ rel. cm}^{-1}$ ) of polyaniline samples SF, CF, and CS.	81
<b>Figure 3.3:</b>	Decomposition of the polaron band region $1300\text{-}1400 \text{ cm}^{-1}$ of polyaniline samples (a) SF, (b) CF, and (c) CS.	83
<b>Figure 3.4:</b>	UV-visible spectra of polyaniline samples (CS, CF, and SF) in m-cresol.	88
<b>Figure 3.5:</b>	Proposed band structures of doped polyaniline sample. (a) Localized polaron/bipolaron model for compact coil conformation in the CS sample. (b) Delocalized polaron (polaron lattice) model for expanded coil conformation, SF and CF samples.	92
<b>Figure 4.1:</b>	Coaxial guided transmission line setup for EMI SE measurements. ....	118
<b>Figure 4.2:</b>	The N(1s), C(1s), and Cl2p XPS core-level spectra and deconvolution for PAN samples prepared with different approaches (SF, CF, and CS).	122
<b>Figure 4.3:</b>	O (1s) XPS core-level spectra and deconvolution for PAN samples prepared with different approaches (SF, CF, and CS).	130
<b>Figure 4.5:</b>	Low frequency electromagnetic shielding potential of 0.06 g HCl-doped PAN (CF, CS, and SF) tested in a coaxial sample holder as a function of frequency measured in the range 100-1500 MHz.	133
<b>Figure 4.6:</b>	Broad band electromagnetic shielding potential of 0.06 g HCl-doped PAN (CF, CS, and SF) tested in a coaxial sample holder as a function of frequency measured in the range 2-14 GHz	134

<b>Figure 5.1:</b>	FTIR spectra of for HCl-doped PAN samples prepared with different approaches.	157
<b>Figure 5.2:</b>	I-V curves from two-terminal measurements on three PAN samples doped with HCl.	164
<b>Figure 5.3:</b>	Frequency dependence on conductivity of HCl-doped PAN samples. ....	167
<b>Figure 5.4:</b>	Frequency dependence of (a) dielectric constant ( $\epsilon'$ ) and (b) dielectric loss factor ( $\epsilon''$ ) for PAN samples.	173
<b>Figure 5.5:</b>	Electric modulus of PAN samples (CS, CF, and SF). .....	176
<b>Figure 5.6:</b>	Complex plane diagram for the electric modulus of PAN samples (CS, CF, and SF).	177
<b>Figure 6.1:</b>	Schematic diagram of the home made cell used for measuring the DC conductivity of the samples.	189
<b>Figure 6.2:</b>	I-V curves from two-terminal measurements on four PAN samples doped with PTSA: CF and SF overlap symbols	202
<b>Figure 6.3:</b>	The TEM images of PTSA-doped PAN samples prepared with different approaches: (a) SL, (b) SF, (c) CS, and (d) CF. Note scale bars of 20 nm (a), 100 nm (b) and 200 (c-d).	204
<b>Figure 6.4:</b>	XRD diffraction pattern of PTSA-doped PAN synthesized under different protocols: SL (top), CS, SF, CF (bottom).	206
<b>Figure 6.5:</b>	UV-visible spectra of polyaniline samples (SL, SF, CS, and CF) in m-cresol.	213
<b>Figure 6.6:</b>	Broad band electromagnetic shielding potential of 0.06 g HCl-doped PAN (SL, CS, SF, and CF) tested in a coaxial sample holder as a function of frequency measured in the range 2-14 GHz.	218
<b>Figure 7.1:</b>	Schematic diagram for different future work trends. ....	247

## LIST OF TABLES

<b>Table 2.1:</b>	The main IR bands for PAN-HCl nanoparticles by synthesis condition. ....	46
<b>Table 2.2:</b>	Absorption intensities and their ratios for PAN-HCl samples. ....	47
<b>Table 2.3:</b>	XRD data analysis summary. ....	51
<b>Table 3.1:</b>	Band assignments from Raman spectra of polyaniline samples (SF,CF, and CS)	77
<b>Table 3.2:</b>	Different possible electronic structures of polyaniline samples SF, CF, and CS obtained by semiquantitative analysis results of the decomposition of the polaron band (1300-1400 cm <sup>-1</sup> )	85
<b>Table 3.3:</b>	Bands assignments of UV-visible spectra of polyaniline samples (CS, CF, and SF) in m-cresol.	89
<b>Table 4.1:</b>	The N(1s), C(1s), O(1s), and Cl(2p) XPS core-level deconvolution results for PAN samples prepared with the three different approaches (SF, CF, and CS).	120
<b>Table 4.2:</b>	The impact of synthesis approach on oxidation/doping level, cross-linking degree, and chlorine radical/chlorine cation ratios of PAN samples	124
<b>Table 4.3:</b>	Summary of EM shielding effectiveness measurements. ....	135
<b>Table 5.1.</b>	The main IR bands for HCl-doped PAN samples prepared with different approaches.	161
<b>Table 5.2.</b>	Domain size, interchain separation, and degree of crystallinity of PAN samples reported in previous work, Chapter 2 in comparison with $\sigma_{DC}$ (S/cm) measured in this work.	170
<b>Table 6.1.</b>	XRD data analysis summary of PTSA-doped PAN samples. ....	207
<b>Table 6.2.</b>	XRD diffraction peak assignments of PTSA-doped PAN samples. ....	208
<b>Table 6.3</b>	Band assignments of UV-visible spectra of polyaniline samples (CS, CF, SL and SF) in m-cresol.	213
<b>Table 6.4</b>	Summary of EM shielding effectiveness (SE) measurements of PTSA-doped band within frequency range 2-14 GHz. ....	217
<b>Table 7.1.</b>	Summary of physicochemical properties of HCl-doped PAN dependence on synthesis approach	236
<b>Table 7.2.</b>	Summary of physicochemical properties of PTSA-doped PAN dependence on synthesis approach	243

## CHAPTER 1

### Introduction to Conducting Polymers for EMI Shielding

#### 1.1. Background and Significance

Nowadays, high-speed communication is an essential concern due to of the rapid progress of technology in all fields. Higher frequency range from the microwave to the millimeter wave is expected to achieve more bandwidth (information-carrying capacity) and satisfies the desired high speed communications.<sup>1</sup> Many electronic instruments with the higher frequency, such as satellite communication, automobile collision prevention radar, accident surveillance of a railroad, millimeter wave wireless LAN and so on, have been developed and applied.<sup>2</sup> As a result, fast growth of high frequency electromagnetic energy emission has been established, leading to electromagnetic interference (EMI) problems, which are unacceptable degradation of the performance of a system or devices by unexpectedly radiated and conducted signals from other electrical origins.<sup>3</sup> In actual fact, EMI has become a serious dilemma, which has impacted almost all electrical and electronic systems from daily life to space exploration.<sup>4</sup> In addition, many types of EM waves may cause health problems<sup>5</sup> such as symptoms of insomnia, nervousness, languidness, and headaches.<sup>6</sup> Rather than rely on ignorance and the potential future knowledge of longer-term health studies, a better and more thorough approach would be to eliminate EMI to the greatest degree possible by current and future technological developments.

Thus, various EMI shielding methods have been developed, not only to reduce the probability of the aforementioned hazards but also to increase the lifetime of electronic devices and their efficiencies. The traditional approach for EMI shielding relies on the use of

metallic materials, which supply excellent shielding effectiveness (SE).<sup>5</sup> However, the conventional metallic shields, in the form of bulk sheets, meshes, plating, coatings, powders, and/or fibers in filled polymer composites or coatings,<sup>7-11</sup> impose severe weight penalties, especially in aerospace applications such as spacecraft and satellite systems.<sup>5</sup> Although great measures are undertaken to overcome such weight penalties, another major drawback of the metallic materials is that the SE degrades greatly in the joints especially where metals simply cannot be employed in a contiguous fashion for many situations.<sup>5</sup> Intrinsically conducting polymers (ICPs) are considered as attractive alternative materials for EMI shielding.<sup>5,12-14</sup> These materials combine high conductivity, ease of processability, low density (far less than that of metals), and corrosion resistance with the unique shielding mechanism high relative absorption (differing from higher reflection terms for metals and carbons).<sup>5</sup>

However, a high level of shielding efficiency can generally not be obtained using conductive polymers alone. Purely conductive materials are able to shield EM waves from electrical sources; but if the EM radiation comes from a magnetic source, they are best shielded by magnetic or magnetizable materials. Recent studies show that magnetic nanoparticles can be used to absorb EM waves.<sup>15,16</sup> The surface effects of small particles only a few nanometers in diameter are also likely important for absorption due to the surface and shape of magnetic anisotropies and surface damping, all of which increase with decreasing diameter. The combination of conducting and nanomagnetic components are thus of much interest in the development of new EMI shielding materials.<sup>13</sup>

The recent research efforts dedicated to enhance EMI shielding performance of ICPs by the development of ICPs-based magnetic nanostructures<sup>17-27</sup> can be grouped as follows: i) the achievement of different magnetic nanoparticles with controlled morphology and

magnetic properties; ii) embedding magnetic nanoparticles into polymeric matrices or obtaining core-shell structures with a magnetic core covered by a conducting polymer shell.<sup>28</sup> The importance of ICPs in the field of EMI shielding is to enhance the shielding-to-weight ratio toward a potential replacement for denser metals, and whatever obtained values, then even more enhancement could be achieved by introducing magnetic materials into a relatively easy to make polymer composite, which could also including some metallic fillers to produce an optimum material that could be fine-tuned in composition for particular applications whether they require plates, films, coatings, or other forms. One particular materials combination of a conducting polymer/magnetic composite with carbon nanotubes is regarded as a future target to optimize EM shielding with mechanical properties as needed.

The present work concerns the possibility of enhancing EM shielding potential of one of the more common and easy to produce conducting polymer candidates, polyaniline (PAN). The selected enhancement strategy based on exploring simple, inexpensive synthesis approaches is to modify the conventional solution-based oxidation method for polymerization by reducing or eliminating the solvent to the concentration that produces the best shielding impact, since this concept has the potential to maximize the shielding potential of polyaniline by providing the optimal reaction conditions for greatest conductivity in the resulting polymer product.

The main goals of this study is investigating and optimizing the dependence of electromagnetic shielding potential of the polyaniline nanoparticles doped with inorganic/organic sulphonic acids on the synthesizing approaches. In addition to establishing a comparison study between the utilized unconventional approach and classic conventional approach for producing doped polyaniline nanoparticles. Moreover, investigating the effect of

the synthesis approach and dopant on different physico-chemical properties of the obtained doped polyaniline, was an important aim to understand how to tune polyaniline properties via unconventional synthesis approach. The long-term goal of this study is the development of new light-weight and affordable high frequency EM shielding materials with an eco-friendly fabrication method.

## 1.2. Theory on Shielding of Electromagnetic Interference

All electromagnetic waves consist of two essential components, a magnetic field (H) and an electric field (E) perpendicular to each other, and the direction of wave propagation is at right angles to the plane containing these two components. The relative magnitude depends upon the waveform and its source. The ratio of E to H is called wave impedance. The intrinsic impedance of free space is  $377\Omega$ .<sup>29</sup>

Shielding effectiveness (SE) is the ratio of impinging energy to the residual energy. The effectiveness of a shield and its resulting EMI attenuation are based on the frequency, the distance of the shield from the source, the thickness of the shield, and the shield material. SE is normally expressed in decibels (dB) as a function of the logarithm of the ratio of the incident and exiting electric (E), magnetic (H), or plane-wave field intensities (F). The subscripts (t) and (i) refer to the transmitted and incident waves:

$$SE = 20 \log \left( \frac{E_t}{E_i} \right)$$

$$SE = 20 \log \left( \frac{H_t}{H_i} \right)$$

$$SE = 20 \log \left( \frac{F_t}{F_i} \right)$$

With any kind of EMI, there are three mechanisms contributing to the effectiveness of a shield. Part of the incident radiation is reflected from the front surface of the shield, part is absorbed within the shield material, and part is reflected from the shield's rear surface to the front where it can aid or hinder the effectiveness of the shield depending on its phase relationship with the incident wave, as shown in Figure 1.1. Therefore, the total SE of a shielding material equals the sum of the absorption factor (A), the reflection factor (R), and the correction factor to account for multiple reflections in thin shields:

$$SE = R + A + B$$

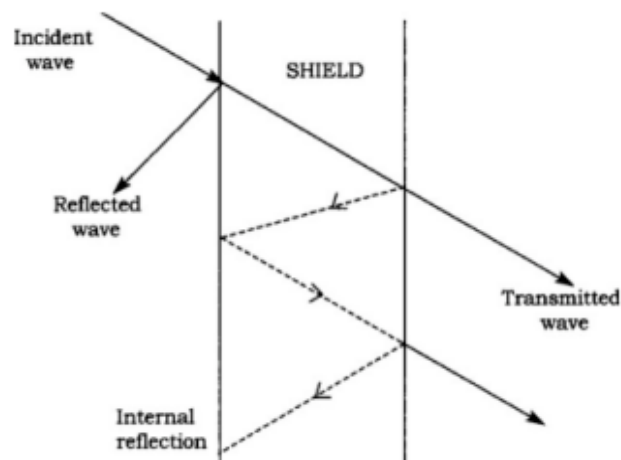


**Figure 1.1.** Simple schematic diagram for the three mechanisms contributing to the attenuation of an electromagnetic wave by a shield.<sup>30</sup>

All SE terms are expressed in dB. The multiple reflection factor, B, can be neglected if the absorption loss, A, is greater than 10 dB. In practical calculations, B can also be neglected for electric fields and plane waves. Absorption losses are a function of the physical characteristics of the shield and are independent of the type of source field.

The decay or absorption loss occurs because currents induced in the medium produce ohmic losses and heating of the material. On the other hand, the reflection loss is related to

the relative mismatch between the incident wave and the surface impedance of the shield. Moreover, the B factor can be mathematically positive or negative (in practice it is always negative) and becomes insignificant when  $A > 6$  dB. B is usually important only at low frequencies (i.e., below approximately 20 kHz). In summary, the amount of reflection loss depends on the impedance of the EM wave and the shield. When an EM wave encounters a shield, if the wave's impedance differs significantly from that of the shield, the wave is partially reflected back.<sup>4</sup>

### 1.3. ICPs Nanostructures

Functionalized nanomaterials, with sizes 1-100 nm, have received great attention in nanoscience and nanotechnology because of their large surface area compared with their bulk materials and the influence of size on the physical properties, which is called as size effect.<sup>31</sup> Multifunctional nanostructures are a special class of materials, which originate from suitable combinations of two or more nanoparticles, have received great attention because of their unique physical properties and wide application potential in diverse areas. Novel properties of nanostructures can be derived from the successful combination of the characteristics of parent constituents into a single material.<sup>32</sup> ICPs nanostructures have unique properties such as  $\pi$ -conjugation polymeric chains, metal-like conductivity, and reversible physical properties by a novel doping/de-doping process that can be used as molecule wires and nanodevices, resulting in attracting attention<sup>33</sup> in nanoscience and nanotechnology.<sup>33</sup>

One of the current interests is the preparation of “core-shell” nanostructured composites, where the inorganic core particles are homogeneously covered with ultra-thin films of conducting polymers. One approach is chemical synthesis of conducting polymer-coated

“core-shell” particles, where the “core” consists of a non-conducting material.<sup>32</sup> These conducting polymer-coated “core-shell” nanoparticles, such as PPy and PAN, have been reported by using poly(N-vinylpyrrolidone) (PVP)-stabilized polystyrene (PS) latex particles as core templates, where the oxidant and monomer were introduced via an aqueous dispersion. This approach demonstrated that better processability and relatively high conductivity can be achieved even with low ICPs loading.<sup>33</sup>

Another approach to improve processability of ICPs (e.g. PAN) is monomer polymerization in the presence of poly(sodium 4-styrenesulfonate) (PSS). It was reported that the conductive core-shell particles were prepared by the deposition of PAN multilayers onto colloidal PS particles via the alternate electrostatic layer-by-layer assembly technique. PSS was used as a polymeric counter ion for multilayer formation as well as a stabilizer and codopant for PAN.<sup>34</sup>

Self-assembled monolayers and adsorbed amphiphilic molecular layers on the surface have been used as the template for growth of ultra-thin films of the conducting polymers. Such templates can afford ordered molecular arrays on the surfaces and be widely used as 2D reaction media to produce ultra-thin polymer films. The method consists of three processes as follows:<sup>33</sup>

- (1) Adsorption of the amphiphilic molecules from aqueous solutions as self-assembled arrays onto a solid surface, which depends on the adsorption behavior (e.g., surface charge for ionic surfactants); the self-assembled arrays can be monolayers or bilayers.
- (2) Partition of the monomer from water into the self-assembled arrays. The rate of the process is controlled by the nature of the surface and interior properties of the self-assembled arrays.

- (3) Polymerization on the solid surface is initiated by adding chemical oxidants and free monomer is generally washed away with water after polymerization, leaving thin ICPs coatings on substrates.

Recently, convenient and adjustable procedures were proposed for the preparation of metal-polymer core-shell and segmented nanostructures.<sup>35</sup> The self-assembly provided a good chemisorbed contact between the metal and polymer segments. In addition, an array of aligned, free-standing gold nanotubes could be prepared from such a nanostructured composite when the matrix of PAN was removed by plasma oxidation.<sup>36</sup>

Surface modification of nanowire or nanorod arrays with ICPs is another type of “core-shell” composites that expected to add more functionality to the system and may lead to completely new nanocomposites.<sup>37</sup> The ability to control the thickness of ICPs coated on each nanowire and the size of the inter-tubular pores is crucial for applications in optoelectronic nano-devices and sensors.<sup>33</sup>

#### **1.4. Electromagnetic Potential Applications of ICPs Nanostructures**

It is well known that conducting polymer-based EMI materials have received great attention in the field of the conducting polymers. Compared with traditional inorganics as EMI materials, the conducting polymer-based materials are advantageous for lower surface mass and relative ease of processing as well as adjustable electromagnetic parameters by changing the doping degree, dopant nature, main polymer chain, and synthesis method and conditions.<sup>30</sup> Among these conducting polymer-based EMI materials, PAN and PPy are regarded as promising because of high conductivity, easy synthesis for large-mass chemical polymerization, and controllable EM parameters by adjusting both oxidation and protonation

state.<sup>6,38</sup> For instance, influence of dopant nature and protonation state on the dielectric properties of PAN in the microwave frequency (8-18 GHz) has been reported. However, most results reported in the literature showed the conducting polymer-based microwave materials belong to typical dielectrical loss materials in the microwave frequencies, which cannot satisfy the application requirements, because both dielectrical and magnetic losses in the microwave region are required for practice EMI shielding materials.<sup>33</sup>

It is necessary to improve the magnetic losses of the conducting polymer-based EMI shielding materials in order to enhance its absorbing efficiency and to expand the absorbing band at the microwave frequency. There are three ways to solve the above issues. One is blending ICPs with inorganic magnetic materials to prepare hybrid composites with both dielectrical and magnetic losses. This is a common approach; however, the surface mass of the hybrid composites is limited by adding magnetic loss materials.<sup>39</sup>

The second way is to synthesize tubular conducting polymers, because theoretical calculations reveal that the tubular materials exhibit a unique absorption character.<sup>40</sup> However, synthesis of large-scaled mass and low-cost for the nanostructured ICPs is a challenge, because hard-templating, as the main feasible method, is unsatisfactory due to size limitations of the membrane used as the hard templates. Since the EM absorbing properties and working frequency of the chiral materials can be adjusted by changing their real and ideal dielectric constant,<sup>41,42</sup> chiral materials have therefore received great attention as a new type of microwave absorbing materials.

It was found that high magnetic loss at the 1-18 GHz region from the PAN- $\beta$ -NSA/D-glucose nanotubes is reasonable, which probably arose from partial ordering of the polarons as charge carries along the tubes. Moreover, the template-free synthesized PAN-DBSA

micro/nanotubes exhibited both dielectric and magnetic losses in the same frequency region while the bulk PAN-DBSA synthesized by a conventional method only showed dielectric loss at microwave frequency without magnetic losses. It could be concluded that tubular materials exhibited novel microwave absorption characters.<sup>33</sup>

Among conducting polymers, PPy is outstanding owing to its high conductivity at room-temperature and stability in air. Moreover, its room-temperature conductivity is generally higher than that of PAN when the same dopants are used. Therefore, the template-free synthesized PPy nanostructures might be used as an excellent microwave absorbing materials. Along this line, large-scaled mass of the PPy-p-TSA nanotubes with a room-temperature conductivity as high as 27 S/cm have been synthesized by a template-free method. Although the magnetic losses observed in the micro/nanotubes are not clearly understood at the present time, it might result from a coordination effect of spin-polaron (i.e., charge carrier) and orientation of polymeric chain along the tubes.<sup>43</sup>

Even though conducting polymer-based EMI shielding materials have received great attention as potential EMI shielding for their high conductivity, tunable dielectro-magnetic properties and light weight, their commercial applications at the current time is limited by their narrow bandwidth due to only having dielectric loss mechanisms and poor mechanical strength. Investigations on conducting polymer-based microwave absorbing materials should therefore move forward to enhancing the absorbing efficiency, expanding bandwidth, and improving mechanical properties. Although hybrid composites of the ICPs with magnetic losses provide a more approach for utilizing the benefits of conducting polymers, restrictive limits to the addition of the magnetic fillers only provide some measure of improvement. It is clear that ICPs nanostructures prepared by some template-free method may open a facile and

efficient approach to fabricate conducting polymer-based microwave materials that satisfy requirements for developing new types of microwave absorbing materials.

### **1.5. Characterization of ICPs Nanostructures**

There are three key steps in the development of ICPs materials: syntheses, property characterizations, and performance. A material's synthesis involves the processing of ICPs nanostructures. The next challenge is to determine the degree and level of dispersion of the ICPs nanostructures. In addition, characterizing ICPs nanostructures is an important issue to correlate the material performance with physical, chemical, and structural features, which are of crucial importance for the development of new ICPs nanostructures and the optimization of existing ones. Comprehensive knowledge of the ICPs nanostructures is critical for their success and realizing how to manipulate properties and production for applications in EMI shielding or any other area. Chemical characterization techniques are essential to identify qualitatively and quantitatively each constituent of the ICPs nanostructures as well as optical and electron spectroscopy and ion spectrometry.<sup>31</sup> Also, characterization involves two more main processes: morphological analysis and materials property measurements. Structure analysis could be carried out using a variety of microscopic and spectroscopic techniques, while property characterization is rather diverse and depends on the application.

#### **1.5.1. Morphological and Chemical Characterization**

Different techniques may be employed for the characterization of ICPs nanostructures, including atomic force microscopy (AFM), scanning tunneling microscopy (STM), Fourier transformed infrared (FTIR) and Raman spectroscopies, X-ray photoelectron spectroscopy

(XPS), nuclear magnetic resonance (NMR), differential scanning calorimetry (DSC), scanning and transmission electron microscopies (SEM/TEM), etc.

For example, AFM is a powerful tool to study the surface even down to the nanometer scale and below in some instances. Simultaneous small-angle X-ray scattering (SAXS) and X-ray diffractometry (XRD) have been used for quantitative characterization of nanostructures and crystallite structures. In addition, theoretical calculations/simulations could be worked out to predict strength properties, including stress/strain curves.<sup>44</sup>

### **1.5.2. Thermal, Electrical and Magnetic Characterization**

Thermogravimetric analysis (TGA) and differential scanning calorimetry (DSC) could be employed to investigate the thermal stability of ICPs nanostructures in inert or oxidant atmosphere, and to determine polymer degradation temperatures, glass transition temperatures, and the mass ratio of the organic and inorganic components of ICPs compositions.<sup>45,46</sup> Standard two-point and four-probe methods are commonly employed for electrical characterization and determination of ICPs resistivity. The nanocomposite powders are pressed into the form of disk pellets with a diameter of 25 mm by applying a pressure up to 95 MPa in a hydraulic press, and the average thickness is about 1 mm. The temperature-dependent resistivity may be used to investigate the electron-transport mechanism in the nanostructures.<sup>47</sup> Magnetic characterization of ICPs nanostructures could be performed with a vibrating sample magnetometer (VSM) to perform susceptibility and magnetization studies<sup>48</sup> or a SQUID magnetometer to determine the coercivity and frequency dependence of the permeability.<sup>49</sup>

### 1.5.3 Electromagnetic Characterization Techniques

Electromagnetic methods for materials characterization generally fall into nonresonant and resonant methods. Nonresonant methods are often used to get a general knowledge of EM properties over a frequency range while resonant methods are used to get accurate dielectric properties at a single frequency or several discrete frequencies.<sup>50</sup> Figure 1.2 shows a general classification. In nonresonant methods, the properties of materials are fundamentally deduced from their impedance and the wave velocities in the materials. When an EM wave propagates from one material to another (e.g., from free space to sample), both the characteristic wave impedance and velocity change, resulting in a partial reflection of the EM wave from the interface. Measurements of this reflection and the transmission through the interface can provide information for the deduction of permittivity and permeability relationships between the two materials.

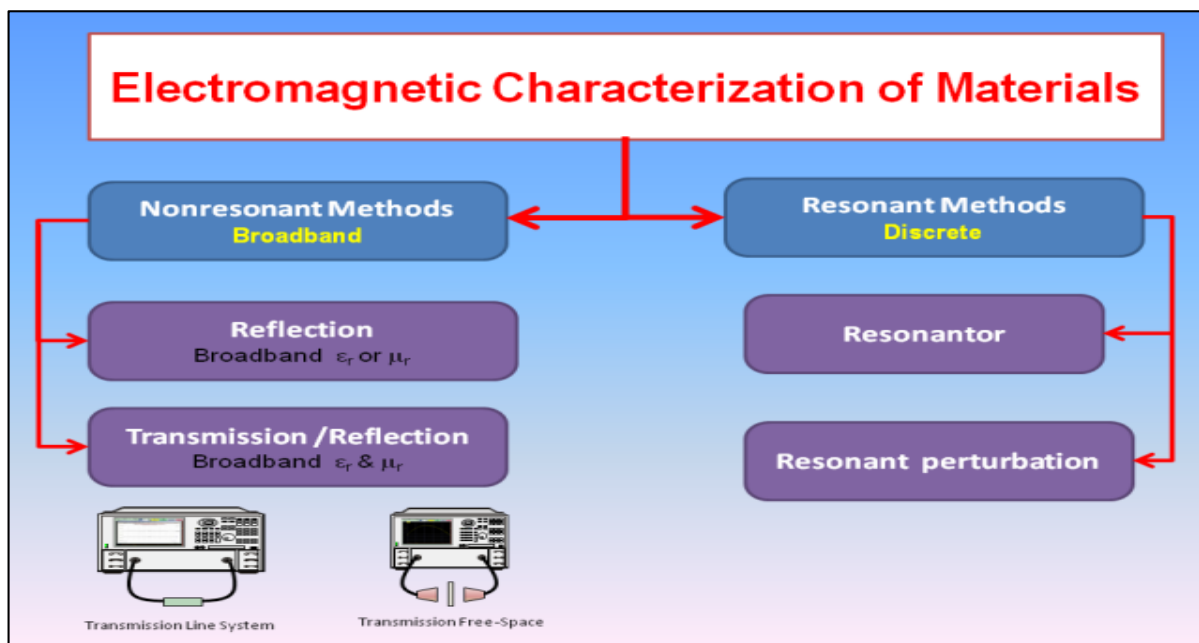


**Figure 1.2.** Classification of electromagnetic characterization methods.

Nonresonant methods mainly include reflection only methods and transmission/reflection methods. In principle, all types of transmission lines can be used to carry the wave for nonresonant methods, such as coaxial line, hollow metallic waveguide, dielectric waveguide, planar transmission line, and even free space. Usually, a reflection method can only measure one parameter, either permittivity or permeability. On the other hand, transmission/reflection is widely used in the measurement of the permittivity and permeability of low conductivity materials. The material under test, which could be ICP nanostructured sample, is inserted into a piece of transmission line, as shown in Figure 1.3, and the properties of the material are deduced on the basis of the reflection from the material and the transmission through the material.

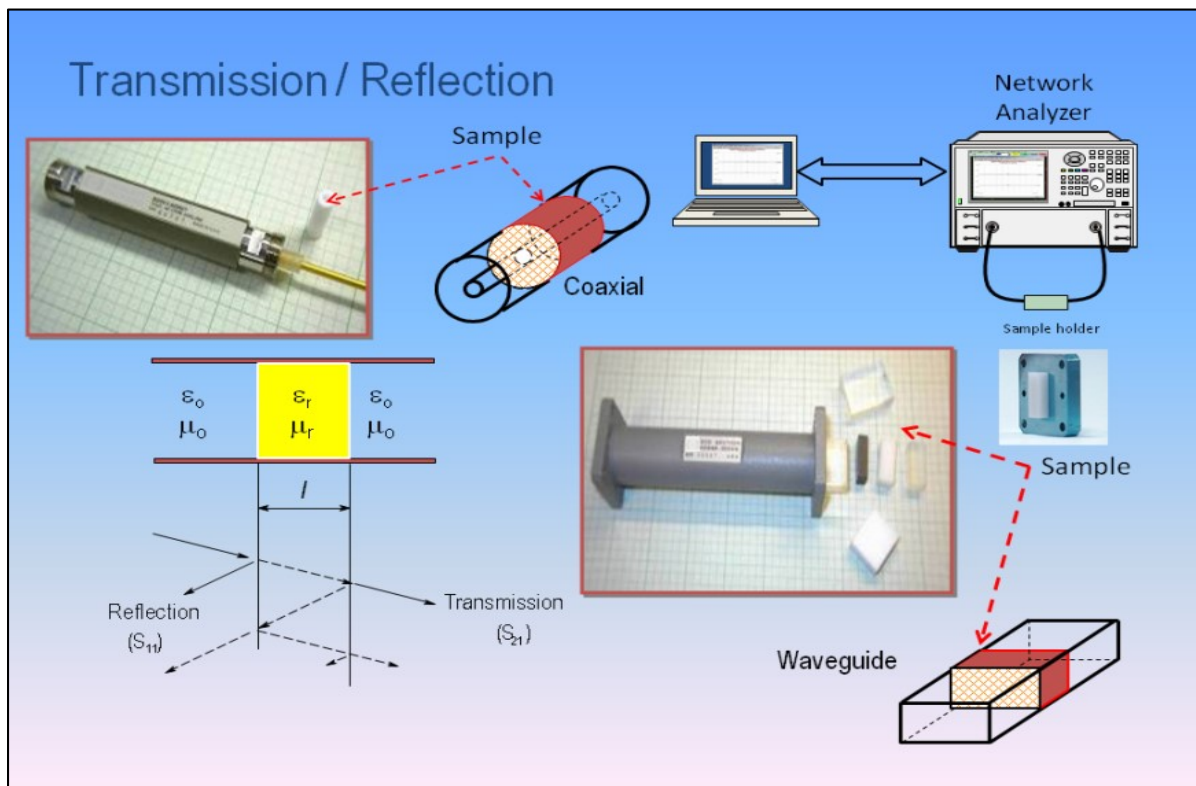


**Figure 1.3.** Transmission/reflection characterization methods.

## 1.6. Perspective and Future Trends

In order to develop new ICP nanostructures and to optimize existing ones, it is important to correlate the electromagnetic shielding performance with physical, chemical, and structural characteristics. This will not happen without establishing a wide base of tremendous experimental results and better understanding of the systems in applications, in addition to expanding the number of selections of conducting polymers and magnetic material candidates for ICP nanostructures. New ICPs and different magnetic ferrites should be investigated. Moreover, tuning the electrical and magnetic characteristics of ICP nanostructures should be investigated along with effects on shielding efficiency. Furthermore, the mass production scale challenges and problems for these electromagnetic ICP nanostructures should be taken into consideration beyond mere scientific interests.

Since the electromagnetic potential of ICP nanostructures depends on their electromagnetic properties of permittivity and magnetic permeability, these could also be varied and controlled in ICPs via the magnetic properties of the additive constituents such as magnetic nanostructured fillers. Thus, the development of new ICP nanostructures or optimization of existing ICPs could be achieved through two parallel steps of selecting optimal ICP(s) and magnetic material(s) individually with the best EM shielding potential. The third step would consider the synergies between the ICP and magnetic material to optimize the composite behavior for relative loadings of each.

The investigation steps of the optimum ICPs should include exploring new dopants, mixed dopants, and synthesis of new ICPs or relevant copolymers. The best candidates should have a broad range for conductivity selection that will be better to control for particular EM shielding potential. On the other hand, different ferromagnetic and ferrimagnetic (ferrites) materials

should be examined. The optimum ferrite candidates as composite shielding material fillers would be expected to have the broadest EM shielding bands. Since ferrites can exist with different crystal structures (cubic or hexagonal), and depending on the crystal structure and the chemical compositions their magnetic behavior can be varied between soft to hard, the correlation between EM shielding potential and crystal structure, chemical compositions, and magnetic activities should be clearly defined and utilized for effective implementations.

During the final step, various issues should be considered for what is assumed to be an optimum design morphology of ICP shell/magnetic ferrite core composite structures, which carrying both magnetic and electrical characteristics. First, the ICP coating process onto magnetic particles or powders should be designed to be feasible and controllable in a large-scale production process and not merely as an interesting lab-scale batch procedure. Second, the effect of the ICP film thickness on the magnetic properties of the ferrite core should be investigated. Third, the effect of ferrite core size, and potentially shape, on the electrical properties of the ICPs should be monitored. Fourth, the impact of the aforementioned issues on the EM shielding potential of the core/shell composite should be clarified. The common magnetic ferrite coating candidates are typically the popular ICPs such as polyaniline and polypyrrole. Less studied ICPs could be explored, such as polythiophenes, poly(3,4-ethylene dioxathiophene), poly(arylene vinylene)s, poly(*p*-phenylene), and poly(*p*-phenylene sulfide) along with many others. On the other hand, there are vast numbers of ferrites already produced for many application areas of interest that could be investigated as fillers, such as spinel  $\text{Fe}_2\text{O}_3 \cdot \text{MeO}$ , where MeO is any transition metal oxide; garnet ( $5\text{Fe}_2\text{O}_3 \cdot 3\text{Me}_2\text{O}_3$ ), where  $\text{Me}_2\text{O}_3$  is a rare earth metal oxide, and magnetoplumbite ( $6\text{Fe}_2\text{O}_3 \cdot \text{MeO}$ ) where MeO is a divalent metal oxide from group II, e.g., BaO, CaO, SrO. Optimum ferrites for maximum

shielding within certain bands should be investigated first, then applying the optimum conducting polymer to ferrite composites follow on investigations of the additivity of effects, whether synergistic or somewhat self-defeating influences contribute to predicted efficiencies for shielding. Then the resultant should be maximize the shielding performance and/or expanding the practical EM shielding frequency band that can be adequately dealt with in applications. Though the present work was unable to extend this far and deep into the expected landscape of potential material composites, it is the main direction of interest for this researcher in future advancements stemming from the accomplishments herein.

### **1.7. Road Map of the Work Plan and Dissertation Outline**

The work presented herein concerns a detailed study exploring the possibility for enhancing electromagnetic (EM) shielding potential of polyanilines (PANs) based on simple, inexpensive alterations from conventional oxidative approaches with solvent such as drastically limiting or even totally eliminating the dispersing solvent(s) in the synthesis of the conducting polymer from its monomeric precursor and doping agent mixture. Based on the obtained results from this research, enhancing the EM shielding potential of PANs beyond this concept would including the addition of magnetic materials as a second in-depth study for future work. Recently, attention has been paid to the preparation of doped-PAN via solvent-free reaction approaches accomplished in a solid or powder/paste-like state.<sup>51-57</sup> This has obvious advantages from eliminating the solvent costs and complications associated therein, including separation, recovery, reuse and proper waste treatment as well as reducing the overall volume and mass of chemicals per final product quantity. Furthermore, a solvent-free reaction is the more environmentally benign method.<sup>52</sup> However, the EM properties of

solvent-free (SF) PAN and their controllability remain largely unstudied, but for the present results and publications by this author, and the EM shielding potential of PAN nanoparticles or nanopowders synthesized by a solvent-free reaction has not been previously evident in available literature.

The main goals of this study are investigating and optimizing the dependence of EM shielding potential of the polyaniline nanoparticles doped with inorganic (HCl) and organic sulphonic acids on the synthesizing approaches. In addition to this, we have established a comparison study between the utilized unconventional approach (solvent free or limited reaction) and classic conventional approach for producing doped polyaniline nanoparticles. Moreover, investigating the effects of the synthesis approach and dopant on different physico-chemical properties of the obtained doped polyaniline was an important aim to understand how to tune polyaniline properties optimally for EM interference shielding and to demonstrate the improvements therein via the unconventional synthesis approach of limited or completely removing the main dispersing solvent from the reaction conditions. The long-term goal of this study is the development of new light-weight and affordable high-frequency EM shielding materials with an eco-friendly fabrication method.

The rest of the dissertation is organized as follows: Chapter 2 presents detailed study of the physico-chemical characteristics of PAN doped with HCl synthesized via a wetted solid state polymerization under mechanical grinding, referred to as a “solvent free” protocol (SF), compared with two conventional chemical approaches for both fast (CF) and slow (CS) oxidation conditions in aqueous solutions of ammonium peroxydisulfate (APS)—the same oxidizing agent used in the solvent-free route. Experimental work demonstrated the chemical, morphological and electrical characteristics of conducting polymer nanoparticles from three

distinctly different chemical synthesis conditions. Results showed that the produced materials with a range of electromagnetic shielding efficiencies for microwave radiation (8–12 GHz) depend on the average extent of oxidation, conductivity and polymer crystallinity.

Chapter 3 represents the first investigations of electronic structure, polymorphism, and chain conformation of HCl-doped polyaniline prepped via solvent free approach in comparison with a classical chemical oxidation approach. In order to get a deep understanding and clear correlations between synthesis approach especially solvent free SF and its impact on electronic structure, polymorphism, and chain conformation of the prepared polyaniline. Moreover, clarifying the sensitivity of polyaniline futures to synthesis condition is a significant aim. Also, addressing the electrical/electromagnetic behavior and correlate it to other parameters such as cross linking, electronic structures, and chain conformations. In order to control and design polyaniline with especial futures for a specific applications.

Chapter 4 represents the first investigations of EM shielding of HCl doped PAN prepared by solvent-free (SF) approach as impacted by electronic structure, polymer chain cross-linking, and chemical structure of HCl-doped PAN in comparison with classical chemical oxidation approaches—the same as discussed previously. Investigating the EM shielding potential of the nanopowders was very important to confirm and validate the results from Chapters 2 and 3. Moreover, addressing the electrical/electromagnetic behavior and correlate it to other physicochemical parameters (cross-linking, chemical and electronic structures) in order to approach specific design requirements toward EM shielding through synthesis processes methodically.

Chapter 5 aims to confirm DC electrical conductivity trends observed previously in Chapter 2. In addition to, elucidating the relative impact of different structure aspects

(hydrogen bonding/branching/cross linking) on electrical/ dielectrical behavior of PAN samples. Moreover, dielectric constant and dielectric loss measurements were employed to estimate the relative degree of charge delocalization of PAN samples, which is considered as an additional aim. Furthermore, elucidating the relation between crystallinity of the HCl-doped PAN samples as was investigated previously in Chapter 2 and electrical/dielectrical properties of PAN sample. In addition to explicate the chemical nature of the HCl-doped PAN samples from each synthetic route to understand and clarify the causal connections between reaction conditions and material products for process control over resulting electrical properties. This chapter continues to expand a fundamental understanding in this regard for methodical expansion to other dopants and on-going studies in shielding materials for mitigating EM interference effects on electronic devices.

Chapter 6 begins the comparative study of *p*-toluene sulfonic acid (PTSA) selected as the dopant candidate of an organic source for contrasting results with the inorganic HCl-doped PAN in order to identify the impacts of synthesis approach on the EM shielding potential of the PTSA-doped PAN samples as may be expected on the cases made for HCl-doped PAN in Chapters 2 and 4. Furthermore, two different “unconventional” approaches of solvent-free and solvent-limited will be tested on the PTSA-doped PAN synthesis products against the two excess solvent regimes of fast and slow oxidant addition, or CF and CS. The EM measurements are expected to confirm the proposed electronic structures for charge delocalization in PTSA-doped PAN samples as examined via UV spectroscopy. EM measurements are correlated to the impact of crystal/electronic/conformational structures and conductivity of the prepared PTSA-doped PAN samples on shielding effectiveness (SE)

behavior with frequency. The impact of crystallinity and conductivity obtained from nanopowders made by the variant synthesis approaches will also be elucidated.

Chapter 7 contains a brief section with comprehensive conclusions and summary of the major chapter-conclusions along with an outline of future work, which was planned from the beginning and has evolved through the details of relevant and ongoing research findings toward a continuously improving design of experiments for this dissertation with a larger perspective in mind beyond the scope of the past few years of the present work.

## 1.8. References

- (1) Pozar, D. M. *Microwave Engineering*; Wiley: New York, 1997.
- (2) Zhang, C. S.; Ni, Q. Q.; Fu, S. Y.; Kurashiki, K. Electromagnetic Interference Shielding Effect of Nanocomposites with Carbon Nanotube and Shape Memory Polymer *Compos. Sci. Technol* **2007**, *67*, 2973-2980.
- (3) Tantawy, H. R.; Weakley, A. T.; Aston, D. E. Chemical Effects of a Solvent-Limited Approach to HCl-Doped Polyaniline Nanopowder Synthesis *J. Phys. Chem. C* **2013**, *118*, 1294-1305.
- (4) Tong, X. C. *Advanced Materials and Design for Electromagnetic Interference Shielding*; CRC Press: Boca Raton, 2009.
- (5) Wang, Y.; Jing, X. Intrinsically Conducting Polymers for Electromagnetic Interference Shielding *Polym. Adv. Technol.* **2005**, *16*, 344-351.
- (6) Kim, B. R.; Lee, H. K.; Park, S. H.; Kim, H. K. Electromagnetic Interference Shielding Characteristics and Shielding Effectiveness of Polyaniline-Coated Films *Thin Solid Films* **2011**, *519*, 3492-3496.
- (7) Ramasubramaniam, R.; Chen, J.; Liu, H. Homogeneous Carbon Nanotube/Polymer Composites for Electrical Applications *Appl. Phys. Lett.* **2003**, *83*, 2928-2930.
- (8) Bigg, D. M. Mechanical, Thermal, and Electrical Properties of Metal Fiber-Filled Polymer Composites *Polym. Eng. Sci.* **1979**, *19*, 1188-1192.
- (9) Wenderoth, K.; Petermann, J.; Kruse, K. D.; ter Haseborg, J. L.; Krieger, W. Synergism on Electromagnetic Inductance (Emi)-Shielding in Metal-and Ferroelectric-Particle Filled Polymers *Polym. Compos.* **1989**, *10*, 52-56.

- (10) Crossman, R. A. Conductive Composites Past, Present, and Future *Polym. Eng. Sci.* **1985**, *25*, 507-513.
- (11) Kortschot, M. T.; Woodhams, R. T. Electromagnetic Interference Shielding with Nickel-Coated Mica Composites *Polym. Compos.* **1985**, *6*, 296-303.
- (12) Saini, P.; Choudhary, V. Structural Details, Electrical Properties, and Electromagnetic Interference Shielding Response of Processable Copolymers of Aniline *J. Mater. Sci.* **2013**, *48*, 797-804.
- (13) Azadmanjiri, J.; Hojati-Talemi, P.; Simon, G. P.; Suzuki, K.; Selomulya, C. Synthesis and Electromagnetic Interference Shielding Properties of Iron Oxide/Polypyrrole Nanocomposites *Polym. Eng. Sci.* **2011**, *51*, 247-253.
- (14) Duan, Y.; Shunhua, L.; Hongtao, G. Investigation of Electrical Conductivity and Electromagnetic Shielding Effectiveness of Polyaniline Composite *STAM* **2005**, *6*, 513-518.
- (15) Wilson, J. L.; Poddar, P.; Frey, N. A.; Srikanth, H.; Mohamed, K.; Harmon, J. P.; Kotha, S.; Wachsmuth, J. Synthesis and Magnetic Properties of Polymer Nanocomposites with Embedded Iron Nanoparticles *J. Appl. Phys.* **2004**, *95*, 1439-1443.
- (16) Guo, X.; Deng, Y.; Gu, D.; Che, R.; Zhao, D. Synthesis and Microwave Absorption of Uniform Hematite Nanoparticles and Their Core-Shell Mesoporous Silica Nanocomposites *J. Mater. Chem.* **2009**, *19*, 6706-6712.
- (17) Singh, K.; Ohlan, A.; Pham, V. H.; Balasubramanian, R.; Varshney, S.; Jang, J.; Hur, S. H.; Choi, W. M.; Kumar, M.; Dhawan, S. Nanostructured Graphene/Fe<sub>3</sub>O<sub>4</sub>

- Incorporated Polyaniline as a High Performance Shield against Electromagnetic Pollution *Nanoscale* **2013**, *5*, 2411-2420.
- (18) Wang, W.; Gumfekar, S. P.; Jiao, Q.; Zhao, B. Ferrite-Grafted Polyaniline Nanofibers as Electromagnetic Shielding Materials *Journal of Materials Chemistry C* **2013**, *1*, 2851-2859.
- (19) Wang, C. P.; Li, C. H.; Bi, H.; Li, J. C.; Zhang, H.; Xie, A. J.; Shen, Y. H. Novel One-Dimensional Polyaniline/Ni<sub>0.5</sub>Zn<sub>0.5</sub>Fe<sub>2</sub>O<sub>4</sub> Hybrid Nanostructure: Synthesis, Magnetic, and Electromagnetic Wave Absorption Properties *Journal of Nanoparticle Research* **2014**, *16*, 1-11.
- (20) Huang, J.; Li, Q.; Li, D.; Wang, Y.; Dong, L.; Xie, H.; Wang, J.; Xiong, C. Fluxible Nanoclusters of Fe<sub>3</sub>O<sub>4</sub> Nanocrystal-Embedded Polyaniline by Macromolecule-Induced Self-Assembly *Langmuir* **2013**, *29*, 10223-10228.
- (21) Tadjarodi, A.; Kerdari, H.; Imani, M. Ba<sub>0.69</sub>Sr<sub>0.17</sub>Cd<sub>0.07</sub>Zn<sub>0.07</sub>Fe<sub>12</sub>O<sub>19</sub> Nanostructures/Conducting Polyaniline Nanocomposites; Synthesis, Characterization and Microwave Absorption Performance *Journal of Alloys and Compounds* **2013**, *554*, 284-292.
- (22) Singh, A. P.; Mishra, M.; Sambyal, P.; Gupta, B. K.; Singh, B. P.; Chandra, A.; Dhawan, S. K. Encapsulation of [Gamma]-Fe<sub>2</sub>O<sub>3</sub> Decorated Reduced Graphene Oxide in Polyaniline Core-Shell Tubes as an Exceptional Tracker for Electromagnetic Environmental Pollution *Journal of Materials Chemistry A* **2014**, *2*, 3581-3593.
- (23) Varshney, S.; Ohlan, A.; Jain, V. K.; Dutta, V. P.; Dhawan, S. K. Synthesis of Ferrofluid Based Nanoarchitected Polypyrrole Composites and Its Application for Electromagnetic Shielding *Mater. Chem. Phys.* **2014**, *143*, 806-813.

- (24) Ahmad, H. Magnetic Polyaniline Composites: Recent Developments in Preparation, Properties and Applications *Journal of Colloid Science and Biotechnology* **2013**, *2*, 155-170.
- (25) Ahmad, H.; Kumar, K.; Rahman, M. A.; Rahman, M. M.; Miah, M. A. J.; Minami, H.; Nuri, M. A. Preparation and Characterization of Conducting Polyaniline Layered Magnetic Nano Composite Polymer Particles *Polym. Adv. Technol.* **2013**, *24*, 740-746.
- (26) Wang, C.; Shen, Y.; Wang, X.; Zhang, H.; Xie, A. Synthesis of Novel NiZn-Ferrite/Polyaniline Nanocomposites and Their Microwave Absorption Properties *Materials Science in Semiconductor Processing* **2013**, *16*, 77-82.
- (27) Zhu, Y. F.; Ni, Q. Q.; Fu, Y. Q.; Natsuki, T. Synthesis and Microwave Absorption Properties of Electromagnetic Functionalized Fe<sub>3</sub>O<sub>4</sub>-Polyaniline Hollow Sphere Nanocomposites Produced by Electrostatic Self-Assembly *Journal of Nanoparticle Research* **2013**, *15*, 1-11.
- (28) Turcu, R.; Nan, A.; Craciunescu, I.; Liebsher, J.; Pana, O.; Bica, D.; Vekas, L.; Mijangos, C. Comparative Study of Hybrid Nanostructures of Polymer-Magnetic Nanoparticles *J. Optoelectron. Adv. M.* **2008**, *10*, 2237-2243.
- (29) Weston, D. A. *Electromagnetic Compatibility : Principles and Applications*; Marcel Dekker: New York, NY 2001.
- (30) Geetha, S.; Rao, C. R. K.; Vijayan, M.; Trivedi, D. C.; Kumar, K. K. S. EMI Shielding: Methods and Materials - a Review *J. Appl. Polym. Sci.* **2009**, *112*, 2073-2086.
- (31) Cao, G. *Nanostructures and Nanomaterials: Synthesis, Properties, and Applications*; Imperial College Press 2004

- (32) Frickel, N.; Gottlieb, M.; Schmidt, A. M. Hybrid Nanocomposites Based on Superparamagnetic and Ferromagnetic Particles: A Comparison of Their Magnetic and Dielectric Properties *Polymer* **2011**, *52*, 1781-1787.
- (33) Wan, M. *Conducting Polymers with Micro or Nanometer Structure*; Tsinghua University Press ; Springer: Beijing; Berlin, 2008.
- (34) Park, M. K.; Onishi, K.; Locklin, J.; Caruso, F.; Advincula, R. C. Self-Assembly and Characterization of Polyaniline and Sulfonated Polystyrene Multilayer-Coated Colloidal Particles and Hollow Shells *Langmuir* **2003**, *19*, 8550-8554.
- (35) Wang, Z.; Yuan, J.; Han, D.; Niu, L.; Ivaska, A. One-Step Synthesis of Gold-Polyaniline Core-Shell Particles *Nanotechnology* **2007**, *18*, 115610.
- (36) Lahav, M.; Weiss, E. A.; Xu, Q.; Whitesides, G. M. Core-Shell and Segmented Polymer-Metal Composite Nanostructures *Nano letters* **2006**, *6*, 2166-2171.
- (37) Zhang, W.; Wen, X.; Yang, S. Synthesis and Characterization of Uniform Arrays of Copper Sulfide Nanorods Coated with Nanolayers of Polypyrrole *Langmuir* **2003**, *19*, 4420-4426.
- (38) Li, X.; Wan, M.; Wei, Y.; Shen, J.; Chen, Z. Electromagnetic Functionalized and Core-Shell Micro/Nanostructured Polypyrrole Composites *J. Phys. Chem. B* **2006**, *110*, 14623-14626.
- (39) Dhawan, S. K.; Ohlan, A.; Singh, K. Designing of Nano Composites of Conducting Polymers for EMI Shielding *Advances in Nanocomposites-Synthesis, InTech, Characterization and Industrial Applications, Rijeka (Croatia)* **2011**, 429-482.
- (40) Wan, M.; Li, J.; Li, S. Microtubules of Polyaniline as New Microwave Absorbent Materials *Polym. Adv. Technol.* **2001**, *12*, 651-657.

- (41) Khan, I. A.; Raghavendra, S. C.; Kulkarni, A. B. Polyester-Based Chiral Materials for Microwave Absorption Applications *Int.J.Electron.* **2003**, *90*, 159-166.
- (42) Sun, G. C.; Yao, K. L.; Liao, H. X.; Niu, Z. C.; Liu, Z. L. Microwave Absorption Characteristics of Chiral Materials with Fe<sub>3</sub>O<sub>4</sub>-Polyaniline Composite Matrix *Int.J.Electron.* **2000**, *87*, 735-740.
- (43) Wan, M. A. Template-Free Method Towards Conducting Polymer Nanostructures *Adv. Mater.* **2008**, *20*, 2926-2932.
- (44) Camargo, P. H. C.; Satyanarayana, K. G.; Wypych, F. Nanocomposites: Synthesis, Structure, Properties and New Application Opportunities *J. Mater. Res* **2009**, *12*, 1-39.
- (45) Zhong, W.; Liu, P.; Shi, H. G.; Xue, D. S. Ferroferric Oxide/Polystyrene (Fe<sub>3</sub>O<sub>4</sub>/Ps) Superparamagnetic Nanocomposite Via Facile in Situ Bulk Radical Polymerization *Express Polym. Lett.* **2010**, *4*, 183.
- (46) Besco, S.; Lorenzetti, A.; Roso, M.; Modesti, M. Pa66/Pa12/Clay Based Nanocomposites: Structure and Thermal Properties *Polym. Adv. Technol.* **2011**, *22*, 1518-1528.
- (47) Mavinakuli, P.; Wei, S.; Wang, Q.; Karki, A. B.; Dhage, S.; Wang, Z.; Young, D. P.; Guo, Z. Polypyrrole/Silicon Carbide Nanocomposites with Tunable Electrical Conductivity *J. Phys. Chem. C* **2010**, *114*, 3874-3882.
- (48) Basavaraja, C.; Jo, E.; Huh, D. S. Characterization and Magnetic Properties of Conducting Poly (N-Vinylcarbazole)-Capped Magnetite Nanocomposite Langmuir-Schaefer Films *Mater. Lett.* **2010**, *64*, 762-764.
- (49) Giri, A. K.; Chowdary, K. M.; Majetich, S. Ac Magnetic Properties of Compacted Fe Co Nanocomposites *Materials Physics and Mechanics (Russia)* **2000**, *1*, 1-10.

- (50) Chen , L. F.; Ong, C. K.; Neo, C. P.; Varadan , V. V.; Varadan, V. K. *Microwave Electronics: Measurement and Materials Characterization*; John Wiley& Sons, Ltd 2004
- (51) Zhou, C. F.; Du, X. S.; Mai, Y. W.; Liu, Z.; Ringer, S. P. Solid Phase Mechanochemical Synthesis of Polyaniline Branched Nanofibers *Synt. Met.* **2009**, *159*, 1302-1307.
- (52) Bekri-Abbes, I.; Srasra, E. Investigation of Structure and Conductivity Properties of Polyaniline Synthesized by Solid–Solid Reaction *J Polym Res* **2011**, *18*, 659-665.
- (53) Abdiryim, T.; Xiao-Gang, Z.; Jamal, R. Comparative Studies of Solid-State Synthesized Polyaniline Doped with Inorganic Acids *Mater. Chem. Phys.* **2005**, *90*, 367-372.
- (54) Du, X. S.; Zhou, C. F.; Wang, G. T.; Mai, Y. W. Novel Solid-State and Template-Free Synthesis of Branched Polyaniline Nanofibers *Chem. Mater.* **2008**, *20*, 3806-3808.
- (55) Abdiryim, T.; Jamal, R.; Nurulla, I. Doping Effect of Organic Sulphonic Acids on the Solid-State Synthesized Polyaniline *J. Appl. Polym. Sci.* **2007**, *105*, 576-584.
- (56) Ding, Y.; Abdiryim, T.; An, S.; Nurulla, I. Effect of B-Cyclodextrin on the Solid-State Synthesized Polyaniline Doped with Hydrochloric Acid *J. Appl. Polym. Sci.* **2008**, *107*, 3864-3870.
- (57) Huang, J.; Moore, J. A.; Acquaye, J. H.; Kaner, R. B. Mechanochemical Route to the Conducting Polymer Polyaniline *Macromolecules* **2004**, *38*, 317-321.

## CHAPTER 2

# A Comparison of Electromagnetic Shielding with Polyaniline Nanopowders Produced in Solvent-limited Conditions

### 2.1 Introduction

The proliferation of electronic devices in the world has caused electromagnetic interference (EMI) to become a vital concern. Although all electronics emit magnetic and electrical energy, if this energy unintentionally interacts with another device and causes it to malfunction, then it is considered interference.<sup>1</sup> In fact, EMI has become a serious dilemma impacting almost all contemporary electrical and electronic systems from daily life to space exploration.<sup>2</sup> A device is considered electromagnetically compatible—having low EMI with its surroundings—if it does not interfere with other devices or itself and it is not affected by emissions from other devices.<sup>3</sup> Therefore, good shielding materials should prevent both incoming and outgoing EMI. Its shielding effectiveness (SE), expressed in decibel (dB) units, is considered adequate for many applications at roughly 30 dB, corresponding to 99.9% attenuation of the EMI radiation.<sup>4</sup> The standard requirements for any application are specific to frequency range and geometry.

Various shielding methods have been developed not only to reduce the probability of EMI occurrence but also to increase device lifetime and efficiency.<sup>1</sup> Traditional approaches to EMI shielding rely on the use of metallic materials, which generally provide excellent SE. However, conventional metallic shields impose severe weight penalties, especially for aerospace applications.<sup>5</sup> Intrinsically conducting polymers (ICPs) are more attractive materials due to

their light weight, versatility, low cost and processability.<sup>6</sup> ICPs have relatively high conductivities ( $\sigma$ ) and dielectric constants ( $\epsilon_r$ ) that are easy to control or design through chemical processing.<sup>7</sup> Moreover, ICPs have significant EMI shielding through absorption that also improves shielding against potential internal EMI, which differs from the dominant metal and carbon-based shielding mechanism of reflection.<sup>8</sup> Among the host of ICPs is polyaniline (PANI), regarded as a promising conductive polymer due to superior conductivity control through doping with relatively easy polymerization of large quantities and its other electromagnetic parameters being flexibly adjustable through both oxidation and protonation states.<sup>5,9,10</sup>

Typically, PANI can be made chemically or electrochemically by oxidative polymerization of aniline.<sup>11</sup> Electrochemical methods have the merit of easier control over morphology and electrical properties but difficulty in mass production. Chemical methods are generally more effective for commercial-scale mass production.<sup>12,13</sup> The conventional chemical synthesis of PANI is based on mixing aniline with an oxidant in aqueous, or nonaqueous, acidic media.<sup>10,14</sup>

Recently, attention has been paid to the preparation of doped-PANI via solvent-free reaction approaches accomplished in a solid state.<sup>15-21</sup> This has obvious advantages by eliminating the solvent costs and complications associated therein, including separation, recovery, reuse and proper waste treatment as well as reducing the overall volume and mass per final product quantity. Furthermore, a solvent-free reaction is the more environmentally benign method.<sup>16</sup> However, the EM properties of solvent-free PANI and their controllability remain largely unstudied, and the electromagnetic shielding potential of PANI nanoparticles or nanopowders synthesized by a solvent-free reaction is not evident in available literature.

The present study details the physico-chemical characteristics of PANI doped with HCl synthesized via a wetted solid state polymerization under mechanical grinding, referred to as a “solvent free” protocol (SF), compared with two conventional chemical approaches for both fast (CF) and slow (CS) oxidation conditions in aqueous solutions of ammonium peroxydisulfate (APS)—the same oxidizing agent used in the solvent-free route—evolving into lyophobic colloidal suspensions. After careful determination of chemical and morphological structures through analysis of Fourier transform-infrared (FTIR) spectra, x-ray diffraction (XRD), and transmission electron microscopy (TEM), the three nanopowders as compressed disks and annuli are tested for conductivity (DC) and electromagnetic wave propagation, respectively, in order to correlate nanomaterial properties with bulk behaviors relevant for EMI shielding. The first comparison of shielding effectiveness (SE) is made on a basis of mass loadings required per area of shielding material to be used within the microwave X-band frequency range (8–12 GHz) for the three conducting nanopowders. This type of synthetic, analytic, applications-oriented process sequence is crucial for the future advancement of affordable, light-weight EMI shielding formulations with these types of nanopowders as filler components in polymer or ceramic matrices, such as for coatings, films, sheets, and paints.

## **2.2 Theory of Electromagnetic Interference Shielding**

Shielding effectiveness (SE) is the ratio of residual energy to impinging energy, usually equivalent to the total electromagnetic (EM) radiation transmitted (subscript  $T$ ) through the shielding divided by the incident (subscript  $i$ ) wave. This can be calculated from any of the energy intensities: electric (E), magnetic (H), electromagnetic power (P):<sup>2,22</sup>

$$SE = -20\log\left(\frac{E_T}{E_i}\right) = -20\log\left(\frac{H_T}{H_i}\right) = -10\log\left(\frac{P_T}{P_i}\right).$$

The EMI attenuation is dependent on frequency, distance between shield and interfering source, shield thickness, and of particular interest, shield material. SE is normally expressed in decibels (dB).<sup>2</sup>

There are three primary EM/material interaction mechanisms contributing to SE. Part of the incident radiation is reflected from the front surface of the shield, part is absorbed within the shield material, and part is reflected from the rear surface to the front where it can either aid or hinder the effectiveness of the shield depending on its phase relationship with the incident wave, as shown in Figure 2.1. Therefore, the total effectiveness of a shielding material ( $SE_{Total}$ ) equals the sum of the absorption losses ( $SE_A$ ), the reflection losses ( $SE_R$ ), and a correction factor ( $M$ ) to account for multiple reflections, which may be significant in thin shields:<sup>23</sup>

$$SE_{Total} = SE_A + SE_R + M.$$

The multiple reflection factor  $M$  is usually neglected where the absorption loss is greater than 10 dB. For simplified calculations, it may be neglected for electric fields and plane waves. Furthermore, absorption losses are a function of the physical characteristics of the shield and are independent of source field type.<sup>2</sup> The absorption, or decay, loss occurs because currents induced in the medium produce ohmic losses and heating of the material.<sup>1</sup> On the other hand, the reflection loss is related to the relative mismatch between the incident wave and the surface impedance of the shield. Moreover, multiple reflection correction factors can be mathematically positive or negative (in practice, it is always negative) and become insignificant when  $SE_A > 6$  dB. It is usually only important at low frequencies (i.e., below approximately 20

kHz)<sup>2</sup> after therefore of insignificant impact to the present study concerning the microwave X-band.

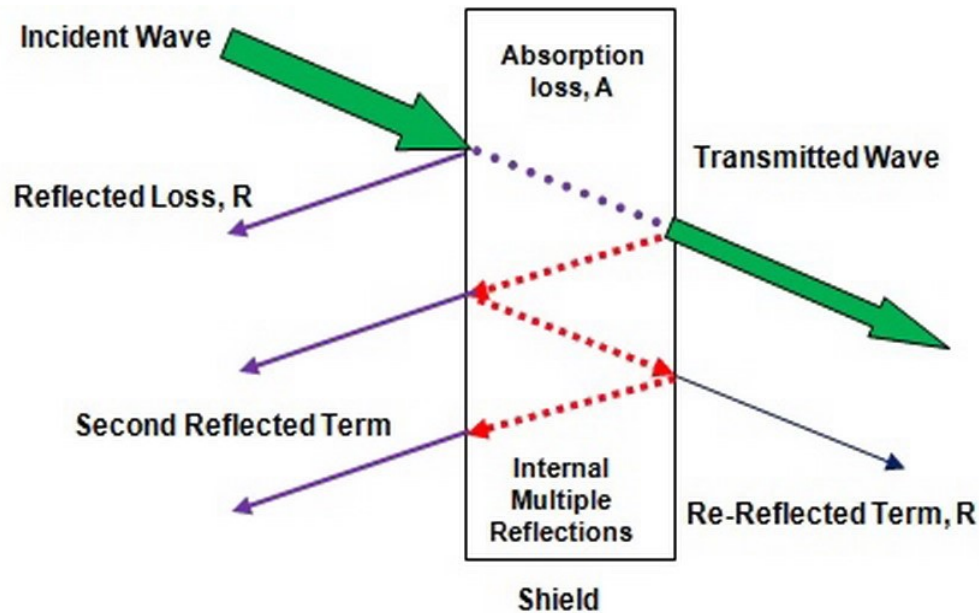


**Figure 2.1** Attenuation schematic of an electromagnetic wave by shielding material.

In a two-port network analysis, EMI SE can be expressed in terms of scattering parameters that quantify the way currents and voltages travel in a transmission line when encountering a discontinuity caused by differing impedances between air and the obstruction or in the dielectric media.<sup>24</sup> In a waveguide, a radiated wave undergoes shielding (reflection, absorption, and transmission) when the incident wave at a point  $i$  passes toward another point  $j$ , and these wave scattering values are expressed as  $S_{ji}$ . For example,  $S_{21}$  is the energy acquisition at point 2 having originated from point 1. Therefore, the scattering parameters  $S_{11}$  and  $S_{21}$  designate the amount of reflected energy and transmitted energy, respectively. In order to investigate the contributions of absorption and reflection to the total EMI SE, the transmittance

( $T_{coef}$ ), reflectance ( $R_{coef}$ ), and absorbance ( $A_{coef}$ ) coefficients can be correlated to  $S$  parameters as follows:<sup>25</sup>

$$T_{coef} = \left[ \frac{E_T}{E_i} \right]^2 = S_{12}^2 = S_{21}^2,$$

$$R_{coef} = \left[ \frac{E_R}{E_i} \right]^2 = S_{11}^2 = S_{22}^2,$$

$$A_{coef} = 1 - T_{coef} - R_{coef}.$$

Here, the term  $A_{coef}$  is given with respect to the power of the incident EM wave. If the effect of multiple reflections between both interfaces of the material is negligible,<sup>26</sup> the relative intensity of the effectively incident EM wave inside the shielding layer after reflection is based on the value of  $(1 - R_{coef})$ . Therefore, the effective absorbance can be described as follows:

$$A_{eff} = \frac{1 - T_{coef} - R_{coef}}{1 - R_{coef}}.$$

Hence, by applying the power balance data,  $SE_R$  and  $SE_A$  can be expressed in terms of transmittance and reflectance, respectively:<sup>27</sup>

$$SE_R = 10 \log(1 - R_{coef}),$$

$$SE_A = 10 \log(1 - A_{coef}) = 10 \log\left(\frac{T_{coef}}{1 - R_{coef}}\right),$$

$$\therefore SE_T = 10 \log\left(\frac{T_{coef}}{1 - R_{coef}}\right) + 10 \log(1 - R_{coef}).$$

## 2.3 Materials and Methods

Batches of HCl-doped polyaniline nanoparticles were produced from three different synthesis protocols to make approximately 5 grams of recovered product per batch using aniline

(99.5%, ACS reagent grade, Aldrich) purified by distillation with zinc dust before use.<sup>21,28</sup> The inorganic acid dopant hydrochloric acid (37.43%, ACS reagent grade, EMD Chemicals) and the oxidant ammonium peroxydisulfate (98%, ACS reagent grade, Aldrich) were used as received. Ammonium peroxydisulfate (APS) was selected from a wide array of potential chemical oxidants based on a summative assessment of the relevant literature indicating generally higher polymer conductivities from APS than others, in conjunction with being a common and affordable chemical.

HCl-doped polyaniline (PAN) nanoparticle samples were prepared by solvent-free (SF) and conventional (solvent-based) chemical oxidations under slow (CS) and fast (CF) production rates as controlled by the addition of aqueous ammonium peroxydisulfate (APS), both described below in detail. All reaction protocols are designed for an targeted 50% level of dopant, which is expected to maximize conductivity in the products, where amine site protonation occurs above 50% and imine sites deprotonate below 50%.<sup>12</sup> However, the precise level of doping achieved is not easily determined and may be an additional source of uncertainty in interpreting physico-chemical behavior. Since all three protocols involve the same constituents, only varying the methods of mixing, an operating hypothesis for similar chemical mechanism(s) producing systematically different product yields is reasonable. In the solvent-free extreme case, local reactant concentrations are maximized, compared to the much more dilute and uniform reaction conditions of the two conventional processes.

Polyaniline doped with HCl is reported to be quite stable regarding thermal and environmental stability.<sup>15-16,22</sup> It should be noted for safety precautions that benzidine is a well-known carcinogen and intermediate product of the electrochemical mechanism for preparing polyaniline, though it is highly susceptible to copolymerization and does not persist in detectible

amounts under final reaction conditions with APS. This is perhaps an important, secondary motivation for avoiding electrochemical methods to alleviate any environmental and health concerns; however, this topic deserves continued awareness and vigilance in the laboratory, for waste management, and potential future technology developments.

### **2.3.1. Solvent-free (SF) Synthesis**

It should be first noted that the “solvent-free” label refers to the aniline monomer and oxidant (APS) being used in their as-prepared and as-received states without first dissolving them in a reaction medium (solvent), though certainly the SF reaction chemicals are not completely void of solvent since the dopant (HCl) is applied from the standard aqueous concentrate. A typical solvent-free polymerization procedure at room temperature (~18–24°C) was followed with freshly distilled aniline (0.05 mole per batch) poured into a porcelain mortar, and then 0.1 mole of the doping acid, i.e., concentrated HCl was added dropwise while grinding manually for 10 min. The acid was added in very small dropwise portions in order to minimize the released fumes and prevent the overheating of the reaction medium since aniline reacts violently with strong acids.<sup>29</sup> The reactant mixture became a white paste after grinding.

Separate grinding of 0.05 mole of APS in another porcelain mortar produced a fine powder, which was subsequently added in small portions to the white paste reactant in order to avoid overheating from the highly exothermic oxidative polymerization.<sup>30,31</sup> Approximately 0.5 g of APS was added in between grinding the reactant mixture for ~1-2 min in cycles until the entire batch was uniformly ground and finally attained the appropriate dark green color indicative of the HCl-doped PAN nanoparticles. This product was transferred to a 2-liter beaker where 100 ml of acetone, 100 ml of ethanol and 800 ml of DI were added then mixed

for 1 h in order to quench the polymerization reaction and to dissolve oligomeric impurities.<sup>32-</sup>

<sup>34</sup> An excess volume of water was used to assure a thorough washing for materials analysis.

A 5- $\mu$ l sample of the mixture was taken and diluted with 10 ml of ethanol for morphological characterization. The rest of the product mixture was filtered and washed with acetone, ethanol, and distilled water, in series, until the initially brown filtrate became colorless in order to confirm the adequate removal of unreacted chemicals and excess acid.<sup>35,36</sup> Less than 500 mL of DI water was typically required for washing. A slower soaking process produced similar results with only 100 mL acetone, 200 mL ethanol and 100 mL DI water. It is likely that ethanol and acetone requirements may be further reduced through future optimizations for practical materials applications for combined quenching and washing. The powder was dried at 40°C for 48 h.

While typical molecular weights for polyaniline prepared by chemical oxidation can be expected of 30,000 g/mol,<sup>37</sup> it will be very important for future work to consider a comparative molecular-weight distribution study of the solvent-free products against the conventional products of the present study.

### **2.3.2. Conventional Chemical Synthesis: Fast (CF) and Slow (CS) Oxidations**

The same freshly distilled aniline in 0.05-mole doses was dissolved in 1000 ml of DI water followed by dropwise addition of 0.1 mole of HCl concentrate with mixing on a magnetic stirrer (1000 rpm) for 15 min. Then 0.05 mole of APS dissolved in 50 ml of DI was added. In case of conventional chemical oxidation with fast reaction (CF), the oxidizing APS solution was added all at once. On the other hand, the slow reaction procedure (CS) added the same APS solution amount with constant rate 0.1 ml/min. Both reaction protocols were conducted at room temperature (~18–24°C). The reaction mixtures were mixed for 12 h after APS

addition. Then 100 ml of acetone and 100 ml of ethanol were added and mixed for 1 h, similar to the SF samples above except that no additional DI water is needed for the conventional solvent-rich synthesis.<sup>32-34</sup> As before, 5- $\mu$ l samples of these mixtures were also taken and diluted with 10 ml of ethanol for comparative morphological characterizations with the SF samples. The remaining products were filtered, washed, and dried identically to the SF samples. However, it must be noted that these conventional chemical synthesis products required in excess of three liters of DI water per batch to wash at the same level of filtrate clarity as the solvent-free product, as well as 500 mL ethanol and 300 mL acetone with clear room for process optimization.

## **2.4. Characterization Methods**

### **2.4.1. Chemical: FTIR**

The doped PAN samples as dry powders were characterized for chemical constituencies with a ThermoNicolet Avatar 370 FTIR spectrometer equipped with an attenuated total reflectance (ATR) attachment. The 16 spectra for each sample type were collected between 1800  $\text{cm}^{-1}$  and 650  $\text{cm}^{-1}$  at a resolution of 4.0  $\text{cm}^{-1}$  and averaged.

### **2.4.2. Morphological: TEM**

Morphological characterization was carried out by transmission electron microscopy (TEM-JEOL JEM 2010) operating 200 kV. A drop of diluted suspension of each sample was applied to a copper grid coated with carbon film (FCF-150-Cu).

### **2.4.3. Crystallinity: XRD**

A Siemens D5000 powder X-ray diffractometer was used for XRD characterization using a copper target (Cu  $K\alpha$  and wavelength ( $\lambda$ ) of 0.15418 nm. Data were collected in the range

of  $2\theta = 10^\circ$  to  $60^\circ$  at a resolution of  $0.02^\circ$  per step with a 1-s integration time per step. The crystallinity of the PAN nanostructures were calculated by “DIFFRACplus EVA” software and obtained as the crystalline area divided by the sum of crystalline and amorphous areas.<sup>33</sup>

The  $d$ -spacings were deduced from the angular position ( $2\theta$ ) of the observed peaks according to the Bragg formula:<sup>38</sup>  $\lambda = 2d\sin\theta$ . The crystalline domain size, or the extent of order  $L$ , of the highest intensity crystallite peak was estimated using the Scherrer formula:<sup>33</sup>  $L = k\lambda/(\beta\cos\theta)$ , where  $k$  is the shape factor for the average crystallite ( $\approx 0.9$ ), and  $\beta$  is the peak’s full width at half-maximum (FWHM) in radians.<sup>39</sup> The inter-chain separation length ( $R$ ), corresponding to the most intense crystallite peak of Bragg diffraction patterns from the PAN samples, was determined from the relation given by Klug and Alexander:<sup>40</sup>  $R = 5\lambda/(8\sin\theta)$ .

#### 2.4.4. Electrical Conductivity

Electrical conductivity of the samples was measured at room temperature on pressed pellets by a two-point probe technique.<sup>17,41,42</sup> Typically, 0.1-g samples were pelletized at 70 MPa for 3 min using a hydraulic press.<sup>43</sup> The obtained pellet dimensions were 13-mm diameter and 1-mm thickness. Three pellets were prepared for each sample. Current-voltage (I-V) measurements were carried out via a Keithley 4200 SCS semiconductor parameter analyzer. Dual sweep mode was operated within a voltage range -1 to 1 V, and 0.01 V stepwise. Five physical locations were measured on each pellet side to confirm consistency within each sample: one location at the center of the pellet and four others nearer the edge in the four adjacent quadrants. Each I-V measurement was repeated five times at least for every location for reproducibility confirmation. The values reported are averaged over 25 readings for each sample.

### 2.4.5. Electromagnetic Shielding

Electromagnetic shielding measurements used an Agilent E8363A PNA vector network analyzer in the X-band (8.2–12.4 GHz). Two open-ended waveguides filled with Teflon at the waveguide end and the sample holder were employed (Figures 2.2 and 2.3).<sup>44</sup> The dimension of the cross-section of the waveguide and the sample holder is 22.86 mm × 10.16 mm.<sup>23</sup> The length of the sample holder is 7 mm. As shown in Figure 2.2 the sample holder was filled with the PAN nanoparticle samples of known masses to specified depths by manual compaction for consistent density between replicates with excellent reproducibility due to careful measurements described below. No matrix material was added. The holder is inserted into the two waveguides as shown in the EMI waveguide measurement setup (Figure 2.3). In order to quantify the S-parameter accurately using the vector network analyzer, the measurement system was calibrated by the Thru–Reflect–Line (TRL) calibration.<sup>23,44</sup> In order to investigate the EM shielding potential of the HCl-doped PAN nanopowders prepared from different synthetic approaches, seven different mass loadings of each sample type were used: 0.1, 0.15, 0.2, 0.25, 0.3, 0.35 and 0.4 g, corresponding to sample areal concentrations, or areal densities, of 0.04, 0.06, 0.09, 0.11, 0.13, 0.15, and 0.17 g/cm<sup>2</sup>, respectively.

This notation was selected to provide a more direct standard for mass loading comparisons with SE trends, since SE is proportional to the shield thickness and areal density factors out the thickness. The 0.1-g samples were compacted to 1.6 mm sample thickness for the conventional nanopowders (CF and CS) and 0.9 mm for the solvent-free product. Each additional 0.05 g of nanoparticles increased the sample thicknesses by 0.8 mm and 0.5 mm, respectively. Compacting depth was measured to within ±0.05 mm. Each sample was tested for the SE<sub>T</sub> of the HCl-doped PAN at different mass loadings as a function of frequency measured

in the 8–12 GHz range for the purpose of discussing the dependence of  $SE_T$  on absorption and reflection losses and the EM shielding potential as a function of the areal concentration with respect to the synthesis conditions.

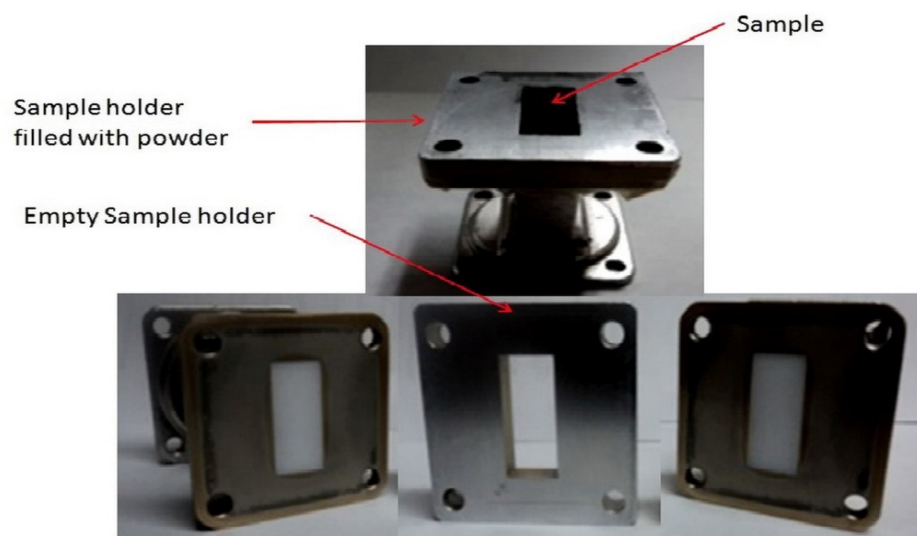


**Figure 2.2.** Waveguide sample holder for X-band measurements performed.

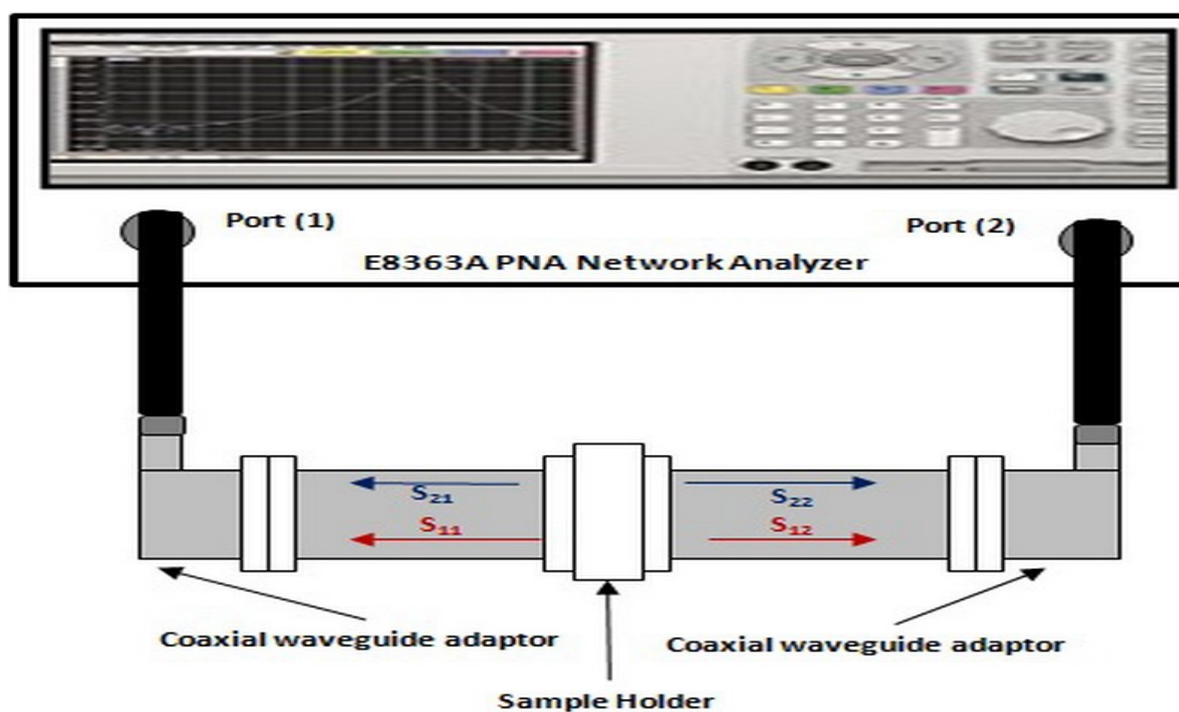


**Figure 2.3.** EMI waveguide measurement setup

## 2.5. Results and Discussion

### 2.5.1. Morphology

TEM micrographs show that fast oxidation of HCl-doped PAN nanoparticles (PAN-HCl-CF) leads to the formation of very regular nano-polygons as well as some irregular spherical nanoparticles (Figure 2.4a). The average particle size is less than 50 nm. There is an obvious contrast with the slow oxidation products (PAN-HCl-CS) giving much larger aggregates with more irregularities to the nano-polygon morphologies and a broad particle size distribution. The largest primary particles typically observed for both CF and CS samples generally do not exceed 50 nm with many more fused clusters in the CS samples. The solvent-free samples (PAN-HCl-SF) consisted of regular nano-polygons and nanospheres with an estimated particle size of 20 nm and less (note the smaller scale in Figure 2.4c from the CF and CS micrographs). It is intriguing that previous studies on solvent-free and solid state synthesis approaches reported nanofibers rather than the nanoparticles produced in this work.<sup>15,18</sup>

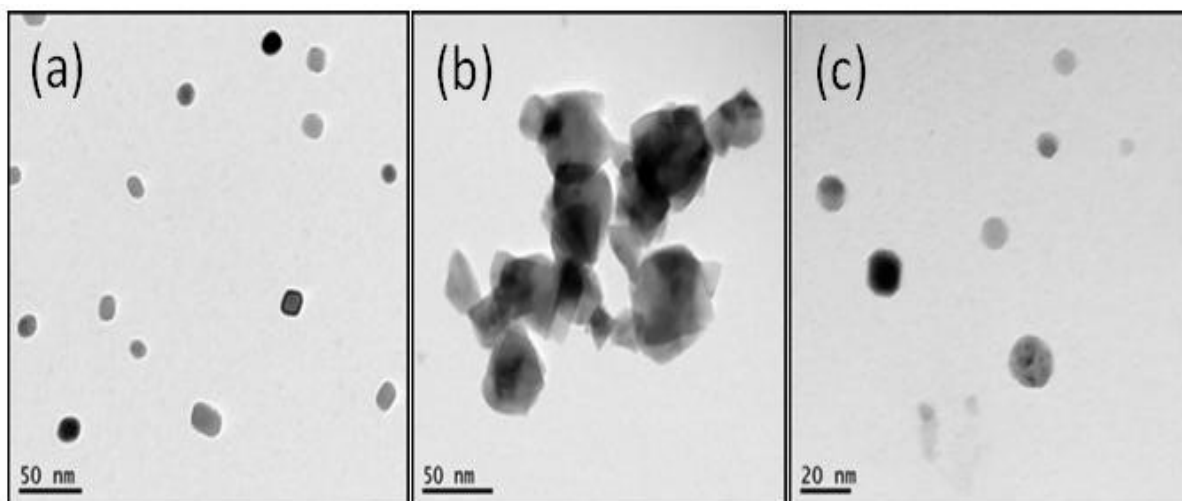


**Figure 2.4.** The TEM images of HCl-doped polyaniline: (a) fast oxidation, (b) slow oxidation, (c) solvent-free formulation. Note scale bars of 50 nm in (a-b) but 20 nm for (c).

### 2.5.2. Current-voltage (I-V) Characterization

The current-voltage (I-V) curves of the HCl-doped PAN samples are shown in Figure 2.5, indicating ohmic behavior in all types at room temperature.<sup>45</sup> All sample types behaved as perfect ohmic conductors with the electrical resistance increasing as follows: SF < CF < CS. The highest conductivity was for SF ( $27.19 \pm 0.26$  S/cm) followed by CF ( $3.28 \pm 0.25$  S/cm) with CS ( $2.94 \pm 0.14$  S/cm) slightly lower. The differences are of course due to the impact of the formulation conditions on the final chemical structure and material crystallinity, which will be discussed later. The experimental values of conventional HCl-doped PAN (CF and CS) fitted within in the range of conductivities previously reported for PAN.<sup>31</sup> However, the nearly order of magnitude increase in conductivity for the SF samples is higher than recently reported.<sup>16,17,21</sup>

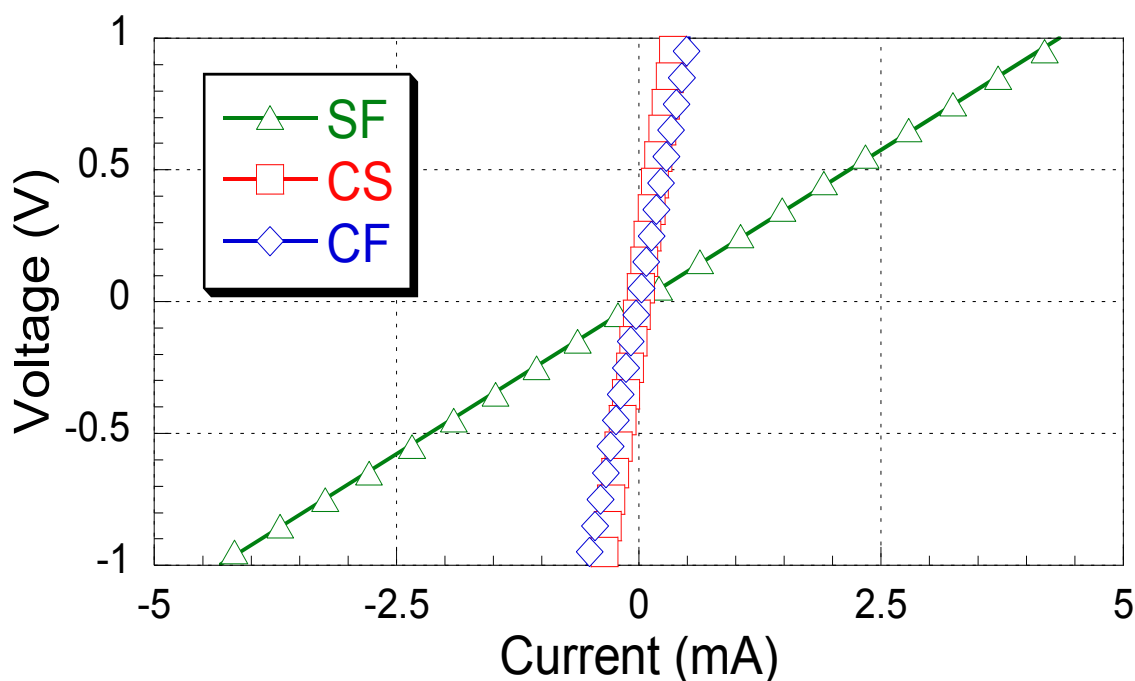


**Figure 2.5.** I-V curves from two-point probe measurements on three polyaniline sample types doped with HCl.

### 2.5.3. Fourier Transform Infrared (FTIR) Spectroscopy Analysis

Representative FTIR spectra of the PAN samples prepared (SF, CF, and CS), are shown in Figure 2.6. The positions of the bands differ only within experimental error from the positions measured by others.<sup>46-49</sup> These previous interpretations of PAN spectra together with corresponding references are summarized in table 1 and associated with the three sample types studied herein.

FTIR spectra are characterized by two major regions I and II. Region I (1100–1700  $\text{cm}^{-1}$ ), in which the C-C and C-N stretching and C-H bending are expected of molecules containing aromatic rings.<sup>48</sup> The pair of bands near 1580  $\text{cm}^{-1}$  and 1490  $\text{cm}^{-1}$  are attributed to C=C stretching of quinonoid (N=Q=N) and benzenoid (N=B=N) ring-stretching vibrations, respectively.<sup>46,50</sup>

Moreover, C-N bending vibration modes are observed near 1295  $\text{cm}^{-1}$  for aromatic amines.<sup>48,51</sup> Furthermore, the bands characteristic of conducting protonated PAN are found at  $\sim 1245 \text{ cm}^{-1}$ , which corresponds to (C-N<sup>+</sup>•) stretching vibration in the polaron structure.<sup>46</sup>

The broad band centered at 1148  $\text{cm}^{-1}$  has been assigned to the vibration mode of the –NH<sup>+</sup>= structure and is associated with the vibrations of the charged polymer units Q=NH<sup>+</sup>–B or B–NH<sup>+</sup>•–B and/or to the aromatic hydrocarbon (C–H) in-plane deformation.<sup>52</sup> The absorption band increases with increasing degree of protonation in the PAN backbone. This band has been related to the high degree of electron delocalization in PAN as well as to strong inter-chain (NH<sup>+</sup>–N) hydrogen bonding.<sup>46,53</sup> The peak located near 1040  $\text{cm}^{-1}$  suggests the presence of sulfonate or bisulfate groups, possibly from the oxidizing agent, attached to the aromatic rings.<sup>46,49,54,55</sup> Alternately, it could be attributed to C–H in-plane bending.<sup>48,49,56</sup>

The PAN-HCl-CS spectrum has two absorption bands of particular interest. The first at  $1445\text{ cm}^{-1}$ , which is attributed to the skeletal (C=C) stretching vibration of substituted aromatic rings,<sup>46,49,54</sup> supports the presence of ortho-coupled and phenazine-like units.<sup>55,57</sup> The second is a weak band at  $1375\text{ cm}^{-1}$ , which is characteristic of standard PAN base material (i.e., undoped) and assigned to C–N stretching in the vicinity of a quinonoid ring,<sup>55,58</sup> also an indication of the existence of phenazine-like structures.<sup>46,57</sup>

Region II ( $<1100\text{ cm}^{-1}$ ), which corresponds to ring deformation,<sup>59</sup> contains the modes related to ring deformations with select C–H out-of-plane vibrations.<sup>48</sup> The observed band near  $820\text{ cm}^{-1}$  is due to the C–H out-of-plane bending vibrations of two adjacent hydrogen atoms on a 1,4-disubstituted benzene ring.<sup>46,48,60</sup>

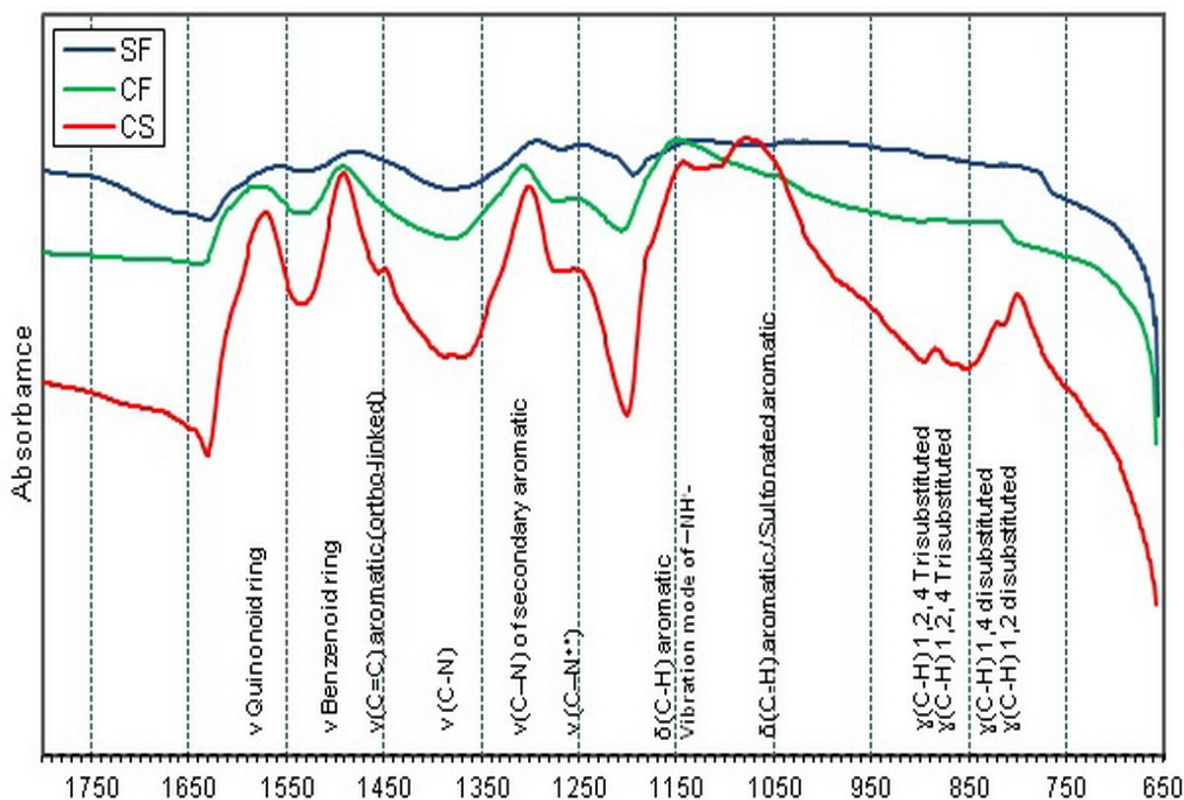


**Figure 2.6.** FTIR spectra (in wavenumbers of  $\text{cm}^{-1}$ ) of HCl-doped polyaniline prepared with different synthesis conditions: SF (top), CF (middle), CS (bottom).

This confirms the dominant para-coupling of constitutional units in the PAN chains. In particular, the PAN-HCl-CS spectrum shows significant amounts of 1,2,4-trisubstituted benzene ring, appearing in bands at  $881\text{ cm}^{-1}$  and  $862\text{ cm}^{-1}$  indicative of the formation of branched and/or substituted phenazine-like segments<sup>54,61</sup> in addition to absorption band at  $796\text{ cm}^{-1}$ , which is attributed to C–H out-of-plane bending vibrations of 1,2-disubstituted benzene ring.<sup>46,49</sup>

**Table 2.1.** The main IR bands for PAN-HCl nanoparticles by synthesis condition.

No.	Wavenumber ( $\text{cm}^{-1}$ )			Assignment	Ref.
	SF	CF	CS		
1	---	---	797	C-H out-of-plane ring bending 1,2-disubstituted	46,49
2	815	823	819	C-H out-of-plane ring bending (1,4 di-substituted ring)	46,48,59,60
3	---	---	862	C–H out-of-plane ring bending (1,2, 4 tri-substituted ring)	50,53,62,63 “
4	---	---	881	“	“
5	1035	1043	1077	C–H in plane bending Sulfonated aromatic ring ( $\text{HSO}_4^-/\text{SO}_2^-$ )	48,49,56 46,49,54,55
6	1121	1147	1140	C–H in plane bending Vibration mode of $-\text{NH}^+$ –	54,64,65
7	1240	1248	1248	C–N Stretching ( $\text{C–N}^{**}$ )	46,53
8	1290	1302	1298	C–N Stretching secondary aromatic amine	46,53,66
9	---	---	1375	C-N Stretching ( $\text{Q=N–B}$ )	46,55,64
10	---	---	1445	C=C aromatic ring or N=N Stretching C=C aromatic ring (ortho-linked)	46 55,57,67
11	1479	1487	1489	Benzenoid (B) ring-stretching	17,31,46,57,64 “
12	1556	1580	1588	Quinonoid (Q) ring-stretching	

Based on the previous data in which the quinonoid and benzenoid units were identified, the intensity ratio of these two absorption bands around  $1580\text{ cm}^{-1}$  and  $1490\text{ cm}^{-1}$  is indicative of the average extent of the oxidation state of the polymer, which reflects the content of the quinoid and benzene ring structures.<sup>59</sup> The intensity ratio  $R$  is calculated as  $I_{\text{quinoid}}$  over  $I_{\text{benzenoid}}$ . Table 2.2 shows that the ordering of  $R$  values is  $\text{SF} > \text{CF} > \text{CS}$ . The results suggest that there is a difference in the extent of oxidation state of the prepared samples depending on the synthesis approach, since the reactants and oxidizer ratios are fixed. The relatively lower oxidation extent in the CS samples could be attributed to its structure, which according to the previous interpretation supports the suggestion of increase in nonlinear chains due to the presence of cross-linking structures from coupling in the ortho- position.<sup>57,67</sup> The CS approach may be favorable for cross-linking and branched PAN allowed by the slower oxidation, which means PAN chains growing with other existing chains, with higher probability of structural defects impacting the electrical and electronic behavior.<sup>57,60</sup>

**Table 2.2.** Absorption intensities and their ratios for PAN-HCl samples.

Synthesis Method	$I_{\text{quinoid}}$	$I_{\text{benzenoid}}$	$R$
CF	0.922	0.957	0.963
CS	0.885	0.948	0.934
SF	0.955	0.980	0.974

#### 2.5.4. XRD characterization

Even though all the three PAN sample types are doped with HCl for the same chemical composition, the XRD patterns show distinct differences between each as shown clearly in Figure 2.7. The similarity between the XRD patterns of the SF and CS samples is relatively

clear with sharper peaks compare to the fast oxidation product (CF), which confirms the presence of high crystallinity and/or ordering in the samples with significant rate-limiting conditions imposed on their reactions. In order to visualize the peaks better and separate the contributions of different crystalline and amorphous constituencies in the XRD pattern, Figures 2.7b–d employ a single-line method using Voigt function.<sup>68,69</sup> The results agree with what has been mentioned in the literature; within  $2\theta$  from  $10^\circ$ – $60^\circ$ , that the three main diffraction peaks of emeraldine salt were resolved. In addition, two weak peaks rise at approximately  $27^\circ$  and  $29^\circ$ , seen in PAN-HCl-CS (Figure 2.7c). The observed  $d$ -spacing of the Bragg reflections are compatible with orthorhombic lattice symmetry.<sup>17,67,70</sup>

Crystalline peaks can be observed near  $15^\circ$  and  $25^\circ$ , which correspond to the (010) and (110) planes of crystalline PAN domains, respectively (table 2.3). An amorphous peak can be seen at  $20^\circ$  that corresponds to the (100) plane<sup>35</sup> and also represents the characteristic distance between the ring planes of benzene in adjacent chains or the close-contact inter-chain distance,<sup>16</sup> while the peaks at  $2\theta = 25^\circ$  may be caused by periodicity perpendicular to the polymer chain. The percentages of crystallinity for each sample type are approximately 54%, 73%, and 66% corresponding to CF, CS, and SF, respectively. The obtained results were the average of three or more XRD measurements. Both SF and CS samples are significantly more crystalline than the CF material.

The high crystallinity of CS could be due to the formation of cross-linking structures from coupling in the ortho- position<sup>67</sup> encouraged by the slow oxidation conditions. In addition, slow exothermic polymerization with no noticeable change in the temperature of the reaction medium is a favorable condition for higher degree of crystallinity<sup>57</sup> compared to CF and SF. The

reason that the SF nanoparticles have higher crystallinity than CF is perhaps due to the formation of its chains under relatively concentrated acidic condition,<sup>17</sup> though it may be difficult to reconcile this with the slow oxidation process at lower local acid concentrations producing the highest crystallinity. Apparently, both slow oxidation and high acidity favor high crystallinity in HCl-doped PAN, supporting the general notion that the degree of crystallinity depends on the synthesis approach.<sup>67</sup>

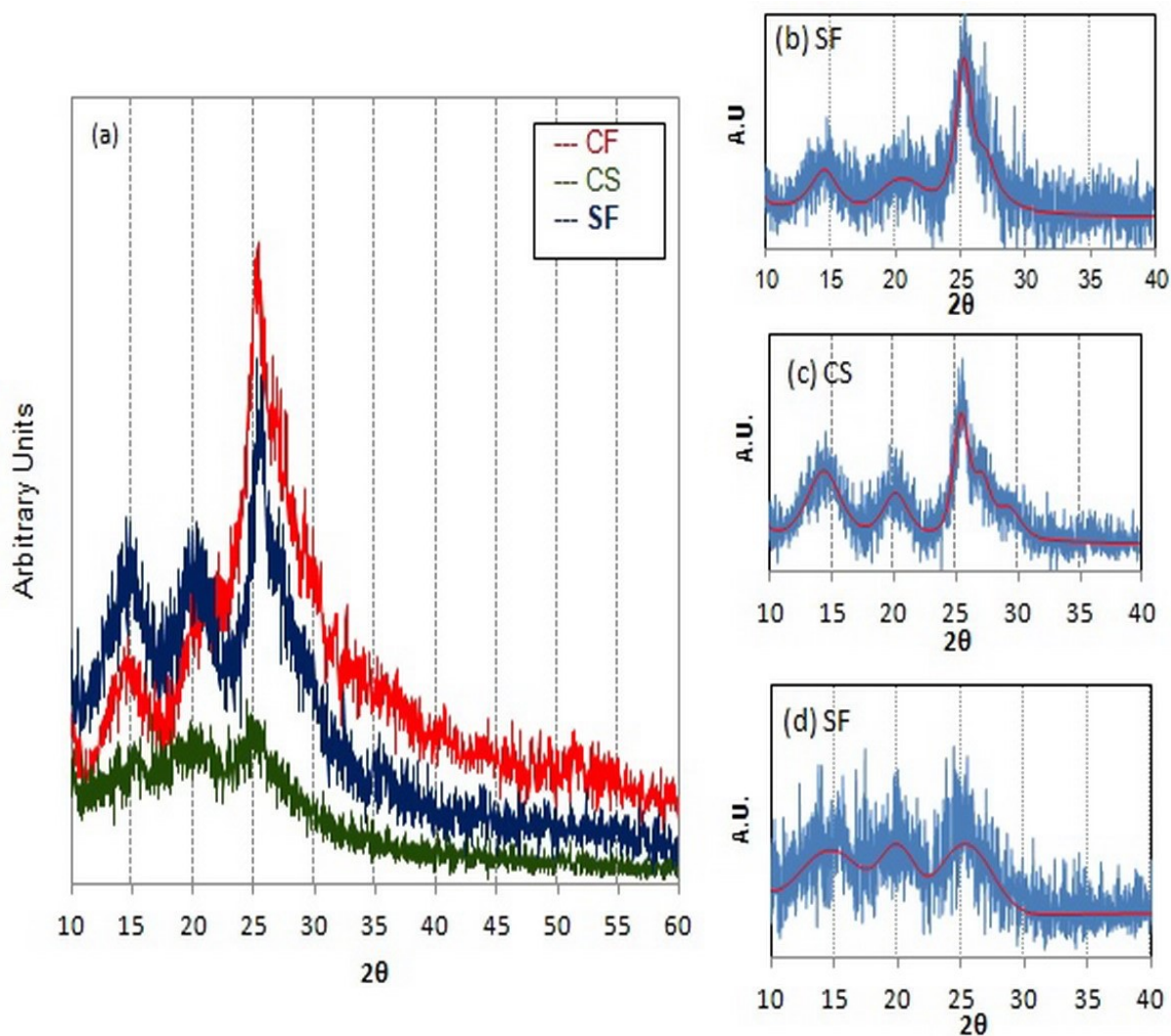


**Figure 2.7.** The XRD patterns of HCl-doped polyaniline nanoparticles from different synthesis.

CF and SF samples consist mainly of linear chains as it was explained from the FTIR discussion. The conventional trends between crystallinity, d-spacing, inter-chain separation, crystalline domain size, and conductivity are clearly observed.<sup>71</sup> The SF samples exhibit larger domain size, shorter d-spacing and inter-chain separation, and higher conductivity than the fast oxidation (CF) product, as might also be expected by differences in linear polymer chain density. The regularity and organized structure defined by crystallinity is a favorable factor mainly for intramolecular mobility of charged species along the chain and to some extent intermolecular hopping because of better and/or closer packing.<sup>71</sup> For this reason, SF nanoparticle samples are roughly ten times more conductive than CF samples. There is, of course, a difficulty in reconciling the highest crystallinity of the three formulations being found for CS samples with the lowest conductivity.

In the particular case of the slow oxidation product, the highly crystalline materials is cross-linked and/or branched more than the other two types, resulting from a shorter conjugated length and localized polarons for a lower conductivity.<sup>60</sup> A further interpretive complication arises from the crystalline domain sizes for CF and CS samples being smaller than the particle sizes observed with the TEM. This suggests that rather than a blend two populations of fully crystalline and fully amorphous PAN nanoparticles, it is more likely that most nanoparticles have an internal blend of crystalline, transition, and amorphous regions.<sup>72</sup> Without knowing the quantitative characteristics in this regard from the analytical techniques and quality available for this work, these variations in nanoparticle morphology could easily account for the relatively lower conductivity of CF and CS sample types with respect to the SF nanopowder. On the other hand, the obtained crystalline domain sizes for SF HCl-doped PAN were very close to the estimated particle size observed with TEM, which may be an indication

of the presence of nearly single-crystal nanoparticles. It may be deduced that the SF approach allows the proper ordering and oxidation extent of PAN molecules and contributes to the higher conductivity than the HCl-doped PAN samples prepared with the classical chemical oxidation approaches (CF and CS).

**Table 2.3.** XRD data analysis summary.

Sample	$2\theta$	$d(\text{\AA})$	Domain size $L(\text{\AA})$	Inter-chain Separation $R(\text{\AA})$	(hkl)	Crystallinity
PAN-HCl-CF	13.90	6.36			(010)	
“	19.67	4.51			(100)	$53.8 \pm 0.3\%$
“	24.36	3.65	$46.33 \pm 8.12$	4.51	(011)	
PAN-HCl-CS	14.54	6.09			(010)	
“	19.70	4.51			(100)	$73.2 \pm 2.9\%$
“	25.60	3.48	$132.32 \pm 9.02$	4.34	(011)	
PAN-HCl-SF	14.64	6.05			(010)	
“	20.94	4.24			(100)	$65.9 \pm 2.1\%$
“	25.24	3.53	$121.63 \pm 9.09$	4.41	(011)	

### 2.5.5. Electromagnetic (EM) measurements

The application of PAN-based nanomaterials in EM shielding manufacturing will be as a filler in some convenient matrix, or perhaps on its own if appropriate forming conditions can be achieved to preserve, or even enhance, final product SE. Therefore, it is important to relate its shielding effectiveness behaviors with the employed amount per unit surface area, also called areal concentration (mass/area). Figure 2.8a-c compiles the average values for  $SE_T$ ,  $SE_A$ , and  $SE_R$  of the all doped PAN sample types and loadings as function of the areal concentrations, showing roughly linear behavior in shielding, with two distinct outliers for the solvent-free samples at the lowest mass loadings. As expected, the total shielding efficiency ( $SE_T$ ) increased with increasing the mass loaded in the sample holder of each sample type (CF, CS,

SF). Figure 2.8a shows  $SE_T$  for PAN samples as a function of EM frequency in the X-band for each mass loading, as well as the absorbance and reflection curves (Figure 2.8b-c). By increasing the amount of nanopowder loaded from 0.1 to 0.4 g, the average  $SE_T$  roughly triples from 5 dB to 14 dB for CF samples. With a constant cross section, this effect is due to the shielding material thickness increasing,<sup>5,7</sup> where the EM wave power traveling through a medium should decay exponentially.<sup>61</sup>

$SE_T$  increased slightly with higher frequencies. This behavior is likely associated with the existence of two types of charged species in doped PAN: 1) polaron/bipolaron systems that are mobile along the chain and 2) other bound charge distributions (e.g., dipoles) with restricted mobility accounting for strong polarization in the system.<sup>12,73</sup> When the frequency of the applied field is increased, the dipoles cannot reorient as rapidly as the applied electric field. This decreases the dielectric constant and increases the number of mobile charges, which results in higher dielectric loss ( $\epsilon''$ ) while the real part ( $\epsilon'$ ) decreases.<sup>26,74,75</sup> The product of angular frequency ( $\omega$ ) and dielectric loss is equivalent to the dielectric conductivity ( $\sigma_{ac}$ , microwave ac conductivity) as follows:<sup>75,76</sup>

$$\sigma_{ac}(\omega) = \omega \epsilon'' = \omega \epsilon_o \epsilon_r'' = 2\pi f \epsilon_o \epsilon_r'' ,$$

where  $\epsilon_o$  is the free space permittivity,  $\epsilon_r''$  is relative dielectric loss of the medium, and  $f$  is the frequency. Higher dielectric loss leads to increasing microwave ac conductivity and the effective conductivity of the medium:<sup>77-79</sup>  $\sigma_e(\omega) = \sigma_{dc}(\omega) + \sigma_{ac}(\omega)$ . This may explain the aforementioned enhancement in  $SE_T$  by increasing the frequency. In the microwave region,  $\sigma_{ac}$  of emeraldine salts is larger than  $\sigma_{dc}$ , though still near the same order of magnitude.<sup>74,80</sup> For this reason,  $\sigma_{dc}$  of PAN still has a significant impact on the SE.

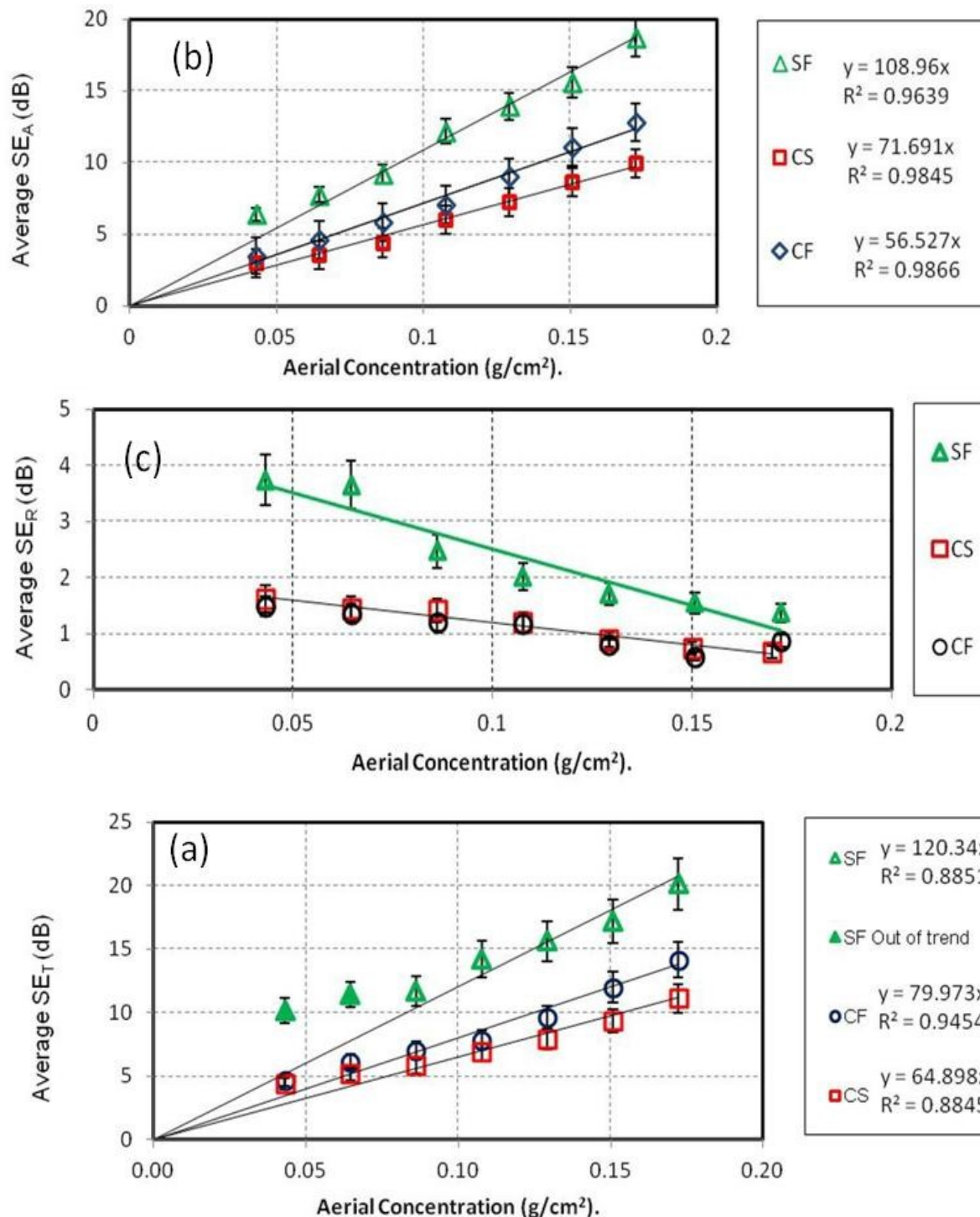


**Figure 2.8.** Shielding effectiveness (SE) averaged over the tested X-band range of 8–12 GHz: (a) total ( $SE_T$ ), (b) absorbance component ( $SE_A$ ), and (c) reflectance component ( $SE_R$ ), identifying linear trends for CF, CS and SF type HCl-doped PAN nanopowders. Error bars represent standard deviations.

The similarly increasing trends for  $SE_A$  with mass loading (Figure 2.8b) show that the absorption mechanism dominates the total shielding and increases from 75% to 90% of the total contribution while  $SE_R$  shows limited impact, decreasing with mass loading from 1.5 dB to 0.9 dB (Figure 2.8c) for both CF and CS samples. The  $SE_A$  contributions for CS are lower (67% to 89% for 0.1 g to 0.4 g, respectively) than found for the CF HCl-doped PAN nanopowders. This could be attributed to an increasing reflection coefficient with sample thickness<sup>81,82</sup> or an impedance mismatch between the incident wave impedance ( $377 \Omega$ ) and the surface impedance expected when dealing with conductive PAN samples.<sup>2</sup> A decreasing trend with frequency has previously been attributed to the decreasing surface impedance with thicker samples.<sup>83,84</sup>

The results for HCl-doped PAN nanoparticles show an interesting contradiction to the general rule that higher crystallinity should increase conductivity,<sup>43,70,85-87</sup> whereas the CS PAN nanopowders are significantly more crystalline (table 2.3) with arguably similar or lower conductivity and slightly lower shielding than CF PAN samples. If high crystallinity were achieved with the formation of cross-linking structures due to coupling in the ortho- position, the proton mobility is expected to be lower than that in linear doped PAN samples in which head-to-tail (i.e., N-para) coupling is predominant.<sup>67</sup> The proposed cross-linking structures in CS samples may arise from the slow oxidation of aniline by restrictive reagent addition (APS solution at 0.1 ml/min  $\approx$  0.11 mmol/min), which fosters PAN chain growth with existing chains as well as other structural defects resulting in lower conductivity.<sup>57,60</sup> Moreover, the slow polymerization produces no noticeable change in temperature of the reacting mixture, which is favorable for higher degrees of crystallinity.<sup>57</sup> Since both fast and slow oxidation products (CF and CS) were synthesized with the same dopant (HCl) ratios, the degree of crystallinity appears to depend

only on the reaction conditions<sup>67</sup> and thus an optimum in conductivity and crystallinity for the maximum shielding potential may be revealed with fine-tuning of the rate and method for oxidant addition.

The solvent-free (SF) HCl-doped PAN nanopowders were the most successful of the three products in shielding the X-band frequencies (Figure 2.8). Similar trends in  $SE_T$  and  $SE_A$  with mass loading follow the results for the conventional products; however, the SE was much greater overall, due mostly to the much higher conductivity. Figure 2.8a indicates significantly greater increases in  $SE_T$  for the lower mass loadings over both CF and CS sample types. Figure 2.8b indicates that relative absorption effects ( $SE_A$  is 63% to 93% of shielding from 0.1 g to 0.4 g) are smallest for SF PAN samples at the lower loadings but match and slightly exceed relative contributions in the other two sample sets. Therefore, the contribution of  $SE_R$  again decreases with mass loading (Figure 2.8c) but is also greater in magnitude for each case compared to the conventional products (3.7 dB to 1.4 dB with increasing mass loads). Clearly, conductivity and not crystallinity is the direct controlling factor herein for the most favorable EM shielding, where losses occur as a result of ohmic current induced in the shield and dissipated as heat; therefore, the magnitude of the EM losses depends on the shield thickness and conductivity.<sup>5,22,88</sup>

It is noteworthy that while both absorption and reflection terms exhibit fairly strong linear correlations, especially for the conventional oxidation products, the  $SE_T$  data trends arguably show some bi-exponential character, viz., upward curvature, across all three nanoparticle formulations. This would seem to support the need for deeper understanding into the function form of the multiple reflection term,  $M$ , according to shield thickness, which was earlier dis-

missed as negligible. The linear trends in  $SE_T$  and  $SE_A$  for increasing areal concentrations generally agree with the fact that the attenuation of the propagating EM wave exponential.<sup>2,89</sup> However, the decreasing trend in average  $SE_R$ , attributed to increasing surface impedance as the thickness increases, currently lacks a clear functional-form connection; that is, no single phenomenological factor appears to suggest an explanation for an apparent exponential decrease in reflective shielding effectiveness due to path length.

## 2.6. Conclusions

The main contribution of this work is highlighting the dependence of EM shielding effectiveness (SE) in conducting polymers on the synthesis approach, particularly in the microwave X-band for polyaniline nanopowders doped with HCl. The solution-free or solvent-limited synthesis in a slightly wetted solid-phase reaction provides substantial material property improvements over conventional solution-rich oxidations with limited or abundant oxidizer (CS and CF samples, respectively). Collective data analysis demonstrates the importance of conductivity over crystallinity for enhancing SE for nanoPAN. The synthesis protocols that lead to maximizing crystallinity (e.g., conventional slow oxidation) in HCl-doped PAN with cross-linked structures or branched chains is not recommended, as there appears to be an intermediate optimum with respect to conductivity and EM shielding.

The total shielding versus nanopowder loading curves exhibit slight but consistent deviations from the expected exponential decay behavior for EM wave propagation, indicative of a significant multiple reflection effect in the nanomaterials. Therefore, it is likely that even greater shielding may be achieved at higher loadings, with alterations in size distributions, and

certainly with the addition of higher reflectance materials, such as metals, in a mixed nanocomposite with a PAN-containing matrix. The latter is a promising approach with potential tradeoffs between materials cost and mass loading as well as an extra controllable parameter for flexibility in fabrication for specific EMI design criteria. In addition, a thin insulating nanoparticle coating, such as PAN without dopant, has the potential to produce higher surface impedance and lower reflection coefficient in the compacted nanopowder to increase  $SE_R$ . In parallel with these studies, the dopant species and level—held constant herein—may be optimized, as well.

## 2.7. References

- (1) Weston, D. A. *Electromagnetic Compatibility : Principles and Applications*; Marcel Dekker: New York, NY 2001.
- (2) Tong, X. C. *Advanced Materials and Design for Electromagnetic Interference Shielding*; CRC Press: Boca Raton, 2009.
- (3) Paul, C. R. *Introduction to Electromagnetic Compatibility*; John Wiley & Sons, Inc.: Hoboken, NJ, 2006.
- (4) Li, L.; Chung, D. D. L. Electrically Conducting Powder Filled Polyimidesiloxane Composites **1991**, 22, 211-218.
- (5) Wang, Y.; Jing, X. Intrinsically Conducting Polymers for Electromagnetic Interference Shielding *Polym. Adv. Technol.* **2005**, 16, 344–351.
- (6) Cao, G. *Nanostructures and Nanomaterials: Synthesis, Properties, and Applications*; Imperial College Press 2004
- (7) Joo, J.; Epstein, A. J. Electromagnetic Radiation Shielding by Intrinsically Conducting Polymers *Appl. Phys. Lett.* **1994** 65 2278-2280
- (8) Skotheim, T. A.; Reynolds, J. R. *Handbook of Conducting Polymers 2, Conjugated Polymers - Processing and Applications*; CRC Press: Boca Raton, Fla. [u.a.], 2007.
- (9) McManus, P. M.; Cushman, R. J.; Yang, S. C. Influence of Oxidation and Protonation on the Electrical Conductivity of Polyaniline *J. Phys. Chem.* **1987**, 91, 744-747.

- (10) Bhadra, S.; Lee, J. H. Synthesis of Higher Soluble Nanostructured Polyaniline by Vapor-Phase Polymerization and Determination of Its Crystal Structure *J. Appl. Polym. Sci.* **2009**, *114*, 331-340.
- (11) Wan, M. *Conducting Polymers with Micro or Nanometer Structure*; Tsinghua University Press ; Springer: Beijing; Berlin, 2008.
- (12) Wallace, G. G.; Spinks, G. M.; Kane-Maguire, L. A. P.; Teasdale, P. R. *Conductive Electroactive Polymers Intelligent Materials Systems*; CRC Press: Boca Raton; London; New York, 2009.
- (13) Toshima, N.; Hara, S. Direct Synthesis of Conducting Polymers from Simple Monomers *Prog. Polym. Sci.* **1995**, *20*, 155-183.
- (14) Han, M. G.; Cho, S. K.; Oh, S. G.; Im, S. S. Preparation and Characterization of Polyaniline Nanoparticles Synthesized from Dbsa Micellar Solution *Synt. Met.* **2002**, *126*, 53-60.
- (15) Zhou, C. F.; Du, X. S.; Mai, Y. W.; Liu, Z.; Ringer, S. P. Solid Phase Mechanochemical Synthesis of Polyaniline Branched Nanofibers *Synt. Met.* **2009**, *159*, 1302-1307.
- (16) Bekri-Abbes, I.; Srasra, E. Investigation of Structure and Conductivity Properties of Polyaniline Synthesized by Solid–Solid Reaction *J Polym Res* **2011**, *18*, 659-665.
- (17) Abdiryim, T.; Xiao-Gang, Z.; Jamal, R. Comparative Studies of Solid-State Synthesized Polyaniline Doped with Inorganic Acids *Mater. Chem. Phys.* **2005**, *90*, 367-372.
- (18) Du, X. S.; Zhou, C. F.; Wang, G. T.; Mai, Y. W. Novel Solid-State and Template-Free Synthesis of Branched Polyaniline Nanofibers *Chem. Mater.* **2008**, *20*, 3806-3808.

- (19) Abdiryim, T.; Jamal, R.; Nurulla, I. Doping Effect of Organic Sulphonic Acids on the Solid-State Synthesized Polyaniline *J. Appl. Polym. Sci.* **2007**, *105*, 576-584.
- (20) Ding, Y.; Abdiryim, T.; An, S.; Nurulla, I. Effect of B-Cyclodextrin on the Solid-State Synthesized Polyaniline Doped with Hydrochloric Acid *J. Appl. Polym. Sci.* **2008**, *107*, 3864-3870.
- (21) Huang, J.; Moore, J. A.; Acquaye, J. H.; Kaner, R. B. Mechanochemical Route to the Conducting Polymer Polyaniline *Macromolecules* **2004**, *38*, 317-321.
- (22) Nalwa, H. S. *Handbook of Organic Conductive Molecules and Polymers 3, Conductive Polymers: Spectroscopy and Physical Properties*; Wiley: Chichester; New York, 1997; Vol. 3.
- (23) Chen, L. F.; Ong, C. K.; Neo, C. P.; Varadan, V. V.; Varadan, V. K. *Microwave Electronics: Measurement and Materials Characterization*; John Wiley & Sons, Ltd 2004
- (24) Yun, J.; Im, J. S.; Lee, Y. S.; Kim, H. I. Effect of Oxyfluorination on Electromagnetic Interference Shielding Behavior of Mwcnt/Pva/Paac Composite Microcapsules *Eur. Polym. J.* **2010**, *46*, 900-909.
- (25) Klemperer, C. J. v.; Maharajb, D. Composite Electromagnetic Interference Shielding Materials *Compos. Struct.* **2009**, *91*, 467-472.
- (26) Boreddy, R. Designing of Nano Composites of Conducting Polymers for Emi Shielding. In *Advances in Nanocomposites - Synthesis, Characterization and Industrial Applications*; Reddy, B. S. R., Ed.; INTECH Open Access Publisher, 2011; pp 429-482.

- (27) Al-Saleh, M. H.; Sundararaj, U. Electromagnetic Interference Shielding Mechanisms of Cnt/Polymer Composites *Carbon* **2009**, *47*, 1738-1746.
- (28) Chowdhury, P.; Saha, B. Potassium Dichromate Initiated Polymerization of Aniline *Indian J. Chem. Technol.* **2005**, *12*, 671-675.
- (29) Pohanish, R. P.; Greene, S. A. *Wiley Guide to Chemical Incompatibilities*, 3 ed.; Wiley: Hoboken, N.J., 2009.
- (30) Fu, Y.; Elsenbaumer, R. L. Thermochemistry and Kinetics of Chemical Polymerization of Aniline Determined by Solution Calorimetry *Chem. Mater.* **1994**, *6*, 671-677.
- (31) Stejskal, J.; Gilbert, R. G. Polyaniline. Preparation of a Conducting Polymer (Iupac Technical Report) *Pure Appl. Chem.* **2002**, *74*, 857.
- (32) Nalwa, H. S. *Handbook of Organic Conductive Molecules and Polymers 2, Conductive Polymers: Synthesis and Electrical Properties.*; Wiley: Chichester; New York, 1997; Vol. 2.
- (33) Bhadra, S.; Khastgir, D. Determination of Crystal Structure of Polyaniline and Substituted Polyanilines through Powder X-Ray Diffraction Analysis *Polym. Test.* **2008**, *27*, 851-857.
- (34) Zhang, X.; Zhu, J.; Haldolaarachchige, N.; Ryu, J.; Young, D. P.; Wei, S.; Guo, Z. Synthetic Process Engineered Polyaniline Nanostructures with Tunable Morphology and Physical Properties *Polymer* **2012**, *53*, 2109-2120.
- (35) Varma, S. J.; Xavier, F.; Jayalekshmi, S.; Varghese, S. Synthesis and Studies of Exceptionally Crystalline Polyaniline Thin Films *Polym. Int.* **2012**, *61*, 743-748.

- (36) Majumdar, D.; Baskey, M.; Saha, S. K. Epitaxial Growth of Crystalline Polyaniline on Reduced Graphene Oxide *Macromol. Rapid Commun.* **2011**, *32*, 1277-1283.
- (37) Freund, M. S.; Deore, B. *Self-Doped Conducting Polymers*; John Wiley & Sons, Ltd: West Sussex, England; Hoboken, NJ, 2007.
- (38) Ladd, M. F. C.; Palmer, R. A. *Structure Determination by X-Ray Crystallography*; Plenum Press: New York, 1994.
- (39) Cullity, B. D. *Elements of X-Ray Diffraction*; Addison-Wesley Pub. Co.: Reading, Mass., 1956.
- (40) Klug, H. P.; Alexander, L. E. *X-Ray Diffraction Procedures for Polycrystalline and Amorphous Materials*; Wiley: New York, 1974.
- (41) Rimbu, G. A.; Stamatina, I.; Jackson, C. L.; Scott, K. The Morphology Control of Polyaniline as Conducting Polymer in Fuel Cell Technology *J. Optoelectron. Adv. M.* **2006**, *8*, 670-674.
- (42) Duan, Y.; Shunhua, L.; Hongtao, G. Investigation of Electrical Conductivity and Electromagnetic Shielding Effectiveness of Polyaniline Composite *STAM* **2005**, *6*, 513-518.
- (43) Zhang, D. On the Conductivity Measurement of Polyaniline Pellets *Polym. Test.* **2007**, *26*, 9-13.
- (44) Ebara, H.; Inoue, T.; Hashimoto, O. Measurement Method of Complex Permittivity and Permeability for a Powdered Material Using a Waveguide in Microwave Band *STAM* **2006**, *7*, 77-83.

- (45) Mzenda, V. M.; Goodman, S. A.; Auret, F. D. Conduction Models in Polyaniline: The Effect of Temperature on the Current–Voltage Properties of Polyaniline over the Temperature Range 30<math>T(K)</math>300 *Synt. Met.* **2002**, *127*, 285-289.
- (46) Trchová, M.; Stejskal, J. Polyaniline: The Infrared Spectroscopy of Conducting Polymer Nanotubes (Iupac Technical Report) *Pure Appl. Chem.* **2011**, *83*, 1801.
- (47) Schrader, B. *Infrared and Raman Spectroscopy: Methods and Applications*; VCH: Weinheim, 1995.
- (48) Boyer, M. I.; Quillard, S.; Rebourt, E.; Louarn, G.; Buisson, J. P.; Monkman, A.; Lefrant, S. Vibrational Analysis of Polyaniline: A Model Compound Approach *J. Phys. Chem. B* **1998**, *102*, 7382-7392.
- (49) Socrates, G. *Infrared and Raman Characteristic Group Frequencies : Tables and Charts*; Wiley: Chichester; New York, 2000.
- (50) Kang, E. T.; Neoh, K. G.; Tan, K. L. Polyaniline: A Polymer with Many Interesting Intrinsic Redox States *Prog. Polym. Sci.* **1998**, *23*, 277-324.
- (51) Ameen, S.; Kim, Y. S.; Shin, H. S.; Akhtar, M. S. Synthesis and Electrochemical Impedance Properties of Cds Nanoparticles Decorated Polyaniline Nanorods *Chem. Eng. J.* **2011**, *181-182*, 806-812.
- (52) Stejskal, J.; Exnerová, M.; Moravková, Z.; Trchová, M.; Hromádková, J.; Prokes, J. Oxidative Stability of Polyaniline *Polym. Degrad. Stab.* **2012**, *97*, 1026-1033.
- (53) Prokes, J.; Trchová, M.; Hlavata, D.; Stejskal, J. Conductivity Ageing in Temperature-Cycled Polyaniline *Polym. Degrad. Stab.* **2002**, *78*, 393-401.

- (54) Stejskal, J.; Trchová, M. Aniline Oligomers Versus Polyaniline *Polym. Int.* **2012**, *61*, 240-251.
- (55) Stejskal, J.; Trchova, M.; Konyushenko, E. N.; Sapurina, I. Oxidation of Aniline: Polyaniline Granules, Nanotubes, and Oligoaniline Microspheres *Macromolecules* **2008**, *41*, 3530-3536.
- (56) Stejskal, J.; Trchova, M.; Prokes, J.; Sapurina, I. Brominated Polyaniline *Chemistry of materials : a publication of the American Chemical Society.* **2001**, *13*, 4083.
- (57) Stejskal, J.; Sapurina, I.; Trchova, M. Polyaniline Nanostructures and the Role of Aniline Oligomers in Their Formation *Prog. Polym. Sci.* **2010**, *35*, 1420-1481.
- (58) Sedenková, I.; Trchová, M.; Stejskal, J.; Bok, J. Polymerization of Aniline in the Solutions of Strong and Weak Acids: The Evolution of Infrared Spectra and Their Interpretation Using Factor Analysis *Applied spectroscopy* **2007**, *61*, 1153-1162.
- (59) Quillard, S.; Louarn, G.; Lefrant, S.; Macdiarmid, A. G. Vibrational Analysis of Polyaniline: A Comparative Study of Leucoemeraldine, Emeraldine, and Pernigraniline Bases *Phys. Rev. B: Condens. Matter* **1994**, *50*, 12496-12508.
- (60) Pan, L. J.; Pu, L.; Shi, Y.; Sun, T.; Zhang, R.; Zheng, Y. O. Hydrothermal Synthesis of Polyaniline Mesostructures *Adv. Funct. Mater.* **2006**, *16*, 1279-1288.
- (61) Hayt, W. H.; Buck, J. A. *Engineering Electromagnetics : 8th Edition*; McGraw hill higher education: London, 2012.
- (62) Miller, F. A.; Mayo, D. W.; Hannah, R. W. *Course Notes on the Interpretation of Infrared and Raman Spectra*; Wiley-Interscience: Hoboken, N.J., 2004.

- (63) Kellenberger, A.; Dmitrieva, E.; Dunsch, L. Structure Dependence of Charged States in “Linear” Polyaniline as Studied by in Situ Atr-Ftir Spectroelectrochemistry *Physical Chemistry B* **2012**, *116*, 4377-4385.
- (64) Trchová, M.; Stejskal, J.; Prokeš, J. Infrared Spectroscopic Study of Solid-State Protonation and Oxidation of Polyaniline *Synt. Met.* **1999**, *101*, 840-841.
- (65) Laslau, C.; Zujovic, Z.; Travas-Sejdic, J. Theories of Polyaniline Nanostructure Self-Assembly: Towards an Expanded, Comprehensive Multi-Layer Theory (Mlt) *Prog. Polym. Sci.* **2010**, *35*, 1403-1419.
- (66) Laska, J.; Widlarz, J. Spectroscopic and Structural Characterization of Low Molecular Weight Fractions of Polyaniline *Polymer* **2005**, *46*, 1485-1495.
- (67) Liu, H.; Hu, X. B.; Wang, J. Y.; Boughton, R. I. Structure, Conductivity, and Thermopower of Crystalline Polyaniline Synthesized by the Ultrasonic Irradiation Polymerization Method *Macromolecules* **2002**, *35*, 9414.
- (68) Banerjee, S.; Saikia, J. P.; Kumar, A.; Konwar, B. Antioxidant Activity and Haemolysis Prevention Efficiency of Polyaniline Nanofibers *Nanotechnology* **2010**, *21*.
- (69) Pramanik, S.; Karak, N.; Banerjee, S.; Kumar, A. Effects of Solvent Interactions on the Structure and Properties of Prepared Pani Nanofibers *J. Appl. Polym. Sci.* **2012**, *26*, 830–836.
- (70) Chaudhari, H. K.; Kelkar, D. S. Investigation of Structure and Electrical Conductivity in Doped Polyaniline *Polym. Int.* **1997**, *42*, 380-384.

- (71) Sinha, S.; Bhadra, S.; Khastgir, D. Effect of Dopant Type on the Properties of Polyaniline *J. Appl. Polym. Sci.* **2009**, *112*, 3135-3140.
- (72) Mazerolles, L.; Folch, S.; Colomban, P. Study of Polyanilines by High-Resolution Electron Microscopy *Macromolecules* **1999**, *32*, 8504-8508.
- (73) Nalwa, H. S. *Advanced Functional Molecules and Polymers*; Gordon and Breach Science Publ.: Amsterdam, 2001.
- (74) Chandrasekhar, P.; Naishadham, K. Broadband Microwave Absorption and Shielding Properties of a Poly(Aniline) *Synt. Met.* **1999**, *105*, 115.
- (75) Micheli, D.; Apollo, C.; Pastore, R.; Marchetti, M. X-Band Microwave Characterization of Carbon-Based Nanocomposite Material, Absorption Capability Comparison and Ras Design Simulation *Compos. Sci. Technol* **2010**, *70*, 400-409.
- (76) Abkowitz, M. A.; Lakatos, A. I. Microwave Dielectric Constant and Conductivity Measurements in the Phthalocyanines *J. Chem. Phys.* **1972**, *57*, 5033-5036.
- (77) John, H.; Thomas, R. M.; Jacob, J.; Mathew, K. T.; Joseph, R. Conducting Polyaniline Composites as Microwave Absorbers *Polym. Compos.* **2007**, *28*, 588.
- (78) John, H.; Thomas, R. M.; Mathew, K. T.; Joseph, R. Studies on the Dielectric Properties of Poly(O-Toluidine) and Poly(O-Toluidine-Aniline) Copolymer *J. Appl. Polym. Sci.* **2004**, *92*, 592-598.
- (79) Moore, J. C.; Fujita, S. Dielectric Properties of Ice Containing Acid and Salt Impurity at Microwave and Low Frequencies *J. Geophys. Res.* **1993**, *98*, 9769-9780.

- (80) Javadi, H.; Cromack, K.; MacDiarmid, A.; Epstein, A. Microwave Transport in the Emeraldine Form of Polyaniline *Physical Review B* **1989**, *39*, 3579-3584.
- (81) Latyshev, A. V.; Yushkanov, A. A. Interaction of the Electromagnetic S-Wave with the Thin Metal Film *Journal of Optical Technology* **2012**, 79316-321
- (82) Rajagopalan, H.; Rahmat-Samii, Y. On the Reflection Characteristics of a Reflectarray Element with Low-Loss and High-Loss Substrates *IEEE Antennas Propag Mag IEEE Antennas and Propagation Magazine* **2010**, *52*, 73-89.
- (83) Avloni, J.; Ouyang, M.; Florio, L.; Henn, A.; Sparavigna, A. Shielding Effectiveness Evaluation of Metallized and Polypyrrole-Coated Fabrics *Journal of Thermoplastic Composite Materials* **2007**, *20*, 241-254.
- (84) Avloni, J.; Florio, L.; Henn, A. R.; Lau, R.; Ouyang, M.; Sparavigna, A. Electromagnetic Shielding with Polypyrrole-Coated Fabrics *Journal of Thermoplastic Composite Materials* **2007**, *20*, 241-254.
- (85) Bohli, N.; Gmati, F.; Mohamed, A. B.; Vigneras, V.; Miane, J. L. Conductivity Mechanism of Polyaniline Organic Films: The Effects of Solvent Type and Casting Temperature *J. Phys. D: Appl. Phys* **2009**, *42*, 205404.
- (86) Chaudhari, H. K.; Kelkar, D. S. X-Ray Diffraction Study of Doped Polyaniline *J. Appl. Polym. Sci.* **1996**, *62*, 15.
- (87) Zhang, K.; Li, Y. Electrical Conductivity Enhancement of Polyaniline by Refluxing *Polym. Adv. Technol.* **2011**, *22*, 2084-2090.

- (88) Geetha, S.; Rao, C. R. K.; Vijayan, M.; Trivedi, D. C.; Kumar, K. K. S. EMI Shielding: Methods and Materials - a Review *J. Appl. Polym. Sci.* **2009**, *112*, 2073-2086.
- (89) Pozar, D. M. *Microwave Engineering*; Wiley: New York, 1997.

## CHAPTER 3

### Chemical Effects of a Solvent-Limited Approach to HCl-Doped

### Polyaniline Nanopowder Synthesis

#### 3.1. Introduction

Polyaniline (PAN) is one of the most interesting conducting polymers due to its environmental stability,<sup>1-4</sup> ease of synthesis and preparation,<sup>5-8</sup> and wide-ranging potential use through its particular electrochemical, optical, and electrical properties.<sup>8-11</sup> The physics and chemistry of polyaniline in its many forms have been the subject of intense study because of its fundamental and important technological properties with their possible applications in rechargeable batteries,<sup>12,13</sup> microelectronics devices,<sup>14</sup> biosensors,<sup>15-17</sup> chemical sensors,<sup>18,19</sup> electrochromic displays,<sup>20</sup> and electromagnetic shielding.<sup>21-25</sup> Superior control over the conductivity of polyaniline through doping is regarded as very promising due to the relative ease of scaling to large quantities and of designing electromagnetic behavior through final oxidation and protonation states determined by adjustable reaction conditions.<sup>6,26,27</sup>

While electropolymerization of aniline has the merit of easier control over morphology and electrical properties, it is not as facile to scale up for commercial production as strictly chemical oxidative methods.<sup>2,6,28-32</sup> Various polyanilines prepared by solvent-limited or solvent-free synthesis—in a largely solid state—are of increasing interest.<sup>10,33-38</sup> This type of protocol has the obvious advantages of eliminating substantial use of solvent and all costs and complications associated therein, including separation, recovery, reuse, and proper waste treatment, as well as reducing the overall reaction volume and mass per final product quantity. Furthermore, a solvent-limited process is more environmentally sound and sustainable.<sup>34</sup>

However, the physical and chemical features of solvent-free PAN and their controllability remain largely unstudied in any comprehensive detail.

Recent preliminary investigations on solvent-limited HCl-doped PAN nanopowders toward electromagnetic shielding materials demonstrated the importance of conductivity over polymer crystallinity for increased effectiveness in the microwave region.<sup>21</sup> The relatively surprising performance of the so-called solvent-free (SF) nanopowder at approximately 27 S/cm over conventional oxidation methods providing only  $\sim 3$  S/cm argues for deeper study into the chemical reasons for increased shielding effectiveness.

This investigation on solvent-free and solvent-limited syntheses provides unique insights from the characterization of electronic structure, polymorphism, and chain conformation of HCl-doped polyaniline compared against two classical oxidation approaches with extremes in rapid and slow additions of reagent, extending from previous developments.<sup>21</sup> Raman and UV-vis spectroscopy studies are applied herein to explicate the chemical nature of the polymer nanopowders from each synthetic route to understand and clarify the causal connections between reaction conditions and material products for process control over the resulting electrical and electromagnetic properties—the focus of current efforts. The three-way comparison of fast oxidation, or rapid addition of oxidizing agent, to slow oxidation and ultimately to a nearly solvent-free reaction process will highlight the significant range of differences in final polymer properties even while using the same dopant at the same quantities. The highly-variant synthesis conditions for one fairly well-studied conductive polymer type establish an example for justification as for the need of deeper understanding into the connections and nuances between reaction process and final nanopowder qualities, especially with a particular future goal for optimizing polymeric materials toward

electromagnetic (EM) shielding applications and related fields. This work continues to expand a fundamental understanding in this regard for methodical expansion to other dopants and ongoing studies in shielding materials for mitigating EM interference effects on electronic devices.

### **3.2. Materials and Methods**

Aniline (99.5%, ACS reagent grade, Aldrich) was purified by distillation with zinc dust before use.<sup>39,40</sup> The inorganic acid dopant hydrochloric acid (37.43%, ACS reagent grade, EMD Chemicals) and the oxidant ammonium peroxydisulfate (98%, ACS reagent grade, Aldrich) were used as received. HCl-doped polyaniline (PAN) nanoparticle samples were prepared by solvent-free (SF) and conventional (solvent-based) chemical oxidations under slow (CS) and fast (CF) production rates as controlled by the addition of aqueous ammonium peroxydisulfate (APS), both described below in detail. Samples from multiple batches produced over several months were tested for conductivity and crystallinity to ensure a reproducible comparison between sample types (SF, CS, CF) can be made.

#### **3.2.1. Solvent-free (SF) Synthesis.**

It should be first noted that the “solvent-free” label refers to the aniline monomer and oxidant (APS) being used in their as-prepared and as-received states without first dissolving them in a reaction medium (solvent), though certainly the SF reaction chemicals are not completely void of solvent since the dopant (HCl) is applied from the standard aqueous concentrate. A typical solvent-free polymerization procedure at room temperature (~18–24°C) was followed with freshly distilled aniline (0.05 mole per batch) poured into a porcelain mortar, and then 0.1 mole of the doping acid, i.e. concentrated HCl, was added dropwise while

grinding manually for 10 min. The acid was added in very small dropwise portions in order to minimize the released fumes and prevent the overheating of the reaction medium since aniline reacts violently with strong acids.<sup>41</sup> The reactant mixture became a white paste after grinding. Separate grinding of 0.05 mole of APS in another porcelain mortar produced a fine powder, which was subsequently added in small portions to the white paste reactant in order to avoid overheating from the highly exothermic oxidative polymerization.<sup>42,43</sup> Approximately 0.5 g of APS was added in between grinding the reactant mixture for ~1-2 min in cycles until the entire batch was uniformly ground and finally attained the appropriate greenish-black color indicative of the HCl-doped PAN nanoparticles. This product was transferred to a 500 mL beaker where 100 mL of acetone, 100 mL of ethanol and 100 mL of DI were added and then mixed for 1 h in order to quench the polymerization reaction and to dissolve oligomeric impurities.<sup>44-46</sup> The rest of the product mixture was filtered and washed with acetone, ethanol, and distilled water, in series, until the filtrate was colorless in order to confirm the adequate removal of unreacted chemicals and excess acid.<sup>47,48</sup> Finally, the powder was dried at 40°C for 48 h.

### **3.2.2. Conventional Chemical Synthesis: Fast (CF) and Slow (CS) Oxidations.**

The same freshly distilled aniline in 0.05-mole doses was dissolved in 1000 mL of DI water followed by dropwise addition of 0.1 mole of HCl concentrate with mixing on a magnetic stirrer (1000 rpm) for 15 min. Then 0.05 mole of APS dissolved in 50 mL of DI was added. In the case of conventional chemical oxidation with fast reaction (CF), the oxidizing APS solution was added all at once. On the other hand, the slow reaction procedure (CS) added the same APS solution amount with constant rate of 0.1 mL/min. Both reaction protocols were conducted at room temperature (~18–24°C). The reaction mixtures were mixed

for 12 h after APS addition. Then 100 mL of acetone and 100 mL of ethanol were added and mixed for 1 h, similar to the SF samples above except that no additional DI water is needed for the conventional solvent-rich synthesis.<sup>44-46</sup> The remaining products were filtered, washed, and dried identically to the SF samples.

### **3.3. Characterization Methods**

#### **3.3.1. Micro-Raman Spectral Analysis of Polyaniline Samples.**

Micro-Raman time-series spectra were acquired from polyaniline samples using a WITec alpha 300R scanning confocal Raman microscope (WITec GmbH, Ulm, Germany). Specifically, spectroscopic analysis was performed on polyaniline suspensions in DI water ( $\approx 10$  mg/mL) in order to prevent thermal decomposition of polyaniline due to interaction with a laser beam. The electronic behavior of PAN produces marked fluorescence, which is a challenge for Raman with 532 nm excitation. To counter this effect, nanopowders of PAN were suspended in water where Raman spectra were continuously collected. A Nikon 20 $\times$  objective (NA = 0.4, WD = 3.8 mm) was used to focus the Raman excitation source (100 mW, 532 nm Nd:YAG laser) at the center of about 3 mL sample suspensions placed in a suitable Petri dish. Upon focusing, the sample was irradiated at a constant attenuated incident power of 8 mW to prevent the thermal destruction of the sample during the study. The average number of particles sampled by the spectrometer was dictated by Brownian motion, particle settling, and CCD integration time: *i.e.*, a Raman spectrum was generated at a frequency of 2 Hz resulting in 1000 total spectra for each PAN sample tested. Spectra were then screened using K-means cluster analysis in WITec Project Plus<sup>TM</sup>. Two parent nodes were sufficient to separate low signal-to-noise ratio (SNR) from high SNR spectra. Roughly 200-500 high SNR

spectra were selected from each set and averaged to yield the final processed spectra herein reported. This process was repeated three times for each PAN type.

The Raman-scattered light was collected in the backscattering configuration and detected using a UHTS-300 spectrometer (WITec). A diffraction grating of 600 lines-mm<sup>-1</sup> was employed giving a spectral coverage of 0–3600 cm<sup>-1</sup> of Raman shift. However, morphologically relevant polyaniline bands were contained in the 200-1700 cm<sup>-1</sup> range. Fluorescence baseline correction was performed using a third-order polynomial, followed by the application of a three-point moving average filter to eliminate most of the perturbing baseline and improve SNR.

### **3.3.2. UV-Vis Characterization.**

The UV analysis was carried out using a SHIMADZU-UV-11700 UV-visible spectrophotometer over the range 350-1100 nm. The testing was carried out taking only the soluble portion of PAN in *m*-cresol and sample concentrations were ≈0.2 mg/mL.

## **3.4. Results and Discussion**

### **3.4.1. Polymorphism, Chemical, and Electronic Structure.**

Raman spectroscopy (RS) aimed to identify and compare (a) polymorphism, (b) the relative structural difference(s) due to cross-linking, and (c) polymer electronic structure as a function of synthesis protocol. In other words, RS should elucidate the impact of the solvent-limited approach on the chemical and electronic structure of polyaniline samples. In general, the Raman spectra of polyaniline samples can be divided into two main regions. Region I represents lower wavenumbers (<1000 rel. cm<sup>-1</sup>) and is shown in Figure 3.1(a). The low wavenumber bands (<400 rel. cm<sup>-1</sup>) of Region I likely isolate polymorphic differences

between polyaniline samples.<sup>49-51</sup> On the other hand, the remaining bands (400-1000 rel.  $\text{cm}^{-1}$ ) indicate ring deformation<sup>52-58</sup> and any band variations between samples indicate a corresponding structural difference due to cross-linking.<sup>4, 7, 9, 15-18</sup> Since RS is a very efficient tool for characterizing radical cations (polaron) and divalent cations (bipolaron) in intrinsically conductive polymers, Figure 3.1(b) shows Region II (1000-1700 rel.  $\text{cm}^{-1}$ ) which has been used to elucidate the relative differences in polaron organization and abundance as a function of synthesis approach.<sup>59-63</sup> Table 3.1 offers a summative interpretation of the Raman bands contained in both regions of interest.

#### 3.4.1.1. Evidence of Various Polyaniline Forms: Region I (<400 $\text{cm}^{-1}$ )

Imine group protonation modifies the nitrogen atom hybridization (from  $\text{sp}^2$  to  $\text{sp}^3$ ) and consequently the chain geometry, which leads to a variety of polyaniline forms, structural conformation, and electronic conductivity.<sup>49</sup> Depending on the preparation methods, two classes of emeraldine chloride salts (ES-I, ES-II) have been distinguished.<sup>49,64-66</sup>

In addition, various kinds of heterogeneity are to be expected within and among these ES forms.<sup>51,67</sup> From a vibrational point-of-view, any disorder in the polyaniline polymeric backbone can result from an irregular arrangement of chemical bonds as well as from the presence of electrical defects, essentially affecting bending and external lattice vibration modes.<sup>49</sup> Low-wavenumber Raman bands elucidate the intramolecular configuration and the arrangement of molecular bricks within the materials and hence can be used to distinguish between ES-I, ES-II, and their heterogeneous mixtures.<sup>49-51</sup>

The low wavenumber Raman spectrum of CS (Figure 3.1a) is best represented by three bands at 125, 200, and 300 rel.  $\text{cm}^{-1}$  corresponding to  $\text{C}_{\text{Ring}}\text{Ar-N-C}_{\text{Ring}}$  deformations and ES-I lattice modes.<sup>49-51</sup> These peaks did not show up in the SF and CF spectra where only one

characteristic band at  $145\text{ cm}^{-1}$ , corresponding to the ES-II form, was observed. The weak shoulder at  $200\text{ cm}^{-1}$  may indicate heterogeneity.<sup>49-51</sup>

It was clear that the CS approach leads to a polyaniline with a predominate ES-I form which has a spinless charged (bipolaron) structure.<sup>68</sup> On the contrary, SF and CF approaches led to a predominately ES-II form that represents a potentially metallic material with a half-filled band.<sup>68</sup> These results and accompanying interpretation support the relatively lower conductivity of CS, which has been reported previously.<sup>21</sup>

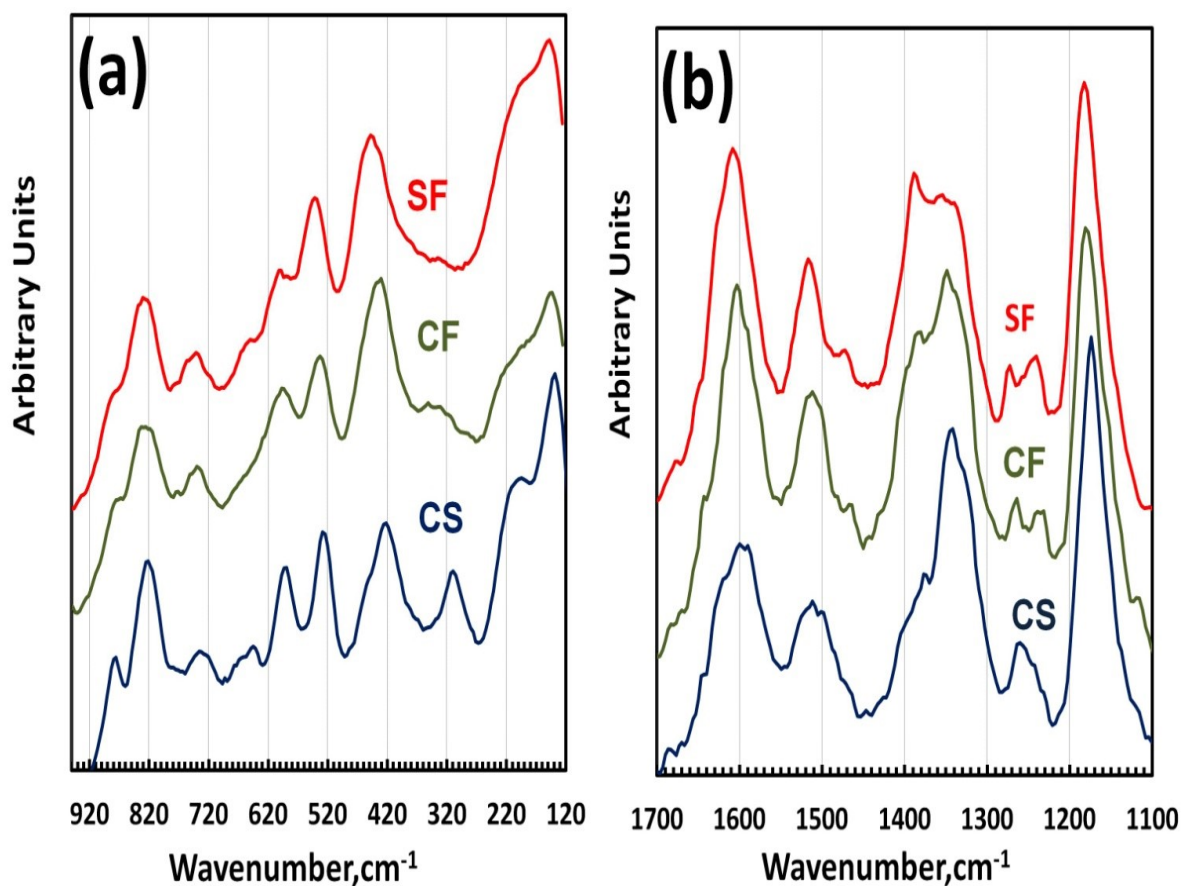


**Figure 3.1.** Raman spectra (in relative wavenumbers) of polyaniline samples (SF,CF, and CS).

**Table 3.1.** Band Assignments from Raman Spectra of Polyaniline Samples (SF,CF, and CS)

Wavenumber(cm <sup>-1</sup> )			Assignment	Ref.
SF	CF	CS		
---	--	125	C-N-C <sub>Ring</sub> Deformation +ES-I Lattice mode	49-51
148	145	---	C <sub>Ring</sub> -N-C <sub>Ring</sub> Deformation +ES-II Lattice mode	49-51
182 sh,vw	182 sh,w	200	C <sub>Ring</sub> -N-C <sub>Ring</sub> Deformation +ES-I Lattice mode C <sub>Ring</sub> -N-C <sub>Ring</sub> (Bipolarons-protonated, spinless units)	49-51 69-71
--	292w	300	C <sub>Ring</sub> -N-C <sub>Ring</sub> Deformation +ES-I Lattice mode C <sub>Ring</sub> -N-C <sub>Ring</sub> (Bipolarons-protonated, spinless units)	49-51,71 69,70
438	422	420	C-N-C-Out-of-plane Torsion Out of plane ring deformation	69,72,73 52-56
533	528	520	C-N-C-Out-of-plane Torsion Out of plane ring deformation	58,72,73 52,53,55
600vw	598w	589	phenazine units (cross-linked units) oxazine/ phenoxazine ring like rings cross-linked units Azo-CN stretching and C=N=N- deformation vibration In-plane amine deformation vibration of (Bipolarons)	52,69,72,74-76 71 77 56
646 sh,w	---	657	In plane ring deformation sulfate anion (ring sulfonation)	57,58,73,78 53,56
737	732	732	Out of plane ring deformation	56,73,78,79
769sh,vw	759w	767w	Phenazine vibration in cross-linked structures	56,70,80
830	825	821	C-H out of plane 1,4-disubstituted Ring deformation C-N-C bending	73,77,78,81 58,70,79 82
877 sh,vw	868w	875	C-H out of plane deformation vibrations substituted Phenazine Cross-linked structures Ring deformation C-N+-C Wag Wag out of Out-of-plane	77 80 53,70,72 73,78
1188	1185	1178	cm-1 C-H bending Aromatic in plane deformation C-H Aromatic in plane deformation (1,4 di-substituted)	57,69,70,80 77,81
1243	1238		C-N stretching (Amines)	57,82-85
1272	1267	1260	C-N stretching in polaronic units	70,72,86
1389	1380	1377	C-N+• stretching- polaronic species	54,74-76
1501	1500	1489	vC=N stretching (Q- Imimes)	52,57,70,74,80
1513	1511	1508	N-H bending	53,70,80
		1546w	Phenazine, safranin or phenoxazine-like segments	72,87
1596	1589	1586	vC=C stretching (Q)	52,82,83,88
1608	1603	1600	vC-C stretching (B)	57,81,83,88
1643vw	1643vw	1643	Cross-linked phenazine, or other aromatic, units	54,74,89

### 3.4.1.2. Cross-linked Polyaniline Structures: Region I (400-1000 $\text{cm}^{-1}$ )

Raman spectroscopy indicated that polyaniline chains may contain significant cross-linking contingent upon synthesis approach, reaction conditions, and any further treatments.<sup>21,74,75,90</sup> Different structures have been proposed for cross-linked segments that represent a heterocyclic ring formed via inter- or intrachain reactions, as previously suggested by Raman studies.<sup>71,74,75,86,91,92</sup> It was reported that polyaniline with cross-linked chains appears to show an intermediate optimum with respect to conductivity.<sup>21</sup> Lower conductivity is observed for a shorter conjugation length and localization of polarons.<sup>21,90</sup> Therefore, the impact of the synthesis approach on cross-linking must be understood to correlate polymeric structure to electrical behavior.

Normal modes related to ring deformations<sup>52-56</sup> (radial, skeletal vibrations) are expected to occur together with select C-H out-of-plane vibrations<sup>73,78,81</sup> and C-N-C stretches in all polyaniline samples analyzed. Vibrations within this wavenumber range are specially modified by the presence of substituents<sup>87</sup> and cross-linking.<sup>71,74,75,86,91,92</sup> Table 3.1 indicates that our band assignments are in general agreement with the literature as shown in Figure 3.1(b).

The advantage of utilizing the solvent-limited approach, in terms of the chemical structure of prepared polyaniline, is shown in Figure 3.1(b). It was found that SF shows the lowest extent of cross-linking as well as the most linear structure relative to CF and CS.

The CS spectrum presents bands showing unique cross-linking relative to the SF and CF spectra: *i.e.*, the relatively strong band at 589  $\text{rel. cm}^{-1}$  appears and belongs to the substituted phenazine structures/ cross-linking units<sup>4, 7, 9, 17-20</sup> and/or oxazine/phenoxazine rings or cross-linked units.<sup>71</sup> This band appears at reduced intensity in CF and only appears as a weak

shoulder in SF. Moreover, the relatively strong band at 875  $\text{rel. cm}^{-1}$  appears in CS spectra and is assigned to substituted phenazine structures/cross-linking.<sup>77</sup> This band also appears with lower intensity in CF and as a weak shoulder in SF. As mentioned previously, cross-linking leads to shortening the conjugation length and hence the localization of polarons for a lower conductivity.<sup>90,93</sup> These spectroscopic observations confirm the lower conductivity of CS polyaniline samples.

#### **3.4.1.3. Electronic Structure of Polyaniline: Region II (1100-1700 $\text{cm}^{-1}$ )**

Figure 3.1(b) spans the range between 1100 and 1650  $\text{rel. cm}^{-1}$  and is primarily comprised of C-N stretching, aromatic stretches, and C-H bending modes. The different vibrational modes were analyzed separately. First, the C-H bending modes between 1100 and 1220  $\text{rel. cm}^{-1}$  (Region II-A) were analyzed followed by the C-N stretching modes (i.e., amines, imines, polarons) between 1220 and 1650  $\text{rel. cm}^{-1}$ . Finally, the C=C ring stretches between 1520 and 1650  $\text{rel. cm}^{-1}$  (Region II-B) were analyzed. For the 1100-1220  $\text{rel. cm}^{-1}$  and the "polaronic" 1300-1400  $\text{rel. cm}^{-1}$  regions, Raman bands were decomposed assuming a Gaussian–Lorentzian line shape where the band area was used to interrogate the relative abundance of distinct vibrations.<sup>61</sup>

#### **3.4.1.4. Average Oxidation Level from C-H Bending: Region II–A (1100 and 1220 $\text{cm}^{-1}$ )**

The C-H bending vibrations are the most external functional groups with respect to the polymer chain and are consequently less perturbed by charge fluctuations on the nitrogens than the C-C vibrations.<sup>61</sup> Therefore, the most straightforward assessment of ring oxidation level is obtained from these modes.<sup>60,94</sup> Three polyaniline base forms are distinguishable by the width and location of the C-H bending mode: leucoemeraldine, emeraldine, and pernigraniline.<sup>73,95</sup> The 1189 and 1165  $\text{cm}^{-1}$  bands are assigned to the polaron lattice and

bipolaronic form, respectively.<sup>96</sup> A red shift (*viz.*, increase in  $\text{rel. cm}^{-1}$ ) in the C–H bending vibration is characteristic of a strongly charged chain<sup>94</sup> and an electronic structure consisting mainly of polaron species. In other words, conductivity in polyaniline forms is maximized where bipolaronic species are minimized.<sup>61</sup> Therefore, the C-H bending mode gives essential information about the possible electronic structures, *i.e.*, the “polaron lattice” and “bipolaronic” forms available in polyaniline samples.<sup>60,61</sup> Furthermore, a broad bandwidth indicates the possible coexistence of different forms (benzenoid/quinoid). To extract this information, one can attempt to resolve the C-H bands numerically where the area is allocated to the individual benzenoid and quinoid contributions. The ratio of the quinoid and benzenoid band areas to the total C-H band area is then used to estimate the extent of polymer oxidation.<sup>60,61</sup>

Figure 3.2 shows the Gaussian-Lorentzian curve fitting for the C-H band of polyaniline samples SF, CF, and CS only for the purpose of relative comparison between sample types, noting that there is no direct validation for quantitative Raman cross-sections. The SF samples achieved the optimum oxidation level ( $A_{\text{benzenoid}}/A_{\text{total}}$ ) of 0.49 for the three samples, thus explaining the relatively high conductivity with respect to CF and CS. CF and CS achieved lower oxidation levels with an estimated areal ratio of 0.43 and 0.38, respectively. The observed band maxima of the three samples were 1188, 1185, and 1178  $\text{cm}^{-1}$ , corresponding to SF, CF, and CS, respectively. These red shifts further indicate that SF preparation results in a more strongly charged chain (on average) than CF, and CS. In other words, the increased prevalence of polaron electronic structures in SF is evident. These results add further support to the structure-property behavior identified in the 400-1000  $\text{cm}^{-1}$  region: *i.e.*, ES-II

predominates in SF, and the CS approach leads to a polyaniline with predominately ES-I structure.

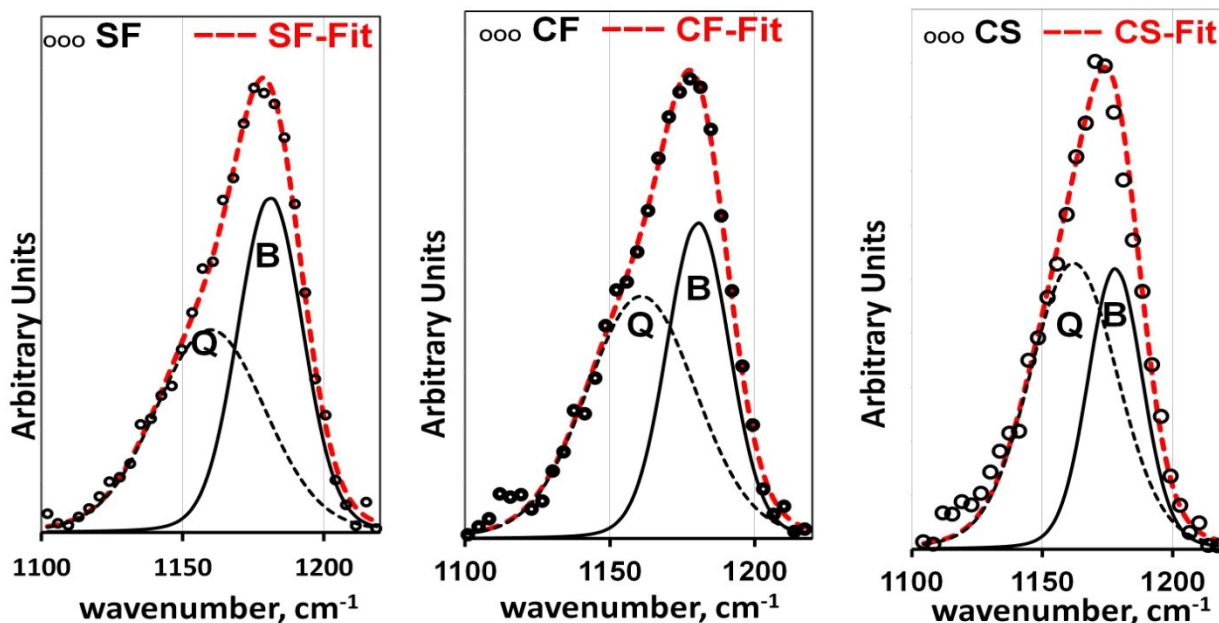


**Figure 3.2.** Gaussian-Lorentzian curve fitting for the C-H band (1100-1220 rel.  $\text{cm}^{-1}$ ) of polyaniline samples SF, CF, and CS.

#### 3.4.1.5. Organization of Charge and Oxidation on the Chain: Region II–B (1220 and 1650 $\text{cm}^{-1}$ )

Raman spectroscopy can be highly sensitive to small structural or electronic alterations.<sup>97</sup> In conducting polymers with strong electron–lattice coupling, the dopant–polymer charge transfer results in the creation of defects such as solitons, polarons, and bipolarons.<sup>98-100</sup> Polaronic lattice and bipolaronic defects can be selectively interrogated via the vibrational study of the radical cation (polaron) and dication (bipolaron) of certain model compounds.<sup>85</sup> Conducting polymers usually show electronic absorptions due to self-localized excitations in the region from visible to near-infrared. It is probable that the C-N stretching mode is the key band that could indicate the delocalization of charge.<sup>85</sup> It was reported that the vibrational

analysis of some conjugated polymers, combined with a model compound approach, yielded evidence that the nature and the ratio of the major species (polarons and/or bipolarons), which are generated by dopants within the polymeric chain, depend on the extent of doping.<sup>60,61,85</sup>

The observed vibration at 1600-1608  $\text{cm}^{-1}$ , characterizes the C-C stretching of the benzene ring<sup>57,81,83,88</sup>, while the shoulder at 1586-1596  $\text{cm}^{-1}$  is associated with C=C stretching of the quinone ring.<sup>52,82,83,88</sup> The observed maximum at 1508-1513  $\text{cm}^{-1}$  is likely assigned to N-H bending.<sup>53,70,80</sup> Overall, the CS bands are broader than SF and CF bands. In fact, these very broad bands contain several components each with distinct chemical and/or electronic structures.<sup>49</sup>

On the other hand, SF bands are the narrowest possibly indicating well-defined structures. A weak band is also observed at 1643  $\text{cm}^{-1}$  and was assigned to cross-linked units<sup>54,74,89</sup> such as phenazine.<sup>56,69,76</sup> This band is observed in the CS spectrum, which further supports cross-linking in CS. A weaker shoulder in the CF spectrum is present indicating some cross-linking behavior possibly to a lesser extent than CS.

An interesting broad band region (1300-1400  $\text{cm}^{-1}$ ) is observed for the three samples shown in Figure 3.3. This broad band region was decomposed under the assumption that at least three smaller bands were contained within it.<sup>61</sup> Based on the literature, it was possible to assign these three bands to the main electronic structures (polaron and bipolaron) found in polyaniline samples where structural heterogeneity was expected.<sup>61,101,102</sup> These three components were centered at: 1320-1327, 1344-1348, and 1374-1388  $\text{cm}^{-1}$  as shown in Figure 3.3.

An additional Gaussian-Lorentzian component at  $1400\text{ cm}^{-1}$  appears in CS and CF samples and indicates the formation of cross-linkages.<sup>54,55,70,72,80</sup> This supports band assignments in Region I indicating CS-PAN is likely the most cross-linked of the three types.

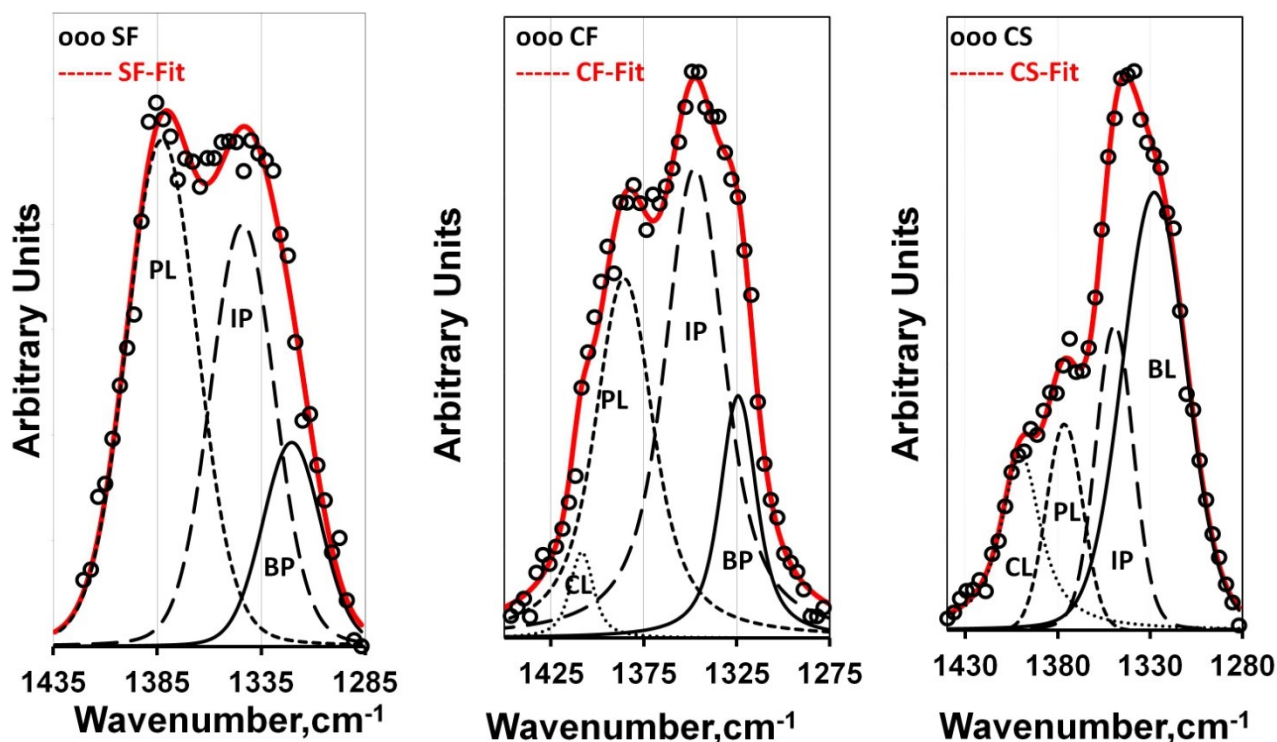


**Figure 3.3.** Decomposition of the polaron band region  $1300\text{-}1400\text{ cm}^{-1}$  of polyaniline samples (a) SF, (b) CF, and (c) CS.

The band observed at  $1375\text{-}1385\text{ cm}^{-1}$  could be assigned to delocalized polaron structure (polaron lattice)<sup>74,85,103-108</sup> and represents the dynamic structure of the free charge carriers. These structures correspond to the electronic absorption characteristic of metallic polyaniline (1 eV).<sup>106</sup> The reported disappearance of this band with very high doping level<sup>58,73,78</sup> confirms its assignment to polaron: *i.e.*, it is possible that a fraction of the polarons initially present in the polymer were converted to bipolarons<sup>109,110</sup> during the formation of heavily doped polyaniline.<sup>64,65</sup> Furthermore, this band is associated with an expanded coil conformation<sup>51,111</sup>

which fosters polaron delocalization and explains the high conductivity.<sup>73,78</sup> Indeed, its presence supports the observed conductivity trends associated with these polyaniline samples.<sup>21</sup>

The loss of long-range crystalline organization allows the trapping/localization of the polarons. Additionally, if phenazine is formed it can be protonated which leads to interchain isolated polarons and a subsequent localization of the electronic state and, hence, a loss in its metallic character.<sup>1</sup> The possible contribution of isolated polarons within the broad polaronic band region (1300-1400  $\text{cm}^{-1}$ ) was assigned to the observed band at 1344-1348  $\text{cm}^{-1}$ .<sup>1,112-116</sup> The association of isolated polarons with bipolaron and/or polaron lattice structures is common.<sup>1</sup> Also, the existence of short conjugation could also be assigned to this band.<sup>58,70,72,75,117</sup> The possible contribution of cross-linked structures could be confirmed if other cross-linking bands are observed. Regardless, short conjugation is expected due to the presence of defects, disorder,<sup>1</sup> and/or cross-linking.<sup>21,90</sup>

Since polarons and bipolarons are almost degenerate and consequently in thermodynamic equilibrium,<sup>110</sup> it was expected to observe a bipolaronic vibration within the broad polaronic band region. The observed band at 1320-1327  $\text{cm}^{-1}$  is assigned to bipolaronic structures.<sup>73,85,94,95,118</sup>

The relative existence of an electronic species (polaron/bipolaron) was determined in order to estimate the predominant electronic species present in each sample. Table 3.2 shows the different possible electronic structures of polyaniline samples SF, CF, and CS obtained using a semiquantitative analysis of the broad polaronic band region (1300-1400  $\text{cm}^{-1}$ ). The predominate electronic structures of polyaniline synthesized using the SF and CF approaches

are polaronic with polaron vibrations occupying 86% and 90% of the total broad band area, respectively.

The higher conductivity of SF is correlated to the fact that 64% of the band area corresponding to SF PAN comprises delocalized forms ( $\text{Area}_{\text{BL}} + \text{Area}_{\text{PL}} / \text{Area}_{\text{Total}}$ ) relative to only 44% delocalization seen in CF. Since delocalization of polaron corresponds to the presence of free carriers in high spin species,<sup>108</sup> the magnitude of conductivity in a conducting polymer depends upon the extent of the charge carrier (delocalization polaron) as well as the polaron mobility and the presence of structural disorder such as non-head-to-tail coupling defects.<sup>59</sup> Moreover, CF has relatively lower crystallinity,<sup>21</sup> which may be the second reason for lower conductivity of CF even though it has predominately polaron electronic structures.

**Table 3.2.** Different Possible Electronic Structures of Polyaniline Samples SF, CF, and CS Obtained by Semiquantitative Analysis Results of the Decomposition of the Polaron Band ( $1300\text{-}1400\text{ cm}^{-1}$ )

		<i>SF</i>	<i>CF</i>	<i>CS</i>	<i>Assignment</i>	<i>Ref.</i>
<i>Bipolarons (BL)</i>	$\nu\text{ (cm}^{-1}\text{)}$	1320	1322	1327	$\nu(\text{C} - \text{N}^{+\blacksquare})$ (bipolaron)	73,85,94,95,118
	Area	0.16	0.1	0.5		
<i>Isolated polarons (IP)</i>	$\nu\text{ (cm}^{-1}\text{)}$	1344	1346	1348	$\nu(\text{C} - \text{N}^{+\blacksquare})$ isolated polarons Phenazine Shorter and/or crosslinked structures	1,112-116 80,119 58,70,72,75,117
	Area	0.36	0.5	0.2		
<i>Polarons Lattice (PL)</i>	$\nu\text{ (cm}^{-1}\text{)}$	1382	1388	1374	$\nu(\text{C} - \text{N}^{+\blacksquare})$ Polaron lattice Electron delocalized Extended coil segments	74,85,103-108 107,111,120 51,111
	Area	0.48	0.4	0.2		
<i>Cross-linking (CL)</i>	$\nu\text{ (cm}^{-1}\text{)}$	-----	---	1400	1394 – 1410 $\text{cm}^{-1}$ phenazine	53-55,70,72
	Area	-----	---	0.1		

Finally, the C-N stretch at  $1228\text{-}1268\text{ cm}^{-1}$  (Figure 3.1b) is, in fact, two modes centered at  $1228\text{-}1238\text{ cm}^{-1}$  and  $1226\text{-}1268\text{ cm}^{-1}$  corresponding to amines<sup>57,82-85</sup> and polaronic units,<sup>70,72,86</sup>

respectively. For the CS sample, a broad C-N band at  $1260\text{ cm}^{-1}$  (possibly the result of many C-N environments) is observed, residing in between the amines and “polaronic units” bands reported.

On the other hand, CF and SF have two resolved bands. This is attributable to these samples having predominately polaronic units as suggested by the semiquantitative analysis presented in Table 3.2. Using Table 3.2 again as a qualitative guide, more heterogeneity is observed for CS where a different predominance of polaronic units (50% bipolaron band area) coexist with the other polaronic units, including substantial cross-linking contribution. The formation of the bipolaronic structure concentrates charge on imine sites and leaves the amine sites free of charge within the polaron lattice structure: *i.e.*, charge is delocalized at all sites.<sup>61</sup> This might partially explain the inability to clearly resolve the C-N stretches as well as explain the relative complexity of the band at  $\sim 1260\text{ rel. cm}^{-1}$ .

Overall, Raman spectroscopy indicates that the CS approach produces polyaniline with a predominately bipolaron electronic structure relative to other polaronic species. This observation agrees with the low wavenumber Raman spectrum of CS, which has ES-I lattice vibrations, predominated by a spinless charged bipolaron structure.<sup>68</sup> The observed cross-linking band at  $1400\text{ cm}^{-1}$  further suggested that the contribution of cross-linking within the isolated polaron band may have led to an increasing percentage of bipolaron electronic structure. In this particular case, slow polymerization of polyaniline produced no noticeable change in the temperature of the reacting mixture, which is favorable for higher molecular weight<sup>92</sup> and more cross-linking.<sup>21</sup> Relatively longer chains may not have been fully protonated, and hence the complete polaron delocalization through the chain may have been hindered<sup>108</sup> leading to shorter conjugation and more polaron localization. This phenomenon

is favorable to form bipolarons.<sup>76</sup> To the best of our knowledge, this study demonstrated ES-I polyaniline formation using an extremely slow oxidation method.

These Raman results show that the solvent-limited approach (SF) leads to ES-II polyaniline with the most linear and fewest number of cross-links relative to the other synthesis approaches tested, as indicated previously. The particular structure that results from SF synthesis is more beneficial to electrical conductivity<sup>121</sup> as polaronic species favor longitudinal charge transfer.<sup>122</sup> Polaron conductivity results from the formation of a polaron lattice with a half occupied polaron band.<sup>123</sup> On the other hand, the CS approach leads to cross-linked structures with cross-linked bipolaronic species and, as a consequence, has low conductivity.<sup>122</sup>

#### **3.4.2. Conformation and Electronic Band Structure Dependence on Synthesis Approach**

In addition to elucidating the possible chain conformations, the features of the polaron, bipolaron, and polaron lattice electronic structures are probed via the electronic absorptions in the region from visible to near-infrared. The primary aim of utilizing UV-vis spectroscopy for these polyaniline samples is to: identify electronic structure(s), investigate the relative conformational differences between the SF, CS, and CF synthesized PAN, and confirm the interpretations derived from Raman spectroscopy (Figure 3.3 and Table 3.2). In general, UV-vis spectra of the polyaniline samples can be roughly divided into four main absorbance contributions as shown in Figure 3.4 and summarized in Table 3.3. The observed absorption band around 430 nm is assigned to the existence of a polaron electronic transition in doped polyaniline which is caused by the presence of radical cations.<sup>30,59,110,122,124-131</sup> This absorption band refers to possible extended coil conformation segments present in polyaniline samples.<sup>132</sup>

Note that this band is observed in the three polyaniline samples with the sharpest and best resolved being in SF spectra as shown in Figure 3.4.

In all likelihood, the polaron in SF-synthesized PAN is the most organized where the possibility of forming a polaron lattice is discussed upon further scrutiny of the UV-vis spectra.

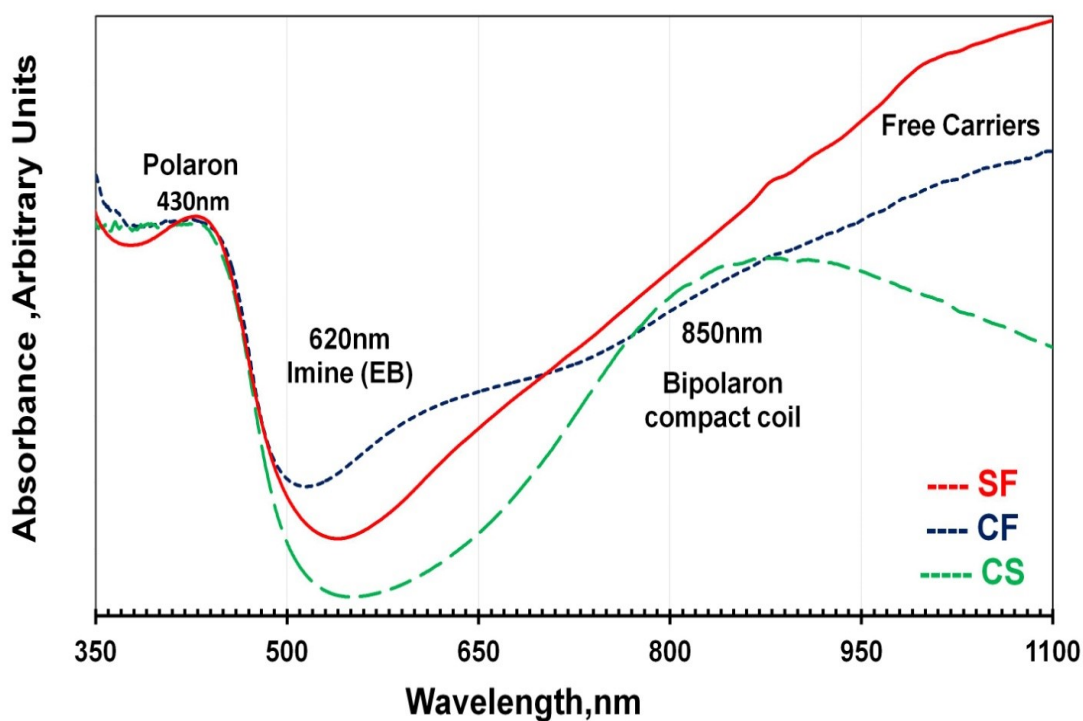


**Figure 3.4.** UV-visible spectra of polyaniline samples (CS, CF, and SF) in *m*-cresol.

On the other hand, this band appears as possibly a broad-shoulder on an adjacent, out-of-range electronic mode in the CF and CS spectra (<350 nm). Taking into account the broadening of the polaron band and previously recorded evidence of bands not-resolved in these spectra,<sup>1</sup> it is probable that different structures, such as isolated polaron, may coexist. In fact, the presence of isolated polaron supported the predicted electronic structure of CF and

CS identified in the previous Raman spectra, *i.e.*, the higher extent of charge localization (isolated polaron) with respect to polarons in CF and CS might be the primary reason for polaron band broadening (Table 3.2, row 3; Figure 3.3). Under these circumstances, a "true polaron lattice" cannot be formed in the CF and CS synthesized PAN which, according to their relative lower conductivity, is consistent with the presence of the predominant random polaron and bipolaronic species. On the contrary, a certain fraction of SF synthesized PAN likely contains the conductive polaron lattice. In general, however, this is only the case when ring moieties are in the polaron configuration in addition to other factors that will be discussed later. It must be emphasized that the presence of polaron in CF and CS synthesized PAN does not guarantee an established polaron lattice.<sup>76</sup>

**Table 3.3.** Bands Assignments of UV-visible spectra of polyaniline samples (CS, CF, and SF) in *m*-cresol.

Absorption band	Assignment	Ref.
<b>430 nm</b>	Polaron transition doped PAN	30,59,110,122,124-131
	Extended coil conformation segments	132
<b>620 nm</b>	Quinonoid segments	52,102,122,133
<b>850 nm</b>	Bipolaron state	59,122,134
	Localized polaronic species	110,129,132,135-141
	Localized polaronic species + compact coil conformation	132,137-141
	Compact coil conformation emeraldine salt	30,132,137-141
	ES-I strong localized polaron	135
<b>&gt;950 nm</b>	Free carrier tails	110,133,141
	Expanded conformation of polyaniline chains	133

The observed band in CF PAN at 620 nm is attributed to  $\pi$ - $\pi^*$  transition of standard PAN base.<sup>70,92,142</sup> Specifically, it is usually ascribed to an exciton, located in the quinoid ring (Q), arising from charge transfer from the adjacent benzenoid rings, with each side contributing half an electron on average.<sup>52,102,122,133</sup> This weak band was distinctly observed in CF spectra

and represents the possible coexistence of unprotonated quinone diamine species.<sup>122</sup> Additionally, it could be an indication for a relatively lower extent of protonation/doping in CF PAN. Its presence might indicate a second possible reason for CF PAN's relatively low conductivity (in addition to the possible significant charge localization of CF due to isolated polarons).

The higher wavelength band observed at ~850 nm indicates significant electronic differences between polyaniline samples. This band is likely contingent upon the existence of dicationic, bipolaron electronic transitions in doped polyaniline,<sup>59,122,134</sup> and/or is caused by localized polaronic species<sup>110,129,132,135-141</sup> with shorter conjugation length.<sup>138</sup> This band appears only in the CS samples, which represents a significantly strong charge localization which may transition to bipolaron depending on synthesis conditions.<sup>76,109</sup> If correct, this band indicates that a polaron transition is favorable in the CS synthesized PAN relative to the other synthesis approaches. Additionally, this band can be attributed to a compact coil conformation of the segments in doped polyaniline,<sup>30,132,137-141</sup> which has been shown to lead to lower conductivity.<sup>139-141</sup> Most notably, the existence of this band in CS confirms its proposed electronic structure and polymorphism obtained via the RS analysis and interpretation. Specifically, the 850-nm band indicates the significant occurrence of bipolaron electronic structures in CS whereas bipolaronic lattice vibrations (ES-I) were observed in the Raman spectra of CS as well.<sup>135</sup> Furthermore, the 850 nm band might support the possibility of cross-linking that was observed when polyaniline contains cross-linked bipolaronic species.<sup>122</sup>

The "free carrier tail," characteristic of metallic conductive materials (delocalization of electrons), is observed above 950 nm.<sup>110,133,141</sup> It is quite telling that the steady increase of free carrier tail in SF was much more pronounced than the CF spectra. This is a very clear

indication of a lower extent of charge delocalization in CF than SF. The relatively dramatic increase in absorbance can be considered a third reasonable explanation for the relatively higher conductivity of SF-PAN. This observation likely explains the order of magnitude differences in conductivity in spite of the general similarities expected for PAN UV-vis spectra.

Moreover, this region can also be attributed to the expanded conformation of polyaniline chains,<sup>133</sup> indicating that SF and CF have a more expanded conformation (on average). It has been previously shown that the delocalization of the polaron along the polyaniline chain in this extended coil conformation results in an enhanced electrical conductivity.<sup>30</sup> Note that the end of the free carrier tail decreases in CS indicating carrier mobility loss.<sup>143</sup> This further confirms a strong charge localization and an increased incidence of compact coil conformations. Furthermore, the presence of cross-linking can induce some nonplanar conformations (more compact coil) that decrease the conjugation length along the polymer backbone owing to an increase of the steric hindrance.<sup>144</sup> UV-vis thus reveals a decrease of the degree of conjugation and hence a dramatic, and initially unexpected, decrease of the conductivity of CS PAN.

Based on the UV-vis spectra, doped polyaniline samples have different electronic structures, which were attributed to differences in conformational structures, resulting from the synthesis approach used. It is clear that polaron is the predominant species in SF and CF. CS spectra show significant indications of localized polaron/bipolaron species which are in firm agreement with the RS analysis and interpretation. Free carriers, corresponding to electron delocalization, were observed in CF and SF UV-vis spectra with a more pronounced presence in SF spectra. In contrast, free electronic absorptions begin to decline as a function

of increasing wavelength in CS. This behavior also agrees with the RS interpretations. The CS approach leads to compact coil conformation, in contrast to SF and CF approaches, which lead to a more extended coil and consequently higher conductivity.<sup>132</sup>

Figure 3.5 shows the proposed band structures of doped polyaniline. Here, the localized polaron/bipolaron model for compact coil conformation (CS sample) and delocalized polaron lattice model for expanded coil conformation in the SF and CF samples are presented.

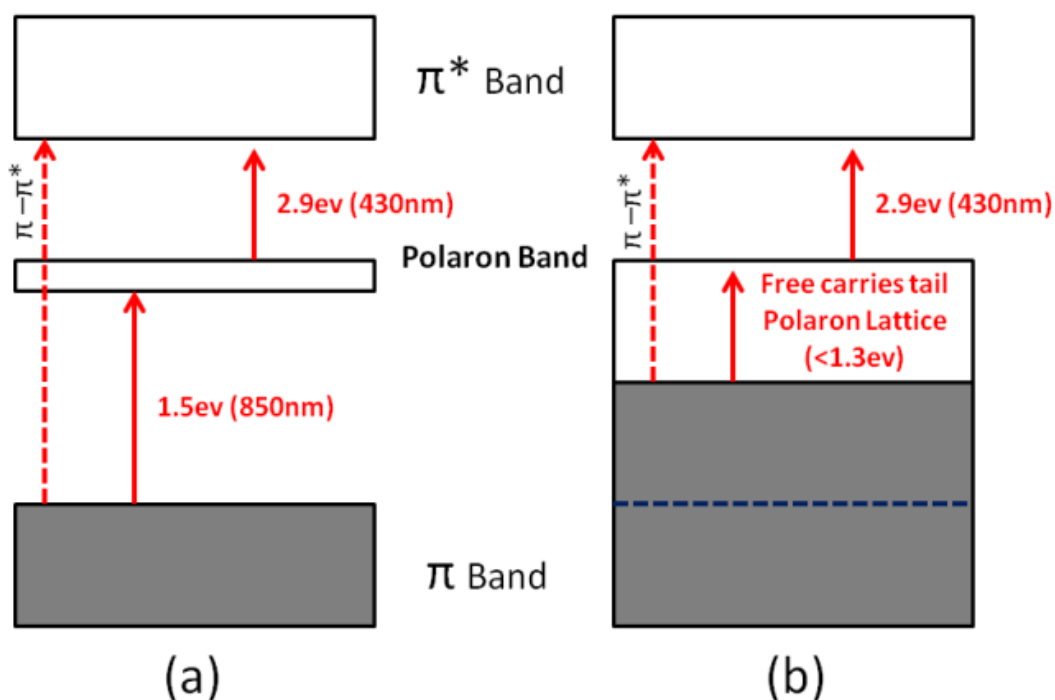


**Figure 3.5.** Proposed band structures of doped polyaniline sample. (a) Localized polaron/bipolaron model for compact coil conformation in the CS sample. (b) Delocalized polaron (polaron lattice) model for expanded coil conformation, SF and CF samples.

This difference in electronic structure can be attributed to their difference in conformation structures as influenced by a synthesis pathway. It has been suggested that HCl-doped polyaniline polymer chains synthesized via the slow oxidation approach lead to a compact coil-like conformation (Figure 3.5(a)). According to prior research, this supports an increase

in nonlinear chains due to the presence of cross-linking structures.<sup>92,145</sup> This leads to isolated polaron chains due to twist defects between aromatic rings.<sup>141</sup>

The slower oxidation encountered via the CS synthesis pathway may be favorable for compact coil generation due to extensive cross-linking and branched PAN structures. Branching behavior may imply that PAN chains grow sequentially from existing chains which results in a higher probability of generating anisotropic, structural defects. This directly impacts the bulk electrical and electronic behavior.<sup>90,92</sup>

It could be suggested that HCl-doped polyaniline polymer chains synthesized via the fast oxidation approach tend to have expanded coil-like conformation (Figure 3.5(b)). Our results indicate that this occurs to a lesser extent than SF. This would explain their similar UV-vis electronic behavior. However, due to the previous three explanations more charge localization, lower protonation/doping, and lower free carrier tail absorbance, CF has not achieved the necessary polaron organization required to facilitate the electron delocalization needed for high conductivity. It is possible to assume that the free carrier band energy of SF is lower than CF.

In general, the band gap structure for CF and SF should have a half-filled polaron band that is formed by the interaction between separate polarons (Figure 3.5(b)). These structure dependences explain the observed optical and electrical properties for the doped polyaniline samples when chains have an extended conformation with minimal twist defects between aromatic rings. Hence, the interaction between the adjacent polarons, therefore, becomes stronger, and the polaron band becomes more dispersed energetically (that is, more delocalized).<sup>146</sup> In both proposed band gap structures, it was interesting to note that the  $\pi -$

$\pi^*$  transition band did not show up in all sample spectra, which could be attributed to broadening of the polaron band at 430 nm<sup>143</sup> as in CS, or it may become very weak and finally disappears possibly because the energy gap between the  $\pi$  band and the polaron band has been eliminated,<sup>146</sup> as in CF and SF. Note, the above assumption concerning conformational change dependence on synthesis approach was consistent with the previously reported conductivity measurements.<sup>21,141</sup>

On the basis of the results of the UV-vis spectra, it was found that the solvent-free and fast oxidation approaches have different electronic structures and conformation than the slow oxidation (CS) approach. The differences in electronic structure can only be attributed to differences in geometric structure within the polymer chain.<sup>141</sup> Sterically-induced valence band narrowing may be a localized electronic phenomenon.<sup>147</sup> When the polymer chains become more like an expanded coil, the polaron band becomes more delocalized, and the carrier mobility and hence the intrachain conductivity increase.<sup>141</sup>

### 3.5. Conclusions

This work highlighted the impact of a solvent-free (SF) synthesis approach on chemical, electronic, and conformational characteristics of HCl-doped polyaniline (PAN) nanopowders compared to conventional oxidation processes for rapid and slow polymerizations. The synthesis of SF-PAN in a slightly wetted solid-phase reaction provided substantial property improvements over conventional solution-rich oxidations using limited or abundant oxidizer. Moreover, PAN polymorphism was significantly affected by the synthesis approach used and thus may be controlled within a certain fine-tuning range for nanopowder products. It was found that the SF approach leads to PAN emeraldine chloride salts of type ES-II, which has a

significant impact on electrical properties of PAN and may favor achieving high electromagnetic (EM) shielding potential—a long-term goal of our research efforts.

Synthesis protocols that lead to compact coils in HCl-doped PAN with cross-linked structures or branched chains (e.g., conventional slow oxidation) are not expected to produce high conductivity or good EM shielding. Further, the evidence for branching and/or cross-linking in the conventional approaches with solvent-rich reactions implies that the solvent-limited synthesis method is closer to a neat, single-reaction type polymerization with its high linearity polymer product. This tentatively suggests the best homogeneity for SF products. Thorough characterization with the current chemical details herein is expected to demonstrate the importance of tuning delocalized polaron electronic structure relative to a bipolaron and/or localized polaron when attempting to enhance average response for EM applications using nanopolyanilines. Optimizing the SF approach for particular solvent-limited conditions toward well-defined polymer needs for conductivity and conformational structures shows inherent promise for future work toward various technological applications.

### 3.6. References

- (1) Nalwa, H. S. *Handbook of Organic Conductive Molecules and Polymers 3, Conductive Polymers: Spectroscopy and Physical Properties*; Wiley: Chichester; New York, 1997; Vol. 3.
- (2) Wan, M. *Conducting Polymers with Micro or Nanometer Structure*; Tsinghua University Press ; Springer: Beijing; Berlin, 2008.
- (3) Jadhav, S. V.; Vijaya, P. Microwave Absorption and Permittivity of Polyaniline Thin Films Using Overlay Technique *Microelectronics Journal* **2008**, *39*, 1472-1475.
- (4) Qiu, H.; Li, H.; Fang, K.; Li, J.; Mao, W.; Luo, S. Micromorphology and Conductivity of the Vacuum-Deposited Polyaniline Films *Synt. Met.* **2005**, *148*, 71-74.
- (5) Xia, H.; Wang, Q. Ultrasonic Irradiation: A Novel Approach to Prepare Conductive Polyaniline/Nanocrystalline Titanium Oxide Composites *Chem. Mater.* **2002**, *14*, 2158-2165.
- (6) Bhadra, S.; Khastgir, D.; Singha, N. K.; Lee, J. H. Progress in Preparation, Processing and Applications of Polyaniline *Prog. Polym. Sci.* **2009**, *34*, 783-810.
- (7) Li, D.; Huang, J.; Kaner, R. B. Polyaniline Nanofibers: A Unique Polymer Nanostructure for Versatile Applications *Acc. Chem. Res.* **2008**, *42*, 135-145.
- (8) Saraswat, A.; Sharma, L. K.; Singh, S.; Singh, R. Electrochemical Assisted Synthesis and Characterization of Perchloric Acid-Doped Aniline-Functionalized Copolymers *Synth. Met.* **2013**, *167*, 31-36.
- (9) Zhang, Y.; Wang, Z.; Ye, W.; Qian, H.; Lin, Z. Enhancement of Polyaniline's Electrical Conductivity by Coagulation Polymerization *Colloid. Polym. Sci.* **2013**, 1-8.

- (10) Abdiryim, T.; Xiao-Gang, Z.; Jamal, R. Comparative Studies of Solid-State Synthesized Polyaniline Doped with Inorganic Acids *Mater. Chem. Phys.* **2005**, *90*, 367-372.
- (11) Kulkarni, M. V.; Charhate, N. A.; Bhavsar, K. V.; Tathe, M. A.; Kale, B. B. Development of Polyaniline-Multiwalled Carbon Nanotube (Pani-Mwcnt) Nanocomposite for Optical Ph Sensor *Mater. Res. Innovations* **2013**, *17*, 238-243.
- (12) Ju, Q.; Shi, Y.; Kan, J. Performance Study of Magnesium-Polyaniline Rechargeable Battery in 1-Ethyl-3-Methylimidazolium Ethyl Sulfate Electrolyte *Synth. Met.* **2013**, *178*, 27-33.
- (13) Zhao, Y.; Si, S.; Liao, C. A Single Flow Zinc//Polyaniline Suspension Rechargeable Battery *J. Power Sources* **2013**, *241*, 449–453.
- (14) Louis, D.; de Poncharra, J. d. P. Microelectronic Device Provided with an Array of Elements Made from a Conductive Polymer with a Positive Temperature Coefficient; US Patent 8,421,230, 2013.
- (15) Xiang, C.; Zou, Y.; Qiu, S.; Sun, L.; Xu, F.; Zhou, H. B. Enzymatic Glucose Biosensor Based on Direct Electrochemistry of Cytochrome C on Gold Nanoparticles/Polyaniline Nanospheres Composite *TALANTA* **2013**, *110*, 96–100.
- (16) Mazeiko, V.; Kausaite-Minkstiniene, A.; Ramanaviciene, A.; Balevicius, Z.; Ramanavicius, A. Gold Nanoparticle and Conducting Polymer–Polyaniline–Based Nanocomposites for Glucose Biosensor Design *Sens. Actuators, B* **2013**.
- (17) Khan, R.; Radhapyari, K.; Das, M. R.; Kotoky, P. Graphene-Polyaniline Nanocomposite Based Biosensor for Detection of Antimalarial Drug Artesunate in Pharmaceutical Formulation and Biological Fluids *TALANTA* **2013**, *111*, 47–53.

- (18) Jaymand, M. Recent Progress in Chemical Modification of Polyaniline *Prog. Polym. Sci.* **2013**, *38*, 1287–1306.
- (19) Kulkarni, M. V.; Kale, B. B. Studies of Conducting Polyaniline (Pani) Wrapped-Multiwalled Carbon Nanotubes (Mwcnts) Nanocomposite and Its Application for Optical Ph Sensing *Sens. Actuators, B* **2013**, *187* 407–412.
- (20) Liu, C. Y.; Chou, J. C.; Liao, Y. H.; Yang, C. J.; Huang, C. J.; Cheng, T. Y.; Hu, J. E.; Chou, H. T. “The Investigation of the Electrochromic Characteristics for the Pani Thin Film by Cyclic Voltammetry and Potentiostatic Method”; Proceedings of the World Congress on Engineering, 2013.
- (21) Tantawy, H. R.; Aston, D. E.; Smith, J. R.; Young, J. L. A Comparison of Electromagnetic Shielding with Polyaniline Nanopowders Produced in Solvent-Limited Conditions *ACS Appl. Mater. Interfaces*, **2013**, *5*, 4648–4658.
- (22) Wang, W.; Gumfekar, S. P.; Jiao, Q.; Zhao, B. Ferrite-Grafted Polyaniline Nanofibers as Electromagnetic Shielding Materials *J. Mater. Chem. C* **2013**, *1*, 2851-2859.
- (23) Saini, P.; Choudhary, V. Enhanced Electromagnetic Interference Shielding Effectiveness of Polyaniline Functionalized Carbon Nanotubes Filled Polystyrene Composites *J. Nanopart. Res.* **2013**, *15*, 1-7.
- (24) Oyharcbal, M.; Olinga, T.; Foulc, M.-P.; Lacomme, S.; Gontier, E.; Vigneras, V. Influence of the Morphology of Polyaniline on the Microwave Absorption Properties of Epoxy Polyaniline Composites *Compos. Sci. Technol.* **2013**, *74*, 107-112.
- (25) Ting, T.-H.; Wu, K.-H. Synthesis and Electromagnetic Wave-Absorbing Properties of Batio<sub>3</sub>/Polyaniline Structured Composites in 2–40 Ghz *J. Polym. Res.* **2013**, *20*, 1-6.

- (26) McManus, P. M.; Cushman, R. J.; Yang, S. C. Influence of Oxidation and Protonation on the Electrical Conductivity of Polyaniline *J. Phys. Chem.* **1987**, *91*.
- (27) Wang, Y.; Jing, X. Intrinsically Conducting Polymers for Electromagnetic Interference Shielding *Polym. Adv. Technol.* **2005**, *16*, 344–351.
- (28) Sharma, A. L.; Kumar, K.; Deep, A. Nanostructured Polyaniline Films on Silicon for Sensitive Sensing of Ammonia *Sens. Actuators, A* **2013**.
- (29) Althaus, C.; Knoll, M. Digital Switching Systems Based on Lateral Self-Oxidation of Aluminum Nanofilm Processors *Electrochem. Commun.* **2013**, *29*, 75–77.
- (30) Wallace, G. G.; Spinks, G. M.; Kane-Maguire, L. A. P.; Teasdale, P. R. *Conductive Electroactive Polymers Intelligent Materials Systems*; CRC Press: Boca Raton; London; New York, 2009.
- (31) Toshima, N.; Hara, S. Direct Synthesis of Conducting Polymers from Simple Monomers *Prog. Polym. Sci.* **1995**, *20*, 155–183.
- (32) Han, M. G.; Cho, S. K.; Oh, S. G.; Im, S. S. Preparation and Characterization of Polyaniline Nanoparticles Synthesized from Dbsa Micellar Solution *Synt. Met.* **2002**, *126*, 53–60.
- (33) Zhou, C. F.; Du, X. S.; Mai, Y. W.; Liu, Z.; Ringer, S. P. Solid Phase Mechanochemical Synthesis of Polyaniline Branched Nanofibers *Synt. Met.* **2009**, *159*, 1302–1307.
- (34) Bekri-Abbes, I.; Srasra, E. Investigation of Structure and Conductivity Properties of Polyaniline Synthesized by Solid–Solid Reaction *J Polym Res* **2011**, *18*, 659–665.
- (35) Du, X. S.; Zhou, C. F.; Wang, G. T.; Mai, Y. W. Novel Solid-State and Template-Free Synthesis of Branched Polyaniline Nanofibers *Chem. Mater.* **2008**, *20*, 3806–3808.

- (36) Abdiryim, T.; Jamal, R.; Nurulla, I. Doping Effect of Organic Sulphonic Acids on the Solid-State Synthesized Polyaniline *J. Appl. Polym. Sci.* **2007**, *105*, 576-584.
- (37) Ding, Y.; Abdiryim, T.; An, S.; Nurulla, I. Effect of B-Cyclodextrin on the Solid-State Synthesized Polyaniline Doped with Hydrochloric Acid *J. Appl. Polym. Sci.* **2008**, *107*, 3864-3870.
- (38) Huang, J.; Moore, J. A.; Acquaye, J. H.; Kaner, R. B. Mechanochemical Route to the Conducting Polymer Polyaniline *Macromolecules* **2004**, *38*, 317-321.
- (39) Chowdhury, P.; Saha, B. Potassium Dichromate Initiated Polymerization of Aniline *Indian J. Chem. Technol.* **2005**, *12*, 671-675.
- (40) Li, Y.; Al-Ghamdi, A. A.; Al-Hartomy, O. A.; El-Tantawy, F.; Yakuphanoglu, F. Semiconducting Properties of Nanofiber Polyaniline Organic Semiconductor *OAM – RC* **2012**, *6*, 235-238.
- (41) Pohanish, R. P.; Greene, S. A. *Wiley Guide to Chemical Incompatibilities*, 3 ed.; Wiley: Hoboken, N.J., 2009.
- (42) Fu, Y.; Elsenbaumer, R. L. Thermochemistry and Kinetics of Chemical Polymerization of Aniline Determined by Solution Calorimetry *Chem. Mater.* **1994**, *6*, 671-677.
- (43) Stejskal, J.; Gilbert, R. G. Polyaniline. Preparation of a Conducting Polymer (Iupac Technical Report) *Pure Appl. Chem.* **2002**, *74*, 857.
- (44) Nalwa, H. S. *Handbook of Organic Conductive Molecules and Polymers 2, Conductive Polymers: Synthesis and Electrical Properties.*; Wiley: Chichester; New York, 1997; Vol. 2.

- (45) Bhadra, S.; Khastgir, D. Determination of Crystal Structure of Polyaniline and Substituted Polyanilines through Powder X-Ray Diffraction Analysis *Polym. Test.* **2008**, *27*, 851-857.
- (46) Zhang, X.; Zhu, J.; Haldolaarachchige, N.; Ryu, J.; Young, D. P.; Wei, S.; Guo, Z. Synthetic Process Engineered Polyaniline Nanostructures with Tunable Morphology and Physical Properties *Polymer* **2012**, *53*, 2109-2120.
- (47) Varma, S. J.; Xavier, F.; Jayalekshmi, S.; Varghese, S. Synthesis and Studies of Exceptionally Crystalline Polyaniline Thin Films *Polym. Int.* **2012**, *61*, 743-748.
- (48) Majumdar, D.; Baskey, M.; Saha, S. K. Epitaxial Growth of Crystalline Polyaniline on Reduced Graphene Oxide *Macromol. Rapid Commun.* **2011**, *32*, 1277-1283.
- (49) Colomban, P.; Folch, S.; Gruger, A. Vibrational Study of Short-Range Order and Structure of Polyaniline Bases and Salts *Macromolecules* **1999**, *32*, 3080-3092.
- (50) Folch, S.; Gruger, A.; Régis, A.; Baddour-Hadjean, R.; Colomban, P. Polymorphism and Disorder in Oligo- and Polyanilines *Synt. Met.* **1999**, *101*, 795-796.
- (51) El Khalki, A.; Gruger, A.; Colomban, P. Bulk–Surface Nanostructure and Defects in Polyaniline Films and Fibres *Synt. Met.* **2003**, *139*, 215-220.
- (52) Stejskal, J.; Exnerova, M.; Moravkova, Z.; Trchova, M.; Hromadkova, J.; Prokes, J. Oxidative Stability of Polyaniline *Polym. Degrad. Stab.* **2012**, *97*, 1026-1033.
- (53) Sedenkova, I.; Trchova, M.; Stejskal, J. Thermal Degradation of Polyaniline Films Prepared in Solutions of Strong and Weak Acids and in Water - Ftir and Raman Spectroscopic Studies *Polym. Degrad. Stab.* **2008**, *93*, 2147-2157.

- (54) Moravkova, Z.; Trchova, M.; Tomsik, E.; Stejskal, J.; Cechvala, J. Enhanced Thermal Stability of Multi-Walled Carbon Nanotubes after Coating with Polyaniline Salt *Polym. Degrad. Stab.* **2012**, *97*, 1405-1414.
- (55) Rozlívková, Z.; Trchová, M.; Sedenková, I.; Spírková, M.; Stejskal, J. Structure and Stability of Thin Polyaniline Films Deposited in Situ on Silicon and Gold During Precipitation and Dispersion Polymerization of Aniline Hydrochloride *Thin Solid Films* **2011**, *519*, 5933-5941.
- (56) Ćirić-Marjanović, G.; Trchová, M.; Stejskal, J. The Chemical Oxidative Polymerization of Aniline in Water: Raman Spectroscopy *J. Raman Spectrosc.* **2008**, *39*, 1375-1387.
- (57) Mažeikienė, R.; Tomkutė, V.; Kuodis, Z.; Niaura, G.; Malinauskas, A. Raman Spectroelectrochemical Study of Polyaniline and Sulfonated Polyaniline in Solutions of Different Ph *Vib. Spectrosc* **2007**, *44*, 201.
- (58) Liu, C.; Zhang, J.; Shi, G.; Chen, F. e. Doping Level Change of Polyaniline Film During Its Electrochemical Growth Process *J. Appl. Polym. Sci.* **2004**, *92*, 171-177.
- (59) Dennany, L.; Innis, P. C.; McGovern, S. T.; Wallace, G. G.; Forster, R. J. Electronic Interactions within Composites of Polyanilines Formed under Acidic and Alkaline Conditions. Conductivity, ESR, Raman, UV-Vis and Fluorescence Studies *PCCP* **2011**, *13*, 3303-3310.
- (60) Bernard, M. C.; Hugot-Le Goff, A. Quantitative Characterization of Polyaniline Films Using Raman Spectroscopy: II. Effects of Self-Doping in Sulfonated Polyaniline *Electrochim. Acta* **2006**, *52*, 728-735.

- (61) Bernard, M. C.; Hugot-Le Goff, A. Quantitative Characterization of Polyaniline Films Using Raman Spectroscopy: I: Polaron Lattice and Bipolaron *Electrochim. Acta* **2006**, *52*, 595-603.
- (62) Fukuda, T.; Takezoe, H.; Ishikawa, K.; Fukuda, A.; Woo, H. S.; Jeong, S. K.; Oh, E. J.; Suh, J. S. Ir and Raman Studies in Three Polyanilines with Different Oxidation Level *Synt. Met.* **1995**, *69*, 175-176.
- (63) Pereira da Silva, J. E.; Temperini, M. L. A.; Córdoba de Torresi, S. I. Secondary Doping of Polyaniline Studied by Resonance Raman Spectroscopy *Electrochim. Acta* **1999**, *44*, 1887-1891.
- (64) Jozefowicz, M. E.; Laversanne, R.; Javadi, H. H. S.; Epstein, A. J.; Pouget, J. P.; Tang, X.; MacDiarmid, A. G. Multiple Lattice Phases and Polaron-Lattice-Spinless-Defect Competition in Polyaniline *Phys. Rev. B: Condens. Matter* **1989**, *39*, 12958-12961.
- (65) Pouget, J. P.; Jozefowicz, M. E.; Epstein, A. J.; Tang, X.; MacDiarmid, A. G. X-Ray Structure of Polyaniline *Macromolecules* **1991**, *24*, 779-789.
- (66) Laridjani, M.; Pouget, J. P.; Scherr, E. M.; MacDiarmid, A. G.; Jozefowicz, M. E.; Epstein, A. J. Amorphography - the Relationship between Amorphous and Crystalline Order. 1. The Structural Origin of Memory Effects in Polyaniline *Macromolecules* **1992**, *25*, 4106-4113.
- (67) Gouadec, G.; Colomban, P. Raman Spectroscopy of Nanomaterials: How Spectra Relate to Disorder, Particle Size and Mechanical Properties *Progress in Crystal Growth and Characterization of Materials* **2007**, *53*, 1-56.

- (68) Varela-Alvarez, A.; Sordo, J. A.; Scuseria, G. E. Doping of Polyaniline by Acid-Base Chemistry: Density Functional Calculations with Periodic Boundary Conditions *JACS* **2005**, *127*, 11318-11327.
- (69) Eftekhari, A. *Nanostructured Conductive Polymers*; Wiley: Chichester, West Sussex, U.K.; Hoboken, N.J., 2010.
- (70) Trchová, M.; Morávková, Z.; Šedáňková, I.; Stejskal, J. Spectroscopy of Thin Polyaniline Films Deposited During Chemical Oxidation of Aniline *Chem. Pap.* **2012**, *66*, 415-445.
- (71) Do Nascimento, G. M. Spectroscopy of Polyaniline Nanofibers. In *Nanofibers*; Kumar, A., Ed.; INTECH, 2010; pp 438.
- (72) Jain, M.; Annapoorni, S. Raman Study of Polyaniline Nanofibers Prepared by Interfacial Polymerization *Synt. Met.* **2010**, *160*, 1727-1732.
- (73) Cochet, M.; Louarn, G.; Quillard, S.; Buisson, J. P.; Lefrant, S. Theoretical and Experimental Vibrational Study of Emeraldine in Salt Form. Part Ii *J. Raman Spectrosc.* **2000**, *31*, 1041-1049.
- (74) Do Nascimento, G. M.; Temperini, M. L. Studies on the Resonance Raman Spectra of Polyaniline Obtained with near-IR Excitation *J. Raman Spectrosc.* **2008**, *39*, 772-778.
- (75) Nobrega, M. M.; Silva, C. H. B.; Constantino, V. R. L.; Temperini, M. L. A. Spectroscopic Study on the Structural Differences of Thermally Induced Cross-Linking Segments in Emeraldine Salt and Base Forms of Polyaniline *J. Phys. Chem. B* **2012**, *116*, 14191-14200.
- (76) Bernard, M. C.; Hugot-Le Goff, A.; Joiret, S.; Arkoub, H.; Saïdani, B. Influence of the Nature of Substituent on the Charge Mechanisms in Substituted Polyanilines (Spani,

- Poma) Studied by Raman and Optical Spectroscopies *Electrochim. Acta* **2005**, *50*, 1615-1623.
- (77) Socrates, G. *Infrared and Raman Characteristic Group Frequencies :Tables and Charts*; Wiley: Chichester; New York, 2000.
- (78) Cochet, M.; Louarn, G.; Quillard, S.; Boyer, M. I.; Buisson, J. P.; Lefrant, S. Theoretical and Experimental Vibrational Study of Polyaniline in Base Forms: Non-Planar Analysis. Part I *J. Raman Spectrosc.* **2000**, *31*, 1029-1039.
- (79) Cochet, M.; Quillard, S.; Buisson, J. P.; Lefrant, S.; Louarn, G. Vibrational Study of the Base Form of Polyaniline: Effect of the 3d Character *Synt. Met.* **1999**, *101*, 793-794.
- (80) Moravkova, Z.; Trchova, M.; Exnerova, M.; Stejskal, J. The Carbonization of Thin Polyaniline Films *Thin Solid Films* **2012**, *520*, 6088-6094.
- (81) Wilhelm, P. "Modern Polymer Spectroscopy", 2008 Weinheim, Germany.
- (82) Mazeikiene, R.; Statino, A.; Kuodis, Z.; Niaura, G.; Malinauskas, A. In Situ Raman Spectroelectrochemical Study of Self-Doped Polyaniline Degradation Kinetics *Electrochemistry Communications* **2006**, *8*, 1082-1086.
- (83) Mazeikiene, R.; Niaura, G.; Malinauskas, A. A Comparative Raman Spectroelectrochemical Study of Selected Polyaniline Derivatives in a Ph-Neutral Solution *Synt. Met.* **2010**, *160*, 1060-1064.
- (84) Lambert, J. B. *Organic Structural Spectroscopy*; Prentice Hall: Boston, 2010.
- (85) Boyer, M. I.; Quillard, S.; Louarn, G.; Froyer, G.; Lefrant, S. Vibrational Study of the FeCl<sub>3</sub>-Doped Dimer of Polyaniline; a Good Model Compound of Emeraldine Salt *J. Phys. Chem. B* **2000**, *104*, 8952-8961.

- (86) Tagowska, M.; Palys, B.; Jackowska, K. Polyaniline Nanotubules—Anion Effect on Conformation and Oxidation State of Polyaniline Studied by Raman Spectroscopy *Synt. Met.* **2004**, *142*, 223-229.
- (87) Bernard, M. C.; Hugot-Le Goff, A.; Arkoub, H.; Saïdani, B. Characterization of Substituted Polyaniline Films Using Raman Spectroscopy: Iii. Study of a Methoxylated Polymer: Poma *Electrochim. Acta* **2007**, *52*, 5030-5038.
- (88) Zhang, J.; Liu, C.; Shi, G. Raman Spectroscopic Study on the Structural Changes of Polyaniline During Heating and Cooling Processes *J. Appl. Polym. Sci.* **2005**, *96*, 732.
- (89) do Nascimento, G. M.; Silva, C. H. B.; Temperini, M. L. A. Electronic Structure and Doping Behavior of Pani-Nsa Nanofibers Investigated by Resonance Raman Spectroscopy *Macromol. Rapid Commun.* **2006**, *27*, 255-259.
- (90) Pan, L. J.; Pu, L.; Shi, Y.; Sun, T.; Zhang, R.; Zheng, Y. O. Hydrothermal Synthesis of Polyaniline Mesostructures *Adv. Funct. Mater.* **2006**, *16*, 1279-1288.
- (91) Mathew, R.; Mattes, B. R.; Espe, M. P. A Solid State Nmr Characterization of Cross-Linked Polyaniline Powder *Synt. Met.* **2002**, *131*, 141.
- (92) Stejskal, J.; Sapurina, I.; Trchova, M. Polyaniline Nanostructures and the Role of Aniline Oligomers in Their Formation *Prog. Polym. Sci.* **2010**, *35*, 1420-1481.
- (93) Cruz-Silva, R.; Romero-García, J.; Angulo-Sánchez, J. L.; Flores-Loyola, E.; Farías, M. H.; Castellón, F. F.; Díaz, J. A. Comparative Study of Polyaniline Cast Films Prepared from Enzymatically and Chemically Synthesized Polyaniline *Polymer* **2004**, *45*, 4711-4717.

- (94) Bernard, M. C.; Joiret, S.; Hugot-Le Goff, A. Spectroelectrochemical Characterization of Aniline/Metanilic Acid Copolymers *Russian Journal of Electrochemistry* **2004**, *40*, 235-244.
- (95) Louarn, G.; Lapkowski, M.; Quillard, S.; Pron, A.; Buisson, J. P.; Lefrant, S. Vibrational Properties of Polyaniline-Isotope Effects *J. Phys. Chem.* **1996**, *100*, 6998-7006.
- (96) Bernard, M. C.; Hugot-Le Goff, A. Raman Spectroscopy for the Study of Polyaniline *Synth. Met.* **1997**, *85*, 1145-1146.
- (97) Furukawa, Y. Electronic Absorption and Vibrational Spectroscopies of Conjugated Conducting Polymers *J. Phys. Chem.* **1996**, *100*, 15644-15653.
- (98) Heeger, A. J.; Kivelson, S.; Schrieffer, J. R.; Su, W. P. Solitons in Conducting Polymers *Reviews of Modern Physics* **1988**, *60*, 781-850.
- (99) Brédas, J. L.; Chance, R. R.; Silbey, R. Comparative Theoretical Study of the Doping of Conjugated Polymers: Polarons in Polyacetylene and Polyparaphenylene *Physical Review B* **1982**, *26*, 5843-5854.
- (100) Chance, R. R.; Silbey, R. Bipolaron Transport in Doped Conjugated Polymers *Physical Review B* **1984**, *29*, 4491-4495.
- (101) Shimano, J. Y.; MacDiarmid, A. G. Phase Segregation in Polyaniline: A Dynamic Block Copolymer *Synth. Met.* **2001**, *119*, 365-366.
- (102) Shimano, J. Y.; MacDiarmid, A. G. Polyaniline, a Dynamic Block Copolymer: Key to Attaining Its Intrinsic Conductivity? *Synth. Met.* **2001**, *123*, 251-262.

- (103) Quillard, S.; Boyer, M. I.; Cochet, M.; Buisson, J. P.; Louarn, G.; Lefrant, S. Spectroelectrochemical Measurements of the Conducting Form of Polyaniline and Related Oligomers *Synth. Met.* **1999**, *101*, 768-771.
- (104) Kumar, A.; Banerjee, S.; Deka, M. *Electron Microscopy for Understanding Swift Heavy Ion Irradiation Effects on Electroactive Polymers*, 2010; Vol. 3.
- (105) Kim, J. Y.; Lee, J. H.; Kwon, S. J. The Manufacture and Properties of Polyaniline Nano-Films Prepared through Vapor-Phase Polymerization *Synth. Met.* **2007**, *157*, 336-342.
- (106) Engert, C.; Umapathy, S.; Kiefer, W.; Hamaguchi, H. o. Dynamic Structure of Charge Carrier in Polyaniline by near-Infrared Excited Resonance Raman Spectroscopy *Chem. Phys. Lett.* **1994**, *218*, 87-92.
- (107) Lapkowski, M.; Berrada, K.; Quillard, S.; Louarn, G. Electrochemical Oxidation of Polyaniline in Nonaqueous Electrolytes: "In Situ" Raman Spectroscopic Studies *Macromolecules* **1995**, *28*, 1233.
- (108) Gospodinova, N.; Dorey, S.; Ivanova, A.; Zhekova, H.; Tadjer, A. Evidence for Generation of Delocalized Polarons in Conducting Polyaniline: A Raman Scattering Spectroscopy Approach *International Journal of Polymer Analysis and Characterization* **2007**, *12*, 251-271.
- (109) Tan, C. K.; Blackwood, D. J. Interactions between Polyaniline and Methanol Vapour *Sensors and Actuators B: Chemical* **2000**, *71*, 184-191.
- (110) Nalwa, H. S. *Handbook of Advanced Electronic and Photonic Materials and Devices*; Academic Press: San Diego, 2001; Vol. 8.

- (111) da Silva, J. E. P.; de Torresi, S. I. C.; de Faria, D. L. A.; Temperini, M. L. A. Raman Characterization of Polyaniline Induced Conformational Changes *Synt. Met.* **1999**, *101*, 834-835.
- (112) Boutaleb, N.; Benyoucef, A.; Salavagione, H. J.; Belbachir, M.; Morallón, E. Electrochemical Behaviour of Conducting Polymers Obtained into Clay-Catalyst Layers. An in Situ Raman Spectroscopy Study *Eur. Polym. J.* **2006**, *42*, 733-739.
- (113) Nastase, C.; Mihaiescu, D.; Nastase, F.; Moldovan, A.; Stamatina, I. Effect of P-Toluene Sulphonic Acid Doping on the Properties of Plasma Polymerized Aniline Thin Films *Synt. Met.* **2004**, *147*, 133-138.
- (114) Nastase, C.; Nastase, F.; Dumitru, A.; Ionescu, M.; Stamatina, I. Thin Film Composites of Nanocarbons-Polyaniline Obtained by Plasma Polymerization Technique *Composites Part A: Applied Science and Manufacturing* **2005**, *36*, 481-485.
- (115) Bernard, M. C.; Cordoba de Torresi, S.; Hugot-Le Goff, A. In Situ Raman Study of Sulfonate-Doped Polyaniline *Electrochim. Acta* **1999**, *44*, 1989-1997.
- (116) Rajendra Prasad, K.; Munichandraiah, N. Electrochemically Deposited Crystalline Thin Film of Polyaniline on Nickel for Redox Reactions at Positive Potentials *Synt. Met.* **2002**, *130*, 17-26.
- (117) Lee, S. Y.; Lim, H.; Choi, G. R.; Kim, J. D.; Suh, E.-K.; Lee, S.-K. Metal-to-Insulating Transition of Single Polyaniline (Pani) Nanowire: A Dedoping Effect *J. Phys. Chem. C* **2010**, *114*, 11936-11939.
- (118) Niaura, G.; Mažeikienė, R.; Malinauskas, A. Structural Changes in Conducting Form of Polyaniline Upon Ring Sulfonation as Deduced by near Infrared Resonance Raman Spectroscopy *Synt. Met.* **2004**, *145*, 105-112.

- (119) Gustavsson, J. M.; Innis, P. C.; He, J.; Wallace, G. G.; Tallman, D. E. Processable Polyaniline-HcSA/Poly(Vinyl Acetate-Co-Butyl Acrylate) Corrosion Protection Coatings for Aluminium Alloy 2024-T3: A SVT and Raman Study *Electrochim. Acta* **2009**, *54*, 1483-1490.
- (120) Furukawa, Y.; Ueda, F.; Hyodo, Y.; Harada, I.; Nakajima, T.; Kawagoe, T. Vibrational Spectra and Structure of Polyaniline *Macromolecules* **1988**, *21*, 1297-1305.
- (121) Yang, C.; Chen, C.; Zeng, Y. Fourier Transform Infrared Spectra of Transition Metal Ion-Containing Polyanilines Synthesized in Different Reaction Conditions *Spectrochim. Acta, Part A* **2007**, *66*, 37-41.
- (122) Gruger, A.; Novak, A.; Regis, A.; Colomban, P. Infrared and Raman Study of Polyaniline. Part II: Influence of Ortho Substituents on Hydrogen Bonding and UV/Vis-near-IR Electron Charge Transfer *J. Mol. Struct.* **1994**, *328*, 153.
- (123) Kurmaev, E. Z.; Katsnelson, M. I.; Moewes, A.; Magnuson, M.; Guo, J. H.; Butorin, S. M.; Nordgren, J.; Ederer, D. L.; Iwami, M. Spectroscopic Observation of Polaron-Lattice Band Structure in the Conducting Polymer Polyaniline *J. Phys.: Condens. Matter* **2001**, *13*, 3907.
- (124) Sinha, S.; Bhadra, S.; Khastgir, D. Effect of Dopant Type on the Properties of Polyaniline *J. Appl. Polym. Sci.* **2009**, *112*, 3135-3140.
- (125) Zhou, Q.; Wang, J.; Ma, Y.; Cong, C.; Wang, F. The Relationship of Conductivity to the Morphology and Crystallinity of Polyaniline Controlled by Water Content Via Reverse Microemulsion *Colloid. Polym. Sci.* **2007**, *285*, 405-411.
- (126) Epstein, A. J.; MacDiarmid, A. G. "Electronic Phenomena in Polyanilines," Defense Technical Information Center, 1992.

- (127) Izumi, C. M. S.; Rodrigues, D. C.; Temperini, M. L. A. The Role of Solvent on the Doping of Polyaniline with Fe(III) Ions *Synt. Met.* **2010**, *160*, 2552-2558.
- (128) Kim, S. C.; Whitten, J.; Kumar, J.; Bruno, F.; Samuelson, L. Self-Doped Carboxylated Polyaniline: Effect of Hydrogen Bonding on the Doping of Polymers *Macromol. Res.* **2009**, *17*, 631-637.
- (129) Han, M. G.; Im, S. S. X-Ray Photoelectron Spectroscopy Study of Electrically Conducting Polyaniline/Polyimide Blends *Polymer* **2000**, *41*, 3253-3262.
- (130) Garai, A.; Chatterjee, S.; Nandi, A. K. Viscoelastic and Conductivity Properties of Thermoreversible Polyaniline-Dnnsa Gel in M-Cresol *Synt. Met.* **2010**, *160*, 1733-1739.
- (131) Inzelt, G. *Conducting Polymers a New Era in Electrochemistry*; Springer: Berlin; New York, 2012.
- (132) Chao, L.; Ho, K. S.; Shen, S. Y.; Pu, H. Y.; Hsieh, T. H.; Kuo, C. W.; Tseng, B. H. Short Polyaniline Nanorod Prepared in the Presence of Para-Phenylenediamine *J. Appl. Polym. Sci.* **2013**, *127*, 1853-1862.
- (133) Anilkumar, P.; Jayakannan, M. Single-Molecular-System-Based Selective Micellar Templates for Polyaniline Nanomaterials: Control of Shape, Size, Solid State Ordering, and Expanded Chain to Coil-like Conformation *Macromolecules* **2007**, *40*, 7311-7319.
- (134) Apesteguy, J.; Jacobo, S. Synthesis of a Soluble Polyaniline-Ferrite Composite: Magnetic and Electric Properties *J. Mater. Sci.* **2007**, *42*, 7062-7068.
- (135) Majidi, M. R.; Kane-Maguire, L. A. P.; Wallace, G. G. Electrochemical Synthesis of Optically Active Polyanilines *Aust. J. Chem.* **1998**, *51*, 23-30.

- (136) Karatchevtseva, I.; Zhang, Z.; Hanna, J.; Luca, V. Electrosynthesis of Macroporous Polyaniline-V<sub>2</sub>O<sub>5</sub> Nanocomposites and Their Unusual Magnetic Properties *Chem. Mater.* **2006**, *18*, 4908-4916.
- (137) Mire, C. A.; Kane-Maguire, L. A.; Wallace, G. G.; in het Panhuis, M. Influence of Added Hydrogen Bonding Agents on the Chiroptical Properties of Chiral Polyaniline *Synt. Met.* **2009**, *159*, 715-717.
- (138) Kane-Maguire, L. A. P.; MacDiarmid, A. G.; Norris, I. D.; Wallace, G. G.; Zheng, W. Facile Preparation of Optically Active Polyanilines Via the in Situ Chemical Oxidative Polymerisation of Aniline *Synt. Met.* **1999**, *106*, 171-176.
- (139) MacDiarmid, A. G.; Epstein, A. J. Secondary Doping in Polyaniline *Synt. Met.* **1995**, *69*, 85-92.
- (140) Min, Y.; Xia, Y.; MacDiarmid, A. G.; Epstein, A. J. Vapor Phase "Secondary Doping" of Polyaniline *Synt. Met.* **1995**, *69*, 159-160.
- (141) Xia, Y.; Wiesinger, J. M.; MacDiarmid, A. G.; Epstein, A. J. Camphorsulfonic Acid Fully Doped Polyaniline Emeraldine Salt: Conformations in Different Solvents Studied by an Ultraviolet/Visible/near-Infrared Spectroscopic Method *Chem. Mater.* **1995**, *7*, 443-445.
- (142) Sedenkova, I.; Konyushenko, E. N.; Stejskal, J.; Trchova, M.; Prokes, J. Solid-State Oxidation of Aniline Hydrochloride with Various Oxidants *Synt. Met.* **2011**, *161*, 1353-1360.
- (143) Rumbau, V.; Pomposo, J. A.; Alduncin, J. A.; Grande, H.; Mecerreyes, D.; Ochoteco, E. A New Bifunctional Template for the Enzymatic Synthesis of Conducting Polyaniline *Enzyme and Microbial Technology* **2007**, *40*, 1412-1421.

- (144) Gök, A.; Sarı, B.; Talu, M. Synthesis and Characterization of Conducting Substituted Polyanilines *Synt. Met.* **2004**, *142*, 41-48.
- (145) Liu, H.; Hu, X. B.; Wang, J. Y.; Boughton, R. I. Structure, Conductivity, and Thermopower of Crystalline Polyaniline Synthesized by the Ultrasonic Irradiation Polymerization Method *Macromolecules* **2002**, *35*, 9414.
- (146) Wise, D. L. *Electrical and Optical Polymer Systems: Fundamentals: Methods, and Applications*; CRC Press, 1998.
- (147) Surwade, S. P.; Agnihotra, S. R.; Dua, V.; Zhang, X.; Manohar, S. K.; Kolla, H. S. Chromism and Molecular Weight of Polyaniline Derivatives *Synt. Met.* **2009**, *159*, 2153-2156.

## CHAPTER 4

### **Broad-band EM Shielding Effects from Solvent-limited Synthesis of HCl-doped Polyaniline Nanopowders**

#### **4.1. Introduction**

In Chapter 2 the main contribution highlighted the dependence of EM shielding effectiveness (SE), particularly in the microwave X-band, for polyaniline (PAN) nanoparticles doped with HCl as it is connected to the synthesis approach. The synthesis protocols (e.g., conventional slow oxidation) that led to maximizing crystalline HCl-doped PAN with cross-linked structures or branched chains were not recommended for EM shielding, as there appears to be an intermediate optimum oxidation rate for the greatest shielding potential, which is the hypothesis upon which the research herein will focus. The solution-free (SF), or extremely restrictive solvent-limited, synthesis product demonstrates the direct importance of conductivity over crystallinity toward the material's SE and represents a nontraditional technique for preparing PAN nanoparticles and bulk nanopowders with an optimum chemical structure and crystallinity for EM shielding.

In this work, detailed investigation about the solvent-free (SF) approach is established. To the best of our knowledge, this research represents the first investigations of EM shielding as impacted by electronic structure, polymer chain cross-linking, and chemical structure of HCl-doped PAN in comparison with classical chemical oxidation approaches—the same as discussed previously. The two extreme comparisons are fast oxidation, or rapid mixing as it was called in some settings, and an extremely slow oxidation, both with significant solvent media. The idea of comparing SF with respect to these two extremes is to highlight possible, significant differences across the literature and new experiments in order to get a deeper

understanding and clear correlations between synthesis approaches, as well as the SF impact on the prepared PAN. Investigating the EM shielding potential of the nanopowders was very important to confirm the above hypothesis and validate the previous work (Chapters 2-3).

The primary aim of utilizing XPS on the HCl-doped PAN nanopowders is to (a) quantitatively determine degree of doping and (b) identify oxidation levels and electronic structures, correlated with Raman and UV-vis spectroscopy results and interpretations from Chapter 3. It is very important to understand deeply why PAN behaves differently, even with the same dopant, from different reaction conditions alone. Moreover, clarifying the sensitivities of PAN properties to synthesis conditions are significant for practical future process design and scale-up to commercial products. Also, it is very important to understand the electrical/electromagnetic behavior and correlate it to other physicochemical parameters (cross-linking, chemical and electronic structures) in order to approach specific design requirements toward EM shielding through synthesis processes methodically.

#### **4.2. Materials and Methods**

Aniline (99.5%, ACS reagent grade, Aldrich) was purified by distillation with zinc dust before use.<sup>1,2</sup> The inorganic acid dopant hydrochloric acid (37.43%, ACS reagent grade, EMD Chemicals) and the oxidant ammonium peroxydisulfate (98%, ACS reagent grade, Aldrich) were used as received. HCl-doped polyaniline (PAN) nanoparticle samples were prepared by solvent-free (SF) and conventional (solvent-based) chemical oxidations under slow (CS) and fast (CF) production rates as controlled by the addition of aqueous ammonium peroxydisulfate (APS), both described previously in detail in chapter

#### 4.2.1. XPS Instrumentation

The X-ray photoelectron spectroscopy (XPS) apparatus was built in-house at the University of Idaho by Prof. David N. McIlroy. XPS was performed under vacuum at base pressure of  $10^{-10}$  Torr at room temperature. During spectral acquisition, the samples were grounded and exposed to a 400-eV electron beam to eliminate spurious charging. All spectra were acquired at room temperature. The X-ray source was generated with an Mg monochromic anode at the  $K_{\alpha}$ -line (*i.e.*, 1253 eV) energized at 15 kV and 400 W. XPS spectra were collected at a fixed takeoff angle of  $90^{\circ}$ , which corresponds to photoelectrons emitted parallel to surface normal.

The binding energies were calibrated by fixing the C 1s neutral carbon peak at 284.6 eV,<sup>3-6</sup> as an internal standard, because the binding energy corresponding to the peak maximum of the C1s spectrum observed for polyanilines is substantially independent of the oxidation state.<sup>7</sup> After background subtraction, the core line envelope was determined to separate the different N, C, O and Cl components in the N(1s), C(1s), O(s1), and Cl(2p) peaks. For each core line envelope, the number of component peaks and their approximate positions were decided based on the chemical functionalities expected for the various forms of PAN. Initial component peaks were set up manually, and the computer program allowed iteration to produce a physically reasonable fit.

All core-level spectra were deconvolved into mixed Gaussian/Lorentzian sub-peaks,<sup>3,8</sup> in which each parameter describing a component peak was varied in turn so as to maximize a “goodness of fit” parameter: specifically by minimizing the weighted sum of squared residuals (WSSR) with the Levenberg-Marquardt method. Each component peak was described by its height, position, full-width-at-half-maximum (FWHM), Gaussian/Lorentzian ratio, and

asymmetry parameter. The FWHM of the Gaussian peak components were kept constant for spectral deconvolution.<sup>4</sup> The Gaussian/Lorentzian ratio of the peaks was set to be equal in each fit.<sup>3</sup>

Photoelectron spectroscopies, such as X-ray photoelectron spectroscopy (XPS), are commonly used for surface characterization due to the very small mean-free path of the outgoing electrons. Generally, the thickness of the analyzed layer does not exceed 10 nm<sup>6,9</sup>, even with an x-ray source. Depth limitations have never appeared as a major drawback when studying the electronic structure of conducting polymers.<sup>10</sup> Indeed, XPS-derived quantitative data, such as the elemental composition of the polymer chain or doping level, are usually close to the results obtained from analysis of bulk material.

#### **4.2.2. Electromagnetic Shielding (SE)**

In a two-port network analysis, the SE for electromagnetic interference (EMI) can be expressed in terms of scattering parameters that quantify the way currents and voltages travel in a transmission line when encountering a discontinuity caused by differing impedances between air and the obstruction or in the dielectric media.<sup>11</sup> Figure 4.1 shows a schematic diagram of the coaxial guided transmission line setup that was used, in comparison with the Chapter 2 waveguide experiments. In order to determine SE of the samples under test and confirm their relative performance, coaxial guided transmission line techniques were employed from the pertinent literature descriptions.<sup>12</sup> A mass of  $0.06 \pm 0.1$  mg of each HCl-doped PAN nanopowders prepared from different synthetic approaches was selected to be pressed inside the sample holder. The dimensions of the sample under testing inside the coaxial holes are  $1.27 \pm 0.05$  mm inner diameter,  $4.56 \pm 0.05$  mm outer diameter and  $6 \pm 0.05$  mm length. Three samples were prepared for each synthetic approach with total nine samples.

Agilent E5061BEP ENA and HP8510C network analyzers were used to investigate EM shielding potential at low frequencies less than 1.5 GHz and broad band from 2-14 GHz, respectively. A full two port calibration was performed before testing in order to remove systematic errors.<sup>13,14</sup> The dependence of SE on absorption and reflection losses were investigated as a function of frequency and synthesis conditions.

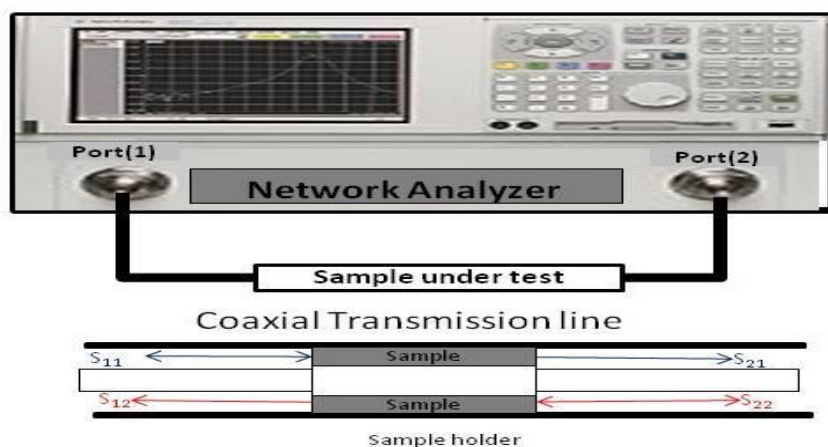


**Figure 4.1.** Coaxial guided transmission line setup for EMI SE measurements.

In order to determine SE of the samples under test and confirm their relative performance, coaxial guided transmission line techniques were employed from the pertinent literature descriptions.<sup>12</sup> A mass of  $0.06\text{g} \pm 0.1 \text{ mg}$  of each HCl-doped PAN nanopowders prepared from different synthetic approaches was selected to be pressed inside the sample holder. The dimensions of the sample under testing inside the coaxial holes are  $1.27 \pm 0.05 \text{ mm}$  inner diameter,  $4.56 \pm 0.05 \text{ mm}$  outer diameter and  $6 \pm 0.05 \text{ mm}$  length. Three samples were prepared for each synthetic approach with total nine samples. Agilent E5061BEP ENA and HP8510C network analyzers were used to investigate EM shielding potential at low frequencies less than 1.5 GHz and broad band from 2-14 GHz, respectively. A full two port calibration was

performed before testing in order to remove systematic errors.<sup>13,14</sup> The dependence of SE on absorption and reflection losses were investigated as a function of frequency and synthesis conditions.

### **4.3. Results and Discussions**

#### **4.3.1. XPS Data Interpretation: Evaluation of Doping Level Dependence on Synthesis Approach**

The electronic structure of the PAN samples prepared using the three different approaches indicated distinctive doping-level differences inferred from XPS spectral interpretations. Model compounds for the amine, imine, polaron, bipolaron, and protonated amine (PA) nitrogen sites potentially present in PAN provided the references for the analysis of the core-level spectra in the nanopowders produced. In particular, the analysis of the nitrogen 1s spectra represents a useful method for accurate determination of the amine-to-imine ratio. The evaluation of the concentration of the different nitrogen species as a function of the synthesis approach is in good agreement with previous Raman results (Chapter 3) as seen by comparison to Table 4.1.

In XPS studies, core-level spectra are often superimposed and/or convolved. Often, the relative contribution of each core-level spectrum, which is attained from various polymeric components, is resolvable given proper references. XPS provides a truly unique tool in the quantitative analysis of the various intrinsic oxidation level of PAN (imine/amine)<sup>9,15</sup> and doping degree as the ratio between the positively-charged nitrogen species to total nitrogen ( $N^+/N$ )<sup>5,7,8</sup>. In addition, XPS elucidates the electronic features of polarons and bipolarons in PAN structures.<sup>7</sup>

**Table 4.1.** The N(1s), C(1s), O(1s), and Cl(2p) XPS core-level deconvolution results for PAN samples prepared with the three different approaches (SF, CF, and CS).

Species	Moiety	BE (eV)	SF (%)	CF (%)	CS (%)	Ref.
N	Imine	398.0±0.1eV	5	4	4	3,4,9,16-20
	Amine	399.4±0.1eV	46	51	54	4,8,9,16,18,20-22
	Polaron	400.4±0.1eV	33	24	18	5,8,19,20,23,24
	Bipolaron	401.6±0.1eV	12	17	19	5,8,18-20,23
	PA	403.4±0.1eV	4	4	6	17,25,26
C	C-C	284.4.0±0.1eV	51	52	44	5,8,27-33
	C-N	285.3±0.1eV	25	28	34	15,32,34-38 (C-N/C=N) <sup>5,30,32,35,38</sup>
	C-O	286.5±0.1eV	14	11	11	5,29,39-41
						(Polaron) <sup>33</sup>
	C=O	288.5±0.1eV	7	7	10	33,34,38,41-44
						(Bipolaron) <sup>45</sup>
$\pi$ - $\pi^*$	290.4±0.1eV	2	2	2	Shake-up <sup>9,46,47</sup>	
O	O=C	531.7 ±0.1eV	77	77	75	22,43,48-50
	C-O-H	533.1±0.1eV	23	23	25	22,43,48-53
Cl	Cl <sup>-</sup>	197.7 ±0.1eV	15	55	52	26,34,44
	Cl <sup>•</sup>	199.0±0.1eV	47	27	32	26,34,44
	-Cl	200.1±0.1eV	38	17	16	10,26,34,54,55

Figure 4.2 shows the XPS core-level spectra with estimated band contributions for PAN samples prepared with the three different approaches (SF, CF, and CS). The binding energies of the deconvolved peaks' maxima as well as their relative percentage areas are reported in

Table 4.1. The N(1s) core-level spectral envelopes of all PAN samples clearly result from more than a single type of nitrogen environment and were successfully decomposed into five peaks<sup>56</sup> using a mixed Gaussian/Lorentzian function.<sup>3,8,28</sup> Two peaks were attributed to neutral nitrogen species; the peak at 398.0 eV is attributed to the imine nitrogen species,<sup>3,4,9,16-20</sup> while a band at 399.4 eV corresponds to the amine nitrogen species.<sup>4,8,9,16,18,20-22</sup> Positively-charged nitrogen species correspond to a particular oxidation level and/or the degree of protonation and are found at binding energies >400 eV.<sup>3,9,18,21,39,56</sup> Three peaks could be assigned to three different positively-charged nitrogen species depending on different environments.<sup>56</sup> The first two, in order of increasing binding energy, could be attributed to polaron and bipolaron states, respectively.<sup>19</sup>

The component at 400.4 eV is attributed to nitrogen atoms with delocalized radical cations (i.e., polaron)<sup>5,8,19,20,23,24</sup> and those observed at 401.6 eV are attributed to the positively-charged imine cation (i.e., bipolaron).<sup>5,8,18-20,23</sup> Positively-charged nitrogen species at 403.4 eV are attributed to protonated amines (PA).<sup>17,25,26</sup> These occur at a higher binding energy because of the stronger electron localization associated with poorer conjugation at sp<sup>3</sup>-bonded sites.<sup>17</sup> The possibility of amine nitrogen protonation is expected, which may lead to (N<sup>+</sup>H<sub>2</sub>)<sup>8,9,57-59</sup> but to a lesser extent than imine nitrogen due to the latter's greater basicity.<sup>60</sup> The presence of protonated amines would likely reduce the  $\pi$ -conjugation and thus bring more uniformly-distributed positive charges on the polymer chain.<sup>8,59</sup> Even the presence of protonated amine (PA) structures may interfere with the formation of polaron and bipolaron,<sup>9,59</sup> though this will not be considered as a determining factor in this study because the observed percentages were fairly low and very similar: 6% for CS case and 4% for both CF and SF.

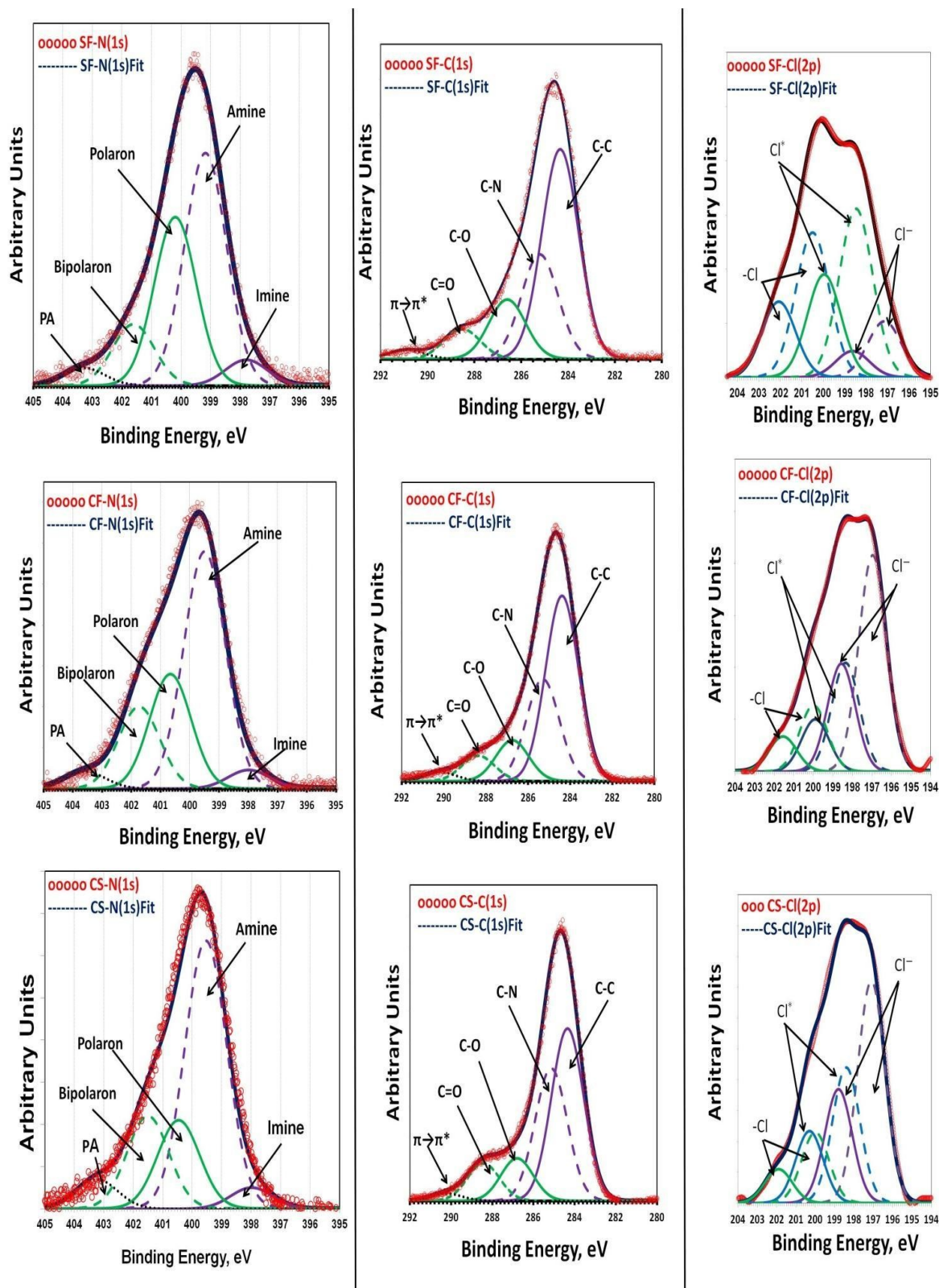


**Figure 4.2.** The N(1s), C(1s), and Cl(2p) XPS core-level spectra and deconvolution for PAN samples prepared with different approaches (SF, CF, and CS).

Generally, well-doped PAN exhibited an almost complete absence of a neutral imine peak.<sup>3</sup> However, due to dynamic vacuum pumping to below  $8 \times 10^{-10}$  Torr during the XPS measurement, unprotonated imine nitrogen may arise due to being partially undoped.<sup>20,54</sup> This may explain the reason for observing neutral imine species in all three doped PAN samples to nearly the same extent (4-5%).

The predominant amine peak appears in all the PAN samples as 46%, 51%, and 54% of the nitrogen moieties in SF, CF, and CS, respectively, as expected for the optimal doping targeted at 50%. Doped PAN samples ideally consist of equal portions of amine and imine (i.e., polaron, bipolaron and undoped).<sup>61,62</sup> The relatively higher percentage of amine for CS, corresponding to the lowest observed imine percentage, indicates a higher extent of cross-linking.<sup>63</sup> The imine sites can be doped (protonated) to the bipolaron emeraldine salt form (dication) or polaron form (radical cations).<sup>62</sup> The suggested coexistence of polarons and bipolarons has been proven.<sup>3,7,64</sup> As expected, most of the imine in the three PAN samples was protonated to form polaron and bipolaron forms. It was already shown (see N1s, Fig. 4.2 and Table 4.1) that the contribution of polaron and bipolaron in the protonated imine peak depends on synthesis approach. Moreover, the imine protonation to polaronic forms predominated in SF and CF as 67% and 53%, respectively. On the other hand, bipolaronic forms dominated over polarons in CS as 44%. These percentages were calculated with respect to the total charged nitrogen atom ( $N^+$ ). Percentages with respect to total neutral nitrogen atoms in Table 4.2 illustrate the dependence on synthesis approach.

It should be noted that polarons are chemically more active than bipolarons although the electrostatic repulsion energy of the former is lower than that of the latter.<sup>7</sup> Moreover, interconversion between polarons and bipolarons requires considerable activation energy

because it is accompanied by an  $sp^3$ - $sp^2$  configuration change.<sup>7,22</sup> Therefore, the relative stability between polarons and bipolarons is dependent on the environment around the positively-charged nitrogen such as the steric effects of the polymer chains.<sup>22</sup> This was discussed in Chapter 3 with Raman and UV-vis spectra. The fact that the major charge carrier of conducting PAN salts is a polaron rather than a bipolaron is confirmed as shown in Tables 4.1, 4.2.

**Table 4.2.** The impact of synthesis approach on oxidation/doping level, cross-linking degree, and chlorine radical/chlorine cation ratios of PAN samples.

	SF	CF	CS
Oxidation Level (=N-/Nh-%)	50	46	42
Doping Level (N <sup>+</sup> /N)%	49	45	40
Polaron/(Polaron +Bipolaron)%	73	59	49
Polaron/(N <sup>+</sup> )%	67	53	42
Bipolaron/(N <sup>+</sup> )%	25	38	44
Cross-Linking Degree (C-C/C-N)	2.0	1.8	1.3
Cl <sup>*</sup> / Cl <sup>-</sup>	3.2	0.49	0.38

These results are in very good agreement with the Raman interpretation from Chapter 3. In order to judge the electric behavior of PAN samples, identifying the type of charged nitrogen (polaron/bipolaron) is extremely important. The oxidation level of PAN samples was found to be dependent on the synthesis approach as 50%, 46%, and 42% for SF, CF, and CS, respectively, where the solvent-free method seems optimal since any higher oxidation produces lower conductivity.<sup>5,61,62</sup> Also, doping level depends on synthesis approach. The observed degree of doping was in the same trending direction 49%, 45%, and 40% corresponding to SF, CF, and CS, respectively. Again, SF shows the greatest degree of doping where 98% of the imine nitrogen is doped.

The relatively lower values for oxidation level and doping level results from the relatively low imine content in CS. This observation confirms the possibility of having the highest crosslinked structure,<sup>28,65,66</sup> which would disrupt linearity and thus prevent polaron delocalization.<sup>67</sup> The relative stability between polarons and bipolarons is, therefore, dependent on the environment around the positively-charged nitrogen such as the steric effects of the polymer chains and the electrostatic interaction with dopant anions.<sup>22</sup> Furthermore, this trend in electronic structure is correlated with conductivity previously as reported.<sup>68</sup> The higher conductivity of the SF with respect to CF and CS is confirmed with the subsequent possibility of some SF organized in a polaron lattice structure because of its oxidation level and degree of doping.<sup>5,61,62</sup>

In comparison with N(1s) core-level spectra, the C(1s) core level of polyaniline is less resolvable. Two C(1s) components at 284.4 eV and 285.3 eV are assigned to C-C<sup>5,8,27-33</sup> and C-N,<sup>15,32,34-38</sup> respectively. The latter band could also be assigned to both C-N and C=N as well,<sup>5,30,32,35,38</sup> since the samples are well-doped. It is possible to consider the presence of C-N only. The intensity ratio C-C to C-N could be helpful to examine the presence of cross-linking in the PAN samples under investigation as a measure of cross-linking degree.<sup>9,42</sup> As shown in Table 1, it was found that SF shows the highest ratio of 2:1, which is the value associated with no cross-linking, thus confirming previous interpretations. On the other hand, the cross-linking degree of 1.8 for CF indicates some significant level of cross-linking whereas the CS value of 1.3 represents the common ratio for highly cross-linked samples, though these are merely semiquantitative measures.

In addition to the two peaks in the C(1s) core-level spectra of the three samples, deconvolution of the high binding energy tail indicates the possibility of three peaks at 286.5 eV, 288.5 eV and 290.4 eV, which could be assigned to C-O,<sup>5,29,39-41</sup> C=O,<sup>33,34,38,41,42</sup> and a  $\pi \rightarrow \pi^*$  shake-up satellite,<sup>9,46,47</sup> respectively. The presence of residual amounts of C-O and C=O species in the C(1s) core-level spectra suggests the PAN sample surfaces are oxidized to some extent. This is consistent with the reactive nature of most conjugated polymer surfaces.<sup>15,43,57-59</sup> Additionally, these oxidation affiliates can also arise from incorporation of significant amount of benzoquinone (BQ) and hydroquinone (HQ) within the polymer chains, which are produced from water molecules during the polymerization.<sup>35,42</sup>

It was interesting to report the significant difference between relative amount of C-O and C=O species within the three sample types. CS had the highest percentage of 10% C=O, where both CF and SF had 7%. On the other hand, SF had the highest percentage of C-O at 14%, where CF and SF had 11%. This observation is attributed to the synthesis approach, as prolonged treatment times of CS in the oxidant solution may readily result in significant hydrolysis of CS instead of increasing the intrinsic oxidation state further.<sup>44</sup> This would lead to the formation of a significant amount of benzoquinone (BQ) and hydroquinone (HQ) with respect to the other samples (SF and CF). This hypothesis would explain the relatively high percentage of C=O in CS but will not explain the high C-O % in SF.

Recall that C(1s) binding energies correlate with fractional carbon atomic charges where decreasing electron density increases, in most cases, the respective binding energy.<sup>69,70</sup> The C(1s) components are associated with the positively polarized or partially charged carbon atoms.<sup>57-59</sup>

The assignment of the high binding energy components in C(1s) and N(1s) core-level spectra to positively polarized species was supported with the near disappearance of these high binding energy species in undoped samples.<sup>55,57-59</sup>

In this current study, this may indicate a correlation between the N(1s) and C(1s) core-level peaks, as the latter is consistent with the simultaneous presence of neutral nitrogen and different polarized nitrogen species. Accordingly, the main three resolved N(1s) peaks at 399.4 eV, 400.4 eV, and 401.6 eV, correspond to neutral nitrogen amine and charged nitrogen as polaron and bipolaron, respectively. Simultaneous presence of neutral carbon (C-N) and two components associated with the positively polarized or partially charged groups were observed also. It is possible that the latter C(1s) components (C-O and C=O) are related to the polaron and bipolaron components of N(1s) based on assignments of higher binding energy components (>286 eV) to carbon bonded to charged/partially-charged nitrogen.<sup>5,8,28-31,33,34,40,42,45,71</sup> Therefore, the two C1s components at 286.5 eV and 288.5 eV are likely carbon species bonded to polaron and bipolaron nitrogen species, respectively. This may explain the increase in the C1s components at 286.5 eV for SF as it has predominantly polaronic nitrogen species. On the other hand, the CS has the highest percentage of the C1s components at 288.5 eV, which is due to bipolaron nitrogen species.

The relative percentage of these to C1s components (polaron/bipolaron) as ratios were found to be 2, 1.5 and 1.1 corresponding to SF, CF, and CS, respectively. This trend agrees with the ratio trend obtained from the N(1s) deconvolution, which was 2.8, 1.4, and 0.9 corresponding to SF, CF, and CS, respectively. These together confirm the importance of the contribution of polarons and bipolarons in C1s components. Of course, the ratios obtained from the C1s are not as quantitatively certain as for N1s due to the difficulty in resolving the

former. Regardless, these ratios are helpful when justifying the high binding energy components of C1s and confirm the various nitrogen charged species.

The small and highest binding energy tails at 290.4 eV could be attributed to the  $\pi-\pi^*$  bonding band,<sup>9,46,47</sup> which is observed in some well-doped (~50%) states.<sup>8</sup> Actually, the interpretation of the size of the satellite shift as function of the type of  $\pi$  conjugation is still restricted or lacked of thereof<sup>43</sup>. Moreover, it was reported that the presence of a C1s satellite 6.5 eV above the main C1s peak could be attributed to  $\pi\rightarrow\pi^*$  transitions in isolated aromatic rings<sup>72</sup> and thus a diagnostic feature indicating the lack of extended conjugation,<sup>9</sup> *i.e.*, it is possible to observe this high-binding energy tail in C1s spectra for defected conjugated systems. This is why it seems to be dependent directly on the doping or oxidation, since conducting polyaniline may not have this high binding energy tail.<sup>34</sup> Additionally, carbonaceous systems containing  $\pi$ -bonds produce obvious satellite peaks approximately 8 eV from the principal line in their C(1s) spectra due to a  $\pi\rightarrow\pi^*$  transition, which is equivalent to certain band-to-band transition for metals.<sup>43</sup> So, the 6.5 eV satellite is slightly lower than common satellites.

Any increase in the positive charge over the carbon-bonded nitrogen atom would result in a corresponding positive shift in the binding energy of the C(1s) line.<sup>73</sup> The highest binding energy tail at 290.4 eV might also be consistent with the third type of charged nitrogen species, *i.e.*, protonated amine (PA). It was notable that both were observed at the highest binding energy of the N1s and C1s core-level spectra, which represent the highest polarized charged state of carbon and nitrogen species. Also, it was obvious that these C1s tails in the three PAN samples have the same percentage with respect to the total C1s peak areas.

This same trend was also observed in the N1s for the protonated amine peak, which suggests a correlation between the nitrogen and carbon species with the general electronic structure of PAN.

Peak deconvolution of the O1s core-level spectra of PAN samples revealed two main components (see Figure 4.3). The first is observed at 531.7 eV and attributed to the oxygen in a carbonyl group (O=C)<sup>22,43,48-50</sup> which results from the hydrolysis of the quinod imine units and aerial oxidation at the sample surface.<sup>34</sup> The second component is observed at 533.1 eV and is attributed to C-OH bonding or hydrogen-bonded water.<sup>22,43,48-52</sup>

Also, the same band was attributed to oxygen in carboxyl groups,<sup>43,48,49</sup> which may result from surface oxidized species.<sup>74</sup> It was reported that water molecules may become trapped in the polymer network.<sup>73</sup> Moreover, the incorporation of significant amounts of benzoquinone and hydroquinone within the polymer chains is still possible.<sup>35,42,44</sup> The relative ratio of these two peaks in the three samples are fairly constant and agree with the literature,<sup>34</sup> *i.e.*, the relative intensity of the oxygen species is independent of the synthesis approach.

The Cl(2p) core-level spectral envelope for the three PAN samples were adequately decomposed into three spin-orbit split doublets (Cl2p<sub>3/2</sub> and Cl2p<sub>1/2</sub>). The binding energy values for the Cl2p peaks resided at 197.7 eV, 199.0 eV, and 200.1 eV. The first and last components suggest the presence of ionic (Cl<sup>-</sup>)<sup>26,34,44</sup> and covalent (-Cl)<sup>10,26,34,54,55</sup> chlorine species, respectively. The chlorine species with intermediate binding energy (Cl•) is more appropriately associated with charge transfer interactions between the halogen and metal-like conducting state of the PAN chain.<sup>9,34,44</sup>

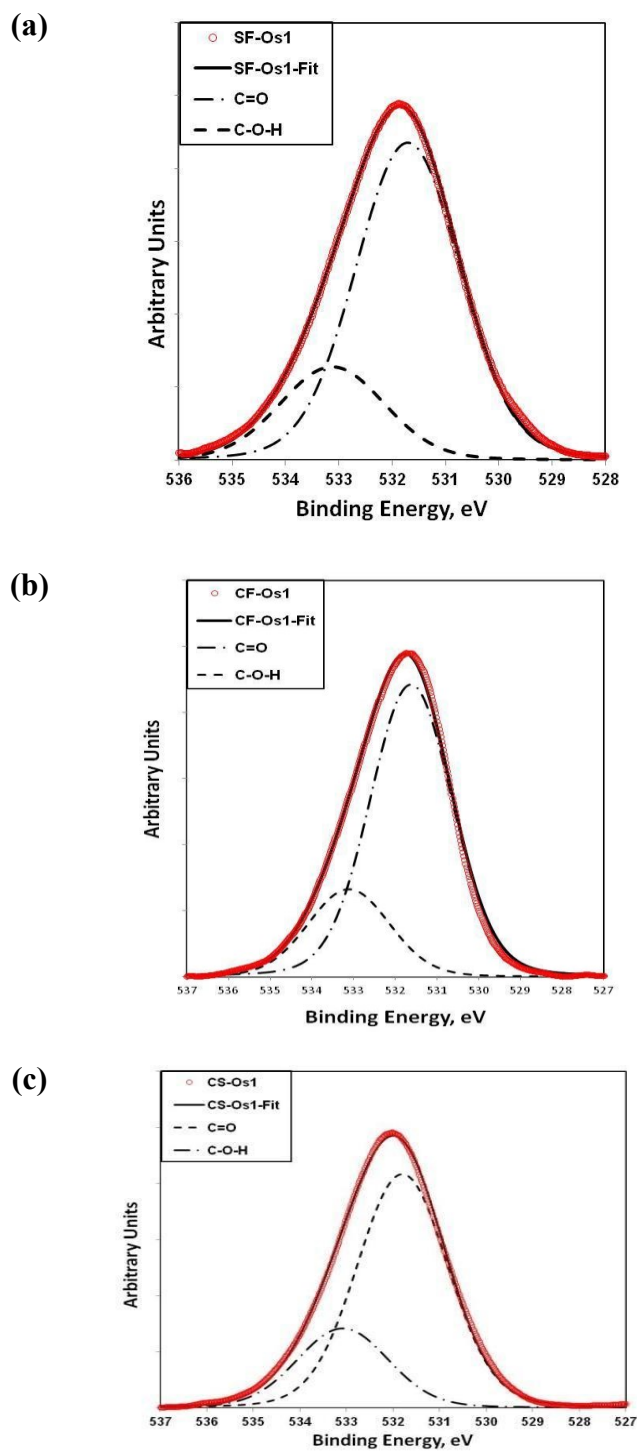


**Figure 4.3.** O (1s) XPS core-level spectra and deconvolution for PAN samples prepared with different approaches (SF, CF, and CS).

It was found that all PAN samples contained covalent chlorine (-Cl) and varied from 16-38% with respect to total chlorine (molar basis). Even this wide range still agrees well with the literature for optimally doped samples (~50%).<sup>26,34,54</sup> Specifically, it was reported that covalent chlorine could be attributed to ring halogenations.<sup>26,34,44,54</sup> On the contrary, covalently-bonded chlorine could be partially removed during the NaOH treatment, suggesting that covalent chlorine formation does not arise entirely from ring substitution.<sup>26</sup>

The possibility of having surface adsorbed Cl<sub>2</sub> and/or HCl on different substrates even under very low pressures as in XPS measurements has been reported.<sup>75-79</sup> It is possible that the covalent component of Cl could be attributed to surface adsorption or trapping within the polymer network. The relatively high value of the covalent component in SF (38%) with respect to CF and CS may confirm the previous assumption, since it agrees with particle size trend of SF<CF<CS, as reported in previous work (Chapter 2),<sup>68</sup> with the average size of SF as smallest (about 10-20 nm) relative to CF and CS (50-100 nm). Essentially, smaller particle size implies a relatively larger surface area to volume ratio and thus higher adsorptivity.<sup>80-82</sup> Additionally, the higher conductivity of SF supports the assumption of adsorbed/network-trapped Cl<sub>2</sub>/HCl over ring chlorination, since the latter has a negative impact on conductivity that is not seen here.<sup>68</sup> Also, it was reported that increasing proportions of covalently-bonded chlorine increases the halogen loading readily,<sup>26</sup> in exact agreement with the observed oxidation and doping level trends as shown in Tables 1 and 2.

The Cl<sup>•</sup> and/or Cl<sup>-</sup> were observed in all conducting forms of the PAN family, corresponding with HCl doping to the positively-charged nitrogen.<sup>24,26,34,44,54,55,57-59,83,84</sup> Since there are two main positive nitrogen species (polaron or bipolaron), it is possible to correlate the Cl species to corresponding N species.

Some reports showed that  $\text{Cl}^-$  was predominant and consistent with relatively lower conductivity and a localized positive charge on the nitrogen species.<sup>9,26,55</sup> On the other hand, increasing the relative proportion of  $\text{Cl}^*$  was consistent with a relative increase in conductivity and delocalized positive charge on nitrogen.<sup>9,44</sup> Based on our results, it is likely that the  $\text{Cl}^*$  and  $\text{Cl}^-$  mainly correspond to the polaron (radical cation) and bipolaron (dication) forms of PAN, respectively. Specifically, SF has the highest proportion of  $\text{Cl}^*$  with respect to CF and CS. The  $\text{Cl}^*/\text{Cl}^-$  ratio for the three samples was found to be 3.3, 0.5, and 0.4 in SF, CF, and CS, respectively. These ratios agree with our previously reported conductivity trend<sup>68</sup> and correlate with the observed oxidation level and degree of doping.

#### **4.3.2. Electromagnetic Measurements**

It was important to identify the structure-property relationships of the synthesis approaches in connection with high-frequency electromagnetic (EM) response to design final properties based on the chemical process steps. The main purpose for EM measurements was to confirm that the electronic structures of PAN samples having polaron and/or polaron lattices—as determined spectroscopically—exhibited the necessary chemical structure and charge delocalization for substantive improvements in EM field responses over existing forms of PAN previously produced and studied. In addition, the SE of PAN samples over a broad band of frequencies was explored. Ultimately, PAN-based nanomaterials as EM shielding media will exist as a filler in some convenient substrate-matrix or perhaps in its native form if appropriate forming conditions can be achieved. This application would preserve, or even enhance, final product SE.

In previous work,<sup>68</sup> it was reported that HCl-doped PAN nanoparticles showed an interesting contradiction to the general rule that higher crystallinity increases conductivity, *i.e.*, the CS PAN nanopowders are significantly more crystalline with demonstrably similar or lower conductivity and lower EM shielding than CF PAN samples.<sup>28,85-88</sup> It was found that if high crystallinity were achieved with the formation of cross-linking structures, the charge mobility is expected to be lower than that in linear doped PAN samples.<sup>89</sup> In this current work, a more detailed explanation addresses the previously observed phenomena from the point-of-view of electronic structure and chain conformation characteristics in reference to Chapter 3. Additionally, EM measurements correlate the impact of chemical, electronic, and conformational structures of the prepared PAN samples on SE behavior. Figures 4.5 and 4.6 show the results obtained from coaxial line measurements over a low frequency bandwidth (100-1500 MHz) and broad bandwidth (2-14 GHz), respectively.

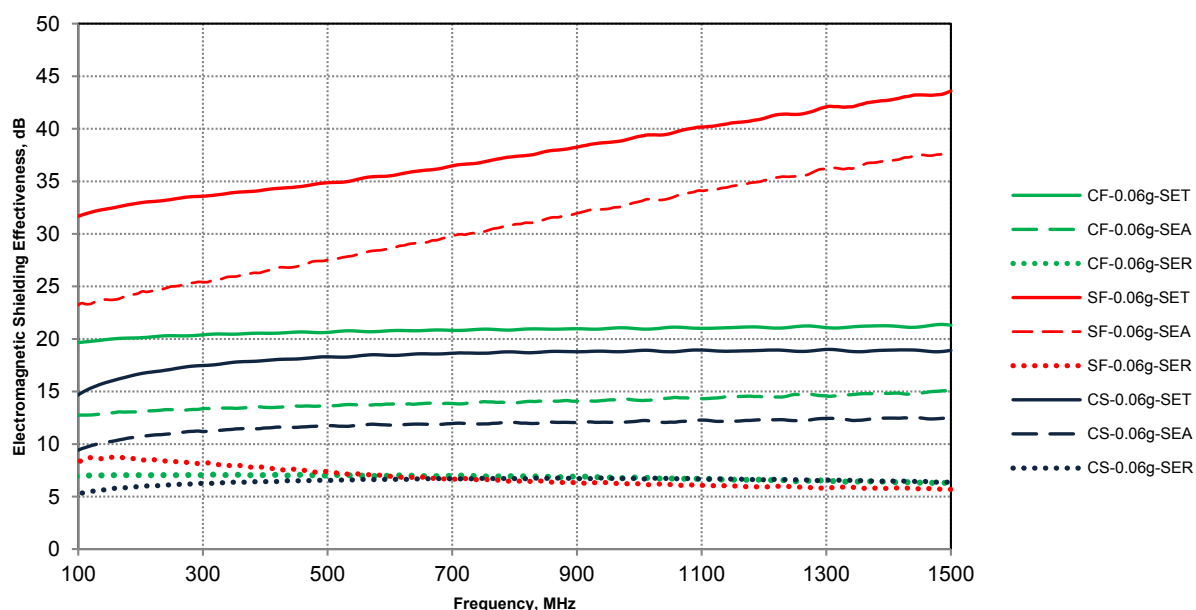


**Figure 4.5.** Low frequency electromagnetic shielding potential of 0.06 g HCl-doped PAN (CF, CS, and SF) tested in a coaxial sample holder as a function of frequency measured in the range 100-1500 MHz.

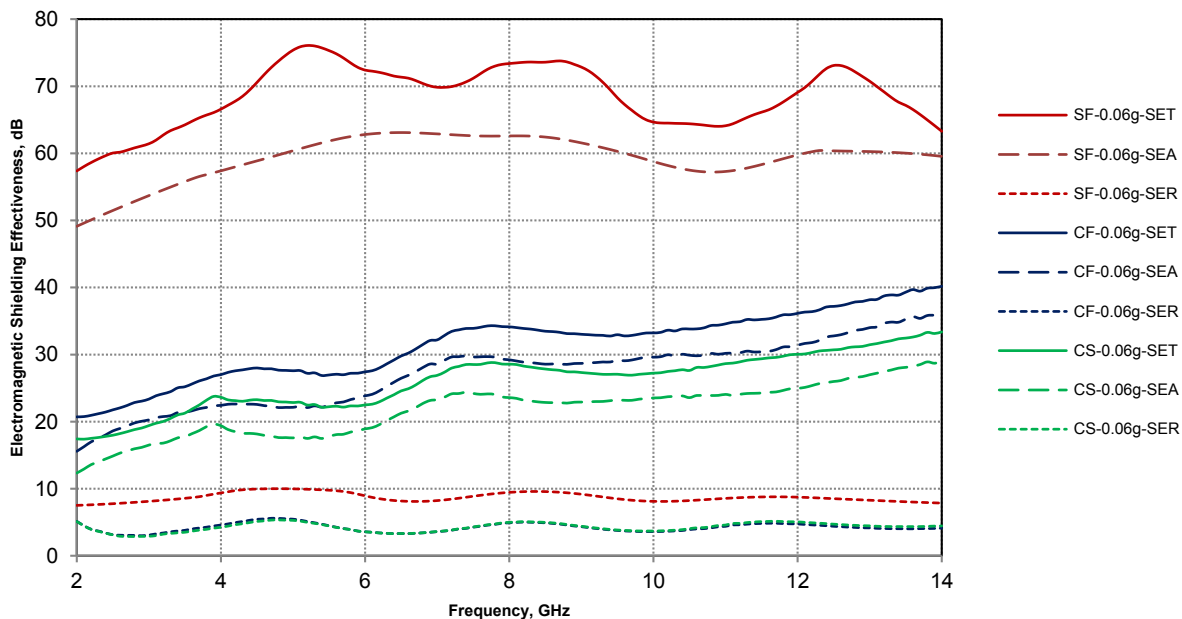


**Figure 4.6.** Broad band electromagnetic shielding potential of 0.06 g HCl-doped PAN (CF, CS, and SF) tested in a coaxial sample holder as a function of frequency measured in the range 2-14 GHz.

It was found that SF PAN was the most successful of the three HCl-doped PAN nano-products at EM shielding, especially at high frequencies. SF PAN achieved the highest average SEs of  $37.6 \pm 3.7$  dB and  $68.7 \pm 4.6$  dB within the 100-1500 MHz and 2-14 GHz bands, respectively. On the other hand, the maximum shielding performance of CF and CS was found to be only  $20.7 \pm 0.5$  dB and  $18.0 \pm 0.18$  dB within the low frequency band (100-1500 MHz), respectively. The same trend was observed at the higher and broader band (2-14 GHz); namely, the maximum shielding performance of CF and CS was found to be  $31.5 \pm 5.1$  dB and  $26.1 \pm 4.1$  dB, respectively. As expected, the SEA dominates the total shielding for all the samples while SER shows limited but still significant impact. In the low-frequency band, the SEA contributions in total shielding were 82%, 67%, and 65% in SF, CF, and CS, respectively. The enhancement of SEA contribution within the higher frequency band was noted.

It was found to be 84%, 87%, and 87% for SF, CF, and CS, respectively, which is a benefit over metals with high reflection contributions, for example. The obtained trends agree with the previous waveguide measurements within the X-band (8-12 GHz).<sup>68</sup> Table 3 summarizes the EM shielding measurements

**Table 4.3.** Summary of EM shielding effectiveness measurements.

SE	Frequency Band	CS	CF	SF
SE <sub>T</sub> (dB)	100-1500 MHz	18.0±1.8	20.7±0.5	37.3±3.7
	2-14 GHz	26.1±4.1	31.5±5.1	68.6±4.6
SE <sub>A</sub> (dB)	100-1500 MHz	11.6±1.2 (65%)	13.9±0.7 (67%)	30.4±4.6 (82%)
	2-14 GHz	21.9±3.9 (84%)	27.3±5.0 (87%)	59.3±3.3 (87%)
SE <sub>R</sub> (dB)	100-1500 MHz	6.40±0.6 (36%)	6.8±0.2 (33%)	6.9±1.0 (19%)
	2-14 GHz	4.3±0.7 (16%)	4.2±0.6 (13%)	8.7±0.7 (13%)

As shown in Figure 4.5, the EM shielding potential of SF is augmented as the frequency increases. This is faster than CF and CS, which were almost constant at low frequencies (Figure 4.6). The successful behavior of SF nanopowders in the waveguide measurements (Chapter 2) is confirmed, since SF samples are more efficient than CF and CS samples at high frequencies. The most interesting observation was the superior broadband shielding effectiveness of SF-PAN, which achieved average shielding effectiveness at 68.6±4.6 dB within the 2-14 GHz band. This superior performance was found to be higher than the recent reported values for HCl-doped PAN<sup>12,61</sup> and even higher than some currently reported performance for doped PAN modified with ferrites and carbon.<sup>90,91</sup>

This shielding effectiveness is very close to the behavior of sulphonic-doped PAN, as will be discussed in detail in Chapter 6.<sup>92,93</sup> To the best of our knowledge, this is the highest electromagnetic shielding by PAN doped with HCl and prepared through a so-called solvent-free approach, having no solvent added other than what dissolves the HCl.

The superior shielding performance of SF within a broad frequency band (2-14 GHz) supports the suggestion that its conjugated structure may have the fastest polaron delocalization<sup>94</sup> with respect to CF and CS. Also, it could be expected that SF has the fastest and enhanced dielectric response at high frequency.<sup>94,95</sup> This results support the presence of a polaron lattice electronic structure of SF. Moreover, the proposed polaron lattice of SF may be the key for enhancing the high-frequency dielectric response due to a long-range displacement of electrons. The SF PAN's superior EM behavior agrees well to previous interpretations of Raman, UV, and XPS. As charge in PAN becomes more delocalized, higher dielectric loss ( $\epsilon''$ ) is expected.<sup>92,96,97</sup> Higher dielectric loss leads to increasing microwave conductivity and the effective conductivity of the medium, as discussed in Chapter 2.<sup>94,95,98-100</sup> This may explain the enhancement in  $SE_T$  by increasing the frequency in the three samples generally and particularly in the SF case.

On contrary, the relative poor EM shielding performance of CF and CS could be correlated to their electronic structure as charge is more localized in both cases. The proposed predominant localized polaron in CF electronic structures may be the cause of its poor EM shielding with respect to SF. Both likely have an expanded coil conformation (found from the UV characterization). At the same time, CF has relatively high degree of disorder.<sup>68</sup> The low conductivity of CF could be attributed to the negative influence of disorder making its polaron structure more localized.<sup>94</sup>

The situation in CS is different than CF since CS has the highest extent of order, *i.e.*, it has the most cross-linked structure relative to SF and CF as it was found before and confirmed in this work.<sup>68</sup> A cross-linked/branched structure may not provide a substantial delocalization length.<sup>94</sup> Additionally, its electronic structure was predominantly bipolaron. Moreover, its compact coil conformation has a negative impact on conductivity. Furthermore, this study indicates that it also has the lowest oxidation level and degree of doping.

#### **4.4. Conclusions**

It was very important to support and confirm the electronic structure in order to understand the impact of the synthesis processes on different properties of HCl-doped PAN to correlate the chemical structure, polymorphism (Chapter 3), and electronic structure to electrical behavior (*viz.*, conductivity). Moreover, the most favorable synthesis approach to achieve the highest possible conductivity is a primary target for practical considerations in fine-tuning production on large scales. The present XPS study demonstrates that the coexistence of polaron and bipolaron is realized in all the polyaniline samples but with different extents dependent on the synthesis approach. Furthermore, polyanilines that have polaron and/or polaron lattices exhibited the necessary chemical structure and charge delocalization for substantive improvements in electromagnetic field responses over existing forms of PAN previously produced and studied. Synthesis protocols that lead to compact coil in HCl-doped PAN with cross-linked structures or branched chains (*e.g.*, conventional slow oxidation) is not recommended as there appears to be poor conductivity and EM shielding.

The SF approach is favorable for synthesizing the relatively linear, expanded coil, PAN conformations encouraging the development of delocalized polaron electronic structures. The SF approach fosters better oxidation and doping degree relative to the CF and CS methods where were found to be important for maximum SE. It could be concluded that SF approach leads to relatively optimum chemical/electronic structure which leads to enhancing dielectric response at higher frequencies, where delocalization processes are prominent, and may ultimately give rise to long-range displacements of electrons in the system<sup>94</sup>. On the other hand, the CS approach was found to be favorable for cross-linking structures, which may arise from the slow oxidation of aniline by restrictive reagent addition (APS solution at 0.1 ml/min  $\approx$  0.1 mmol/min), which fosters PAN chain growth with existing chains as well as other structural defects resulting in lower conductivity than in relatively linear, doped PAN.<sup>89,101,102</sup> Moreover, slow polymerization produces no noticeable change in temperature of the reacting mixture, which is favorable for higher degrees of crystallinity.<sup>101</sup> The higher cross-linked structures<sup>28,65,66</sup> would also disrupt crystallinity/linearity and thus prevent polaron delocalization.<sup>67</sup>

It was found that the oxidation level of PAN samples was found to be dependent on the synthesis approach, and SF approach leads to an optimum oxidation level (50%), and doping level also was found to be dependent on synthesis approach, with the SF approach leading to the greatest degree of doping where 98% of the imine nitrogens are doped. Since both fast and slow oxidation products (CF and CS) were synthesized with the same dopant (HCl) ratios, the chemical, electronic structures and chain conformation appear to depend only on the reaction conditions<sup>89</sup> and thus an optimum in conductivity for the maximum shielding potential may be revealed with fine-tuning of the rate and method for oxidant addition.

XPS results indicate that increasing radical chlorine concentrations correlate with better conductivity, oxidation level, and degree of doping for higher polaron content. The SF approach may ultimately give rise to increased long-range electron displacement in PAN systems for optimal dielectric response at high frequency.

This work highlighted the impact of a solvent-free synthesis approach on chemical, electronic, and conformational characteristics of HCl-doped PAN nanopowders. Moreover, the proposed polaron lattice of SF may be the key for enhancing the high-frequency dielectric response due to a long-range displacement of electrons. Ultimately, an extensive characterization was performed to investigate the effective role of these parameters in EM shielding effectiveness (SE), particularly in the microwave band. SF synthesis in a slightly wetted solid-phase reaction provided substantial property improvements over conventional solution-rich oxidations using limited or abundant oxidizer. It was found that SF PAN was the most successful of the three HCl-doped PAN nano-products at EM shielding, especially at high frequencies. This superior performance (SE of  $37.6 \pm 3.7$  dB and  $68.7 \pm 4.6$  dB within 100-1500 MHz and 2-14 GHz, respectively) was found to be higher than the recent reported values for HCl-doped PAN<sup>12,61</sup> and even higher than some currently reported performance for doped PAN modified with ferrites and carbon.<sup>90,91</sup> Thorough characterization demonstrates the importance of generating a predominantly delocalized polaron electronic structure relative to a bipolaron and/or localized polaron when attempting to enhance SE in nano-PAN. The superior shielding performance of SF within a broad frequency band (2-14 GHz) supports the suggestion that its conjugated structure may have the fastest polaron delocalization<sup>94</sup> with respect to CF and CS.

#### 4.5. References

- (1) Chowdhury, P.; Saha, B. Potassium Dichromate Initiated Polymerization of Aniline *Indian J. Chem. Technol.* **2005**, *12*, 671-675.
- (2) Li, Y.; Al-Ghamdi, A. A.; Al-Hartomy, O. A.; El-Tantawy, F.; Yakuphanoglu, F. Semiconducting Properties of Nanofiber Polyaniline Organic Semiconductor *OAM – RC* **2012**, *6*, 235-238.
- (3) Karatchevtseva, I.; Zhang, Z.; Hanna, J.; Luca, V. Electrosynthesis of Macroporous Polyaniline–V<sub>2</sub>O<sub>5</sub> Nanocomposites and Their Unusual Magnetic Properties *Chem. Mater.* **2006**, *18*, 4908-4916.
- (4) Chen, S. A.; Lin, L. C. Polyaniline Doped by the New Class of Dopant, Ionic Salt: Structure and Properties *Macromolecules* **1995**, *28*, 1239-1245.
- (5) Sreedhar, B.; Sairam, M.; Chattopadhyay, D. K.; Mitra, P. P.; Rao, D. V. Thermal and Xps Studies on Polyaniline Salts Prepared by Inverted Emulsion Polymerization *J. Appl. Polym. Sci.* **2006**, *101*, 499-508.
- (6) Heide, V. d. *X-Ray Photoelectron Spectroscopy an Introduction to Principles and Practices*; Wiley: Hoboken, N.J., 2012.
- (7) Inoue, M. B.; Nebesny, K. W.; Fernando, Q.; Inoue, M. X-Ray Photoelectron Spectroscopy of New Soluble Polyaniline Perchlorates: Evidence for the Coexistence of Polarons and Bipolarons *J. Mater. Chem.* **1991**, *1*, 213-216.
- (8) Han, M. G.; Im, S. S. X-Ray Photoelectron Spectroscopy Study of Electrically Conducting Polyaniline/Polyimide Blends *Polymer* **2000**, *41*, 3253-3262.

- (9) Nalwa, H. S. *Handbook of Organic Conductive Molecules and Polymers 3, Conductive Polymers: Spectroscopy and Physical Properties*; Wiley: Chichester; New York, 1997; Vol. 3.
- (10) Snauwaert, P.; Lazzaroni, R.; Riga, J.; Verbist, J. J.; Gonbeau, D. A Photoelectron Spectroscopic Study of the Electrochemical Processes in Polyaniline *J. Chem. Phys.* **1990**, *92*, 2187.
- (11) Yun, J.; Im, J. S.; Lee, Y. S.; Kim, H. I. Effect of Oxyfluorination on Electromagnetic Interference Shielding Behavior of Mwcnt/Pva/Paac Composite Microcapsules *Eur. Polym. J.* **2010**, *46*, 900-909.
- (12) Wang, Y.; Jing, X. Intrinsically Conducting Polymers for Electromagnetic Interference Shielding *Polym. Adv. Technol.* **2005**, *16*, 344-351.
- (13) Phang, S. W.; Hino, T.; Abdullah, M. H.; Kuramoto, N. Applications of Polyaniline Doubly Doped with P-Toluene Sulphonic Acid and Dichloroacetic Acid as Microwave Absorbing and Shielding Materials *Mater. Chem. Phys.* **2007**, *104*, 327-335.
- (14) Chen, L. F.; Ong, C. K.; Neo, C. P.; Varadan, V. V.; Varadan, V. K. *Microwave Electronics: Measurement and Materials Characterization*; John Wiley & Sons, Ltd 2004
- (15) Chen, Y.; Kang, E. T.; Neoh, K. G.; Lim, S. L.; Ma, Z. H.; Tan, K. L. Intrinsic Redox States of Polyaniline Studied by High-Resolution X-Ray Photoelectron Spectroscopy *Colloid. Polym. Sci.* **2001**, *279*, 73-76.
- (16) Kulkarni, V. G.; Campbell, L. D.; Mathew, W. R. Thermal Stability of Polyaniline *Synt. Met.* **1989**, *30*, 321-325.

- (17) Wei, X. L.; Fahlman, M.; Epstein, A. J. Xps Study of Highly Sulfonated Polyaniline *Macromolecules* **1999**, *32*, 3114-3117.
- (18) Zeng, X. R.; Ko, T. M. Structures and Properties of Chemically Reduced Polyanilines *Polymer* **1998**, *39*, 1187-1195.
- (19) Han, M. G.; Cho, S. K.; Oh, S. G.; Im, S. S. Preparation and Characterization of Polyaniline Nanoparticles Synthesized from Dbsa Micellar Solution *Synt. Met.* **2002**, *126*, 53-60.
- (20) Chen, S. A.; Hwang, G. W. Water-Soluble Self-Acid-Doped Conducting Polyaniline: Structure and Properties *JACS* **1995**, *117*, 10055-10062.
- (21) Ren, G.; Qiu, H.; Wu, Q.; Li, H.; Fan, H.; Fang, C. Thermal Stability of Composites Containing Hcl-Doped Polyaniline and Fe Nanoparticles *Mater. Chem. Phys.* **2010**, *120*, 127-133.
- (22) Chan, H. S. O.; Ho, P. K. H.; Ng, S. C.; Tan, B. T. G.; Tan, K. L. A New Water-Soluble, Self-Doping Conducting Polyaniline from Poly (O-Aminobenzylphosphonic Acid) and Its Sodium Salts: Synthesis and Characterization *JACS* **1995**, *117*, 8517-8523.
- (23) Jousseume, V.; Morsli, M.; Bonnet, A. Xps Study of Aged Polyaniline Films *J. Appl. Polym. Sci.* **2003**, *90*, 3730-3736.
- (24) Yue, J.; Epstein, A. J. Xps Study of Self-Doped Conducting Polyaniline and Parent Systems *Macromolecules* **1991**, *24*, 4441-4445.
- (25) Abe, T.; Watanabe, A. X-Ray Photoelectron Spectroscopy of Nitrogen Functional Groups in Soil Humic Acids *Soil science* **2004**, *169*, 35-43.
- (26) Kang, E. T.; Neoh, K. G.; Tan, T. C.; Khor, S. H.; Tan, K. L. Structural Studies of Poly(P-Phenyleneamine) and Its Oxidation *Macromolecules* **1990**, *23*, 2918-2926.

- (27) Ashraf, S. A.; Kane-Maguire, L. A. P.; Majidi, M. R.; Pyne, S. G.; Wallace, G. G. Influence of the Chiral Dopant Anion on the Generation of Induced Optical Activity in Polyanilines *Polymer* **1997**, *38*, 2627-2631.
- (28) Zhang, K.; Li, Y. Electrical Conductivity Enhancement of Polyaniline by Refluxing *Polym. Adv. Technol.* **2011**, *22*, 2084-2090.
- (29) Tan, H. H.; Neoh, K. G.; Liu, F. T.; Kocherginsky, N.; Kang, E. T. Crosslinking and Its Effects on Polyaniline Films *J. Appl. Polym. Sci.* **2001**, *80*, 1-9.
- (30) Mosqueda, Y.; Pérez-Cappe, E.; Arana, J.; Longo, E.; Ries, A.; Cilense, M.; Nascente, P. A. P.; Aranda, P.; Ruiz-Hitzky, E. Preparation and Characterization of  $\text{LiNi}_{0.8}\text{Co}_{0.2}\text{O}_2/\text{PANI}$  Microcomposite Electrode Materials under Assisted Ultrasonic Irradiation *J. Solid State Chem.* **2006**, *179*, 308-314.
- (31) Boutaleb, N.; Benyoucef, A.; Salavagione, H. J.; Belbachir, M.; Morallón, E. Electrochemical Behaviour of Conducting Polymers Obtained into Clay-Catalyst Layers. An in Situ Raman Spectroscopy Study *Eur. Polym. J.* **2006**, *42*, 733-739.
- (32) Golczak, S.; Kanciurzevska, A.; Fahlman, M.; Langer, K.; Langer, J. J. Comparative Xps Surface Study of Polyaniline Thin Films *Solid State Ionics* **2008**, *179*, 2234-2239.
- (33) OnáChan, H. S.; MingáGan, L.; HaráChew, C.; HowáSeow, S. Characterization of Chemically and Electrochemically Prepared Polyanilines in Inverse Microemulsions *J. Mater. Chem.* **1993**, *3*, 1109-1115.
- (34) Monkman, A. P.; Stevens, G. C.; Bloor, D. X-Ray Photoelectron Spectroscopic Investigations of the Chain Structure and Doping Mechanisms in Polyaniline *J. Phys. D: Appl. Phys* **1991**, *24*, 738-749.

- (35) Chen, W. C.; Wen, T. C.; Gopalan, A. The Inductive Behavior Derived from Hydrolysis of Polyaniline *Electrochim. Acta* **2002**, *47*, 4195-4206.
- (36) Beard, B. C.; Spellane, P. Xps Evidence of Redox Chemistry between Cold Rolled Steel and Polyaniline *Chem. Mater.* **1997**, *9*, 1949-1953.
- (37) Liu, Y. Synthesis and Characterization of Metal-Polyaniline Thin Films and Membranes, University of Missouri, 2004.
- (38) Wu, M. S.; Wen, T. C.; Gopalan, A. Electrochemical Copolymerization of Diphenylamine and Anthranilic Acid with Various Feed Ratios *J. Electrochem. Soc.* **2001**, *148*, D65-D73.
- (39) Kohut-Svelko, N.; Reynaud, S.; Dedryvère, R.; Martinez, H.; Gonbeau, D.; François, J. Study of a Nanocomposite Based on a Conducting Polymer: Polyaniline *Langmuir* **2005**, *21*, 1575-1583.
- (40) Hardy, S. Use of Polythiophene and Poly (Thiophene-3-Acetic Acid) as Charge-Selective Films for Amperometric Flow-Cell Detectors *J. Mater. Chem.* **1995**, *5*, 631-637.
- (41) Watts, J. F.; Wolstenholme, J. *An Introduction to Surface Analysis by Xps and Aes*; J. Wiley: Chichester, West Sussex, England; New York, 2003.
- (42) Hu, C. C.; Lin, J. Y. Effects of the Loading and Polymerization Temperature on the Capacitive Performance of Polyaniline in Nano<sub>3</sub> *Electrochim. Acta* **2002**, *47*, 4055-4067.
- (43) Barr, T. L. *Modern Esca : The Principles and Practice of X-Ray Photoelectron Spectroscopy*; CRC Press: Boca Raton, 1994.

- (44) Kang, E. T.; Neoh, K. G.; Tan, K. L. Polyaniline: A Polymer with Many Interesting Intrinsic Redox States *Prog. Polym. Sci.* **1998**, *23*, 277-324.
- (45) Barthet, C.; Armes, S. P.; Chehimi, M. M.; Bilem, C.; Omastova, M. Surface Characterization of Polyaniline-Coated Polystyrene Latexes *Langmuir* **1998**, *14*, 5032-5038.
- (46) Rajagopalan, R.; Iroh, J. O. Characterization of Polyaniline–Polypyrrole Composite Coatings on Low Carbon Steel: A Xps and Infrared Spectroscopy Study *Appl. Surf. Sci.* **2003**, *218*, 58-69.
- (47) Ameen, S.; Song, M.; Kim, D. G.; Im, Y. B.; Seo, H. K.; Kim, Y. S.; Shin, H. S. Iodine Doped Polyaniline Thin Film for Heterostructure Devices Via Pecvd Technique: Morphological, Structural, and Electrical Properties *Macromol. Res.* **2012**, *20*, 30-36.
- (48) Gerenser, L. J.; Elman, J. F.; Mason, M. G.; Pochan, J. M. Esca Studies of Corona-Discharge-Treated Polyethylene Surfaces by Use of Gas-Phase Derivatization *Polymer* **1985**, *26*, 1162-1166.
- (49) Zhou, J. H.; Sui, Z. J.; Zhu, J.; Li, P.; Chen, D.; Dai, Y. C.; Yuan, W. K. Characterization of Surface Oxygen Complexes on Carbon Nanofibers by Tpd, Xps and Ft-Ir *Carbon* **2007**, *45*, 785-796.
- (50) Briggs, D.; Beamson, G. Xps Studies of the Oxygen 1s and 2s Levels in a Wide Range of Functional Polymers *Anal. Chem.* **1993**, *65*, 1517-1523.
- (51) López, G. P.; Castner, D. G.; Ratner, B. D. Xps O1s Binding Energies for Polymers Containing Hydroxyl, Ether, Ketone and Ester Groups *Surf. Interface Anal.* **1991**, *17*, 267-272.

- (52) Fan, J.; Hao, Y.; Munuera, C.; Garcia-Hernandez, M.; Güell, F.; Johansson, E. M. J.; Boschloo, G.; Hagfeldt, A.; Cabot, A. *The Journal of Chemical Physics* *J. Phys. Chem. C* **2013**.
- (53) Puziy, A.; Poddubnaya, O. I.; Socha, R. P.; Gurgul, J.; Wisniewski, M. *Xps and Nmr Studies of Phosphoric Acid Activated Carbons* *Carbon* **2008**, *46*, 2113-2123.
- (54) Aldissi, M.; Armes, S. P. *X-Ray Photoelectron Spectroscopy Study of Bulk and Colloidal Polyaniline* *Macromolecules* **1992**, *25*, 2963-2968.
- (55) Tan, K. L.; Tan, B. T.; Kang, E. T.; Neoh, K. G. *X-Ray Photoelectron Spectroscopy Studies of the Chemical Structure of Polyaniline* *Physical Review B* **1989**, *39*, 8070-8073.
- (56) Barra, G. M. O.; Leyva, M. E.; Gorelova, M. M.; Soares, B. G.; Sens, M. *X-Ray Photoelectron Spectroscopy and Electrical Conductivity of Polyaniline Doped with Dodecylbenzenesulfonic Acid as a Function of the Synthetic Method* *J. Appl. Polym. Sci.* **2001**, *80*, 556-565.
- (57) Kang, E. T.; Neoh, K. G.; Tan, K. L. "Esca Studies of Charge Transfer Interactions in Electroactive Polymers"; *Makromolekulare Chemie. Macromolecular Symposia*, 1992.
- (58) Kang, E. T.; Neoh, K. G.; Woo, Y. L.; Tan, K. L. *X-Ray Photoelectron Spectroscopic Studies of H<sub>2</sub>SO<sub>4</sub> Protonated Polyaniline* *Polymer* **1992**, *33*, 2857-2859.
- (59) Kang, E. T.; Neoh, K. G.; Tan, K. L.; Tan, B. T. G. *Protonation of the Amine Nitrogens in Emeraldine — Evidence from X-Ray Photoelectron Spectroscopy* *Synt. Met.* **1992**, *46*, 227-233.
- (60) Colomban, P.; Folch, S.; Gruger, A. *Vibrational Study of Short-Range Order and Structure of Polyaniline Bases and Salts* *Macromolecules* **1999**, *32*, 3080-3092.

- (61) Wan, M. *Conducting Polymers with Micro or Nanometer Structure*; Tsinghua University Press ; Springer: Beijing; Berlin, 2008.
- (62) Wallace, G. G.; Spinks, G. M.; Kane-Maguire, L. A. P.; Teasdale, P. R. *Conductive Electroactive Polymers Intelligent Materials Systems*; CRC Press: Boca Raton; London; New York, 2009.
- (63) Mathew, R.; Mattes, B. R.; Espe, M. P. A Solid State Nmr Characterization of Cross-Linked Polyaniline Powder *Synt. Met.* **2002**, *131*, 141.
- (64) Varela-Alvarez, A.; Sordo, J. A. A Suitable Model for Emeraldine Salt *J. Chem. Phys.* **2008**, *128*.
- (65) Nand, A. V.; Ray, S.; Gizdavic-Nikolaidis, M.; Travas-Sejdic, J.; Kilmartin, P. A. The Effects of Thermal Treatment on the Antioxidant Activity of Polyaniline *Polym. Degrad. Stab.* **2011**, *96*, 2159-2166.
- (66) Bhadra, S.; Khastgir, D. Extrinsic and Intrinsic Structural Change During Heat Treatment of Polyaniline *Polym. Degrad. Stab.* **2008**, *93*, 1094-1099.
- (67) Laslau, C.; Zujovic, Z.; Travas-Sejdic, J. Theories of Polyaniline Nanostructure Self-Assembly: Towards an Expanded, Comprehensive Multi-Layer Theory (Mlt) *Prog. Polym. Sci.* **2010**, *35*, 1403-1419.
- (68) Tantawy, H. R.; Aston, D. E.; Smith, J. R.; Young, J. L. A Comparison of Electromagnetic Shielding with Polyaniline Nanopowders Produced in Solvent-Limited Conditions *ACS Appl. Mater. Interfaces*, **2013**, *5*, 4648-4658.
- (69) Hendrickson, D. N.; Hollander, J. M.; Jolly, W. L. Core-Electron Binding Energies for Compounds of Boron, Carbon, and Chromium *Inorg. Chem.* **1970**, *9*, 612-615.

- (70) Van der Heide, P. *X-Ray Photoelectron Spectroscopy: An Introduction to Principles and Practices*; John Wiley & Sons, 2011.
- (71) Paterno, L. G.; Manolache, S.; Denes, F. Synthesis of Polyaniline-Type Thin Layer Structures under Low-Pressure Rf-Plasma Conditions *Synt. Met.* **2002**, *130*, 85-97.
- (72) Lee, Y. M.; Kim, J. H.; Kang, J. S.; Ha, S. Y. Annealing Effects of Dilute Polyaniline/Nmp Solution *Macromolecules* **2000**, *33*, 7431-7439.
- (73) Kumar, S. N.; Gaillard, F.; Bouyssoux, G.; Sartre, A. High-Resolution Xps Studies of Electrochemically Synthesized Conducting Polyaniline Films *Synt. Met.* **1990**, *36*, 111-127.
- (74) Boehm, H. P. Surface Oxides on Carbon and Their Analysis: A Critical Assessment *Carbon* **2002**, *40*, 145-149.
- (75) Kishi, K.; Ikeda, S. X-Ray Photoelectron Spectroscopic Study of the Reaction of Evaporated Metal Films with Chlorine Gas *J. Phys. Chem.* **1974**, *78*, 107-112.
- (76) Brichka, S. Y.; Prikhod'ko, G. P.; Sementsov, Y. I.; Brichka, A. V.; Dovbeshko, G. I.; Paschuk, O. P. Synthesis of Carbon Nanotubes from a Chlorine-Containing Precursor and Their Properties *Carbon* **2004**, *42*, 2581-2587.
- (77) Ordonez, S.; Díez, F. V.; Sastre, H. Characterisation of the Deactivation of Platinum and Palladium Supported on Activated Carbon Used as Hydrodechlorination Catalysts *Appl. Catal., B* **2001**, *31*, 113-122.
- (78) Ordóñez, S.; Sastre, H.; Díez, F. V. Thermogravimetric Determination of Coke Deposits on Alumina-Supported Noble Metal Catalysts Used as Hydrodechlorination Catalysts *Thermochim. Acta* **2001**, *379*, 25-34.

- (79) Papirer, E.; Lacroix, R.; Donnet, J. B.; Nansé, G.; Fioux, P. Xps Study of the Halogenation of Carbon Black—Part 2. Chlorination *Carbon* **1995**, *33*, 63-72.
- (80) Maeda, S.; Armes, S. P. Surface Area Measurements on Conducting Polymer-Inorganic Oxide Nanocomposites *Synt. Met.* **1995**, *73*, 151-155.
- (81) Croissant, M. J.; Napporn, T.; Léger, J. M.; Lamy, C. Electrocatalytic Oxidation of Hydrogen at Platinum-Modified Polyaniline Electrodes *Electrochim. Acta* **1998**, *43*, 2447-2457.
- (82) Xia, H.; Wang, Q. Preparation of Conductive Polyaniline/Nanosilica Particle Composites through Ultrasonic Irradiation *J. Appl. Polym. Sci.* **2003**, *87*, 1811-1817.
- (83) Nicolau, Y. F.; Ermolieff, A. Xps Characterization of Polyaniline Filled N<sup>+</sup> Type Porous Silicon *Synt. Met.* **1995**, *71*, 2073-2074.
- (84) Bedekar, B. A.; Rama, H. S.; Kaushik, V. K. Structural Analysis and Electrical Behavior of Polyaromatic Diamines *Polym. Plast. Technol. Eng.* **2001**, *40*, 321-340.
- (85) Zhang, D. On the Conductivity Measurement of Polyaniline Pellets *Polym. Test.* **2007**, *26*, 9-13.
- (86) Chaudhari, H. K.; Kelkar, D. S. Investigation of Structure and Electrical Conductivity in Doped Polyaniline *Polym. Int.* **1997**, *42*, 380-384.
- (87) Bohli, N.; Gmati, F.; Mohamed, A. B.; Vigneras, V.; Miane, J. L. Conductivity Mechanism of Polyaniline Organic Films: The Effects of Solvent Type and Casting Temperature *J. Phys. D: Appl. Phys* **2009**, *42*, 205404.
- (88) Chaudhari, H. K.; Kelkar, D. S. X-Ray Diffraction Study of Doped Polyaniline *J. Appl. Polym. Sci.* **1996**, *62*, 15.

- (89) Liu, H.; Hu, X. B.; Wang, J. Y.; Boughton, R. I. Structure, Conductivity, and Thermopower of Crystalline Polyaniline Synthesized by the Ultrasonic Irradiation Polymerization Method *Macromolecules* **2002**, *35*, 9414.
- (90) Gairola, S. P.; Verma, V.; Kumar, L.; Dar, M. A.; Annapoorni, S.; Kotnala, R. K. Enhanced Microwave Absorption Properties in Polyaniline and Nano-Ferrite Composite in X-Band *Synt. Met.* **2010**, *160*, 2315-2318.
- (91) Moon, Y. E.; Yun, J.; Kim-II, H. Synergetic Improvement in Electromagnetic Interference Shielding Characteristics of Polyaniline-Coated Graphite Oxide/G-Fe<sub>2</sub>O<sub>3</sub>/BaTiO<sub>3</sub> Nanocomposites *J. Ind. Eng. Chem.* **2012**.
- (92) Chandrasekhar, P.; Naishadham, K. Broadband Microwave Absorption and Shielding Properties of a Poly(Aniline) *Synt. Met.* **1999**, *105*, 115.
- (93) Saini, P.; Choudhary, V.; Sood, K. N.; Dhawan, S. K. Electromagnetic Interference Shielding Behavior of Polyaniline/Graphite Composites Prepared by in Situ Emulsion Pathway *J. Appl. Polym. Sci.* **2009**, *113*, 3146-3155.
- (94) Yan, X. Z.; Goodson, T. High Dielectric Hyperbranched Polyaniline Materials *J. Phys. Chem. B* **2006**, *110*, 14667-14672.
- (95) Guo, M.; Yan, X.; Kwon, Y.; Hayakawa, T.; Kakimoto, M. A.; Goodson, T. High Frequency Dielectric Response in a Branched Phthalocyanine *JACS* **2006**, *128*, 14820-14821.
- (96) Boreddy, R. Designing of Nano Composites of Conducting Polymers for Emi Shielding. In *Advances in Nanocomposites - Synthesis, Characterization and Industrial Applications*; Reddy, B. S. R., Ed.; INTECH Open Access Publisher, 2011; pp 429-482.

- (97) Micheli, D.; Apollo, C.; Pastore, R.; Marchetti, M. X-Band Microwave Characterization of Carbon-Based Nanocomposite Material, Absorption Capability Comparison and Ras Design Simulation *Compos. Sci. Technol* **2010**, *70*, 400-409.
- (98) John, H.; Thomas, R. M.; Jacob, J.; Mathew, K. T.; Joseph, R. Conducting Polyaniline Composites as Microwave Absorbers *Polym. Compos.* **2007**, *28*, 588.
- (99) John, H.; Thomas, R. M.; Mathew, K. T.; Joseph, R. Studies on the Dielectric Properties of Poly(O-Toluidine) and Poly(O-Toluidine-Aniline) Copolymer *J. Appl. Polym. Sci.* **2004**, *92*, 592-598.
- (100) Moore, J. C.; Fujita, S. Dielectric Properties of Ice Containing Acid and Salt Impurity at Microwave and Low Frequencies *J. Geophys. Res.* **1993**, *98*, 9769-9780.
- (101) Stejskal, J.; Sapurina, I.; Trchova, M. Polyaniline Nanostructures and the Role of Aniline Oligomers in Their Formation *Prog. Polym. Sci.* **2010**, *35*, 1420-1481.
- (102) Pan, L. J.; Pu, L.; Shi, Y.; Sun, T.; Zhang, R.; Zheng, Y. O. Hydrothermal Synthesis of Polyaniline Mesostructures *Adv. Funct. Mater.* **2006**, *16*, 1279-1288.

## CHAPTER 5

### **Dielectric Behavior and Conductivity HCl-Doped Polyaniline by Solvent-Limited Synthesis**

#### **5.1.Introduction**

In previous chapters 2, 3 and 4, the impact of solvent free/limited approach on HCl-doped polyanilines (PANs) was investigated from several aspects. One of the main summative conclusions therein was that the SF approach leads to moderate crystallinity and minimum cross-linking and/or branching, which may be the most important reason for its relatively high conductivity, with the best impact on EMI shielding. On the other hand, the highest crystalline/ordered HCl-doped PAN prepared by the CS approach has the lowest conductivity with respect to SF and CF PANs. The suggested explanation was that the CS approach leads to maximizing cross-linking/branching, which results in a shorter conjugated length and localized charge and hence lower conductivity. This previous explanation was confirmed in chapter 3 with Raman and UV investigations<sup>1</sup>. In addition, XPS and EM shielding measurements support the aforementioned explanation as mentioned in chapter 4.

In order to understand how the synthesis approach could enhance electrical/dielectrical properties through tuning electronic structure of HCl-doped PAN and correlate this impact with chemical structure and degree of delocalization of electronic structure (polaron/polaron lattice), deeper investigations were employed and covered in this chapter. It was interesting to consider more details about the possible tuning of the chemical structure of the doped PAN as a result of manipulating preparation conditions. Distinguishing between the impact of cross-linking and branching on electrical/dielectrical properties of HCl-doped PAN was an

important aim of this chapter. In many sources, cross-linking and branching were assumed to be largely dependent<sup>2-7</sup>. It could be helpful to understand how to distinguish between cross-linking and branching doped PAN samples for the purpose of tuning synthesis conditions toward a given application requirements of electrical behavior, whether increasing or decreasing either cross-linking or branching for the desired result.

The current study aims to confirm the reason for DC electrical conductivity trends observed previously in chapter 2, electrical conductivity was out with different approach than the used in chapter 2. In addition to elucidating the relative impact of different structural aspects (hydrogen bonding/branching/cross-linking) on electrical/dielectrical behavior of PAN samples. Moreover, dielectric constant and dielectric loss measurements were employed to estimate the relative degree of charge delocalization, which can be correlated at least in relative trends with the average extent of cross-linking and branching. Furthermore, elucidating the relation between the crystallinity of the HCl-doped PAN samples investigated in chapter 2 with respect to molecular structure and electrical/dielectrical properties will be discussed.

FTIR spectroscopy and AC/DC studies of HCl-doped PAN samples are applied herein to explicate the chemical nature of the HCl-doped PAN samples from each synthetic route to understand and clarify the causal connections between reaction conditions and material products for process control over resulting electrical properties. Full FTIR band characterization ( $400\text{ cm}^{-1} - 4000\text{ cm}^{-1}$ ) was carried out for HCl-doped PAN nanopowders. Moreover, PAN samples were subjected to AC conductivity and dielectric permittivity measurements in the frequency range of 1Hz-1MHz in order to estimate the relative degree of charge delocalization of the samples. By integrating the conclusions from this current work

and previous chapters, in addition to recalling some reported facts about the observed significant crystallinity in undoped/dedoped polyaniline<sup>8-11</sup>, the former model that assumed doped PAN as macroscopic metallic domains (conductive/crystalline) sprinkled throughout a disordered insulating matrix (amorphous barriers)<sup>12-15</sup> may need to be clarified and updated.

The three-way comparison of fast oxidation, or rapid addition of oxidizing agent, to slow oxidation and ultimately to a nearly solvent-free reaction process will highlight the significant range of differences in final polymer properties even while using the same dopant at the same quantities. The highly-variant synthesis conditions for one fairly-well studied conductive polymer type establishes an example for justification as to the need of a much deeper understanding into the connections and nuances between reaction conditions and final PAN qualities, especially with a particular future goal for optimizing polymeric materials toward enhancing dielectrical properties of PAN for electromagnetic (EM) shielding applications and related fields as part of this dissertation's goal. This work continues to expand a fundamental understanding in this regard for methodical future expansion to other dopants and ongoing studies in shielding materials for mitigating EM interference effects on electronic devices.

## **5.2. Materials and Methods**

The same materials and procedures aforementioned in chapter 2, 3, and 4 were used to prepare the PAN samples in this current work<sup>16-18</sup> from solvent-free (SF) and conventional (solvent-based) chemical oxidations under slow (CS) and fast (CF) production rates as controlled by the addition of aqueous ammonium peroxydisulfate (APS).

### 5.2.1. Chemical Characterization

In order to confirm the chemical composition of the obtained HCl-doped PAN samples and investigate any significant difference in the chemical structures (cross-linking/branching/hydrogen bonding) of PAN samples as functions of synthesis approach, FTIR was employed. The final obtained dry powder of the prepared doped PAN were characterized with ThermoNicolet Avatar 370 FTIR spectrometer. Tested samples were prepared as KBr pellets (ca. 0.3 % by mass in KBr). The spectra were collected using 128 scans between 4000  $\text{cm}^{-1}$  and 400  $\text{cm}^{-1}$  at a resolution of 2.0  $\text{cm}^{-1}$ .

### 5.2.2. DC/AC Conductivity and Dielectric Permeativity Measurements

Typically, 0.05-g samples were pelletized in a special homemade cell, unlike chapter 2. The dimensions of the pellet under test were 5-mm diameter and  $1.2 \pm 0.1$ -mm thickness. DC conductivity ( $\sigma_{DC}$ ) of the samples was measured at room temperature on pressed pellets by a two-point probe technique<sup>19-21</sup>, the value of which was calculated by the following equation<sup>22</sup>:

$$\sigma_{DC} = \frac{L_c}{R * A_c}$$

where  $L_c$  is sample thickness,  $A_c$  is sample surface area, and  $R$  is the measured resistance of the sample.

Three pellets were prepared for each sample. Current-voltage (I-V) measurements were carried out via a Keithley 4200 SCS semiconductor parameter analyzer. Dual sweep mode was operated within a voltage range of -0.1 to 0.1 V, in 0.01 V steps. Each I-V measurement was repeated 11 times at least for every pellet for reproducibility confirmation. The values reported are averaged over 33 readings for each sample. After DC conductivity measurements, samples in the same homemade cell were subjected to AC conductivity and

dielectric permittivity measurements, which were performed in the frequency range of 1Hz-1MHz. These two parameters were evaluated by measuring the equivalent capacitance and conductance of the samples at room temperature using a VersaSTAT 3 Impedance Analyzer.

### **5.3.Results and Discussions**

#### **5.3.1. FTIR Interpretation**

FTIR spectroscopy aimed to distinguish between PAN samples from the viewpoint of branching and cross-linking as a function of synthesis protocol, whereas most previous work did not distinguish between cross-linking and branching but rather treated both as having the same impact on material properties. In other words, they should exist dependently<sup>2-7</sup>. To clarify this point, recall the reported suggestions that cross-linking structures are based on pre-existing branched chains, which undergo oxidative intermolecular cyclization<sup>23-25</sup>. Then it is easy to conclude if FTIR spectra of PAN show the bands corresponding to more than the expected 1,4 di-substitutes, such as 1,2,4 tri-substitutes; here there are two possibilities. The first is the possibility of having branched structures, and the second is having cross-linked structures. To distinguish between these, it is important to find out if there are more bands corresponding to intermolecular cyclization units. If these bands exist, this supports the cross-linking possibility; if these bands are absent, this indicates branching only. According to the previous strategy, FTIR spectra of PAN samples were interpreted in this fashion in order to distinguish bands mainly corresponding to linear, branched, and cross-linked PAN structures. Linear PAN is well distinguishable with the predominant IR bands corresponding to the 1,4 disubstituted ring and the absence of any other bands corresponding to any other polysubstitution. The possibility of having significant branching will depend on the

observation of any poly substitution bands coexist with the 1,4 disubstituted bands, and the absence of bands corresponding to intermolecular cyclization, such as phenazine. The coexistence of all of these bands will indicate heterogeneity in PAN samples. Additionally, the FTIR spectra were examined for significant hydrogen bonding in the samples as a function of the synthesis approach, in order to investigate and confirm the presence of supramolecular assemblies<sup>25</sup> and cross-linking phenazine-like units, as it will be discussed later.

Representative FTIR spectra of the PAN samples prepared (SF, CF, and CS) are shown in Figure 5.1. The positions of the bands differ only within experimental error from the positions measured by others<sup>26-29</sup>. These previous interpretations of PAN spectra together with corresponding references are summarized in table 5.1 and associated with the three samples types studied herein. FTIR spectra are characterized by three major regions: 3000-3500  $\text{cm}^{-1}$ , 1100-1700  $\text{cm}^{-1}$ , and  $<1100 \text{ cm}^{-1}$ .<sup>28</sup>

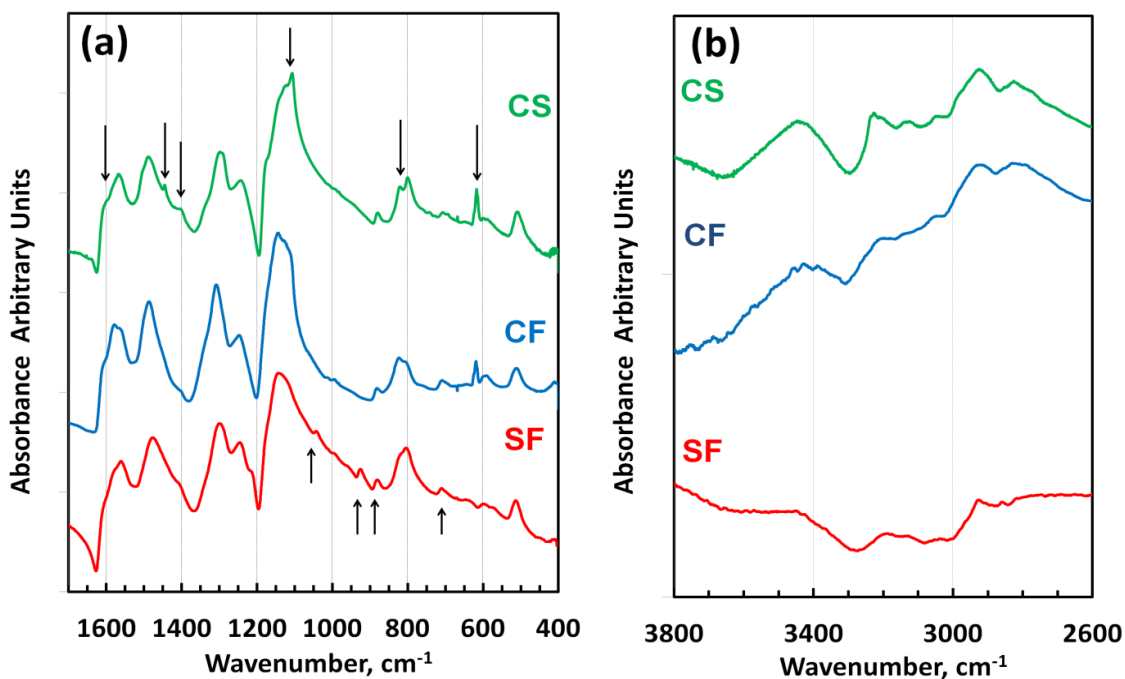


**Figure 5.1.** FTIR spectra of for HCl-doped PAN samples prepared with different approaches.

Region I ( $<1100\text{ cm}^{-1}$ ) contains the modes related to ring deformations<sup>30</sup> with select C–H out-of-plane vibrations<sup>28</sup>. Aromatic ring deformation bands (out-of-plane and in-plane) are quite sensitive to changes in the nature and position of substitutions<sup>29</sup>. Figure 5.1(a) shows the FTIR spectra within region I of PAN samples show bands that elucidate the possibility of having PAN with a significant branched or cross-linked structure. Interpreting the bands in this region could give an estimate about the impact of the synthesis approach on chemical structures of PAN samples. Three main features are expected for the PAN chains. The observed bands that relate to linear PAN are found in or near the ranges of 508-511 and 800-801  $\text{cm}^{-1}$  corresponding to aromatic ring deformations of 1,4 di-substituted benzene rings<sup>24,29,31,32</sup> and attributed to the C–H out-of-plane bending vibrations<sup>24,26,29,32</sup>. This confirms the para-coupling of constitutional units in the PAN chains. These bands are observed in all three PAN sample types representing the main chemical structure. As was expected, the PAN samples were not ideal in purity of structural composition. Indications of cross-linking and/or branched features were also found in all three PAN samples. The bands related to branched structures were found near 706-709, 879-881, and  $\sim 913\text{ cm}^{-1}$ . These bands are attributed to the C–H out-of-plane bending vibrations of the 1,2,4 trisubstituted benzene ring<sup>4,24,26,32-38</sup>. If branched PAN chains undergo oxidative intermolecular cyclization, they form cross-linked phenazine structural units<sup>39</sup>. Absorption bands related to cross-linking structures were observed mainly in CS and CF samples. These cross-linking bands observed near 616-617 and 825-828  $\text{cm}^{-1}$  are attributed to skeletal vibrations in the phenazine ring<sup>24,37,39-41</sup>.

Region II ( $1100\text{-}1700\text{ cm}^{-1}$ ) specifies where the C-C and C-N stretching and C-H bending modes are expected for molecules containing aromatic rings<sup>28</sup>. Figure 5.1(a) also shows the pair of FTIR spectral bands near 1558-1568 and 1489-1474  $\text{cm}^{-1}$  that are attributed

to C=C stretching of quinonoid (N=Q=N) and benzenoid (N=B=N) ring-stretching vibrations, respectively <sup>19,23,26,42,43</sup>. Moreover, C–N stretching modes are observed near 1300 cm<sup>-1</sup> for secondary aromatic amines <sup>7,26,44</sup>. This band is attributed to  $\pi$ -electron delocalization by protonation <sup>38,45-47</sup>. Furthermore, the bands characteristic of conducting protonated PAN are found at ~1245 cm<sup>-1</sup>, which corresponds to stretching vibration in the polaronic structure <sup>7,24,26,32,46,48</sup>.

The broad band centered at ~1145 cm<sup>-1</sup> has been assigned to the vibration mode of the polaronic structure and is associated with vibrations of charged polymer units <sup>4,32,35,38,46,49</sup>. The absorption band increases and become broader with increasing degree of electron delocalization in the PAN backbone <sup>47</sup>. In addition, this band is associated with aromatic hydrocarbon (C–H) in-plane deformation <sup>26,47,50-52</sup> and confirm the 1,4 di-substituted chain structure <sup>29</sup> along with the previous observed bands within region I. This band's appearance is very interesting because it has different shapes according to the three PAN sample types. The SF has a symmetrical shape with a single maximum at 1145 cm<sup>-1</sup>. The broadness of this band in SF suggests high degree of delocalization <sup>47</sup>. In case of CF it is not symmetrical and broad as SF. This could be an indication about expected charge localization of CF. Also, CF has a shoulder at 1124 cm<sup>-1</sup>, which corresponding to skeletal and C-H in-plane deformation of phenazine structures <sup>40</sup>, similar to CS. This band was asymmetric with the main maximum at 1107 cm<sup>-1</sup>, which corresponds to substituted phenazine units/intramolecular cyclization <sup>24,25,53</sup>. An observed shoulder at 1140 cm<sup>-1</sup> corresponds to polaronic structures <sup>4,32,35,38,46,49</sup> and aromatic hydrocarbon (C–H) in-plane deformations <sup>26,47,50-52</sup>. This band shows a significant difference in chain structure of PAN samples as a function of the synthesis approach. It could be suggested that CS and CF have significant cross-linking and charge localization with

respect to SF. Within region II, the CS spectrum has two more absorption bands of particular interest. The first at  $1445\text{ cm}^{-1}$ , which is attributed to the skeletal (C=C) stretching vibration of substituted aromatic rings<sup>2,26,29</sup>, supports the presence of ortho-coupled<sup>43,54,55</sup> and phenazine-like units<sup>32,40</sup>. The second is a weak band at  $1400\text{ cm}^{-1}$ , which is characteristic of phenazine ring stretching<sup>24-26,40</sup>.

Interpreting the IR bands in region II shows that the 1,4 di-substituted PAN chains exist, in agreement with the corresponding bands in region I. Also, the possible cross-linking within CF and CS was confirmed with poly-substituted bands observed in region I as the cross-linking structures are based on pre-existing branched chains that undergo oxidative intermolecular cyclization<sup>23-25</sup>. The CS spectrum shows more bands corresponding to cross-linking than CF, which indicates that CS (the solvent-rich, slow addition of oxidant) could be the more highly cross-linked.

Region III ( $3000\text{-}3500\text{ cm}^{-1}$ ) bands show a significant difference between PAN samples as a function of synthesis approach. Figure 5.1(b) reveals the relatively strong and clear spectral bands observed especially in the case of CS type samples, which are weaker in the CF type and almost vanish in SF samples.

Two types of modes within region III are expected. The N-H and C-H stretching could include hydrogen bonding indicative of the self-organization of PAN chains<sup>35,40,49,53,56</sup>, secondary aromatic amines<sup>24,26,29,35,57,58</sup>, protonated amine (NH<sub>2</sub><sup>+</sup>)/protonated imine (NH<sup>+</sup>)<sup>29,59-62</sup>, and intermolecular phenazine-like structures<sup>29,37,40,60,63</sup>. The assignment of individual peaks for PAN has been proposed in the literature (Table 5.1). Absorption bands connected with nitrogen-containing groups, the secondary amine –NH– and protonated imine –NH<sup>+</sup>–, reflect the hydrogen bonds involving these groups<sup>61</sup>.

**Table 5.1.** The main IR bands for HCl-doped PAN samples prepared with different approaches.

Features	Wavenumber (cm <sup>-1</sup> )			Assignment	Ref.
	SF	CF	CS		
Linear	509	511	508	Aromatic ring deformation 1,4 disubstituted	24,29,31,32
Phz	----	618	617	Skeletal vibrations in the phenazine ring	24,39,41,64
Branched	706	709	708	$\gamma$ (C – H) 1,2,4 trisubst & 1,2 disubst'd	4,24,33,34
Linear	800	800	801	$\gamma$ (C – H) 1,4 di-substituted	24,26,29,32
Phz	--	823	825	Skeletal vibrations in the phenazine ring $\gamma$ (C – H) 1,2 di-substituted	24,37,40,60,64 65,66
Branched	879	881	879	$\gamma$ (C – H) 1,2,4-trisubstituted	24,32,35,37,38,53,67
Branched	913	---	---	$\gamma$ (C – H) 1,2,4 trisubsteuted	26,35,36,67
Branched	1034	---	---	(C – H) deformation in-plane 1,2,4 trisubsteuted	29,60,68,69
Phz	-----	-----	1107	Substituted phenazine units/intramolecular cyclization	24,25,53,60
Phz	---	1124sh	1123	Skeletal and C-H in-plane deformation (phenazine) C-H aromatic in plane deformation	40 50
Linear Polaronic	1140	1143	1140sh	C-H aromatic in plane deformation C-H aromatic in plane deformation (1,4 di-substituted) C–N stretching polaronic structure Degree of electron delocalization	26,47,50-52 29 4,32,35,38,46,49
Phz			1170sh	C–N stretching phenazine units	60,70
Polaronic	1244	1246	1243	C–N stretching polaronic structure	7,24,26,32,46,48,
Polaronic	1298	1307	1299	C–N stretching secondary aromatic amine $\pi$ electron delocalization by protonation	7,26,44 38,45-47
Phz	--	--	1400	Phenazine ring starching	24-26,40
Phz			1445	N=N stretching $\nu$ (C=N)/ $\nu$ (C=C) phenazine	26 32,37,39,40,71
B	1474	1486	1489	Benzenoid (B) ring-stretching	19,23,26,42,43
Q	1558	1560	1568	Quinonoid (Q) ring-stretching	19,23,26,42,43
Phz			1600sh	$\nu$ (C=C) phenazine	37
Phz			1628	Substituted phenazine units/ Intramolecular cyclization	24,25,40
H-bonded Phz $\nu$ (N-H) $\nu$ (N-H+) $\nu$ (N-H2+)	---	2820	2827	-NH2+ Interchain hydrogen bonding $\nu$ (C-H) phenazine	29,59 49,53,72 40
	2925w	2921	2926	NH2+ $\nu$ (C-H) phenazine like structures	59,60,73 40
	----	3044	3048	$\nu$ (N-H) H-bonded $\nu$ (C-H) phenazine	2,24,26,49,74 29,37,40,60
	----	3196	3124	3160 cm <sup>-1</sup> N-H---H (H-bonded) $\nu$ (N-H+) $\nu$ (N-H) phenazine	35,40,49,53,56 61 29
	3184vw	3200	3227	N-H---H (H-bonded) $\nu$ (N-H), $\nu$ (N-H+) $\nu$ (N-H) phenazine like structures	2,4,25,26,49,75 35,61,72 40,63
	3441vw	3450	3443	$\nu$ (N-H) H-bonded or (=NH+) H-bonded $\nu$ (N-H) secondary aromatic amines $\nu$ (N-H), $\nu$ (N-H+), $\nu$ (N-H2+), $\nu$ (N-H) phenazine like structures	24,59,74 24,26,29,35,57,58 62 40,63

The clear presence of the bands corresponding to hydrogen bonding indicates highly cross-linked structure<sup>65</sup>. So, the relatively clear bands of CS may indicate that charge is the most localized in this case as dications (bipolaron). On the other hand, the weakness of these bands in SF and CF suggest that the charge is more delocalized as a result of partial masking by the extended absorption tail of the protonated PAN<sup>61</sup>. Moreover, the presence of strong hydrogen bonding is indicative of the self-organization of CS-PAN chains that may have led to supramolecular assemblies;<sup>25</sup> under hydrogen bonding conditions for cross-linking, CS-PAN should have the most compact coil chain confirmation,<sup>76</sup> which agrees with previous UV measurements<sup>77</sup> mentioned in chapter 3. In addition, it has the most significant amount of intramolecular cyclic phenazine-like units. On the other hand, the spectra suggest that SF-PAN has the lowest cross-linking and the most expanded coil confirmation. It seems that CF-PAN has heterogeneous mixed structures. It could be suggested that increasing the degree of charge localization increases the possibility of having strong hydrogen bonding. The CS approach may be favorable for cross-linking allowed by the slower oxidation, which means PAN chains growing with other existing chains, with higher probability of structural defects impacting the electrical and electronic behavior 4,43. By contrast then, SF may be favorable for limited branching in PAN.

Based on FTIR data interpretation, the observation of abortion bands corresponding to the 1,2,4 trisubstituted ring in the SF-PAN spectra suggest that under certain solvent-limited conditions the radical semiquinone cations on the main chain of PAN can initiate limited polymerization. The development of side chains resulted in limited side branches. While in the cases of CS and CF, the corresponding abortion bands to the 1,2,4 trisubstituted ring in addition to the phenazine bands were observed in CF- and CS-PAN spectra.

This supports the idea that under conventionally solvent-rich polymerization conditions (viz., CF and CS) the reactivity of the radical semiquinone cations would be favorable to cross-linking reactions between the PAN chain and resulted in more cross-linked structures. In other words, the branched PAN chains undergo oxidative intermolecular cyclization into cross-linking phenazine structural units<sup>39</sup>. However, under SF conditions the impact of limited solvent may prevent cross-linking in favor of branching. The reason that CS shows the most cross-linking could be due to the slower oxidation rate in a kinetic reactivity sense rather than as a direct consequence of the presence or absence of solvent in a geometric sense; this means PAN chains growing with other existing chains with a higher probability of structural defects impacting the electrical and electronic behavior<sup>4,43</sup>. It seems that CF has a mixed structure in between CS and SF, while SF may be favorable for limited branching in PAN when and where desired by application needs.

### 5.3.2. DC Electrical Conductivity ( $\sigma_{DC}$ )

The current-voltage (I-V) curves of HCl-doped PAN samples are shown in Figure 5.2, indicating ohmic behavior in all types at room temperature<sup>78</sup>. All samples behaved as perfect ohmic conductors with the electrical resistance trend as SF < CF < CS. The highest  $\sigma_{DC}$  was for SF ( $55.2 \pm 0.2$  S/cm) followed by CF ( $6.0 \pm 0.4$  S/cm) with CS ( $1.6 \pm 0.7$  S/cm) the lowest; values differ here from Chapter 2 due to batch differences as well as changes in the sample compression for improving consistency and accuracy in two-point measurements. The significant differences between sample types are of course due to the impact of the formulation conditions on the final chemical structure and material crystallinity, which were discussed in previous work<sup>18</sup> and reconfirmed in this chapter.

The experimental values of conventional HCl-doped PAN (CF and CS) fitted within a factor of 2 in conductivities previously reported herein and within the same range for other HCl-doped PANs<sup>23</sup>. However, the nearly order of magnitude increase in conductivity for the SF samples is substantially higher than recently reported elsewhere<sup>19,79,80</sup> and even significantly greater than found in our initial studies (Chapter 3)<sup>18</sup>. The negative impact of cross-linking on conductivity is obvious and agrees with other findings<sup>4,18</sup>, whereas SF-PAN with its limited branching structures and minimum cross-linking achieves the highest  $\sigma_{DC}$ .

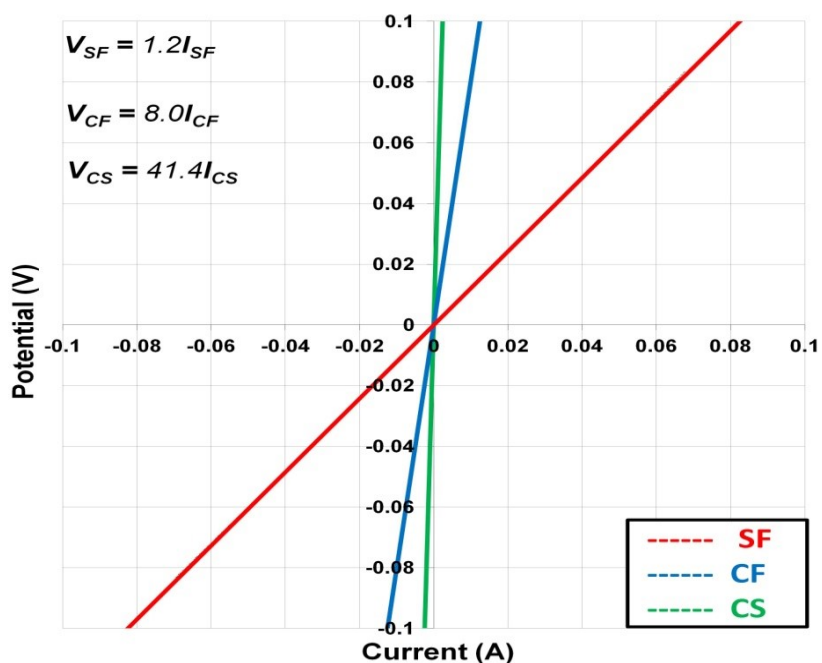


**Figure 5.2.** I-V curves from two-terminal measurements on three PAN samples doped with HCl.

### 5.3.3. AC Conductivity ( $\sigma_{AC}$ )

In general, the AC electrical conductivity  $\sigma_{AC}(\omega)$  of disordered materials, measured in the frequency ( $f$ ) range from 0.01 Hz to 10 MHz ( $\omega = 2\pi f$ ), presents an almost universal behavior, exhibits two frequency regions, one plateau at low frequencies (the DC plateau) followed by a region of increasing conductivity, obeying  $\sigma_{AC}(\omega) \propto \omega^s$ , where  $0, s \leq 1$

<sup>13,81,82</sup>. The transition between the first plateau and the frequency-dependent region defines a critical frequency,  $\omega_c$ . Conductive polymers are usually classified as highly disordered materials and are very attractive materials since their DC conductivities may vary, reversibly, by orders of magnitude under chemical doping–dedoping <sup>13,83</sup>. The enhancement of conductivity comes from the generation of extended states in doped molecules correlating, in a molecular scale, charged defects with electronic structures having intermediate energetic levels in the forbidden gap, attributed to the creation of solitons and/or polarons <sup>84</sup>. Electronic transport in isotropic-disordered media depends strongly on irregularities in material structure that determine the degree of carrier delocalization <sup>13</sup>. The increase in  $\sigma_{AC}(\omega)$  can be attributed to the decrease in the charge binding energy and the transformation of the lattice structure from localization to delocalization <sup>81</sup>. In the case of PAN, the formation of delocalized charge leads to enhancing its metallic character <sup>85,86</sup>.

It was reported that the electric response of  $\sigma_{AC}$  in doped PAN must be considered as the sum of two components. The first is due to dielectric relaxation in the polymer backbone and the second is related to the oscillations of polarons and bipolarons about their pinning centers <sup>15,87,88</sup>. This last mechanism becomes more valuable as the doping level increases <sup>87</sup>. The total measured conductivity at a given temperature and frequency arises from both DC and AC components, in general, obeying a power law with frequency <sup>82,89,90</sup>:

$$\sigma_{AC}(\omega) = \sigma_{DC} + \sigma_{AC}(\omega).$$

Figure 5.3 shows a log-log plot of  $\sigma_{AC}(f)$  of doped PAN samples synthesized with the three different approaches. One may infer that SF-PAN behaves like a metal in the sense that its conductivity will tend toward a frequency-independent behavior across the whole frequency range <sup>13</sup>.

It is clear that SF-PAN has a zero value of  $s$  within the measuring frequency range (1 Hz-1 MHz), as  $\sigma_{DC}(f)$  represents a straight line corresponding to its  $\sigma_{DC}$  values. In case of CF, it behaves almost like SF as its  $\sigma_{AC}(f)$  tends toward an almost frequency-independent behavior up to 0.7 MHz as  $\sigma_{AC}(f)$  represents straight line corresponding to its  $\sigma_{DC}$  values. Then CF  $\sigma_{AC}(f)$  starts to be frequency dependent with  $s$  value of 0.16. CS-PAN has a significantly different  $\sigma_{AC}(f)$  behavior than SF-PAN and behaves as more frequency-dependent than CF-PAN. CS has two values of  $s$ , first zero up to 0.5 MHz represents its  $\sigma_{DC}$  value, and then it becomes 0.51. It is obvious that CS starts to be frequency dependent at lower frequencies than CF with about 0.2 MHz, and CS shows greater frequency dependence than CF. The metallic character of HCl-doped PAN is strongly affected by synthesis approach.

The observed metallic character agrees with the DC conductivity values and trend. The relatively low conductivity of CS with respect to SF and CF is confirmed again but for AC behavior, whereas DC measurements and their trends hid any frequency dependence<sup>15</sup>. Also, this behavior indicates that the predominate charge binding energy has the general trend CS > CF > SF, which corresponds inversely as a generally increasing delocalized electronic structure (viz., SF > CF > CS)<sup>81</sup>.

The behavior of  $\sigma_{AC}(f)$  strongly depends on the PAN synthesis approach, pushing the critical frequency,  $f_c$  ( $f_c = \omega_c/2\pi$ ), to higher values with increasing conductivity and /doping level in the sample<sup>13,90</sup>. However, CS-PAN is the only one here that has a clear  $f_c$  within the measuring frequency range. Above  $f_c$ , the conductivity increases with frequency. It could be suggested that this increase in  $\sigma_{AC}(\omega)$  with frequency above  $f_c$  is due to the transformation of the its electronic/polaron lattice structure to more delocalization<sup>81</sup>.

This behavior indicates that CS-PAN has the most localized electronic structure of the three sample types and appears to behave as if it is the most disordered, since the transition in  $\sigma_{AC}(\omega)$  above  $f_c$  from the DC plateau into a dispersive high-frequency region is common with disordered materials <sup>13,81</sup>.

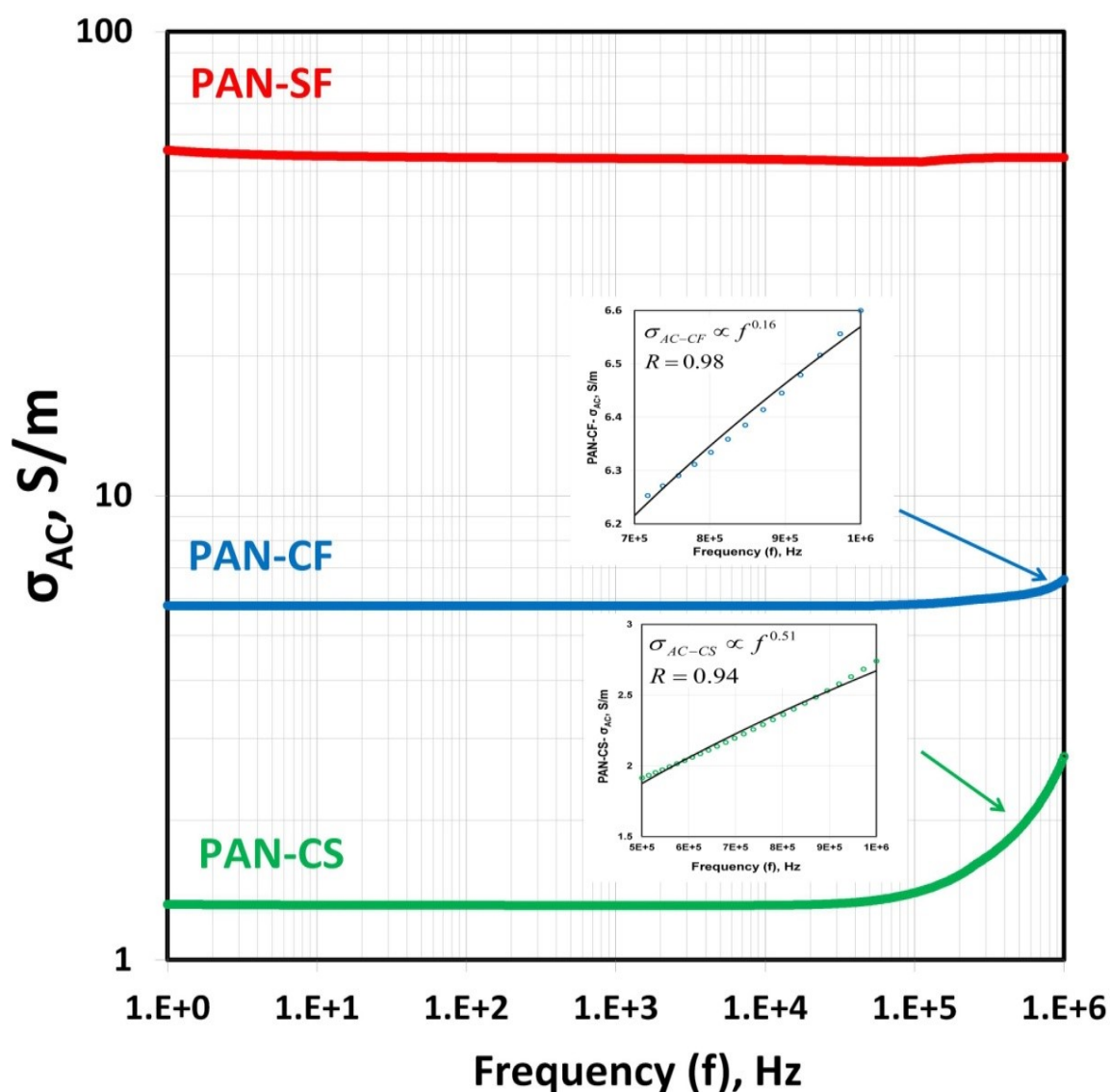


**Figure 5.3.** Frequency dependence on conductivity of HCl-doped PAN samples.

There is an unexpected contradiction with crystallinity being highest in CS-PAN, which should be the most ordered with respect to CF and SF (see Table 5.1), where crystallinity represents regularity and structural organization. This should thus be a favorable factor for intramolecular mobility of charged species along the chain and to some extent intermolecular hopping because of better and/or closer packing<sup>91</sup>. But  $\sigma_{AC}(\omega)$  measurements show that the electronically-inferred disordered trends do not agree with crystallinity, interchain separation, or crystalline domain size trends.

To explain how CS-PAN with the highest degree of crystallinity behaves as the most disordered polymeric material, we need to recall the fact that an increase in  $\sigma_{AC}(\omega)$  is attributed to a decrease in charge binding energy and the predomination of delocalized electronic structure<sup>81</sup>. Therefore,  $\sigma_{AC}(\omega)$  depends mainly on electronic structure, even in spite of apparent molecular disorder as indicated from x-ray diffraction data. If a relatively high degree of crystallinity, short interchain separation, and large crystalline domain size exist but predominate electronic structure is localized, this leads to poor electrical behavior of PAN. Poor electrical behavior of CS-PAN could be due to the formation of cross-linking structures<sup>54</sup>, encouraged by the slow oxidation conditions<sup>18</sup>. The previous conditions may foster PAN chain growth with existing chains as well as other structural defects resulting in lower conductivity<sup>4,43</sup>, but it still facilitate high molecular ordering. In addition, slow exothermic polymerization with no noticeable change in the temperature of the reaction medium is a favorable condition for higher degree of crystallinity<sup>43</sup> compared to the more rapid and thus more thermally energetic reactions in CF and SF methods. On the other hand, CF and SF PANs consist mainly of chains with lower extent of cross-linking/hydrogen bonding, as explained in the FTIR discussion. The reason that the SF-PAN has the greatest conductivity

and a higher degree of crystallinity than CF is perhaps due to the formation of SF-PAN chains under relatively concentrated acidic conditions <sup>19</sup>, though it may be difficult to reconcile this with the slow oxidation process at lower local acid concentrations that produce the highest crystallinity and highest delocalized electronic structure.

The conventional trends between crystallinity, d-spacing, inter-chain separation, crystalline domain size, and conductivity are clearly observed <sup>91</sup>. The SF samples exhibit larger domain size, shorter d-spacing and inter-chain separation, and higher conductivity than the fast oxidation (CF) product, as might also be expected by differences in polymer cross-link density. The molecular regularity and organized structure defined by crystallinity is a favorable factor mainly for intramolecular mobility of charged species along the chain and to some extent intermolecular hopping because of better and/or closer packing <sup>91</sup>. For this reason, SF samples are roughly ten times more conductive than CF samples. There is, of course, the sustained difficulty in reconciling the highest crystallinity of the three formulations being found for CS samples with the lowest conductivity. Apparently, both fast or moderate oxidation rate and high acidity favor good electrical behavior coupled with high crystallinity in HCl-doped PAN with predominate delocalized electronic structure, as indicated by weak frequency dependence of  $\sigma_{AC}$ . SF and CF PANs seem to be more homogeneous and ordered <sup>82</sup>, which could be attributed to the predomination of delocalized electronic structure (polaron/polaron lattice). The obtained results support the general notion that the degree of crystallinity depend on the synthesis approach <sup>54</sup>. In addition, this highlights the importance of the synthesis approach impact on the degree of delocalization for prepared HCl-doped PAN.

It may be deduced that the SF approach allows the proper ordering and electronic delocalization extent in PAN molecules that contribute to the highest conductivity. The results for HCl-doped PAN show an interesting contradiction to the general rule that higher crystallinity should increase conductivity<sup>92-96</sup>. Since both fast and slow oxidation products (CF and CS) were synthesized with the same dopant (HCl) ratios, the degree of electronic delocalization appears to depend only on the reaction conditions<sup>54</sup>. Thus, an optimum in crystallinity for the maximum degree of electronic delocalization to provide the highest conductivity may be revealed with future fine-tuning of the oxidation rate and method for oxidant addition.

**Table 5.2.** Domain size, interchain separation, and degree of crystallinity of PAN samples reported in previous work, chapter 2<sup>18</sup> in comparison with  $\sigma_{DC}$  (S/cm) measured in this work.

Sample	Domain size L(Å)	Inter-chain Separation R(Å)	Crystallinity	$\sigma_{DC}$ S/cm
PAN-HCl-SF	121.6 ± 9.0	4.4	66%	55.2 ± 0.2
PAN-HCl-CF	46.3 ± 8.1	4.5	54%	6.0 ± 0.4
PAN-HCl-CS	132.3 ± 9.0	4.3	73%	1.6 ± 0.7

#### 5.3.4. Dielectric Permittivity

Typically, the frequency-dependent dielectric permittivity in organic polymers is dominated by reorientation of molecular dipoles<sup>81,97</sup>. In dealing with conducting polymers, it must be realized that they usually contain a number of hopping charge carriers, which may lead to a great difference in the dielectric properties from insulators. A hopping charge carrier shows both dielectric characteristics, like a jumping dipole in its reciprocating motions, and conducting characteristics<sup>98</sup>. The hopping of charge carriers can make a very substantial

contribution to  $\epsilon'$ , and  $\epsilon''$ , which are closely related to the polarization<sup>99</sup>. The general dielectric behavior of conducting polymers often exhibits a relatively high dielectric constant at low frequency and a sharp decrease as frequency increases<sup>100</sup>. It has been reported that the dielectric constant of doped PAN increases in the macroscopic metallic domains<sup>101</sup>, as dielectric constant increases with the increase in conductivity<sup>14,81</sup>.

Figure 5.4 represents the measured real part of complex permittivity,  $\epsilon'$  (relative permittivity or dielectric constant), and the imaginary part of complex permittivity,  $\epsilon''$  (dielectric loss factor), from PAN samples (SF, CF, and CS). As  $\epsilon'$  represents the capacitive nature and  $\epsilon''$  represents the conductive nature, the electrical behavior of a sample can be traced by elucidating the dielectrical behavior involving  $\epsilon'$  and  $\epsilon''$  from the complex permittivity  $\epsilon^*$ , which are related as<sup>100</sup>

$$\epsilon^*(\omega) = \epsilon'(\omega) - i \epsilon''(\omega) = \epsilon'(\omega) - i \left[ \frac{\sigma(\omega)}{\epsilon_0 \omega} \right].$$

As shown in Figure 5.4, a relatively high dielectric constant ( $\epsilon'$ ) was observed at low frequency and a rapid decrease with frequency as typical characteristics of a conducting polymer<sup>14,82,100,102</sup>. However,  $\epsilon'$  slowly decreases with frequency at  $f < 100$ -1000 Hz, which may be due to the vanishing polarization angle changes (i.e., no polarization losses) at relatively higher frequencies<sup>81</sup>. The impact of synthesis approach on  $\epsilon'$  corresponding to PAN samples is apparent. At low frequencies, the dielectric constant decreases as frequency increases, whereas upon reaching 100-1000 Hz, it became less dependent on frequency exhibiting a low value plateau at higher frequencies<sup>100</sup>, where CF-PAN provides a typical example. Overall, the SF-PAN  $\epsilon'$  is highest with respect to CF and CS products across the frequency band under investigation. It was found that  $\epsilon''$  was also largest for SF-PAN, decreasing almost linearly in all samples<sup>14,100,102</sup> with a slope of -1 indicating that  $\epsilon''$  is

proportional to  $1/f$ , and accordingly the AC conductivity is a constant, viz., the same as  $\sigma_{DC}$ , up to 1 MHz. This agrees with what was reported <sup>99</sup>.

The presence of a plateau in  $\epsilon'$  and the absence of a well-defined loss peak in  $\epsilon''$  are characteristic of charge-carrier systems <sup>99,100</sup>. The obvious and significant impact of synthesis approach on  $\epsilon'$  and  $\epsilon''$  reveals differences that may be due to chemical and electronic structures in the nanopowders. It is obvious that electric charges being displaced inside the CS (stronger localization) <sup>100</sup>. Synthesis approach which leads to higher doping can be in accord with the electrical conduction <sup>89</sup>. The observed dielectric trends of the three HCl-doped PAN sample types agree with conductivity trends and their interdependence on each other <sup>81,100,103</sup>, where their dielectric behavior can be elucidated in terms of the contribution of non-negligible  $\sigma_{DC}$  on measured loss ( $\epsilon''$ ) in the following way <sup>99,104</sup>:

$$\epsilon_r'' = \epsilon_{rA}'' + \frac{\sigma_{DC}}{\omega\epsilon_0}$$

And the corresponding  $\sigma_{AC}$  is expressed as follows:

$$\sigma_{AC} = \omega\epsilon_0\epsilon_r'' = \omega\epsilon_0\epsilon_{rA}'' + \sigma_{DC}$$

where  $\epsilon_{rA}''$  represents the loss caused only by alternating mechanisms in a conducting polymer. In fact, the high density of free charges able to cross the sample is too high and hides potential polarization phenomena. A high dielectric constant encountered at low  $f$  is linked to the heterogeneity of materials, and true values are often hidden by electrode polarization effects <sup>105</sup>. It is clear that the measured loss ( $\epsilon_r''$ ) includes contributions of both  $\epsilon_{rA}''$  and  $\sigma_{DC}$ , because the measuring instrument cannot differentiate between them. Consequently,  $\sigma_{AC}$  is also composed of these two contributions: the DC conductivity and the dielectric loss. If  $\sigma_{DC} = 0$  or is very low,  $\implies \epsilon_r'' = \epsilon_{rA}''$  and  $\sigma_{AC} = \omega\epsilon_0\epsilon_{rA}''$ ; this is the case for insulating materials. On the other hand, if  $\sigma_{DC}$  is large,  $\implies \epsilon_r'' \approx \frac{\sigma_{dc}}{\omega\epsilon_0}$  and  $\sigma_{AC} = \sigma_{DC} =$

constant at low frequency; this is the case for conducting polymers. Therefore, the DC mechanism may dominate in measured loss at low frequency and AC loss may dominate at high frequency in conducting polymers<sup>14,99</sup>. This is why the AC conductivity of SF-PAN was constant, and nearly so for CF-PAN, across the measuring frequency band 1 Hz-1 MHz, as shown in Figure 5.4. In the case of CS-PAN, conductivity was also roughly constant except at the high-frequency end where it increases but remains lower still than for CF-PAN. The variance in CS samples is likely due to it having the lowest  $\sigma_{DC}$ .

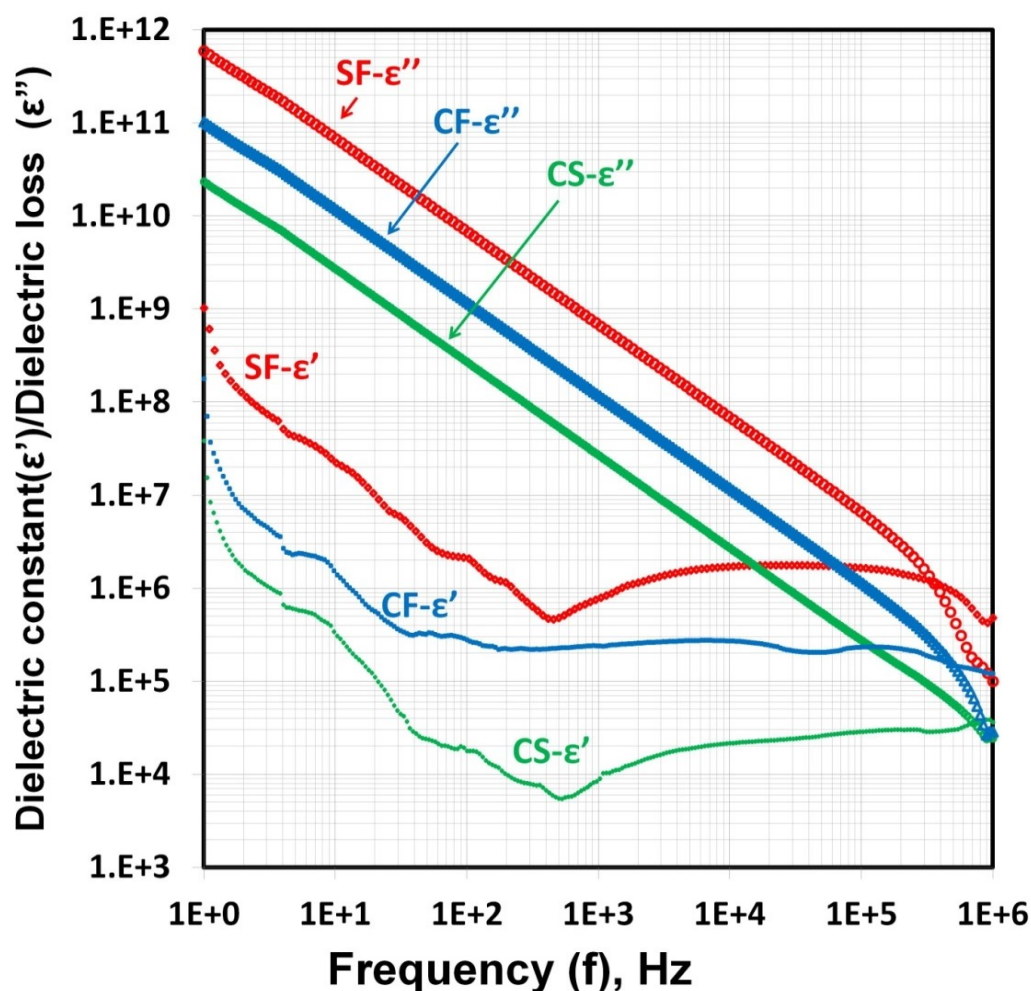


**Figure 5.4.** Frequency dependence of (a) dielectric constant ( $\epsilon'$ ) and (b) dielectric loss factor ( $\epsilon''$ ) for PAN samples.

It could be assumed that the density of charge carriers in SF-PAN is the highest; then it is expected that the dispersion of  $\epsilon'$  and  $\epsilon''$  would be the strongest, especially at low frequency<sup>99</sup>. On the other hand, the relatively high  $\epsilon'$  and  $\epsilon''$  values of the SF-PAN (by roughly an order of magnitude over CS and CF PANs) imply that  $\sigma_{DC}$  still plays an important role in determining their magnitudes. Therefore, a high  $\sigma_{DC}$  value may generally be expected to provide high microwave absorptivity; consequently, finding methods for producing conducting PAN with enhanced conductivity is key to obtain a good EM absorber.

### 5.3.5. Electric Modulus

To analyze the conductivity relaxation property in more depth, the complex permittivity ( $\epsilon^*$ ) is converted to the complex electric modulus  $M^*(\omega)$ , because  $\epsilon^*$  is not completely suitable to describe the electrical properties of conjugated polymers<sup>89,100,106</sup>. The real and imaginary parts ( $M'$  and  $M''$ ) of the electric modulus can be calculated from  $\epsilon'$  and  $\epsilon''$  as follows<sup>14,100</sup>:

$$M' = \frac{\epsilon'}{(\epsilon'^2 + \epsilon''^2)}$$

$$M'' = \frac{\epsilon''}{(\epsilon'^2 + \epsilon''^2)}$$

The complex electric modulus is also expressed by

$$M^*(\omega) = M'(\omega) + i M''(\omega)$$

$M^*(\omega)$ , which is inversely proportional to the complex dielectric permittivity<sup>106</sup>, characterizes the dynamic aspects of the charge motion in conductors in terms of a relaxation in an electric field. Hence, this  $M^*(\omega)$  description can explain the dispersion of  $\epsilon^*$  with the frequency without any “molecular” polarization phenomena<sup>100</sup>. From the  $M'$  and  $M''$  of PAN samples shown in Figure 5.5, the dispersions of  $M'$  and  $M''$  indicate the presence of the relaxation-time

distribution of conduction.  $M'$  in Figure 5.5(a) approaches zero at low frequencies, indicating that the electrode polarization gives a negligible low contribution to  $M'$  and can be ignored<sup>100</sup>. After keeping a low value,  $M'$  steeply increases after 0.07, 0.09 and 0.5 MHz, respectively, for CS, CF, and SF PAN nanopowders. Figure 5.5(b) shows the frequency dependence of the imaginary part of the electric modulus doped with three different approaches. As expected, CF and CS PANs seem to have maximum  $M''$  in these frequency regions at 0.6 MHz and 0.64 MHz, respectively. On the other hand, SF-PAN has a peak maximum of the  $M''$  curve appears to be located beyond the interval of frequencies used in these measurements, which may be attributed to mixed conduction or an enhanced contribution of DC conductivity to the measured AC conductivity<sup>89</sup>. The latter is expected due the relatively higher conductivity of SF with respect to CF and CS.

It was obvious that manipulating the synthesis approach leads to the appearance of  $M''$  in the higher-frequency regions, which means enhanced DC conductivity 14,100,105, as can be seen in the SF case. The intensity of the electric modulus seems to be inversely dependent on the DC conductivity 100. For lower conductivity, the observed  $\epsilon'$  and  $\epsilon''$  values are relatively low and the  $M''$  relaxation peak (conductivity relaxation 102,105) is seen at relatively low frequency 100,107; this peak shifts toward higher frequencies with increasing DC conductivity 100. This behavior indicates a significant difference between PAN samples, due to possible relative differences in delocalized charge density 100 as a direct impact of their synthesis approach. The localized charge carriers under an applied AC electric field can hop to neighboring sites like the reciprocating motion of a jumping dipole or can jump to neighboring sites, which form a continuous connected network, allowing the charges to travel through the entire physical dimensions of the sample and causing the electric conduction<sup>102</sup>.

The non-monomodal distribution of the electric modulus in the higher-frequency region could not be found because of the limitation of the measurement region. This may also be due to the complicated conduction process or various PAN phases<sup>100</sup>

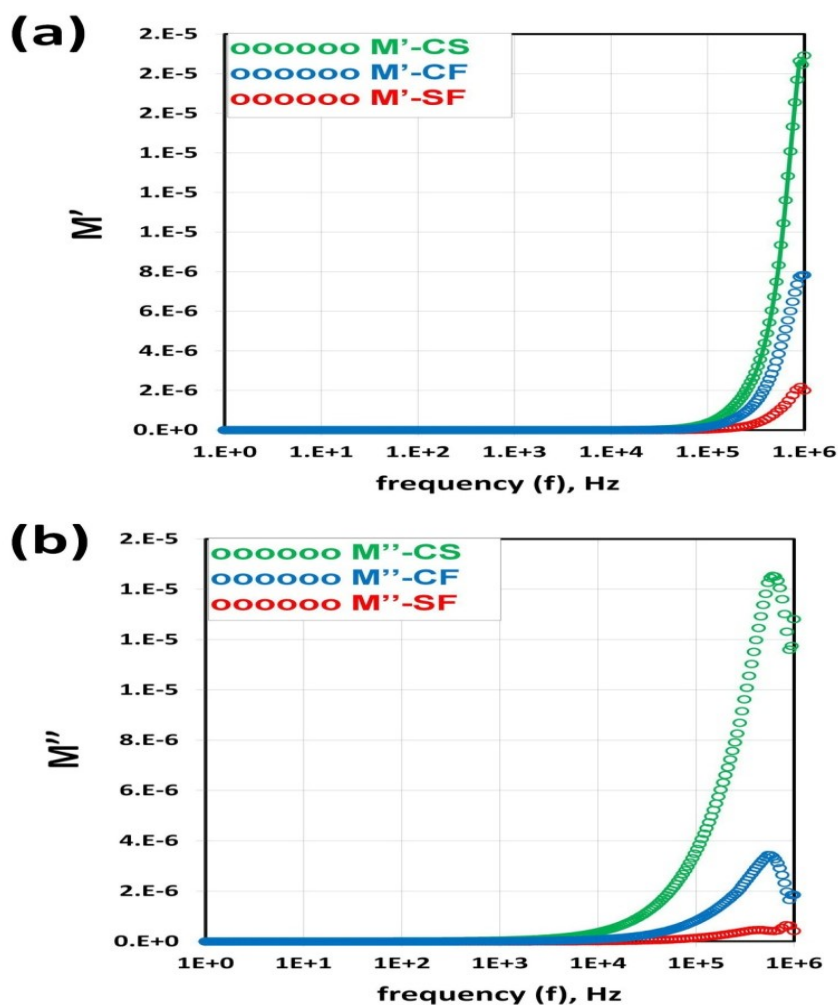


**Figure 5.5.** Electric modulus of PAN samples (CS, CF, and SF).

Figure 5.6 shows the complex plane of  $M'$  and  $M''$  for all three PAN sample types, represented as arcs with their centers and the radii of the arcs seeming to be dependent on the synthesis approach, e.g., CS, CF, SF. It has been reported that the radius of the arc of the

complex plane diagram is dependent on the electrical conductivity of the samples, as the larger arc means lower electrical conductivity<sup>87,100,106</sup>.

It was found that the samples have different radii of their arcs, showing also differences in the length of the arc, which means different chain structures<sup>100</sup> and doping levels<sup>106</sup>, irrespective of the impact of synthesis approach. When complex planes for the electric modulus do not form semicircles, it can be concluded that different conduction mechanisms are employed since it conflicts with the ideal Debye model of a single relaxation time<sup>100</sup>. The observed dielectric behavior of HCl-doped PANs represent a significant difference in polymer chain structure<sup>100</sup> relating to the synthesis condition effects. The difference in chain structure is likely due to different degrees of cross-linking and hydrogen bonding as shown in the FTIR interpretation.

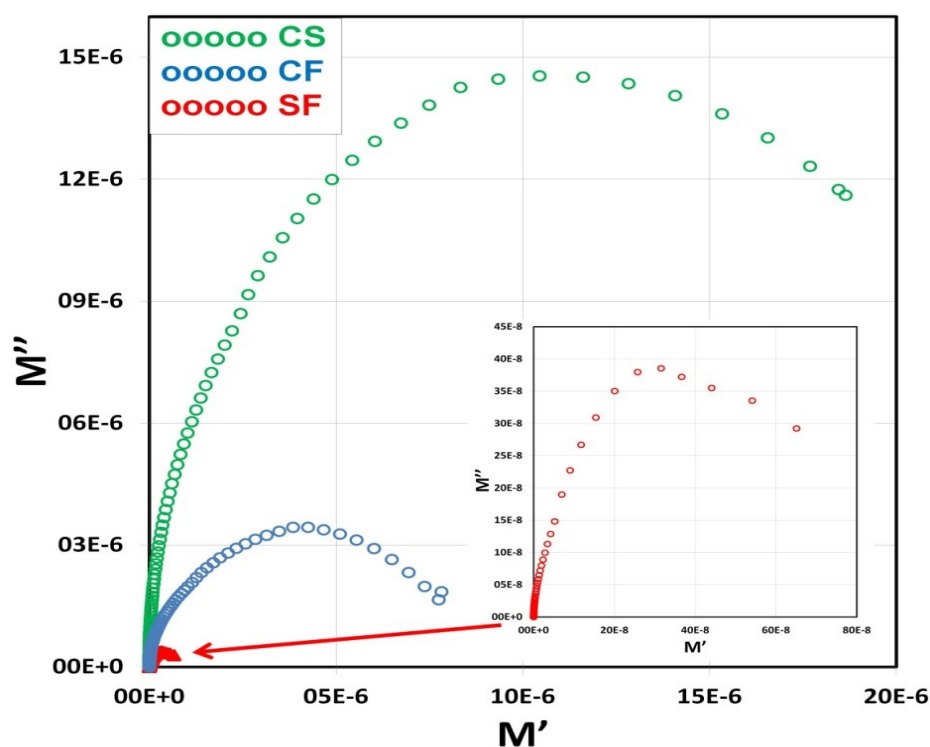


**Figure 5.6.** Complex plane diagram for the electric modulus of PAN samples (CS, CF, and SF).

#### 5.4. Conclusions

In this current work, it was possible to distinguish between branching and cross-linking in HCl-doped PAN samples prepared with different synthesis approaches (CF, CS, and SF) by utilizing full FTIR band characterization (400 – 4000  $\text{cm}^{-1}$ ). The relative extent of branching and/or cross-linking in PAN samples was estimated from the predominance of IR bands corresponding to 1,4-disubstituted rings and the absence of any other bands corresponding to any other polysubstitution. The possibility of having significant branching was estimated from the observation of (or lack thereof) any polysubstitution bands coexistent with the 1,4-disubstituted bands and the absence of bands corresponding to intermolecular cyclization such as phenazine. The coexistence of all the previous bands could indicate significant heterogeneity in the PAN sample.

The CS approach is favorable for maximizing the extent of intramolecular cyclic phenazine as cross-linking units and hydrogen bonding. As a result, the charge is probably the most localized as dications (bipolaron) in CS-PAN. Its chains may furthermore have supramolecular assemblies<sup>25</sup> and the most compact-coil chain confirmation<sup>76</sup>, which both agree with UV-Vis and XPS analyses in chapter 3. These features may be preferred by the slower oxidation rates, which means PAN chains growing with other existing chains (rather than by monomer addition), with a higher probability of structural defects impacting the electrical and electronic behavior<sup>4,43</sup>. On the other hand, the SF and CF approaches appear favorable for relatively limited branching in PAN with low extent of cross-linking and hydrogen bonding, thus indicating that the charge is more delocalized as a result of partial masking or screening as suggested by the extended absorption tail of the protonated PAN<sup>61</sup>.

If a relatively high degree of crystallinity, short interchain separation, and large crystalline domain size exist but predominate electronic structure is localized, this leads to poor electrical behavior of PAN materials. The AC conductivity ( $\sigma_{AC}(\omega)$ ) and dielectric permittivity measurements ( $\epsilon'$  and  $\epsilon''$ ) showed an unexpected contradiction to the highly oversimplified general rule that higher crystallinity should provide increases conductivity and dielectric permittivity<sup>92-96</sup>. It was found that CS-PAN, the most crystalline (~77%) material of the three synthesis methods, acts as the most disordered sample with respect to SF and CF PANs in electrical properties; it has the most localized electronic structure of the three sample types. On the other hand, SF-PAN with a moderate crystallinity (~66%) behaves more like a metal in the sense that its conductivity tends toward a frequency-independent behavior<sup>13</sup> across the tested frequency range (1 Hz-1 MHz). Apparently, both fast/moderate oxidation rate and high acidity favor HCl-doped PAN synthesis with delocalized electronic structures (polaron/polaron lattice), as indicative from poor frequency dependence of  $\sigma_{AC}$  (Co in SF and CF PANs<sup>82</sup>).

Dielectric permittivity measurements showed that the SF approach leads to the highest values of  $\epsilon'$  and  $\epsilon''$ . The relatively high  $\epsilon'$  and  $\epsilon''$  values imply that  $\sigma_{DC}$  still plays an important role in determining the magnitudes of  $\epsilon'$  and  $\epsilon''$ . The lowest values in CS-PAN confirm that it has the strongest charge localization of the three<sup>100</sup>. The observed dielectric trends of PAN samples agree with conductivity trends and the reported conductivity/dielectric dependence. Therefore, a high  $\sigma_{DC}$  value may generally indicate high microwave absorptivity; consequently, raising the DC conductivity of a conducting polymer PAN is the key to obtain a good electromagnetic interference (EMI) absorber.

The SF approach enhanced the dielectric constant and dielectric loss with about an order of magnitude over conventional synthesis, which has high promise as a process application for maximizing EMI shielding in PAN-based materials.

It is further deduced that the unconventional solvent-free or solvent limited approaches are likely key to prevent the cyclization of branched chains and minimize the possibility of hydrogen bonding/cross-linking in HCl-doped PAN that would reduce the effectiveness for EM shielding. The solvent and/or oxidant concentration and accessibility to each other appear to provide a fine-tuning potential for controlling the property outcomes for doped PAN polymerization. The SF approach seems to lead to proper ordering and electronic delocalization extent in HCl-doped PAN molecules to contribute to enhanced conductivity over the classical chemical oxidation approaches (CF and CS). These conventional methods are not recommended since they lead to maximizing crystallinity with cross-linked structures. There appears to be an intermediate optimum in crystallinity with respect to electrical/dielectrical behavior. Since both fast and slow oxidation products (CF and CS) were synthesized in excess solvent with the same dopant (HCl) ratios, the degree of electronic delocalization appears to depend on the reaction condition rather than on the doping level<sup>54</sup>. Therefore, an optimization between conductivity and crystallinity for the maximum degree of electronic delocalization should be revealed with fine-tuning of the rate and method for oxidant addition.

## 5.5.References

- (1) Tantawy, H. R.; Weakley, A. T.; Aston, D. E. Chemical Effects of a Solvent-Limited Approach to HCl-Doped Polyaniline Nanopowder Synthesis *J. Phys. Chem. C* **2013**, *118*, 1294-1305.
- (2) Stejskal, J.; Trchová, M. Aniline Oligomers Versus Polyaniline *Polym. Int.* **2012**, *61*, 240-251.
- (3) Nand, A. V.; Ray, S.; Gizdavic-Nikolaidis, M.; Travas-Sejdic, J.; Kilmartin, P. A. The Effects of Thermal Treatment on the Antioxidant Activity of Polyaniline *Polym. Degrad. Stab.* **2011**, *96*, 2159-2166.
- (4) Pan, L. J.; Pu, L.; Shi, Y.; Sun, T.; Zhang, R.; Zheng, Y. O. Hydrothermal Synthesis of Polyaniline Mesostructures *Adv. Funct. Mater.* **2006**, *16*, 1279-1288.
- (5) Okamoto, H.; Okamoto, M.; Kotaka, T. Structure Development in Polyaniline Films During Electrochemical Polymerization. Ii: Structure and Properties of Polyaniline Films Prepared Via Electrochemical Polymerization *Polymer* **1998**, *39*, 4359-4367.
- (6) Wang, J.; Wang, J.; Wang, Z.; Zhang, F. A Template-Free Method toward Urchin-Like Polyaniline Microspheres *Macromol. Rapid Commun.* **2009**, *30*, 604-608.
- (7) Prokes, J.; Trchova, M.; Hlavata, D.; Stejskal, J. Conductivity Ageing in Temperature-Cycled Polyaniline *Polym. Degrad. Stab.* **2002**, *78*, 393-401.
- (8) Pouget, J. P.; Hsu, C. H.; MacDiarmid, A. G.; Epstein, A. J. Structural Investigation of Metallic PAN-CSA and Some of Its Derivatives *Synt. Met.* **1995**, *69*, 119-120.
- (9) Pouget, J. P.; Jozefowicz, M. E.; Epstein, A. J.; Tang, X.; MacDiarmid, A. G. X-Ray Structure of Polyaniline *Macromolecules* **1991**, *24*, 779-789.

- (10) Pouget, J. P.; Oblakowski, Z.; Nogami, Y.; Albouy, P. A.; Laridjani, M.; Oh, E. J.; Min, Y.; Macdiarmid, A. G.; Tsukamoto, J.; Ishiguro, T.; Epstein, A. J. Recent Structural Investigations of Metallic Polymers *Synt. Met.* **1994**, *65*, 131-140.
- (11) Pouget, J. P.; Zhao, S. L.; Wang, Z. H.; Oblakowski, Z.; Epstein, A. J.; Manobar, S. K.; Wiesinger, J. M.; Macdiarmid, A. G.; Hsu, C. H. Poly(0-Ethoxyaniline): Control of Structure and Charge Transport through Derivatization *Synt. Met.* **1993**, *55*, 341-346.
- (12) Pelster, R.; Nimtz, G.; Wessling, B. Fully Protonated Polyaniline: Hopping Transport on a Mesoscopic Scale *Phys. Rev. B: Condens. Matter* **1994**, *49*, 12718.
- (13) Bianchi, R. F.; Ferreira, G. F.; Lepienski, C. M.; Faria, R. M. Alternating Electrical Conductivity of Polyaniline *J. Chem. Phys.* **1999**, *110*, 4602.
- (14) Soares, B. G.; Leyva, M. E.; Barra, G. M. O.; Khastgir, D. Dielectric Behavior of Polyaniline Synthesized by Different Techniques *Eur. Polym. J.* **2006**, *42*, 676-686.
- (15) Javadi, H. H. S.; Zuo, F.; Cromack, K. R.; Angelopoulos, M.; MacDiarmid, A. G.; Epstein, A. J. Charge Transport in the "Emeraldine" Form of Polyaniline *Synt. Met.* **1989**, *29*, 409-416.
- (16) Chowdhury, P.; Saha, B. Potassium Dichromate Initiated Polymerization of Aniline *Indian J. Chem. Technol.* **2005**, *12*, 671-675.
- (17) Li, Y.; Al-Ghamdi, A. A.; Al-Hartomy, O. A.; El-Tantawy, F.; Yakuphanoglu, F. Semiconducting Properties of Nanofiber Polyaniline Organic Semiconductor *OAM-RC* **2012**, *6*, 235-238.
- (18) Tantawy, H. R.; Aston, D. E.; Smith, J. R.; Young, J. L. A Comparison of Electromagnetic Shielding with Polyaniline Nanopowders Produced in Solvent-Limited Conditions *ACS Appl. Mater. Interfaces*, **2013**, *5*, 4648-4658.

- (19) Abdiryim, T.; Xiao-Gang, Z.; Jamal, R. Comparative Studies of Solid-State Synthesized Polyaniline Doped with Inorganic Acids *Mater. Chem. Phys.* **2005**, *90*, 367-372.
- (20) Rimbu, G. A.; Stamatina, I.; Jackson, C. L.; Scott, K. The Morphology Control of Polyaniline as Conducting Polymer in Fuel Cell Technology *J. Optoelectron. Adv. M.* **2006**, *8*, 670-674.
- (21) Duan, Y.; Shunhua, L.; Hongtao, G. Investigation of Electrical Conductivity and Electromagnetic Shielding Effectiveness of Polyaniline Composite *STAM* **2005**, *6*, 513-518.
- (22) Blythe, A. R.; Bloor, D. *Electrical Properties of Polymers*; Cambridge University Press: Cambridge; New York, 2005.
- (23) Stejskal, J.; Gilbert, R. G. Polyaniline. Preparation of a Conducting Polymer (Iupac Technical Report) *Pure Appl. Chem.* **2002**, *74*, 857.
- (24) Dmitrieva, E.; Dunsch, L. How Linear Is "Linear" Polyaniline? *J. Phys. Chem. B* **2011**, *115*, 6401-6411.
- (25) Stejskal, J.; Sapurina, I.; Trchová, M.; Konyushenko, E. N.; Holler, P. The Genesis of Polyaniline Nanotubes *Polymer* **2006**, *47*, 8253-8262.
- (26) Trchová, M.; Stejskal, J. Polyaniline: The Infrared Spectroscopy of Conducting Polymer Nanotubes (Iupac Technical Report) *Pure Appl. Chem.* **2011**, *83*, 1801.
- (27) Schrader, B.; Bougeard, D. *Infrared and Raman Spectroscopy Methods and Applications*; VCH: Weinheim; New York, 1995.
- (28) Boyer, M. I.; Quillard, S.; Rebourt, E.; Louarn, G.; Buisson, J. P.; Monkman, A.; Lefrant, S. Vibrational Analysis of Polyaniline: A Model Compound Approach *J. Phys. Chem. B* **1998**, *102*, 7382-7392.

- (29) Socrates, G. *Infrared and Raman Characteristic Group Frequencies :Tables and Charts*; Wiley: Chichester; New York, 2000.
- (30) Quillard, S.; Louarn, G.; Lefrant, S.; Macdiarmid, A. G. Vibrational Analysis of Polyaniline: A Comparative Study of Leucoemeraldine, Emeraldine, and Pernigraniline Bases *Phys. Rev. B: Condens. Matter* **1994**, *50*, 12496-12508.
- (31) Cochet, M.; Louarn, G.; Quillard, S.; Boyer, M. I.; Buisson, J. P.; Lefrant, S. Theoretical and Experimental Vibrational Study of Polyaniline in Base Forms: Non-Planar Analysis. Part I *J. Raman Spectrosc.* **2000**, *31*, 1029-1039.
- (32) Tang, S. J.; Wang, A. T.; Lin, S. Y.; Huang, K. Y.; Yang, C. C.; Yeh, J. M.; Chiu, K. C. Polymerization of Aniline under Various Concentrations of Aps and Hcl *Polymer* **2011**, *43*, 667-675.
- (33) Lambert, J. B. *Organic Structural Spectroscopy*; Prentice Hall: Boston, 2010.
- (34) Miller, F. A.; Mayo, D. W.; Hannah, R. W. *Course Notes on the Interpretation of Infrared and Raman Spectra*; Wiley-Interscience: Hoboken, N.J., 2004.
- (35) Tang, J.; Jing, X.; Wang, B.; Wang, F. Infrared Spectra of Soluble Polyaniline *Synt. Met.* **1988**, *24*, 231-238.
- (36) Han, C. C.; Bai, M. Y.; Yang, K. F.; Lee, Y. S.; Lin, C. W. A Novel Method for Making Highly Dispersible Conducting Polymer and Concentric Graphitic Carbon Nano-Spheres Based on an Undoped and Functionalized Polyaniline *J. Mater. Chem.* **2008**, *18*, 3918-3925.
- (37) Chiba, K.; Ohsaka, T.; Ohnuki, Y.; Oyama, N. Electrochemical Preparation of a Ladder Polymer Containing Phenazine Rings *J. Electroanal. Chem. Interfacial Electrochem.* **1987**, *219*, 117-124.

- (38) Sedenkova, I.; Trchova, M.; Stejskal, J. Thermal Degradation of Polyaniline Films Prepared in Solutions of Strong and Weak Acids and in Water - Ftir and Raman Spectroscopic Studies *Polym. Degrad. Stab.* **2008**, *93*, 2147-2157.
- (39) Dmitrieva, E.; Harima, Y.; Dunsch, L. Influence of Phenazine Structure on Polaron Formation in Polyaniline: In Situ Electron Spin Resonance– Ultraviolet/Visible– near-Infrared Spectroelectrochemical Study *J. Phys. Chem. B* **2009**, *113*, 16131-16141.
- (40) Stammer, C.; Taurins, A. Infrared Spectra of Phenazines *Spectrochimica Acta* **1963**, *19*, 1625-1654.
- (41) Chalmers, J. M.; Griffiths, P. R. *Handbook of Vibrational Spectroscopy. 3*; J. Wiley: New York, 2002.
- (42) Trchová, M.; Stejskal, J.; Prokeš, J. Infrared Spectroscopic Study of Solid-State Protonation and Oxidation of Polyaniline *Synt. Met.* **1999**, *101*, 840-841.
- (43) Stejskal, J.; Sapurina, I.; Trchova, M. Polyaniline Nanostructures and the Role of Aniline Oligomers in Their Formation *Prog. Polym. Sci.* **2010**, *35*, 1420-1481.
- (44) Laska, J.; Widlarz, J. Spectroscopic and Structural Characterization of Low Molecular Weight Fractions of Polyaniline *Polymer* **2005**, *46*, 1485-1495.
- (45) Chen, T.; Dong, C.; Li, X.; Gao, J. Thermal Degradation Mechanism of Dodecylbenzene Sulfonic Acid- Hydrochloric Acid Co-Doped Polyaniline *Polym. Degrad. Stab.* **2009**, *94*, 1788-1794.
- (46) Trchova, M.; Sedenkova, I.; Stejskal, J. In-Situ Polymerized Polyaniline Films 6. Ftir Spectroscopic Study of Aniline Polymerisation *Synt. Met.* **2005**, *154*, 1-4.

- (47) Sedenkova, I.; Trchova, M.; Stejskal, J.; Prokes, J. Conformational Transition in Polyaniline Films - Spectroscopic and Conductivity Studies of Ageing *Polym. Degrad. Stab.* **2008**, *93*, 428-435.
- (48) Mažeikienė, R.; Tomkutė, V.; Kuodis, Z.; Niaura, G.; Malinauskas, A. Raman Spectroelectrochemical Study of Polyaniline and Sulfonated Polyaniline in Solutions of Different Ph *Vib. Spectrosc* **2007**, *44*, 201.
- (49) Trchová, M.; Morávková, Z.; Šeděnková, I.; Stejskal, J. Spectroscopy of Thin Polyaniline Films Deposited During Chemical Oxidation of Aniline *Chem. Pap.* **2012**, *66*, 415-445.
- (50) Trchová, M.; Šeděnková, I.; Tobolková, E.; Stejskal, J. FTIR Spectroscopic and Conductivity Study of the Thermal Degradation of Polyaniline Films *Polym. Degrad. Stab.* **2004**, *86*, 179-185.
- (51) Mohamad, A.; Sawsan, Z. Nanostructured Crosslinked Polyaniline with High Surface Area: Synthesis, Characterization and Adsorption for Organic Dye *Chem. Eng. J.* **2012**, *204-206*, 79-86.
- (52) Sariciftci, N.; Kuzmany, H.; Neugebauer, H.; Neckel, A. Structural and Electronic Transitions in Polyaniline: A Fourier Transform Infrared Spectroscopic Study *J. Chem. Phys.* **1990**, *92*, 4530.
- (53) Trchová, M.; Šeděnková, I.; Konyushenko, E. N.; Stejskal, J.; Holler, P.; Ćirić-Marjanović, G. Evolution of Polyaniline Nanotubes: The Oxidation of Aniline in Water *J. Phys. Chem. B* **2006**, *110*, 9461-9468.

- (54) Liu, H.; Hu, X. B.; Wang, J. Y.; Boughton, R. I. Structure, Conductivity, and Thermopower of Crystalline Polyaniline Synthesized by the Ultrasonic Irradiation Polymerization Method *Macromolecules* **2002**, *35*, 9414.
- (55) Stejskal, J.; Trchova, M.; Konyushenko, E. N.; Sapurina, I. Oxidation of Aniline: Polyaniline Granules, Nanotubes, and Oligoaniline Microspheres *Macromolecules* **2008**, *41*, 3530-3536.
- (56) Brožová, L.; Holler, P.; Kovářová, J.; Stejskal, J.; Trchová, M. The Stability of Polyaniline in Strongly Alkaline or Acidic Aqueous Media *Polym. Degrad. Stab.* **2008**, *93*, 592-600.
- (57) Mostafa, T. B.; El-Sherif, H. Polyaniline Nanostructures with Controlled Morphology Via Pseudo-High Dilution Technique *J. Macromol. Sci., A: Pure Appl. Chem.* **2011**, *48*, 742-750.
- (58) Kuzmany, H.; Sariciftci, N. S.; Neugebauer, H.; Neckel, A. Evidence for Two Separate Doping Mechanisms in the Polyaniline System *Phys. Rev. Lett.* **1988**, *60*, 212.
- (59) Nastase, C.; Mihaiescu, D.; Nastase, F.; Moldovan, A.; Stamatina, I. Effect of P-Toluene Sulphonic Acid Doping on the Properties of Plasma Polymerized Aniline Thin Films *Synt. Met.* **2004**, *147*, 133-138.
- (60) Kellenberger, A.; Dmitrieva, E.; Dunsch, L. The Stabilization of Charged States at Phenazine-Like Units in Polyaniline under P-Doping: An in Situ ATR-FTIR Spectroelectrochemical Study *Phys. Chem. Chem. Phys.* **2011**, *13*, 3411-3420.
- (61) Šeděnková, I.; Trchová, M.; Blinova, N. V.; Stejskal, J. In-Situ Polymerized Polyaniline Films. Preparation in Solutions of Hydrochloric, Sulfuric, or Phosphoric Acid *Thin Solid Films* **2006**, *515*, 1640-1646.

- (62) Abdiryim, T.; Jamal, R.; Nurulla, I. Doping Effect of Organic Sulphonic Acids on the Solid-State Synthesized Polyaniline *J. Appl. Polym. Sci.* **2007**, *105*, 576-584.
- (63) Ćirić-Marjanović, G.; Blinova, N. V.; Trchová, M.; Stejskal, J. Chemical Oxidative Polymerization of Safranines *J. Phys. Chem. B* **2007**, *111*, 2188-2199.
- (64) Mitchell, M. B.; Smith, G. R.; Guillory, W. A. Matrix-Isolation Triplet (T) State Ir Spectroscopy of Acridine and Phenazine *J. Chem. Phys.* **1981**, *75*, 44.
- (65) Zujovic, Z. D.; Laslau, C.; Bowmaker, G. A.; Kilmartin, P. A.; Webber, A. L.; Brown, S. P.; Travas-Sejdic, J. Role of Aniline Oligomeric Nanosheets in the Formation of Polyaniline Nanotubes *Macromolecules* **2009**, *43*, 662-670.
- (66) Krishna, A.; Laslau, C.; Waterhouse, G. I.; Zujovic, Z. D.; Travas-Sejdic, J. Effect of Ionic Liquid on Polyaniline Chemically Synthesised under Falling-Ph Conditions *Chem. Pap.* **2013**, *67*, 995-1001.
- (67) Hasik, M.; Drelinkiewicz, A.; Wenda, E.; Paluszkiwicz, C.; Quillard, S. FTIR Spectroscopic Investigations of Polyaniline Derivatives–Palladium Systems *J. Mol. Struct.* **2001**, *596*, 89-99.
- (68) Nyquist, R. A. *Interpreting Infrared, Raman, and Nuclear Magnetic Resonance Spectra. Volume 2*; Academic Press: San Diego, 2001.
- (69) Nalwa, H. S. *Handbook of Advanced Electronic and Photonic Materials and Devices*; Academic Press: San Diego, 2001; Vol. 8.
- (70) Zujovic, Z. D.; Zhang, L.; Bowmaker, G. A.; Kilmartin, P. A.; Travas-Sejdic, J. Self-Assembled, Nanostructured Aniline Oxidation Products: A Structural Investigation *Macromolecules* **2008**, *41*, 3125-3135.

- (71) Stejskal, J.; Exnerova, M.; Moravkova, Z.; Trchova, M.; Hromadkova, J.; Prokes, J. Oxidative Stability of Polyaniline *Polym. Degrad. Stab.* **2012**, *97*, 1026-1033.
- (72) Wu, C. G.; Yeh, Y. R.; Chen, J. Y.; Chiou, Y. H. Electroless Surface Polymerization of Ordered Conducting Polyaniline Films on Aniline-Primed Substrates *Polymer* **2001**, *42*, 2877-2885.
- (73) Khuspe, G. D.; Bandgar, D. K.; Sen, S.; Patil, V. B. Fussy Nanofibrous Network of Polyaniline (Pani) for  $\text{NH}_3$  Detection *Synt. Met.* **2012**, *162*, 1822-1827.
- (74) Moravkova, Z.; Trchova, M.; Exnerova, M.; Stejskal, J. The Carbonization of Thin Polyaniline Films *Thin Solid Films* **2012**, *520*, 6088-6094.
- (75) Zheng, W.; Angelopoulos, M.; Epstein, A. J.; MacDiarmid, A. G. Experimental Evidence for Hydrogen Bonding in Polyaniline: Mechanism of Aggregate Formation and Dependency on Oxidation State *Macromolecules* **1997**, *30*, 2953-2955.
- (76) Li, Y.; Zheng, J. L.; Feng, J.; Jing, X. L. Polyaniline Micro-/Nanostructures: Morphology Control and Formation Mechanism Exploration *Chem. Pap.* **2013**, *67*, 876-890.
- (77) Wang, W.; Gumfekar, S. P.; Jiao, Q.; Zhao, B. Ferrite-Grafted Polyaniline Nanofibers as Electromagnetic Shielding Materials *Journal of Materials Chemistry C* **2013**, *1*, 2851-2859.
- (78) Mzenda, V. M.; Goodman, S. A.; Auret, F. D. Conduction Models in Polyaniline: The Effect of Temperature on the Current–Voltage Properties of Polyaniline over the Temperature Range  $30 < T(K) < 300$  *Synt. Met.* **2002**, *127*, 285-289.
- (79) Bekri-Abbes, I.; Srasra, E. Investigation of Structure and Conductivity Properties of Polyaniline Synthesized by Solid–Solid Reaction *J Polym Res* **2011**, *18*, 659-665.

- (80) Huang, J.; Moore, J. A.; Acquaye, J. H.; Kaner, R. B. Mechanochemical Route to the Conducting Polymer Polyaniline *Macromolecules* **2004**, *38*, 317-321.
- (81) Banerjee, S.; Kumar, A. Dielectric Behavior and Charge Transport in Polyaniline Nanofiber Reinforced Pmma Composites *J. Phys. Chem. Solids* **2010**, *71*, 381-388.
- (82) Dutta, P.; Biswas, S.; De, S. Alternating-Current Conductivity and Dielectric Permittivity of Polyaniline Doped with B-Naphthalene Sulphonic Acid *J. Phys.: Condens. Matter* **2001**, *13*, 9187.
- (83) Wan, M. *Conducting Polymers with Micro or Nanometer Structure*; Tsinghua University Press ; Springer: Beijing; Berlin, 2008.
- (84) Bredas, J. L.; Street, G. B. Polarons, Bipolarons, and Solitons in Conducting Polymers *Acc. Chem. Res* **1985**, *18*, 309-315.
- (85) Bernard, M. C.; Hugot-LeGoff, A.; Joiret, S.; Arkoub, H.; Saïdani, B. Influence of the Nature of Substituent on the Charge Mechanisms in Substituted Polyanilines (Spani, Poma) Studied by Raman and Optical Spectroscopies *Electrochim. Acta* **2005**, *50*, 1615-1623.
- (86) Bernard, M. C.; Hugot-Le Goff, A. Quantitative Characterization of Polyaniline Films Using Raman Spectroscopy: I: Polaron Lattice and Bipolaron *Electrochim. Acta* **2006**, *52*, 595-603.
- (87) Matveeva, E. S. Residual Water as a Factor Influencing the Electrical Properties of Polyaniline. The Role of Hydrogen Bonding of the Polymer with Solvent Molecules in the Formation of a Conductive Polymeric Network *Synt. Met.* **1996**, *79*, 127-139.
- (88) Zuo, F.; Angelopoulos, M.; MacDiarmid, A. G.; Epstein, A. J. Ac Conductivity of Emeraldine Polymer *Phys. Rev. B: Condens. Matter* **1989**, *39*, 3570-3578.

- (89) Singh, R.; Arora, V.; Tandon, R. P.; Mansingh, A.; Chandra, S. Dielectric Spectroscopy of Doped Polyaniline *Synt. Met.* **1999**, *104*, 137-144.
- (90) Barrau, S.; Demont, P.; Peigney, A.; Laurent, C.; Lacabanne, C. Dc and Ac Conductivity of Carbon Nanotubes-Polyepoxy Composites *Macromolecules* **2003**, *36*, 5187-5194.
- (91) Sinha, S.; Bhadra, S.; Khastgir, D. Effect of Dopant Type on the Properties of Polyaniline *J. Appl. Polym. Sci.* **2009**, *112*, 3135-3140.
- (92) Zhang, D. On the Conductivity Measurement of Polyaniline Pellets *Polym. Test.* **2007**, *26*, 9-13.
- (93) Chaudhari, H. K.; Kelkar, D. S. Investigation of Structure and Electrical Conductivity in Doped Polyaniline *Polym. Int.* **1997**, *42*, 380-384.
- (94) Bohli, N.; Gmati, F.; Mohamed, A. B.; Vigneras, V.; Miane, J. L. Conductivity Mechanism of Polyaniline Organic Films: The Effects of Solvent Type and Casting Temperature *J. Phys. D: Appl. Phys* **2009**, *42*, 205404.
- (95) Chaudhari, H. K.; Kelkar, D. S. X-Ray Diffraction Study of Doped Polyaniline *J. Appl. Polym. Sci.* **1996**, *62*, 15.
- (96) Zhang, K.; Li, Y. Electrical Conductivity Enhancement of Polyaniline by Refluxing *Polym. Adv. Technol.* **2011**, *22*, 2084-2090.
- (97) Malecki, J.; Hilczer, B. Dielectric Behaviour of Polymers and Composites *Mech. Corros. Prop. A, Key Eng. Mater.* **1994**, *92-93*, 181-216.
- (98) Chen, S. A.; Liao, C. S. Conductivity Relaxation and Chain Motions in Conjugated Conducting Polymers: Neutral Poly(3-Alkylthiophenes) *Macromolecules* **1993**, *26*, 2810-2816.

- (99) Lian, A.; Besner, S.; Dao, L. Broadband Dielectric and Conducting Properties of Poly(N-Alkylanilines) *Synt. Met.* **1995**, *74*, 21-27.
- (100) Han, M. G.; Im, S. S. Dielectric Spectroscopy of Conductive Polyaniline Salt Films *J. Appl. Polym. Sci.* **2001**, *82*, 2760-2769.
- (101) Joo, J.; Oblakowski, Z.; Du, G.; Pouget, J. P.; Oh, E.; Wiesinger, J. M.; Min, Y.; MacDiarmid, A. G.; Epstein, A. J. Microwave Dielectric Response of Mesoscopic Metallic Regions and the Intrinsic Metallic State of Polyaniline *Phys. Rev. B: Condens. Matter* **1994**, *49*, 2977.
- (102) Lee, H. T.; Chuang, K. R.; Chen, S. A.; Wei, P. K.; Hsu, J. H.; Fann, W. Conductivity Relaxation of 1-Methyl-2-Pyrrolidone-Plasticized Polyaniline Film *Macromolecules* **1995**, *28*, 7645-7652.
- (103) Lian, A.; Besner, S.; Dao, L. Dielectric Relaxation of Polyaniline/Polyvinylalcohol Blends *Mater. Lett.* **1994**, *21*, 215-220.
- (104) Jonscher, A. K. Dielectric Relaxation in Solids *J. Phys. D: Appl. Phys* **1999**, *32*, R57.
- (105) Nalwa, H. S. *Handbook of Organic Conductive Molecules and Polymers 3, Conductive Polymers: Spectroscopy and Physical Properties*; Wiley: Chichester; New York, 1997; Vol. 3.
- (106) Matveeva, E. S.; Calleja, R. D.; Parkhutik, V. P. Impedance Study of Chemically Synthesized Emeraldine Form of Polyaniline *Electrochim. Acta* **1996**, *41*, 1351-1357.
- (107) Lee, H. T.; Liao, C. S.; Chen, S. A. Conductivity Relaxation of Polyaniline *Makromol. Chem.* **1993**, *194*, 2443.

## CHAPTER 6

### **Solvent-Limited versus Solvent-Free Unconventional Approaches for Synthesizing Nano-PTSA-Doped PAN for Broadband EM Shielding**

#### **6.1. Introduction**

In previous Chapters (2-5), the impact of HCl-doped PAN prepared via different approaches on different physical and chemical properties of the prepared PAN were studied in detail. According to the results, the synthesis approach of limiting available solvent plays a critical role in the fine-tuning of chemical/electronic/conformational structure(s) and crystallinity in addition to affecting the (bulk) electrical/dielectrical properties and electromagnetic (EM) shielding potential of the HCl-doped PAN directly through doping levels as all interconnected. In previous work <sup>1</sup>, it was reported that HCl-doped PAN nanoparticles showed an interesting contradiction to the general rule that higher crystallinity increases conductivity <sup>2-6</sup>, *i.e.*, the PAN nanopowders prepared via a slow oxidation approach (CS) were significantly more crystalline with similar or lower conductivity and lower EM shielding than PAN samples prepared via fast oxidation (CF).

In this chapter, a similar study is carried out utilizing another dopant to test the recently supported working hypothesis that the solvent addition method is critical in PAN synthesis with simultaneous doping and to investigate similarities and differences that might be related to the dopant species of interest. The organic species p-toluene sulfonic acid (PTSA) was selected as the dopant candidate for this work rather than another inorganic acid in order to look for greater variation in comparisons with HCl doping.

It was important to identify the impact of synthesis approach on the EM shielding potential of the PTSA-doped PAN samples as it was clarified in the case of the HCl-doped PAN in Chapters 2 and 4. One of the main aims of utilizing another dopant candidate is to confirm a general effect of limiting solvent—either to a minimum or to some optimum level and mixing procedure—on the relation between conductivity, crystallinity, chemical/electronic conformation and EM shielding. A second hypothesis that will be tested by UV-vis and EM measurements ( sections 6.4.4 and 6.4.5 respectively) is that the extent of delocalized charge distributions and/or polaron lattice-supporting polymer structures can be finely tuned toward optimal conditions for EM interference (EMI) shielding applications by the synthesis approach of carefully controlling solvent availability during doping-polymerization.

Furthermore, two different “unconventional” approaches will be tested on the PTSA-doped PAN synthesis products. Whereas the HCl studies for “solvent-free (SF)” nanopowders all used HCl concentrate (36%) without the addition of more solvent—the water available in the HCl solution only cannot be totally removed—to compare against the two excess solvent regimes (fast and slow addition with pure water diluting the reaction conditions; CF and CS), the use of PTSA also a more truly solvent-free reaction in a similar method of grinding for simultaneous polymerization and doping. While the SF medium for HCl-doped PAN production was a paste with some very low water content, the PTSA is solid powder allowing a completely solvent-free reaction, other than what trace amounts of water may absorb from atmospheric conditions, etc. In order to explore the impact of the limited solvent more completely than was possible in the case of HCl-PAN, a direct comparison between truly solvent-free conditions and carefully controlled, limited addition of solvent (water) can be

accomplished with PTSA for the first time, to the best of our knowledge. A very limited amount of water was applied to the reaction medium in order to have a paste comparable to the HCl-PAN “solvent-free” conditions, as described in the methodology section. This later approach is now referenced as SL in this chapter to distinguish it from the SF procedure for PTSA, where again no solvent is present. Thus, two unconventional approaches are compared with the conventional approach (used in the previous Chapters) with fast (CF) and slow (CS) reactions controlled by addition rate of oxidizing solution (see Chapter 2 for details).

Finally, it was very important in this current work to examine any changes in the shielding potential, as the primary property for ultimate application, of the PAN doped with the conventional approach in switching the dopant from HCl (Chapters 2 and 3) to PTSA (current study). The structure-property relationships of the nanopowders from different synthetic procedures will be utilized to examine the PTSA case in connection with high-frequency EM response observed in the previous case of HCl (Chapters 2 and 4). The EM measurements are expected to confirm the proposed electronic structures for charge delocalization in PTSA-doped PAN samples as examined via UV spectroscopy—exhibiting the necessary charge delocalization for substantial improvements in EM field responses over existing forms of PAN previously produced and studied, both in this dissertation and in the current literature. In this chapter, EM measurements are correlated to the impact of crystal/electronic/conformational structures and conductivity of the prepared PTSA-doped PAN samples on shielding effectiveness (SE) behavior with frequency. The impact of crystallinity and conductivity obtained from nanopowders made by the variant synthesis approaches will also be elucidated.

## 6.2. Materials and Methods

Aniline (99.5%, ACS reagent grade, Aldrich) was purified by distillation with zinc dust before use <sup>7,8</sup>. The sulfonic acid dopant p-toluene sulfonic acid (98.5%, ACS reagent grade, Alfa Aesar Chemicals) and the oxidant ammonium peroxydisulfate (98%, ACS reagent grade, Aldrich) were used as received. PTSA-doped PAN samples were prepared similarly to the previous reported procedures <sup>1</sup>. PAN samples were prepared with solvent-limited (SL), solvent-free (SF) and conventional (solvent-based) chemical oxidations under slow (CS) and fast (CF) production rates as controlled by the addition of aqueous ammonium peroxydisulfate (APS), both described below in detail.

### 6.2.1. Solvent-Limited (SL)/Solvent-Free (SF) Synthesis

It should be first noted that the “solvent-limited (SL)” label refers to the aniline monomer, dopant (PTSA), and oxidant (APS) being used in their as-prepared and as-received states with a small amount of solvent in a reaction medium compared to the two conventional methods. On the other hand, “solvent-free (SF)” label refers to reactants being used in their as-prepared and as-received states without first dissolving them in a reaction medium (solvent), though certainly the SF reaction chemicals are completely void of solvent, unlike the HCl-PAN scenario.

A typical SL polymerization procedure at room temperature (~18–24°C) was followed with 0.1 mole of the doping acid PTSA with 5 mL of DI water ground in a 250-mL glass mortar. Freshly distilled aniline (0.05 mole per batch) was added dropwise while grinding manually for 10 min. Very small dropwise portions are needed in order to minimize the released fumes and prevent overheating of the reaction medium since aniline reacts violently with acids <sup>9</sup>. The reactant mixture became a white paste after grinding. Separate grinding of

0.05 mole APS in an agate mortar produced a fine powder, which was subsequently added in small portions to the white paste reactant in order to avoid overheating from the highly exothermic oxidative polymerization<sup>10,11</sup>. Approximately 0.5 g APS was added in between grinding the reactant mixture for ~1-2 min in cycles until the entire batch was uniformly ground and finally attained the appropriate greenish-black color indicative of the PTSA-doped PAN nanoparticles reproducibly from batch to batch. This product was transferred to a 500-mL beaker where 50 mL of acetone, 100 mL of ethanol and 100 mL of DI were added then mixed for 1 h in order to quench the polymerization reaction and to dissolve oligomeric impurities<sup>12-14</sup>. The rest of the product mixture was filtered and washed with acetone, ethanol, and distilled water, in series, until the filtrate from each solvent stage was colorless in order to confirm the adequate removal of unreacted chemicals and excess acid<sup>15,16</sup>. Finally, the powder was dried at room temperature for 72 h. A typical SF polymerization at room temperature (~18–24°C) had the same previous procedures as SL except that the 5 mL DI water was not added during the grinding reaction steps.

### **6.2.2. Conventional Chemical Synthesis: Fast (CF) and Slow (CS) Oxidations**

Typically, 0.1 mole of PTSA was dissolved in 1000 mL of DI water with mixing on a magnetic stirrer (1000 rpm) for 15 min, followed by dropwise addition of 0.05 mole of the same freshly distilled aniline with mixing for another 15 min. Then 0.05 mole of APS dissolved in 50 mL of DI water was added. In case of conventional chemical oxidation with fast reaction (CF), the oxidizing APS solution was added all at once to the reactor vessel. On the other hand, the slow reaction procedure (CS) added the same APS solution amount with constant rate of 0.1 mL/min. Both reaction protocols were conducted at room temperature (~18–24°C). The reaction solutions were mixed for 12 h after APS addition. Then 50 mL of

acetone and 100 mL of ethanol were added and mixed for 1 h, similar to the SL and SF samples above except that no additional DI water is needed for the conventional solvent-rich synthesis<sup>12-14</sup>. The remaining products were filtered, washed, and dried identically to the SL and SF samples.

### 6.3. Characterization

#### 6.3.1. DC Conductivity Measurements

Typically, 0.05-g samples were pelletized in a special homemade cell. The dimensions of the standard pellet under testing were 5-mm diameter and  $1.2\pm 0.1$ -mm thickness. Figure 6.1 shows a schematic diagram of the home made cell used for measuring the DC conductivity of the samples.

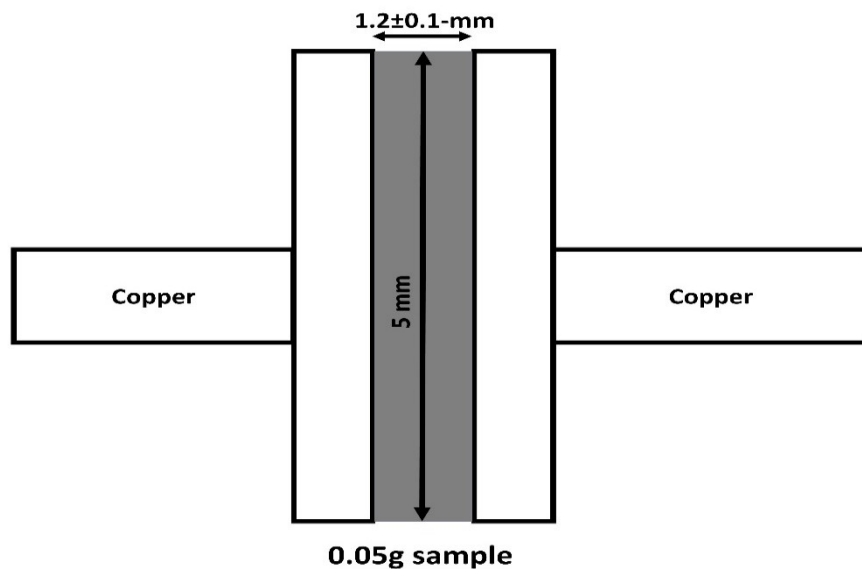


**Figure 6.1** Schematic diagram of the home made cell used for measuring the DC conductivity of the samples.

DC conductivity ( $\sigma_{DC}$ ) of the samples was measured at room temperature on pressed pellets by a two-point probe technique<sup>17-19</sup>. Sample ( $\sigma_{DC}$ ) was calculated by the following equation<sup>20</sup>:

$$\sigma_{DC} = \frac{L_c}{R \cdot A_c}$$

where  $L_c$  is sample thickness,  $A_c$  is sample surface area, and  $R$  is the measured resistance of the sample.

Three pellets were prepared for each sample. Current-voltage (I-V) measurements were carried out via a Keithley 4200 SCS semiconductor parameter analyzer. Dual sweep mode was operated within a voltage range -0.1 to 0.1 V, and 0.01 V stepwise. Each I-V measurement was repeated 11 times at least for every pellet for reproducibility confirmation. The values reported are averaged over 33 readings for each sample.

### 6.3.2. Morphology: TEM

Morphological characterization was carried out by transmission electron microscopy (TEM-JEOL JEM 2010) operating at 200 kV. A drop of diluted suspension of each sample was applied to a copper grid coated with carbon film (FCF-150-Cu).

### 6.3.3. Crystallinity: XRD

A Siemens D5000 powder X-ray diffractometer (XRD) was used with a copper target (Cu K $\alpha$ ) and wavelength ( $\lambda$ ) of 0.15418 nm. Data were collected in the range of  $2\theta = 2^\circ$  to  $40^\circ$ <sup>21,22</sup> at a resolution of  $0.01^\circ$  per step with an 11-s integration time per step. The  $d$ -spacings were deduced from the angular position ( $2\theta$ ) of the observed peaks according to the Bragg formula<sup>23</sup>:  $\lambda = 2d\sin\theta$ . The crystalline domain size, or the extent of order  $L$ , of the highest intensity crystallite peaks was estimated using the Scherrer formula<sup>13</sup>:  $L = k\lambda/(\beta\cos\theta)$ , where

$k$  is the shape factor for the average crystallite ( $\approx 0.9$ ), and  $\beta$  is the peak's full width at half-maximum (FWHM) in radians<sup>24</sup>. The inter-chain separation length ( $R$ ), corresponding to the most intense crystallite peak of Bragg diffraction patterns from the PAN samples, was determined from the relation given by Klug and Alexander<sup>25</sup>:  $R = 5\lambda/(8\sin\theta)$ . The percent crystallinity has been calculated by using the Manjunath's formula<sup>5,26-28</sup>. According to this, the resolution of the peak  $R$  for X-ray spectrum with heights  $h_1$  and  $h_2$ , and minima  $m_1$  is given by

$$R = \frac{2 m_1}{h_1 + h_2}$$

In the case of polymers, where there are more than two peaks as in polyaniline, all the peaks and the minima between them are measured. Thus, for any polymer

$$R = \frac{m_1 + 2m_2 + \dots + m_n}{h_1 + h_2 + \dots + h_n}$$

where  $m_1, m_2, \dots$  are the heights of minima between two peaks and  $h_1, h_2, \dots$  are the heights of peaks from the baseline. Then  $(1-R)$  gives the lateral order or the index of crystallinity.

#### 6.3.4. UV-Visible Spectra

The UV analysis was carried out using a SHIMADZU-UV-11700 UV-visible spectrophotometer over the range 350-1100nm. The testing was carried out taking only the soluble portion of PAN in m-cresol, sample concentrations were  $\approx 0.2$  mg/ml.

#### 6.3.5. Electromagnetic Shielding Efficiency (SE)

In order to determine SE of the samples under test and confirm their relative performance, coaxial-guided transmission line techniques were employed from the pertinent literature descriptions.<sup>29,30</sup> A mass of  $0.06 \text{ g} \pm 0.01 \text{ mg}$  of each PTSA-doped PAN

nanopowders prepared from different synthetic approaches was selected to be pressed inside the sample holder. The dimensions of the sample under testing inside the coaxial holes are  $1.27 \pm 0.05$  mm inner diameter,  $4.56 \pm 0.05$  mm outer diameter and  $6 \pm 0.05$  mm length. Three samples were prepared for each synthetic approach with a total of 12 samples. HP8510C network analyzers were used to investigate EM shielding potential within a broad band of 2-14 GHz. A full two-port calibration was performed before testing in order to remove systematic errors<sup>30,31</sup>. The dependence of SE on absorption and reflection losses were investigated as a function of frequency and synthesis conditions. The coaxial-guided transmission line setup was used in this Chapter was in similar fashion as shown in Chapter 4 (Figure 4.1), in contrast to the Chapter 2 waveguide experiments.

## 6.4. Results and Discussions

### 6.4.1. DC Electrical Conductivity ( $\sigma_{DC}$ )

The current-voltage (I-V) curves of the PTSA-doped PAN samples are shown in Figure 6.2, indicating ohmic behavior in all types at room temperature<sup>32</sup> with electrical resistance increasing as follows: SL ( $15.4 \pm 0.6$  S/cm) < CS ( $4.5 \pm 0.1$  S/cm) < SF ( $1.6 \pm 0.4$  S/cm) < CF ( $1.3 \pm 0.3$  S/cm). The differences are likely due to the impact of the formulation conditions on the final chemical/electronic/conformational structure and material crystallinity, as it was suggested in previous chapters and by others. The experimental values of PTSA-doped PAN (CS, CF and SF) fitted within the range of conductivities previously reported for HCl-doped PAN<sup>2,33-35</sup>. However, the nearly order of magnitude increase in conductivity for the SL samples is higher than CF and SF and almost four times higher than the CS. It is now further substantiated through this very different dopant system that the synthesis approach is

capable of tuning electrical properties of PTSA-doped PAN, similar to what was observed in case HCl-doped PAN but with a different trend. The possible explanation about different electrical behavior trends observed in the PTSA-PAN will be discussed later.

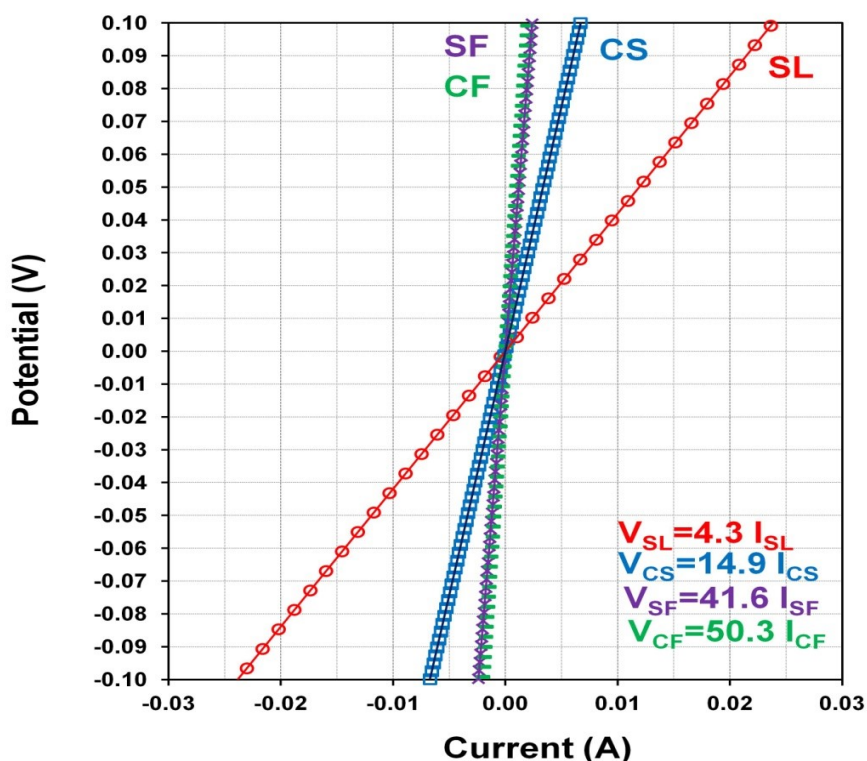


**Figure 6.2.** I-V curves from two-terminal measurements on four PAN samples doped with PTSA: CF and SF overlap symbols.

#### 6.4.2. Morphology

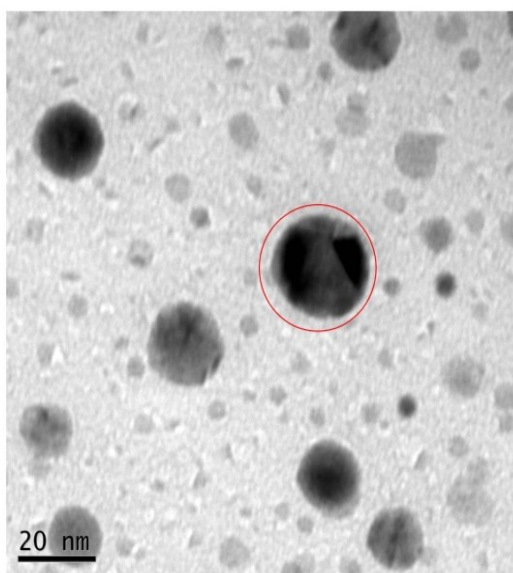
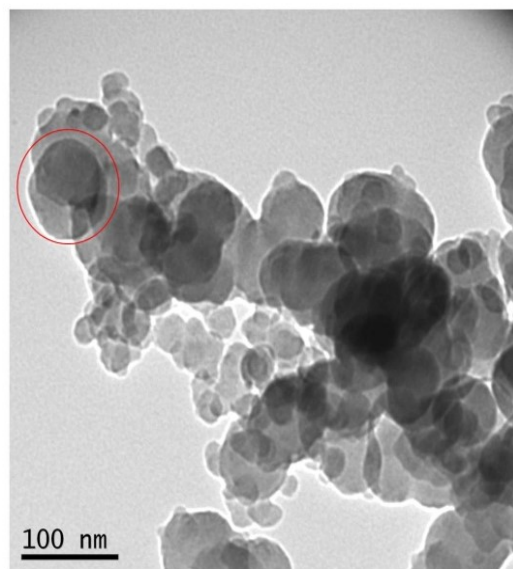
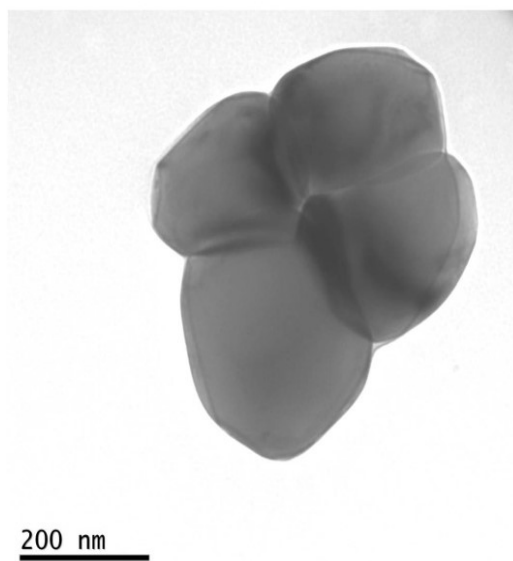
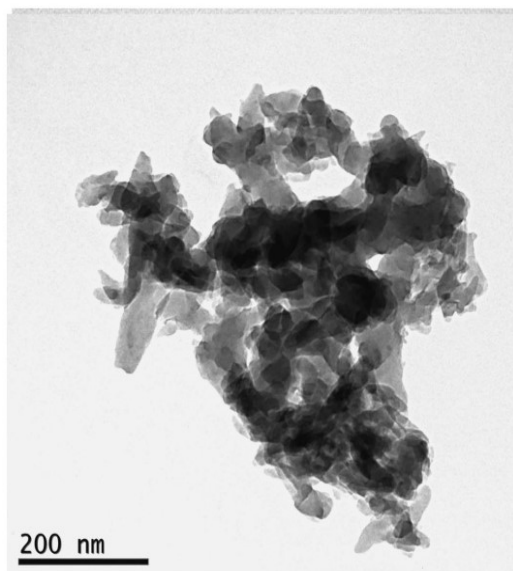
It was interesting to observe that utilizing different synthesis approaches led to significant differences in morphology and particle size range for the PTSA-doped PAN. Regarding the unconventional approaches SF and SL (Figure 6.3a-b), it seems tuning up the SF approach with a limited amount of solvent, as mentioned in the methodology section, led to a significant change in particle size distributions. The SL approach produced regular nanoparticles and nanospheres with an estimated particle size of 20-30 nm and less. On the other

hand, the SF method without solvent led to PAN nanoparticles also with regular nano-polygons and nanospheres but of an estimated particle size of 100-200 nm and less.

The similarity in particle shapes between SL and SF as shown by the red circle in Figure 6.3a and 6.3b may be an indication of similarity in crystal structure (distributions), to be discussed later in the XRD section. This could be suggestive that tuning the solvent ratio with respect to reactants may play an important role in controlling particle size (distributions) and possibly other morphological properties of the prepared PTSA-doped PAN.

The representative TEM micrograph of slow oxidation products (CS) shows the largest aggregates of nano-polygon morphologies (Figure 6.3c). The average particle size is about 200-300 nm. Recalling the observation in Chapter 2 about the impact of the CS approach on particle size in HCl-doped PAN<sup>1</sup>, the relatively large sized PTSA-doped PAN builds to a generalized expectation that slow oxidant addition will likely bias toward larger primary polymer particles. Moreover, the shape of the CS nanoparticles may indicate different crystalline structure(s) with respect to the unconventional approaches of SF and SL (see XRD section).

There is an obvious contrast with the fast oxidation products CF (Figure 6.3d) giving the most irregularities to the nano-polygon morphologies and a broad particle size and shape distribution. These noticeable irregularities could be due to the mixed PAN phases, discussed later with XRD results. It is difficult to estimate the particle size quantitatively due to the broad-ranging character of irregular shapes, though they appear to vary from 30 to 300 nm. It is intriguing and perhaps indirectly relevant for future expansion on this work that previous studies on solvent-free and solid state synthesis approaches reported nanofibers rather than the nanoparticles produced in this work<sup>36,37</sup>.

**(a) SL****(b) SF****(c) CS****(d) CF**

**Figure 6.3.** The TEM images of PTSA-doped PAN samples prepared with different approaches: (a) SL, (b) SF, (c) CS, and (d) CF. Note scale bars of 20 nm (a), 100 nm (b) and 200 (c-d).

### 6.4.3. XRD Characterization

X-ray diffraction data allows examination of the impact of particular synthesis approaches on the crystal structure, crystallinity, and polymorphism of the prepared PTSA-doped PAN nanopowders. The XRD patterns show distinct differences between each PTSA-PAN sample type, which have almost identical chemical compositions (Figure 6.4). The relative clarity and sharpness of the observed peaks represent the impact of synthesis approach on PAN chain ordering, crystal structure and crystallinity as reported in Table 6.1. The intensity (peak height) represents the population of crystallite in certain planes and the sharpness of the peak represents the degree of regularity or ordered arrangement of polymer chains in that crystallite type<sup>38</sup>. Depending on the synthesis protocol, two different crystalline forms as well as significantly different degrees of crystallinity of PTSA-doped PAN were observed to be 54%, 70%, 77% and 63% corresponding to CF, CS, SF and SL, respectively (Table 6.1). The differences in broadness observed (Figure 6.4) show that the disorder is very anisotropic (not the same in all directions)<sup>39</sup>.

The main diffraction peaks of PAN salt were resolved. Comparison of the measured d-spacings and Bragg intensities of PAN samples with literature values led to the identification of two polymorphic families, ES-I and ES-II<sup>21,40-45,46,47-50</sup>, as shown in Table 6.1. As reported previously, class I consists of PAN prepared in the conducting doped PAN salt form, while class II consists of materials prepared in the insulating PAN base form<sup>3,40-42</sup>. In the current work, both classes (I and II) were prepared from the conducting PTSA-doped PAN salt form of aniline.

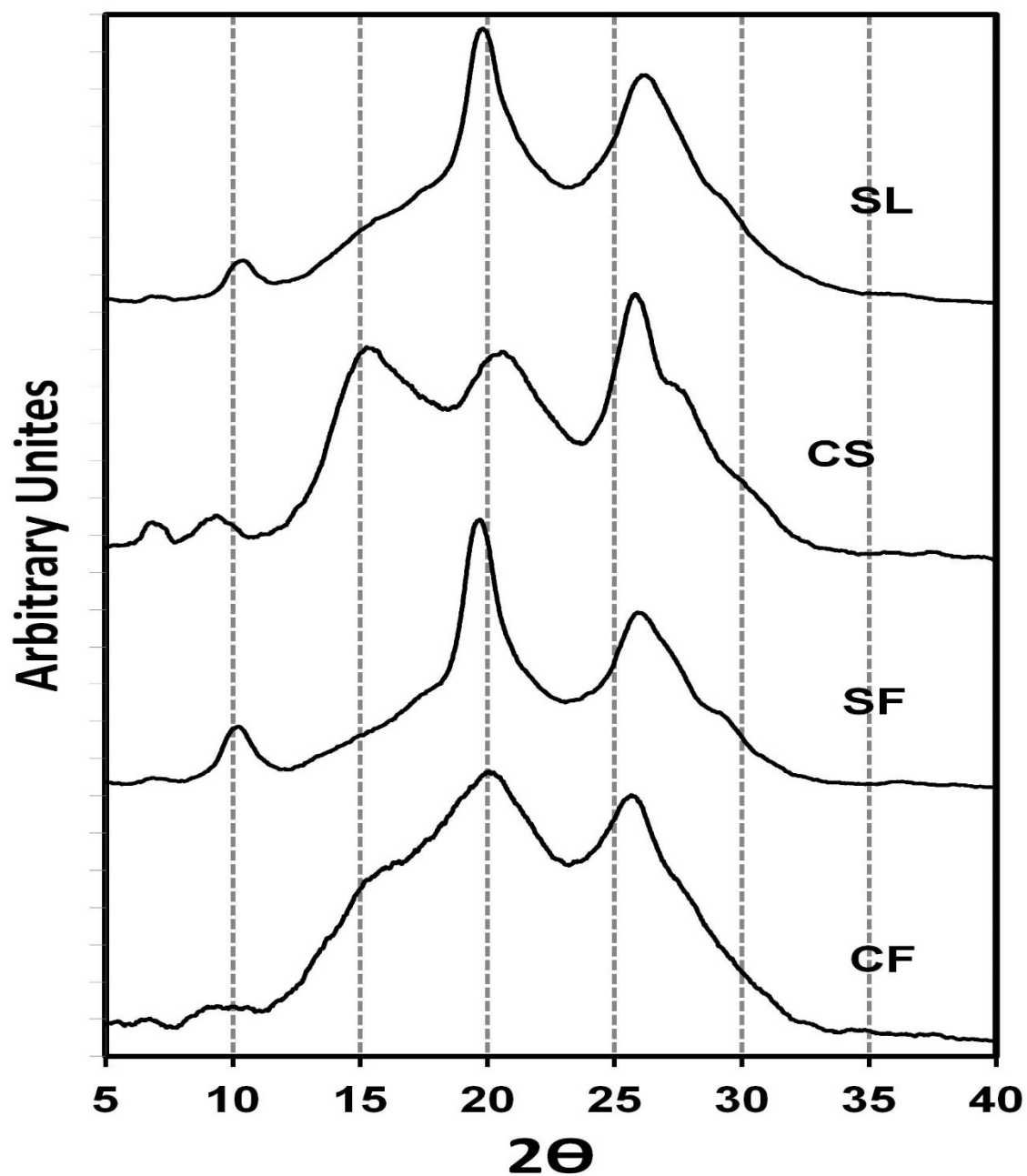


**Figure 6.4.** XRD diffraction pattern of PTSA-doped PAN synthesized under different protocols: SL (top), CS, SF, CF (bottom).

**Table 6.1.** XRD data analysis summary of PTSA-doped PAN samples<sup>21,40-45,46,47-50</sup>

<i>Sample</i>	<i>2θ</i>	<i>d(Å)</i>	<i>Domain size L(Å)</i>	<i>Inter-chain Separation R(Å)</i>	<i>hkl</i>	<i>Phase</i>	<i>Crystallinity %</i>
<b>CF</b>	6.5vw	13.6				Mixed	54
	9.1vw	9.7			(001) ES-I	(ES-I/ES-II)	
	10.1vw	8.8			(010) ES-II		
	15.6sh	5.7			(010) ES-I		
	<b>20.1</b>	<b>4.4</b>	<b>27.2</b>	<b>5.6</b>	(100) ES-I		
					(020) ESII		
	<b>25.5</b>	<b>3.5</b>	<b>40.0</b> ⊥	<b>4.4</b>	(110) ESI		
					(020) ESII		
<b>CS</b>	6.8	12.9	113.8			ES-I	70
	9.0	9.8	58.1		(001) ES-I	pseudo orthorhombic	
	<b>15.1</b>	<b>5.9</b>	34.0		(010) ESI		
	20.4	4.4	40.4	5.5	(100) ESI		
	<b>25.2</b>	<b>3.5</b>	<b>66.6</b> ⊥	<b>4.4</b>	(110) ESI		
	26.9sh	3.3			(111) ESI		
<b>SF</b>	9.5	9.3	90.5		(010) ESII	ES-II	77
	<b>19.2</b>	<b>4.6</b>	<b>81.4</b>	<b>5.8</b>	(020) ESII	Orthorhombic	
	25.6	3.5	65.4⊥	4.4	(200) ESII		
	28.6sd	3.1			(210) ESII		
<b>SL</b>	9.9	8.9			(010) ESII	ES-II	63
	<b>19.2</b>	<b>4.6</b>	<b>74.7</b>	<b>5.7</b>	(020) ESII	Orthorhombic	
	25.5	3.5	35.6⊥	4.3	(200) ESII		
	29.0sh	3.0			(210) ESII		

Table 6.2 shows the diffraction peaks of the samples and the proper assignments. It was found that all the samples have two main diffraction peaks can be seen at 20° (4.4 Å) and 25° (3.5 Å). The first one corresponds to the (100) plane and/or (020) plane of ES-I and ES-II, respectively (Table 6.2). This diffraction peak arises from periodicity parallel to PAN chains<sup>51-57</sup>. The second one corresponding to (110) plane and/or (200) plane of ES-I and ES-II, respectively (Table 6.1). This diffraction peak arises from periodicity perpendicular to PAN chains<sup>52-58</sup>. The observed diffraction peak at 15° (5.9 Å) corresponds to the (010) plane of ES-I, which assigned repeating units of PAN chain<sup>51,54,59</sup>. The d-spacing of 5.9 Å could correspond to the compact packing distance between dopant within the dopant layer<sup>40</sup>.

The diffraction peaks at  $9^\circ$  (9.8 Å) and  $10^\circ$  (8.8 Å) are corresponding to (001) and (010) of ES-I and ES-II, respectively. These peaks arise from the periodicity of repeating units of PAN chains<sup>51,54,59</sup>.

**Table 6.2.** XRD diffraction peak assignments of PTSA-doped PAN samples.

2θ (Degree)				Assignments	Refs.
SL	SF	CS	CF		
6.3vw	6.5vw	6.5	6.5	Aniline/dopant acid salt penetration Long-range order.	51,52,58 51,52
9.9	9.5	9	9.1/10.1	repeating units of PAN chain	51,54,59
	---	15.1	15.6sh	ES-I interchain reflection.	39,42,47,50
19.2	19.2	20.4	20.1	Periodicity parallel to PAN chains	51-57
25.5	25.6	25.2	25.5	Periodicity perpendicular to PAN chains	52-58
-----	28.6 <sub>sd</sub>	26.9 <sub>wsh</sub>		Periodicity of $\pi$ - $\pi$ stacking of rigid phenazine-like/cross-linking structures.	52,56,58,60,61

The XRD patterns indicate that the SL and SF approaches lead to mainly ES-I, where the majority of SL and SF PAN chains is orderly arranged on the  $d_{200}$  crystal plane. SF and SL diffraction patterns are compatible pseudo-orthorhombic lattice structures<sup>41,42,62,63</sup>, where the chains have their zigzag backbone in-phase<sup>39</sup>. The possibility of being also compatible with monoclinic lattice<sup>39,43,64</sup> or triclinic<sup>64</sup> still exists. The SF peaks are sharper and more intense than SL, which confirms the presence of high crystallinity and/or ordering in the SF with solvent-free conditions imposed on their reactions. Also, it was observed that crystalline coherent length in polymer chain direction and transverse ( $L_{\parallel}$ ) and ( $L_{\perp}$ ) of SF is relatively longer than SL. This agrees with the observed crystallinity trend (Table 6.1) and the expectation that concentrated acidic conditions favor higher crystallinity for doped PANs<sup>1,17</sup>. Higher crystallinity may also correlate with more cross-linking<sup>1,55</sup>.

In the SF diffraction curve, a shoulder at  $29^\circ$  ( $3 \text{ \AA}$ ) could be assigned to the periodicity of  $\pi$ - $\pi$  stacking of rigid phenazine-like/cross-linking structures<sup>52,56,58,60,61</sup>. This same shoulder is weaker in SL samples, perhaps indicating an intermittent crystallinity and/or lower extent of cross-linking compared to SF PTSA-doped PAN, supporting the general notion that while the degree of crystallinity depends on the synthesis approach<sup>65</sup> it is not the only factor of importance to maximize conductivity.

The diffraction pattern of CS PAN indicate that the majority of polymer chains are orderly arranged on the  $d_{110}$  crystal plane. The pattern is compatible with the ES-II orthorhombic lattice<sup>39,42,43,64,66</sup> composed of layers of chains having their zigzag backbone out of phase<sup>39</sup>. The observed diffraction peak at  $6.5^\circ$  ( $12.9 \text{ \AA}$ ) is corresponding to aniline/dopant acid salt penetration<sup>51,52,58</sup> and/or long-range order<sup>51,52</sup>. The diffraction from ES-I and ES-II structures mainly differs by the interchain (010) reflection at  $d \approx 5.9 \text{ \AA}$  in ES-I and at  $d \approx 8.9 \text{ \AA}$  in ES-II, and the intrachain (001) reflection at  $d \approx 9.9 \text{ \AA}$  in ES-I, which is not allowed in ES-II<sup>42</sup>. The (100) and (110) ES-I reflections at  $d = 4.4 \text{ \AA}$  and  $3.56 \text{ \AA}$  are very close to the (020) and (200) interchain reflections observed at  $d = 4.1 \text{ \AA}$  and  $3.5 \text{ \AA}$ , respectively, in the ES-II structure<sup>42</sup>.

Also, it was observed that the CS crystalline coherent lengths in the polymer chain direction and transverse ( $L_{\parallel}$ ) and ( $L_{\perp}$ ) are relatively shorter than for SF (Table 6.1), which agrees also with the crystallinity trend. The relatively high crystallinity and low conductivity of CS with respect to SL could be attributed to CS samples having relatively high cross-linked, as its diffraction pattern has a shoulder at  $26.9^\circ$  ( $3 \text{ \AA}$ ), which could be assigned to the periodicity of  $\pi$ - $\pi$  stacking of rigid phenazine-like/cross-linking structures<sup>52,56,58,60,61</sup>. Again, the negative impact of cross linking on conductivity is confirmed.

In the case of CF-produced nanopowders, the observation of two relatively weak and broad diffraction peaks corresponding to d-spacings of about  $9.1^\circ$  ( $9.7 \text{ \AA}$ ) and shoulder at  $15.6^\circ$  ( $5.7 \text{ \AA}$ ), associated with the (010) reflection of the ES-II and ES-I structures<sup>42</sup>, respectively, suggests that there is a mixture of ES-I and ES-II local orders and the chains are not orderly arranged on a certain crystal plane. The CF crystalline coherent lengths ( $L_{\parallel}$ ) and ( $L_{\perp}$ ) are found to be the shortest with respect all the PTSA-doped samples (Table 6.1), which agrees also with the crystallinity trend. The CS method is apparently favorable for increasing crystallinity over the CF protocol<sup>1,67</sup>, even though both conventional approaches provide solvent-rich conditions, which agrees with the HCl-PAN cases, as well. Though the origin of the polymorphism (classes I and II) was recognized in many sources<sup>27,40-43,48,50,68</sup>, the fact that the form seems to depend on the synthesis route and not on the anion suggests it is due to the arrangement and the nature of chains<sup>39</sup>.

A further interpretive complication arises from the crystalline domain sizes for CF, CS, and SF samples being smaller than the particle sizes observed with the TEM. Cross-linking leads to shorter conjugated lengths and more localized polarons for a lower conductivity<sup>1,55</sup>. These two details suggest that rather than a whole-particle mix of two populations of fully crystalline and fully amorphous PAN nanoparticles, it is more likely that most nanoparticles have an internal blend of crystalline, transition, and amorphous regions<sup>1,50</sup>. Without knowing the quantitative characteristics in this regard from the analytical techniques available for this work and their limitations, these variations in nanoparticle morphology could easily account for the relatively lower conductivity in CF, CS and SF sample types with respect to the SL nanopowder. On the other hand, the obtained crystalline domain sizes for SL PTSA-doped PAN were very close to the estimated particle size observed

with TEM, which may be an indication of the presence of nearly single-crystal nanoparticles in the SL case. It may be deduced that the SL approach allows the proper/optimal ordering extent of PAN molecules and contributes to the higher conductivity than the other approaches.

One report observed that doped PAN can exhibit intermediate crystallinity with a more “metallic” nature than either relatively higher or lower crystallinity samples<sup>42</sup> while others showed slight degradation of metallic behavior in spite of an increase in crystalline domain size<sup>40</sup>. In concert with the observations from this current dissertation, an optimum crystallinity for maximum conductivity should correspond to an optimum chemical/electronic/conformational structure for EM shielding efficiency. This optimum, perhaps accessible through fine-tuning the synthesis approach with key reactor compositions of monomer, dopant and oxidant, would effectively be setting the specific reaction kinetics mechanism(s) and rate(s) for particular outcomes. Studying the chemical kinetics of the synthesis approaches from this work would be an important future focus. The possibility of having the same class of PAN salts (ES-I/ES-II), the same dopant, and same reactant amounts and ratios, and at the end getting an order of magnitude difference in conductivity leads to an intriguing possibility: that each approach (CS, CF, SF, SL) may control the polymerization reaction differently in a fundamental fashion.

#### **6.4.4. UV-Vis Interpretation**

The main aim of utilizing UV-vis spectroscopy for these PAN samples is to: identify electronic structures and investigate the relative conformational differences between the SL, SF, CS, and CF synthesis products. In addition to elucidating the probable chain conformations, the features of the polaron, bipolaron, and polaron lattice electronic structures are probed via the electronic absorptions in the region from visible to near-infrared.

In addition to previous aims, it was important to elucidate the relationship between the observed conductivity trends of different PAN samples and the possible conformation and electronic structure dependence on synthesis approach. In order to get a deep understanding of the last aim, the UV analysis results and conductivity trends of PTSA-doped PAN samples were put in comparison with the HCl-doped PAN samples (Chapter 3) to explain or at least understand possible agreements or contrasts.

In general, UV-vis spectra of the PAN samples can be roughly divided into four main absorbance contributions as shown in Figure 6.5 and summarized in Table 6.3. The absorption band around 430 nm is assigned to the existence of a polaron electronic transition in doped polyaniline that is caused by the presence of radical cations<sup>69-80</sup>. This absorption band refers to possible extended coil conformation segments present in polyaniline samples<sup>81</sup>. Note, this band is observed in the four PAN samples with the sharpest and best-resolved being in SL and CS spectra as shown in Figure 6.5. In all likelihood, the polaron in SL- and CS-synthesized PANs are the most organized. On the other hand, this band appears as possibly a broad-shoulder on an adjacent, out-of-range electronic mode in the CF and SF spectra (<350 nm). Taking into account the broadening of the polaron band and previously recorded evidence of bands not-resolved in these spectra<sup>45</sup>, it is probable that different structures, such as isolated polarons, may coexist. In fact, the presence of isolated polarons indicates that the electronic structure of CF and SF may have higher extents of charge localization (isolated polaron) with respect to polarons in CS and SF might be the primary reason for polaron band broadening. The observed band in CF PAN at 620 nm is attributed to  $\pi$ - $\pi^*$  transition of standard PAN base.<sup>67,82,83</sup> Specifically, it is usually ascribed to an exciton located in the quinoid ring (Q) and arising from charge transfer from the adjacent benzenoid rings, with each side contributing

half an electron on average<sup>73,84-86</sup>. This weak band was distinctly observed in CF spectra and represents the possible coexistence of unprotonated quinone diamine species<sup>73</sup>. Additionally, it could be an indication for a relatively lower extent of protonation/doping in CF PAN.

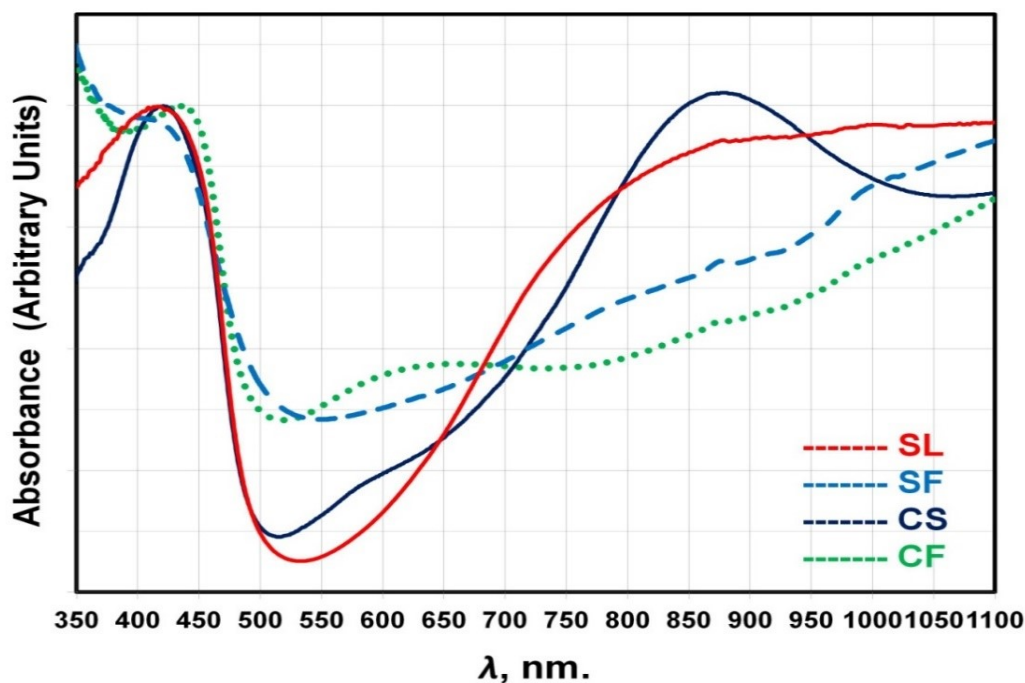


**Figure 6.5.** UV-visible spectra of polyaniline samples (SL, SF, CS, and CF) in *m*-cresol.

**Table 6.3.** Band assignments of UV-visible spectra of polyaniline samples (CS, CF, SL and SF) in *m*-cresol.

<i>Absorption band</i>	<i>Assignment</i>	<i>Ref.</i>
430 nm	Polaron transition doped PAN	69-80
	Extended coil conformation segments	81
620 nm	Quinonoid segments	73,84-86
850 nm	Bipolaron state	73,80,87
	Localized polaronic species	75,77,81,88-94
	Localized polaronic species + compact coil conformation	81,90-94
	Compact coil conformation emeraldine salt	74,81,90-94
	ES-I strong localized polaron	88
>950 nm	Free carrier tails	75,85,94
	Expanded conformation of polyaniline chains	85

The higher wavelength band observed at ~850 nm indicates significant electronic differences between PAN samples. This band is likely contingent upon the existence of dicationic, bipolaron electronic transitions in doped PAN<sup>73,80,87</sup> and/or is caused by localized polaronic species<sup>75,77,81,88-94</sup> with shorter conjugation length<sup>91</sup>. This band appears only in the CS samples, which represents a significant charge localization that may transition to a bipolaron depending on synthesis conditions<sup>95,96</sup>. Additionally, this band can be attributed to a compact coil conformation of the segments in doped PAN<sup>74,81,90-94</sup>, which has been shown to lead to lower conductivity<sup>92-94</sup>. Most notably, the existence of this band in CS confirms its proposed polymorphism obtained via the XRD analysis and interpretation. Specifically, the 850-nm band indicates the predomination of ES-I structures in CS<sup>88</sup>. It is important to notice that this band is not as broad as it was observed before in Chapter 3 with the HCl-doped PAN prepared from the slow oxidation. This may suggest that the bipolaron/compact coil band in case of PTSA is not as strong as in the CS HCl-doped PAN. Therefore, PTSA-doped PAN may not have the predominant bipolaron electronic structure/compact coil conformation of the CS HCl-doped PAN. This could explain why the conductivity is not the lowest with respect to the SL, SF, and CF) samples, as in the HCl study. In addition to the coiled conformation of CS-PTSA-PAN not being totally randomly coiled, the possibility of having helically-coiled conformation with retained conjugation, and thus conductivity, is still feasible<sup>81,88,97,98</sup>. This assumption may explain why this band looks different than the observed corresponding band in HCl-PAN (Chapter 3).

The "free carrier tail" characteristic of metallic conductive materials (i.e., delocalization of electrons) is observed above 950 nm<sup>75,85,94</sup>. The steady increase of free carrier tail in SF PAN was more pronounced than in the CF spectra. This is a very clear

indication of a lower extent of charge delocalization in CF. The relative increase in absorbance can be considered a third reasonable explanation for the relative higher conductivity of SF-PAN. Moreover, this region can also be attributed to the expanded conformation of polyaniline chains<sup>85</sup>, indicating that SF and CF have expanded conformation. Recalling the possible higher extent of charge localization in both sample types as indicated by their polaron band broadening, the obscurity of the polaron band may suggest an explanation of the conductivity trend. Moreover, the presence of the  $\pi$ - $\pi^*$  transition of standard PAN base in CF products might indicate a second possible reason for CF-PAN's being the lowest conductivity.

The UV spectrum of SL-PAN shows a nearly flat plateau of well-developed carrier-tails covering almost the entire NIR region as shown in Figure 6.5, indicating SL-PAN molecules are highly conjugated<sup>81,92,99</sup> for relatively high conductivity/metallic character<sup>92</sup> and the expanded conformation of polyaniline chains<sup>85</sup>. By comparing the UV spectra of SL, SF, and CF samples with similar PAN UV spectra<sup>81,92,100,101</sup>, the SL-PAN could be considered to have the most well-developed, free carrier tail and the highest conjugation. This later observation with the well-organized polaron in SL-synthesized PAN likely explains the order of magnitude increase in conductivity. However, it still has a strong absorption in the visible light region (a V-shape at the visible region)<sup>81</sup>. Luckily, the CS-PAN absorption at the visible region can be depressed (U-shape at the visible region), and a peak at the NIR region appeared at 850 nm as an indication of relatively shortened conjugation length in CS-PAN with respect to SL<sup>81</sup> as shown in Figure 6.4 (CS). It is important again to notice that this band it not decreasing as much as it was observed to in the CS-HCl-PAN (Chapter 3). This may suggest that loss of carrier mobility is not as large for PTSA as for HCl. Therefore, PTSA-doped PAN may still have significant free-carrier mobility.

The organized polarons in CS-synthesized PAN (compared to SF and CF) likely explains its conductivity being lower than SL because of partially localized charge/short conjugated lengths (850 nm absorption band) and its free carrier band being not as steady and straight as for SL.

Based on the UV-vis spectra, doped polyaniline samples have different electronic structures, which were attributed to differences in conformational structures. The polaron is the predominant feature in SL, SF and CF while CS spectra indicate partially localized polaron/bipolaron species. Free carriers, corresponding to electron delocalization, were observed in all UV-vis spectra with the best developed and steady appearance for SL. Under these circumstances, a "true polaron lattice" cannot be formed in the CF and SF synthesized PANs which, according to their lower conductivities, may be attributed to the presence of the predominant random polaron and bipolaronic species (Chapter 3). On the contrary, a certain fraction of SL and CS synthesized PAN likely contains the conductive polaron lattice. In general, however, this is only the case when ring moieties are in the polaron configuration in addition to other factors that will be discussed later. It must be emphasized that the presence of polarons in CF and SF synthesized PAN does not guarantee an established polaron lattice.<sup>95</sup>

#### **6.4.5. Electromagnetic Measurements**

Figure 6.6 shows the results obtained from coaxial line measurements over a broad bandwidth (2-14 GHz). Table 6.4 summarizes the EM shielding measurements. It was found that SL-PAN was the most successful of the four PTSA-doped nano-powders at EM shielding. SL-PAN achieved the highest average SE of  $73.6 \pm 3.6$  dB, with CS second ranked with average SE of  $36 \pm 6.3$  dB while the lowest shielding performance was found to be only about 16.5 dB for both CF and SF, which is surprising since the two synthesis methods were at the

solvent extremes. As expected from HCl-doped PAN (Chapters 2 and 4), the  $SE_A$  dominates for all samples (97% and 95% of SE in SL and CS types with lowest at 81% in SF and CF types) while  $SE_R$  shows limited but significant impact. The predominant absorption loss is a benefit over metals, which have high reflection contributions and negligible absorption. The enhancement of SE within the higher frequency band was noted to increase more rapidly with frequency in the case of CS more than CF and SF.

There are three differing trends in EM shielding with frequency, which correlates quite closely to the conductivity trend and the three different electronic spectral types with their varied degrees of charge delocalization implied, as observed through UV-vis results. While the SE for SL-PAN nanopowders fluctuates about its average, having the highly conjugated molecules with well-developed carrier-tails (Figure 6.5)<sup>81,92,99</sup>, CS-PAN samples show significantly increasing trends with frequency, which agrees with more localized electronic structure suggested by UV-vis response. The generally increasing SE for CF and SF material types are of substantially lower slope and nearly overlay each other, as did their UV-vis spectra, with even more highly localized charge domains.

**Table 6.4.** Summary of EM shielding effectiveness (SE) measurements of PTSA-doped band within frequency range 2-14 GHz.

<i>SE</i>	<i>SL</i>	<i>SF</i>	<i>CS</i>	<i>CF</i>
$SE_T$ (dB)	$73.6 \pm 3.6$	$16.4 \pm 2.7$	$36.6 \pm 6.3$	$16.6 \pm 2.8$
$SE_A$ (dB)	$74.5 \pm 3.8$ (97%)	$13.2 \pm 2.7$ (81%)	$33.1 \pm 6.7$ (95%)	$13.5 \pm 2.7$ (81%)
$SE_R$ (dB)	$2.3 \pm 0.8$ (3%)	$3.2 \pm 0.4$ (19%)	$4.4 \pm 1.5$ (5%)	$3.2 \pm 0.6$ (19%)

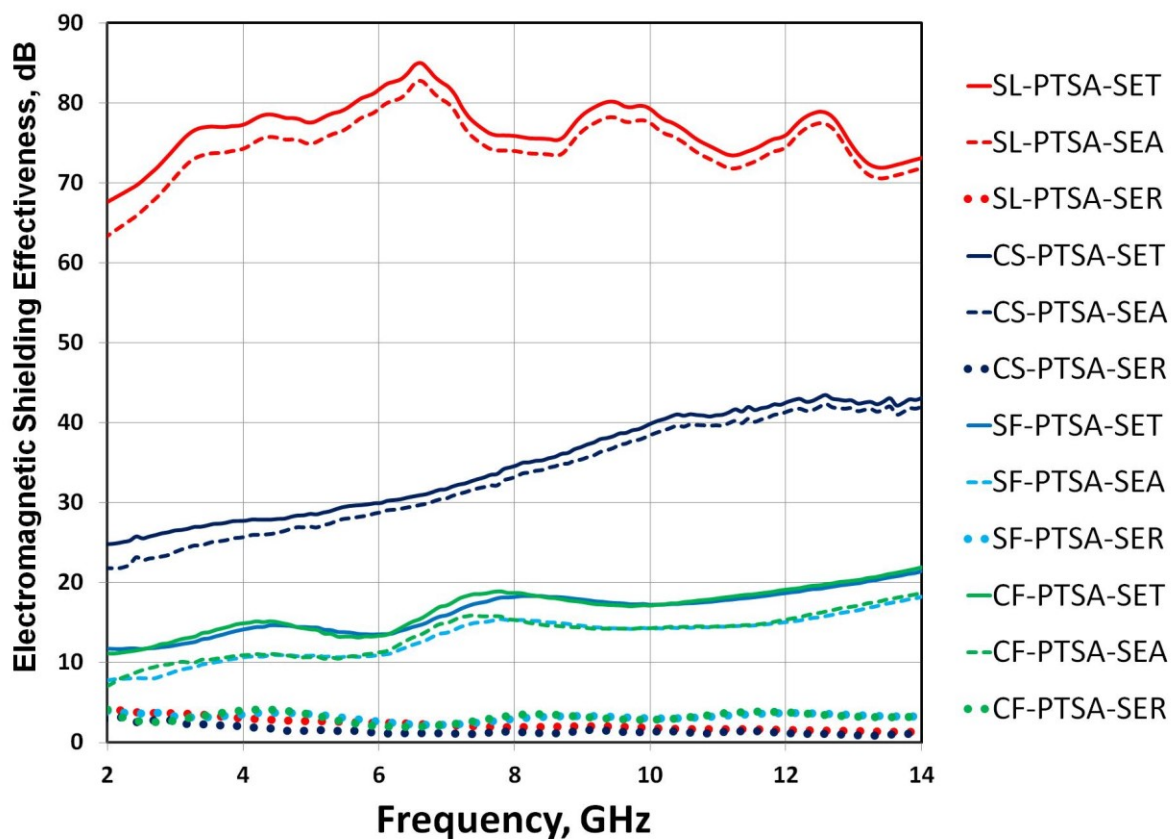


**Figure 6.6.** Broad band electromagnetic shielding potential of 0.06 g HCl-doped PAN (SL, CS, SF, and CF) tested in a coaxial sample holder as a function of frequency measured in the range 2-14 GHz.

The most interesting observation remains that the nano-PAN types with highest and lowest crystallinity (SF and CF, respectively) produce the worst shielding and conductivity, similar to the HCl-doped PAN study<sup>1</sup> discussed in depth (Chapters 2-4) and attributed to the negative influence of disorder on polaron structure delocalization<sup>102</sup>. The clearest discrepancy between PTSA and HCl (Chapters 2 and 4) doping is in comparing the CS synthesis method outcome. CS-HCl-PAN achieved the worst EM shielding potential (with most localized electronic structure) whereas CS-PTSA-PAN gave the second best result (Table 6.3), though only half as effective as for the SL product.

Finally, the critical impact of just the very small amount of solvent (DI water) in the SL preparation on electrical behavior must be emphasized as furthering the overall objective of this dissertation. Even though both SF and SL nanopowders have the same ES-II type, they differ in crystallinity and UV-vis spectra significantly. The superior shielding performance of SL within a broad frequency band (2-14 GHz) supports the suggestion that its conjugated structure may have the fastest polaron delocalization<sup>102</sup> and is expected to have the fastest, enhanced dielectric response at high frequency<sup>102,103</sup>. These results support the presence of a polaron lattice electronic structure in SL-produced PTSA-doped PAN, which may be the key for enhancing high-frequency dielectric response due to a long-range displacement of electrons by fine-tuning the electronic structure, enhancing charge delocalization, and contributing to higher dielectric loss ( $\epsilon''$ ) as expected from relative previous reports<sup>104-106</sup>.

## 6.5. Conclusions

One of the main contributions of this work is highlighting the dependence of EM shielding effectiveness (SE) in conducting polymers on the synthesis approach, specifically on reaction conditions and dopant speciation, particularly in the microwave band (2-14 GHz) for PAN nanopowders doped with PTSA compared to HCl. The possibility of tuning the EM shielding potential via utilizing different approaches is now well established. It could be concluded that synthesis approach controls, at least to some significant and highly efficacious degree, the polymerization reaction in a certain fashion based on synthesis conditions, directing the reaction to form predominate electronic structures from which the bulk conductivity and EM shielding emerge.

It is difficult to tell quantitatively the relative compactness or expanding of PAN chains, but the impact of synthesis approach on electronic structures (well developed polaron lattice) is clear and obvious for the observed electrical conductivity behavior of PTSA-doped samples. Based on the previous conclusions from Chapters 2-4, it could be assumed that the approach which leads to doped PAN with predominant polaron/polaron lattice leads to enhancing charge delocalization and conductivity, and vice versa.

Secondly, the difference between solvent-free (SF) and solvent-limited (SL) syntheses, both unconventional approaches, is elucidated. SL synthesis in a slightly wetted solid paste reaction provides substantial material property improvements over the unconventional SF and conventional solvent-rich oxidations with rate-limited addition or abundant oxidizer (CS and CF samples, respectively). The enhancement of the DC conductivity of PTSA-PAN prepared with the SL approach indicates the importance of tuning the solvent amount in PAN polymerization medium as a powerful and promising tool to be utilized for further enhancements. Collective data analysis demonstrates the importance of conductivity over crystallinity for enhancing SE for nanoPAN. The synthesis protocols that lead to maximizing crystallinity are not recommended, as there appears to be an intermediate optimum with respect to conductivity and EM shielding.

The results of XRD make it clear that the PAN structures are very sensitive to synthesis conditions even when the same composition nanopowder is produced. Furthermore, PAN polymorphism (ES-I and/or ES-II) was significantly affected by the synthesis approach used and thus may be controlled within a certain fine-tuning range for nanopowder products. It was found that the SL, SF and CS approaches lead to PAN emeraldine PTSA salts of type ES-II. On the other hand, the CF approach leads to mixed phases (ES-I/II), respectively. The impact

of emeraldine PTSA salt type alone on electrical properties of PAN is therefore not the key concern for predicting or designing particular crystallinity or conductivity..

The superior shielding performance of SL within a broad frequency band (2-14 GHz) supports the suggestion that the SL approach leads to PTSA-doped PAN with the most conjugated structure and the (inferred) fastest polaron delocalization <sup>102</sup> with respect to CS, CF and SF. Also, it could be expected that SL has the faster and improved dielectric response at high frequency<sup>102,103</sup>. This result supports the presence of a polaron lattice electronic structure in SL PAN products. Moreover, the proposed polaron lattice may be the key feature for enhancing high-frequency dielectric response due to a long-range displacement of electrons as the governing characteristic.

Thorough characterization with the current chemical details herein is expected to demonstrate the importance of tuning delocalized polaron electronic structure (viz., increasing their extreme) relative to bipolarons and/or localized polarons when attempting to enhance average response for EM applications using nano-PANs, and perhaps can be generally extended to other doping/polymerizing systems. Optimizing the SL approach for particular solvent-limited conditions (e.g., what is the optimum amount of solvent to maximize SE for a given dopant species) toward well-defined polymer needs for conductivity and conformational structures shows inherent promise for future work toward various technological applications. It is difficult to tell quantitatively the relative compactness or expandness of PAN chains, but the impact of synthesis approach on electronic structures (well developed polaron lattice) is clear and obvious for the observed electrical conductivity behavior of PTSA-doped samples.

## 6.6. References

- (1) Tantawy, H. R.; Aston, D. E.; Smith, J. R.; Young, J. L. A Comparison of Electromagnetic Shielding with Polyaniline Nanopowders Produced in Solvent-Limited Conditions *ACS Appl. Mater. Interfaces*, **2013**, *5*, 4648–4658.
- (2) Zhang, D. On the Conductivity Measurement of Polyaniline Pellets *Polym. Test.* **2007**, *26*, 9-13.
- (3) Chaudhari, H. K.; Kelkar, D. S. Investigation of Structure and Electrical Conductivity in Doped Polyaniline *Polym. Int.* **1997**, *42*, 380-384.
- (4) Bohli, N.; Gmati, F.; Mohamed, A. B.; Vigneras, V.; Miane, J. L. Conductivity Mechanism of Polyaniline Organic Films: The Effects of Solvent Type and Casting Temperature *J. Phys. D: Appl. Phys* **2009**, *42*, 205404.
- (5) Chaudhari, H. K.; Kelkar, D. S. X-Ray Diffraction Study of Doped Polyaniline *J. Appl. Polym. Sci.* **1996**, *62*, 15.
- (6) Zhang, K.; Li, Y. Electrical Conductivity Enhancement of Polyaniline by Refluxing *Polym. Adv. Technol.* **2011**, *22*, 2084-2090.
- (7) Chowdhury, P.; Saha, B. Potassium Dichromate Initiated Polymerization of Aniline *Indian J. Chem. Technol.* **2005**, *12*, 671-675.
- (8) Li, Y.; Al-Ghamdi, A. A.; Al-Hartomy, O. A.; El-Tantawy, F.; Yakuphanoglu, F. Semiconducting Properties of Nanofiber Polyaniline Organic Semiconductor *OAM – RC* **2012**, *6*, 235-238.

- (9) Pohanish, R. P.; Greene, S. A. *Wiley Guide to Chemical Incompatibilities*, 3 ed.; Wiley: Hoboken, N.J., 2009.
- (10) Fu, Y.; Elsenbaumer, R. L. Thermochemistry and Kinetics of Chemical Polymerization of Aniline Determined by Solution Calorimetry *Chem. Mater.* **1994**, *6*, 671-677.
- (11) Stejskal, J.; Gilbert, R. G. Polyaniline. Preparation of a Conducting Polymer (Iupac Technical Report) *Pure Appl. Chem.* **2002**, *74*, 857.
- (12) Nalwa, H. S. *Handbook of Organic Conductive Molecules and Polymers 2, Conductive Polymers: Synthesis and Electrical Properties.*; Wiley: Chichester; New York, 1997; Vol. 2.
- (13) Bhadra, S.; Khastgir, D. Determination of Crystal Structure of Polyaniline and Substituted Polyanilines through Powder X-Ray Diffraction Analysis *Polym. Test.* **2008**, *27*, 851-857.
- (14) Zhang, X.; Zhu, J.; Haldolaarachchige, N.; Ryu, J.; Young, D. P.; Wei, S.; Guo, Z. Synthetic Process Engineered Polyaniline Nanostructures with Tunable Morphology and Physical Properties *Polymer* **2012**, *53*, 2109-2120.
- (15) Varma, S. J.; Xavier, F.; Jayalekshmi, S.; Varghese, S. Synthesis and Studies of Exceptionally Crystalline Polyaniline Thin Films *Polym. Int.* **2012**, *61*, 743-748.
- (16) Majumdar, D.; Baskey, M.; Saha, S. K. Epitaxial Growth of Crystalline Polyaniline on Reduced Graphene Oxide *Macromol. Rapid Commun.* **2011**, *32*, 1277-1283.
- (17) Abdiryim, T.; Xiao-Gang, Z.; Jamal, R. Comparative Studies of Solid-State Synthesized Polyaniline Doped with Inorganic Acids *Mater. Chem. Phys.* **2005**, *90*, 367-372.

- (18) Rimbu, G. A.; Stamatini, I.; Jackson, C. L.; Scott, K. The Morphology Control of Polyaniline as Conducting Polymer in Fuel Cell Technology *J. Optoelectron. Adv. M.* **2006**, *8*, 670-674.
- (19) Duan, Y.; Shunhua, L.; Hongtao, G. Investigation of Electrical Conductivity and Electromagnetic Shielding Effectiveness of Polyaniline Composite *STAM* **2005**, *6*, 513-518.
- (20) Blythe, A. R.; Bloor, D. *Electrical Properties of Polymers*; Cambridge University Press: Cambridge; New York, 2005.
- (21) Stejskal, J.; Riede, A.; Hlavatá, D.; Prokeš, J.; Helmstedt, M.; Holler, P. The Effect of Polymerization Temperature on Molecular Weight, Crystallinity, and Electrical Conductivity of Polyaniline *Synt. Met.* **1998**, *96*, 55-61.
- (22) Stejskal, J.; Hlavatá, D.; Holler, P.; Trchová, M.; Prokeš, J.; Sapurina, I. Polyaniline Prepared in the Presence of Various Acids: A Conductivity Study *Polym. Int.* **2004**, *53*, 294-300.
- (23) Ladd, M. F. C.; Palmer, R. A. *Structure Determination by X-Ray Crystallography*; Plenum Press: New York, 1994.
- (24) Cullity, B. D. *Elements of X-Ray Diffraction*; Addison-Wesley Pub. Co.: Reading, Mass., 1956.
- (25) Klug, H. P.; Alexander, L. E. *X-Ray Diffraction Procedures for Polycrystalline and Amorphous Materials*; Wiley: New York, 1974.
- (26) Seshadri, D. T.; Bhat, N. V. Structural and Electrical Properties of Crystals of Substituted Polyaniline *J. Polym. Sci., Part B: Polym. Phys* **2007**, *45*, 1127-1137.

- (27) Manjunath, B. R.; Venkataraman, A.; Stephen, T. The Effect of Moisture Present in Polymers on Their X-Ray Diffraction Patterns *J. Appl. Polym. Sci.* **1973**, *17*, 1091-1099.
- (28) Tang, Q.; Wu, J.; Li, Y.; Lin, J.; Tang, Z.; Huang, M. Facile Secondary-Template Synthesis of Polyaniline Microtube Array for Enhancing Glucose Biosensitivity *J. Mater. Chem.* **2011**, *21*, 12927-12934.
- (29) Wang, Y.; Jing, X. Intrinsically Conducting Polymers for Electromagnetic Interference Shielding *Polym. Adv. Technol.* **2005**, *16*, 344–351.
- (30) Phang, S. W.; Hino, T.; Abdullah, M. H.; Kuramoto, N. Applications of Polyaniline Doubly Doped with P-Toluene Sulphonic Acid and Dichloroacetic Acid as Microwave Absorbing and Shielding Materials *Mater. Chem. Phys.* **2007**, *104*, 327-335.
- (31) Chen, L. F.; Ong, C. K.; Neo, C. P.; Varadan, V. V.; Varadan, V. K. *Microwave Electronics: Measurement and Materials Characterization*; John Wiley & Sons, Ltd 2004
- (32) Mzenda, V. M.; Goodman, S. A.; Auret, F. D. Conduction Models in Polyaniline: The Effect of Temperature on the Current–Voltage Properties of Polyaniline over the Temperature Range 30 <math>T(K)</math> 300 *Synt. Met.* **2002**, *127*, 285-289.
- (33) Abdiryim, T.; Jamal, R.; Nurulla, I. Doping Effect of Organic Sulphonic Acids on the Solid-State Synthesized Polyaniline *J. Appl. Polym. Sci.* **2007**, *105*, 576-584.
- (34) Bhadra, S.; Khastgir, D.; Singha, N. K.; Lee, J. H. Progress in Preparation, Processing and Applications of Polyaniline *Prog. Polym. Sci.* **2009**, *34*, 783-810.
- (35) Jung, W. H.; Lee, Y. M.; Jo, N. J.; Lee, J. O. Control of Polyaniline Particle Shapes *Macromol. Chem. Phys.* **2008**, *209*, 1083-1093.

- (36) Zhou, C. F.; Du, X. S.; Mai, Y. W.; Liu, Z.; Ringer, S. P. Solid Phase Mechanochemical Synthesis of Polyaniline Branched Nanofibers *Synt. Met.* **2009**, *159*, 1302-1307.
- (37) Du, X. S.; Zhou, C. F.; Wang, G. T.; Mai, Y. W. Novel Solid-State and Template-Free Synthesis of Branched Polyaniline Nanofibers *Chem. Mater.* **2008**, *20*, 3806-3808.
- (38) Bhadra, S.; Lee, J. H. Synthesis of Higher Soluble Nanostructured Polyaniline by Vapor-Phase Polymerization and Determination of Its Crystal Structure *J. Appl. Polym. Sci.* **2009**, *114*, 331-340.
- (39) Colombari, P.; Folch, S.; Gruber, A. Vibrational Study of Short-Range Order and Structure of Polyaniline Bases and Salts *Macromolecules* **1999**, *32*, 3080-3092.
- (40) Pouget, J. P.; Hsu, C. H.; MacDiarmid, A. G.; Epstein, A. J. Structural Investigation of Metallic PAN-CSA and Some of Its Derivatives *Synt. Met.* **1995**, *69*, 119-120.
- (41) Pouget, J. P.; Jozefowicz, M. E.; Epstein, A. J.; Tang, X.; MacDiarmid, A. G. X-Ray Structure of Polyaniline *Macromolecules* **1991**, *24*, 779-789.
- (42) Pouget, J. P.; Oblakowski, Z.; Nogami, Y.; Albouy, P. A.; Laridjani, M.; Oh, E. J.; Min, Y.; MacDiarmid, A. G.; Tsukamoto, J.; Ishiguro, T.; Epstein, A. J. Recent Structural Investigations of Metallic Polymers *Synt. Met.* **1994**, *65*, 131-140.
- (43) Jozefowicz, M. E.; Laversanne, R.; Javadi, H. H. S.; Epstein, A. J.; Pouget, J. P.; Tang, X.; MacDiarmid, A. G. Multiple Lattice Phases and Polaron-Lattice-Spinless-Defect Competition in Polyaniline *Phys. Rev. B: Condens. Matter* **1989**, *39*, 12958-12961.
- (44) Tang, S. J.; Wang, A. T.; Lin, S. Y.; Huang, K. Y.; Yang, C. C.; Yeh, J. M.; Chiu, K. C. Polymerization of Aniline under Various Concentrations of Aps and Hcl *Polymer* **2011**, *43*, 667-675.

- (45) Nalwa, H. S. *Handbook of Organic Conductive Molecules and Polymers 3, Conductive Polymers: Spectroscopy and Physical Properties*; Wiley: Chichester; New York, 1997; Vol. 3.
- (46) Inoue, M.; Monica Castillo-Ortega, M.; Inoue, M. B. Polyaniline Toluenesulfonates: X-Ray Diffraction and Electrical Conductivity *Journal of Macromolecular Science, Part A: Pure and Applied Chemistry* **1997**, *34*, 1493-1497.
- (47) Lubentsov, B.; Timofeeva, O.; Saratovskikh, S.; Krinichnyi, V.; Pelekh, A.; Dmitrenko, V.; Khidekel, M. The Study of Conducting Polymer Interaction with Gaseous Substances Iv. The Water Content Influence on Polyaniline Crystal Structure and Conductivity *Synt. Met.* **1992**, *47*, 187-192.
- (48) Pouget, J. P.; Zhao, S. L.; Wang, Z. H.; Oblakowski, Z.; Epstein, A. J.; Manobar, S. K.; Wiesinger, J. M.; Macdiarmid, A. G.; Hsu, C. H. Poly(0-Ethoxyaniline): Control of Structure and Charge Transport through Derivatization *Synt. Met.* **1993**, *55*, 341-346.
- (49) Winokur, M. J.; Mattes, B. R. Polyaniline as Viewed from a Structural Perspective *J. Reinf. Plast. Compos.* **1999**, *18*, 875-884.
- (50) Mazerolles, L.; Folch, S.; Colombari, P. Study of Polyanilines by High-Resolution Electron Microscopy *Macromolecules* **1999**, *32*, 8504-8508.
- (51) Zhang, L.; Long, Y.; Chen, Z.; Wan, M. The Effect of Hydrogen Bonding on Self-Assembled Polyaniline Nanostructures *Adv. Funct. Mater.* **2004**, *14*, 693-698.
- (52) Zujovic, Z. D.; Laslau, C.; Bowmaker, G. A.; Kilmartin, P. A.; Webber, A. L.; Brown, S. P.; Travas-Sejdic, J. Role of Aniline Oligomeric Nanosheets in the Formation of Polyaniline Nanotubes *Macromolecules* **2009**, *43*, 662-670.

- (53) Yin, J.; Zhao, X.; Xia, X.; Xiang, L.; Qiao, Y. Electrorheological Fluids Based on Nano-Fibrous Polyaniline *Polymer* **2008**, *49*, 4413-4419.
- (54) Zhang, L.; Wan, M. Chiral Polyaniline Nanotubes Synthesized Via a Self-Assembly Process *Thin Solid Films* **2005**, *477*, 24-31.
- (55) Pan, L. J.; Pu, L.; Shi, Y.; Sun, T.; Zhang, R.; Zheng, Y. O. Hydrothermal Synthesis of Polyaniline Mesostructures *Adv. Funct. Mater.* **2006**, *16*, 1279-1288.
- (56) Zujovic, Z. D.; Laslau, C.; Travas-Sejdic, J. Lamellar-Structured Nanoflakes Comprised of Stacked Oligoaniline Nanosheets *Asian J. Chem* **2011**, *6*, 791.
- (57) Hopkins, A. R.; Lipeles, R. A.; Hwang, S. J. Morphology Characterization of Polyaniline Nano- and Microstructures *Synt. Met.* **2008**, *158*, 594-601.
- (58) Laslau, C.; Ingham, B.; Zujovic, Z. D.; Čapková, P.; Stejskal, J.; Trchová, M.; Travas-Sejdic, J. Synchrotron X-Ray Scattering Reveals Early-Stage Crystallinity During the Self-Assembly of Polyaniline Nanotubes with Rectangular Cross-Sections *Synt. Met.* **2012**, *161*, 2739-2742.
- (59) Wan, M.; Li, J. Microtubules of Polyaniline Doped with HCl and Hbf<sub>4</sub> *J. Polym. Sci., Part A: Polym. Chem.* **1999**, *37*, 4605-4609.
- (60) Gawlicka-Chruszcz, A.; Stadnicka, K. A Comparative Study of Intermolecular Interactions in the Crystal Structures of Phenyl/Phenyl End-Capped Oligoanilines *Acta Crystallogr., C: Cryst. Struct. Commun.* **2002**, *58*, o416-o420.
- (61) Thalladi, V. R.; Smolka, T.; Boese, R.; Sustmann, R. Reproducible Phenazine Molecular Stacks *Cryst. Eng. Comm.* **2000**, *2*, 96-101.

- (62) Jozefowicz, M. E.; Epstein, A. J.; Pouget, J. P.; Masters, J. G.; Ray, A.; MacDiarmid, A. G. X-Ray Structure of the Polyaniline Derivative Poly (O-Toluidine): The Structural Origin of Charge Localization *Macromolecules* **1991**, *24*, 5863-5866.
- (63) Banerjee, S.; Saikia, J. P.; Kumar, A.; Konwar, B. Antioxidant Activity and Haemolysis Prevention Efficiency of Polyaniline Nanofibers *Nanotechnology* **2010**, *21*.
- (64) Joo, J.; Long, S. M.; Pouget, J. P.; Oh, E. J.; MacDiarmid, A. G.; Epstein, A. J. Charge Transport of the Mesoscopic Metallic State in Partially Crystalline Polyanilines *Phys. Rev. B: Condens. Matter* **1998**, *57*, 9567-9580.
- (65) Liu, H.; Hu, X. B.; Wang, J. Y.; Boughton, R. I. Structure, Conductivity, and Thermopower of Crystalline Polyaniline Synthesized by the Ultrasonic Irradiation Polymerization Method *Macromolecules* **2002**, *35*, 9414.
- (66) Mani, A.; Athinarayanasamy, K.; Kamaraj, P.; Tamil Selvan, S.; Ravichandran, S.; Phani, K.; Pitchumani, S. Crystalline Order in Polyaniline *J. Mater. Sci. Lett.* **1995**, *14*, 1594-1596.
- (67) Stejskal, J.; Sapurina, I.; Trchova, M. Polyaniline Nanostructures and the Role of Aniline Oligomers in Their Formation *Prog. Polym. Sci.* **2010**, *35*, 1420-1481.
- (68) Minto, C. D. G.; Vaughan, A. S. Orientation and Conductivity in Polyaniline: 1 *Polymer*. **1997**, *38*, 2683-2688.
- (69) Sinha, S.; Bhadra, S.; Khastgir, D. Effect of Dopant Type on the Properties of Polyaniline *J. Appl. Polym. Sci.* **2009**, *112*, 3135-3140.

- (70) Zhou, Q.; Wang, J.; Ma, Y.; Cong, C.; Wang, F. The Relationship of Conductivity to the Morphology and Crystallinity of Polyaniline Controlled by Water Content Via Reverse Microemulsion *Colloid. Polym. Sci.* **2007**, *285*, 405-411.
- (71) Epstein, A. J.; MacDiarmid, A. G. "Electronic Phenomena in Polyanilines," Defense Technical Information Center, 1992.
- (72) Izumi, C. M. S.; Rodrigues, D. C.; Temperini, M. L. A. The Role of Solvent on the Doping of Polyaniline with Fe(II) Ions *Synt. Met.* **2010**, *160*, 2552-2558.
- (73) Gruger, A.; Novak, A.; Regis, A.; Colomban, P. Infrared and Raman Study of Polyaniline. Part II: Influence of Ortho Substituents on Hydrogen Bonding and Uv/Vis-near-IR Electron Charge Transfer *J. Mol. Struct.* **1994**, *328*, 153.
- (74) Wallace, G. G.; Spinks, G. M.; Kane-Maguire, L. A. P.; Teasdale, P. R. *Conductive Electroactive Polymers Intelligent Materials Systems*; CRC Press: Boca Raton; London; New York, 2009.
- (75) Nalwa, H. S. *Handbook of Advanced Electronic and Photonic Materials and Devices*; Academic Press: San Diego, 2001; Vol. 8.
- (76) Kim, S.-C.; Whitten, J.; Kumar, J.; Bruno, F.; Samuelson, L. Self-Doped Carboxylated Polyaniline: Effect of Hydrogen Bonding on the Doping of Polymers *Macromol. Res.* **2009**, *17*, 631-637.
- (77) Han, M. G.; Im, S. S. X-Ray Photoelectron Spectroscopy Study of Electrically Conducting Polyaniline/Polyimide Blends *Polymer* **2000**, *41*, 3253-3262.
- (78) Garai, A.; Chatterjee, S.; Nandi, A. K. Viscoelastic and Conductivity Properties of Thermoreversible Polyaniline-Dnnsa Gel in M-Cresol *Synt. Met.* **2010**, *160*, 1733-1739.

- (79) Inzelt, G. *Conducting Polymers a New Era in Electrochemistry*; Springer: Berlin; New York, 2012.
- (80) Dennany, L.; Innis, P. C.; McGovern, S. T.; Wallace, G. G.; Forster, R. J. Electronic Interactions within Composites of Polyanilines Formed under Acidic and Alkaline Conditions. Conductivity, ESR, Raman, UV-Vis and Fluorescence Studies *J. Phys. Chem.* **2011**, *113*, 3303-3310.
- (81) Chao, L.; Ho, K. S.; Shen, S. Y.; Pu, H. Y.; Hsieh, T. H.; Kuo, C. W.; Tseng, B. H. Short Polyaniline Nanorod Prepared in the Presence of Para-Phenylenediamine *J. Appl. Polym. Sci.* **2013**, *127*, 1853-1862.
- (82) Trchová, M.; Morávková, Z.; ÁedÄ›nková, I.; Stejskal, J. Spectroscopy of Thin Polyaniline Films Deposited During Chemical Oxidation of Aniline *Chem. Pap.* **2012**, *66*, 415-445.
- (83) Sedenkova, I.; Konyushenko, E. N.; Stejskal, J.; Trchova, M.; Prokes, J. Solid-State Oxidation of Aniline Hydrochloride with Various Oxidants *Synt. Met.* **2011**, *161*, 1353-1360.
- (84) Stejskal, J.; Exnerova, M.; Moravkova, Z.; Trchova, M.; Hromadkova, J.; Prokes, J. Oxidative Stability of Polyaniline *Polym. Degrad. Stab.* **2012**, *97*, 1026-1033.
- (85) Anilkumar, P.; Jayakannan, M. Single-Molecular-System-Based Selective Micellar Templates for Polyaniline Nanomaterials: Control of Shape, Size, Solid State Ordering, and Expanded Chain to Coil-like Conformation *Macromolecules* **2007**, *40*, 7311-7319.
- (86) Shimano, J. Y.; MacDiarmid, A. G. Polyaniline, a Dynamic Block Copolymer: Key to Attaining Its Intrinsic Conductivity? *Synt. Met.* **2001**, *123*, 251-262.

- (87) Apesteguy, J.; Jacobo, S. Synthesis of a Soluble Polyaniline-Ferrite Composite: Magnetic and Electric Properties *J. Mater. Sci.* **2007**, *42*, 7062-7068.
- (88) Majidi, M. R.; Kane-Maguire, L. A. P.; Wallace, G. G. Electrochemical Synthesis of Optically Active Polyanilines *Aust. J. Chem.* **1998**, *51*, 23-30.
- (89) Karatchevtseva, I.; Zhang, Z.; Hanna, J.; Luca, V. Electrosynthesis of Macroporous Polyaniline-V<sub>2</sub>O<sub>5</sub> Nanocomposites and Their Unusual Magnetic Properties *Chem. Mater.* **2006**, *18*, 4908-4916.
- (90) Mire, C. A.; Kane-Maguire, L. A.; Wallace, G. G.; in het Panhuis, M. Influence of Added Hydrogen Bonding Agents on the Chiroptical Properties of Chiral Polyaniline *Synt. Met.* **2009**, *159*, 715-717.
- (91) Kane-Maguire, L. A. P.; MacDiarmid, A. G.; Norris, I. D.; Wallace, G. G.; Zheng, W. Facile Preparation of Optically Active Polyanilines Via the in Situ Chemical Oxidative Polymerisation of Aniline *Synt. Met.* **1999**, *106*, 171-176.
- (92) MacDiarmid, A. G.; Epstein, A. J. Secondary Doping in Polyaniline *Synt. Met.* **1995**, *69*, 85-92.
- (93) Min, Y.; Xia, Y.; MacDiarmid, A. G.; Epstein, A. J. Vapor Phase "Secondary Doping" of Polyaniline *Synt. Met.* **1995**, *69*, 159-160.
- (94) Xia, Y.; Wiesinger, J. M.; MacDiarmid, A. G.; Epstein, A. J. Camphorsulfonic Acid Fully Doped Polyaniline Emeraldine Salt: Conformations in Different Solvents Studied by an Ultraviolet/Visible/near-Infrared Spectroscopic Method *Chem. Mater.* **1995**, *7*, 443-445.
- (95) Bernard, M. C.; Hugot-LeGoff, A.; Joiret, S.; Arkoub, H.; Saïdani, B. Influence of the Nature of Substituent on the Charge Mechanisms in Substituted Polyanilines (Spani,

- Poma) Studied by Raman and Optical Spectroscopies *Electrochim. Acta* **2005**, *50*, 1615-1623.
- (96) Tan, C. K.; Blackwood, D. J. Interactions between Polyaniline and Methanol Vapour *Sensors and Actuators B: Chemical* **2000**, *71*, 184-191.
- (97) Pornputtkul, Y.; Kane-Maguire, L. A. P.; Innis, P. C.; Wallace, G. G. Asymmetric Proliferation with Optically Active Polyanilines *Chem. Commun.* **2005**, 4539-4541.
- (98) Wessling, B. New Insight into Organic Metal Polyaniline Morphology and Structure *Polymers* **2010**, *2*, 786-798.
- (99) Hsieh, B. Z.; Chuang, H. Y.; Chao, L.; Li, Y.-J.; Huang, Y. J.; Tseng, P. H.; Hsieh, T. H.; Ho, K. S. Formation Mechanism of a Nanotubular Polyanilines Prepared by an Emulsion Polymerization without Organic Solvent *Polymer* **2008**, *49*, 4218-4225.
- (100) MacDiarmid, A. G.; Epstein, A. J. The Concept of Secondary Doping as Applied to Polyaniline *Synt. Met.* **1994**, *65*, 103-116.
- (101) Feng, J.; MacDiarmid, A. G.; Epstein, A. J. Conformation of Polyaniline: Effect of Mechanical Shaking and Spin Casting *Synt. Met.* **1997**, *84*, 131-132.
- (102) Yan, X. Z.; Goodson, T. High Dielectric Hyperbranched Polyaniline Materials *J. Phys. Chem. B* **2006**, *110*, 14667-14672.
- (103) Guo, M.; Yan, X.; Kwon, Y.; Hayakawa, T.; Kakimoto, M. A.; Goodson, T. High Frequency Dielectric Response in a Branched Phthalocyanine *JACS* **2006**, *128*, 14820-14821.

- (104) Boreddy, R. Designing of Nano Composites of Conducting Polymers for EMI Shielding. In *Advances in Nanocomposites - Synthesis, Characterization and Industrial Applications*; Reddy, B. S. R., Ed.; INTECH Open Access Publisher, 2011; pp 429-482.
- (105) Chandrasekhar, P.; Naishadham, K. Broadband Microwave Absorption and Shielding Properties of a Poly(Aniline) *Synt. Met.* **1999**, *105*, 115.
- (106) Micheli, D.; Apollo, C.; Pastore, R.; Marchetti, M. X-Band Microwave Characterization of Carbon-Based Nanocomposite Material, Absorption Capability Comparison and Resonance Design Simulation *Compos. Sci. Technol* **2010**, *70*, 400-409.

## CHAPTER 7

### Conclusions and Future Work

#### 7.1. Summary and Concluding Remarks

This dissertation work both demonstrates and deeply elucidates the possibility and likely extent of enhancing EM shielding potential of polyanilines (PANs)—and by extension to conducting, doped polymers in general, based on utilizing a simple and inexpensive, unconventional synthesis approach. The utilized unconventional approach was an optimally wetted solid state polymerization under mechanical grinding, referred to as a “solvent-free” or “solvent-limited” (SL) protocol and herein restricted to aqueous polymerizations. Both were compared with two conventional chemical approaches for both fast (CF) and slow (CS) oxidation conditions in aqueous solutions of ammonium peroxydisulfate (APS)—the same oxidizing agent used in the SF/SL route. Two dopant candidate types were employed for this research, HCl as an inorganic dopant and p-toluenesulfonic acid (PTSA) as organic acid dopant. Moreover, the effect of the synthesis approach and dopant on different physicochemical properties of the obtained doped polyaniline was investigated. The most favorable synthesis approach to achieve the highest possible EM shielding effectiveness (SE) is a primary target for practical considerations in fine-tuning production on large scales for feasible commercialization.

Table 7.1 shows the summary of the most important results as the impact of different synthesis methods on physicochemical properties of HCl-doped PAN first, with obvious dependence of EM SE on the synthesis approach over a broad frequency band particularly in the microwave band (2-14 GHz).

**Table 7.1.** Summary of physicochemical properties of HCl-doped PAN dependence on synthesis approach

	<i>SF-HCl</i>	<i>CF-HCl</i>	<i>CS-HCl</i>
<b><i>Morphology</i></b>			
<i>Average size</i>	≤20 nm	≤50 nm	≤100 nm
<i>Shape</i>	Regular	Regular	Irregular
<b><i>Conductivity</i></b>			
<i>DC (S/cm)</i>	27.19 ± 0.26	3.28 ± 0.25	2.94 ± 0.14
<i>AC (1 Hz-1 MHz)</i>	Maximum	Moderate	Minimum
<i>Metallicity</i>	Maximum	Moderate	Minimum
<b><i>EM Shielding</i></b>			
<i>100-1500 MHz</i>	Max	Moderate	Minimum
<i>2-14 GHz</i>	37 ± 4 dB	21 ± 1 dB	18 ± 2 dB
	69 ± 5 dB	32 ± 5 dB	26 ± 4 dB
<b><i>Crystallinity</i></b>	<b>66%</b>	<b>54%</b>	<b>73%</b>
<b><i>Chemical Structure</i></b>			
<i>Cross linking</i>	Minimum	Moderate	Maximum
<i>Hydrogen bonding</i>	Minimum	Moderate	Maximum
<b><i>Electronic Structure</i></b>			
<i>Polaron</i>	Maximum	Moderate	Minimum
<i>Bipolaron</i>	Minimum	Moderate	Maximum
<i>Charge delocalization</i>	Maximum	Moderate	Minimum
<b><i>Conformation</i></b>	Expanded	Expanded	Compact

Synthesis protocols that lead to compact coils in HCl-doped PAN with cross-linked structures or branched chains (e.g., conventional slow (CS) oxidation) are not expected to produce high conductivity or good EM shielding. Further, the evidence for branching and/or cross-linking in the conventional approaches (CS and CF) with solvent-rich reactions implies that a solvent-limited synthesis is closer to a neat, single-reaction type polymerization with its highly linear polymer product.

This tentatively suggests the best homogeneity would be found in SF products. Thorough characterization with the current chemical details herein demonstrates the importance of tuning delocalized polaron electronic structure relative to a bipolaron and/or localized polaron when attempting to enhance average response for EM applications using nanoPANs. Optimizing the SF approach for particular solvent-limited (SL) conditions in the HCl-PAN preparations toward defined targets (that is, just the right amount of solvent added) regarding conductivity and chemical/conformational structures in the polymer nanopowders shows inherent promise. Moreover, PAN polymorphism (Chapters 3 and 6) was significantly affected by the synthesis approach used and thus may be controlled within a certain fine-tuning range for nanopowder products. It was found that the SF approach leads to PAN emeraldine chloride salts of type ES-II, which has a significant impact on electrical properties and may favor achieving high electromagnetic (EM) shielding potentials a long-term goal of ongoing research efforts.

The XPS study (Chapter 4) demonstrates that the coexistence of polaron and bipolaron is realized in all the polyaniline samples but with different extents dependent on the synthesis approach. Furthermore, PANs that have polaron and/or bipolaron lattices exhibited the necessary chemical structure and charge delocalization for substantive improvements in electromagnetic field responses over existing forms of PAN previously produced and studied. Synthesis protocols that lead to compact coil in HCl-doped PAN with cross-linked structures or branched chains (e.g., conventional slow oxidation) are not recommended as there appears to be poor conductivity and EM shielding in these cases.

The SF approach is favorable for synthesizing the relatively linear, expanded coil, PAN conformations encouraging the development of delocalized polaron electronic structures.

The SF approach fosters better oxidation and doping degree relative to the CF and CS methods found to be important for maximum SE. Perhaps the SF approach leads to relatively optimum chemical/electronic structure that enhances dielectric response at higher frequencies, where delocalization processes are prominent, and may ultimately give rise to long-range displacements of electrons in the system.<sup>1</sup> On the other hand, the CS approach was found to be favorable for cross-linking structures, which may arise because of slow oxidation of aniline by restrictive reagent addition, which fosters PAN chain growth with existing chains as well as other structural defects resulting in lower conductivity than in relatively linear, doped PAN.<sup>2-4</sup> Moreover, slow polymerization produces insignificant change in temperature of the reacting mixture, which is favorable for higher degrees of crystallinity.<sup>2</sup> The higher cross-linked structures<sup>5-7</sup> also disrupt polaron delocalization.<sup>8</sup>

It was found that the oxidation level of PAN samples also depends on the synthesis approach, and the SF protocol gives an optimum oxidation level (50%), and the doping level also was found to be dependent on synthesis approach, with SF leading to the greatest degree of doping where 98% of the imine nitrogens are doped. Since both fast and slow oxidation products (CF and CS) were synthesized with the same dopant (HCl) ratios, the chemical structures, electronic structures and chain conformations appear to depend only on the reaction conditions,<sup>4</sup> and thus an optimum in conductivity for the maximum shielding potential may be revealed with fine-tuning of the rate and method for oxidant addition. XPS results also indicate that increasing radical chlorine concentrations correlate with better conductivity, oxidation level, and degree of doping for higher polaron content. The SF approach may ultimately give rise to increased long-range electron displacement in PAN systems for optimal dielectric response at high frequency.

Moreover, the proposed polaron lattice of SF may be the key for enhancing the high-frequency dielectric response due to a long-range displacement of electrons. Ultimately, an extensive characterization was performed to investigate the effective role of these parameters in EM SE, particularly in the microwave band. SF synthesis in a slightly wetted solid-phase reaction provided substantial property improvements over conventional solution-rich oxidations using limited or abundant oxidizer. It was found that SF PAN was the most successful of the three HCl-doped PAN nano-products at EM shielding, especially at high frequencies.

This superior performance (SE of  $37.6 \pm 3.7$  dB and  $68.7 \pm 4.6$  dB within 100-1500 MHz and 2-14 GHz, respectively) was found to be higher than the recent reported values for HCl-doped PAN<sup>9,10</sup> and even higher than some currently reported performance for doped PAN modified with ferrites and carbon.<sup>11,12</sup> Thorough characterization demonstrates the importance of generating a predominantly delocalized polaron electronic structure relative to a bipolaron and/or localized polaron when attempting to enhance SE in nano-PAN. The superior shielding performance of SF within a broad frequency band (2-14 GHz) further supports the suggestion that its conjugated structure may have the fastest polaron delocalization<sup>1</sup> with respect to CF and CS.

Full FTIR band characterization ( $400 - 4000 \text{ cm}^{-1}$ ) shows that it was possible to distinguish between branching and cross-linking in HCl-doped PAN samples prepared with different synthesis approaches (CF, CS, and SF). The relative extent of branching and/or cross-linking in PAN samples was estimated from the predomination of IR bands corresponding to 1,4-disubstituted rings and the absence of any other bands corresponding to any other polysubstitution.

The possibility of having significant branching was estimated from the observation of (or lack thereof) any polysubstitution bands coexistent with the 1,4-disubstituted bands and the absence of bands corresponding to intermolecular cyclization such as phenazine. The coexistence of all the previous bands could indicate significant heterogeneity in the PAN sample. It could be concluded that the CS approach is favorable for maximizing the extent of intramolecular cyclic phenazine as cross-linking units and hydrogen bonding. As a result, the charge is probably the most localized as dications (bipolarons) in CS-PAN. Its chains may furthermore have supramolecular assemblies<sup>13</sup> and the most compact-coil chain confirmation,<sup>14</sup> which both agree with UV-Vis and XPS analyses (Chapter 3). These features may be preferred by the slower oxidation rates, which means PAN chains growing with other existing chains (rather than by monomer addition), with a higher probability of structural defects impacting the electrical and electronic behavior.<sup>2,3</sup>

On the other hand, the SF and CF approaches appear favorable for relatively limited branching in PAN with low extent of cross-linking and hydrogen bonding, thus indicating that the charge is more delocalized as a result of partial masking or screening as suggested by the extended absorption tail (i.e., free carriers) of the protonated PAN,<sup>15</sup> which is confirmed through UV-vis spectroscopy as greater delocalization. If a relatively high degree of crystallinity, short interchain separation, and large crystalline domain size exist but the predominant electronic structure is localized, this leads to poor electrical behavior of PAN materials. The AC conductivity ( $\sigma_{AC}(\omega)$ ) and dielectric permittivity measurements ( $\epsilon'$  and  $\epsilon''$ ) showed an unexpected contradiction to the highly oversimplified general rule that higher crystallinity should provide increases conductivity and dielectric permittivity.<sup>5,16-19</sup>

It was found that CS-PAN, the most crystalline (~77%) material of the three synthesis methods, acts as the most disordered sample with respect to SF and CF PANs in electrical properties; it has the most localized electronic structure of the three sample types. On the other hand, SF-PAN with a moderate crystallinity (~66%) behaves more like a metal in the sense that its conductivity tends toward a frequency-independent behavior<sup>20</sup> across the tested frequency range (1 Hz-1 MHz). Apparently, both fast/moderate oxidation rate and high acidity favor HCl-doped PAN synthesis with delocalized electronic structures (polaron/polaron lattice), as indicative from weak frequency dependence of  $\sigma_{AC}$  in SF and CF PANs.<sup>21</sup>

Dielectric permittivity measurements showed that the SF approach leads to the highest values of  $\epsilon'$  and  $\epsilon''$ . The relatively high  $\epsilon'$  and  $\epsilon''$  values imply that  $\sigma_{DC}$  still plays an important role in determining their magnitudes. The lowest values in CS-PAN confirm that it has the strongest charge localization of the three.<sup>22</sup> The observed dielectric trends of PAN samples agree with conductivity trends and the reported conductivity/dielectric dependence. Therefore, a high  $\sigma_{DC}$  value may generally indicate high microwave absorptivity; consequently, raising the DC conductivity of a polymer is the key to obtain a good electromagnetic interference (EMI) absorber. The SF approach enhanced the dielectric constant and dielectric loss by about an order of magnitude over conventional synthesis, which has high promise as a process application for maximizing EMI shielding in PAN-based materials.

It is further deduced that the unconventional solvent-limited approaches are likely the key to prevent cyclization of branched chains and minimize the possibility of hydrogen bonding/cross-linking in PAN doped with inorganic acids (e.g., HCl) that would reduce the effectiveness for EM shielding. The solvent and/or oxidant concentration and accessibility to

each other appear to provide a fine-tuning potential for controlling the property outcomes for doped PAN polymerization. The SF approach seems to lead to proper ordering and electronic delocalization extent in HCl-doped PAN molecules to contribute to enhanced conductivity over the classical chemical oxidation approaches (CF and CS). These conventional methods are not recommended since they lead to maximizing crystallinity with cross-linked structures (such as CS) or minimizing crystallinity (such as CF). There appears to be an intermediate optimum in crystallinity with respect to electrical/dielectrical behavior. Since both fast and slow oxidation products (CF and CS) were synthesized in excess solvent with the same dopant (HCl) ratios, the relative degree of electronic delocalization appears to depend on the reaction conditions in particular rather than on the doping level in general.<sup>4</sup> Therefore, an optimization between conductivity and crystallinity for the maximum degree of electronic delocalization should be revealed with fine-tuning of the rate and method for oxidant addition.

#### *Organic Acid Dopant vs. Inorganic Dopant*

To expand on the already supported hypothesis for a general effect of limiting solvent—either to a minimum or to some optimum level and mixing procedure—on the relation between conductivity, crystallinity, chemical/electronic conformation and EM shielding, a similar study was carried out utilizing PTSA as the organic acid dopant for comparison to the extensively characterized but inorganically-doped (HCl) PAN nanopowders. Two different unconventional approaches were tested on the PTSA-doped PAN synthesis products against the two excess solvent regimes (fast and slow addition; CF and CS), since PTSA-PAN protocols could be truly solvent-free, where no water is induced with acid as was unavoidable with concentrated HCl solution.

Table 7.2 shows the summary of the most important results as the impact of the now four different synthesis protocols (rather than the three only for HCl-PAN) on physicochemical properties of PTSA-doped PAN nanopowders.

**Table 7.2.** Summary of physicochemical properties of PTSA-doped PAN dependence on synthesis approach

	<i>SL-PTSA</i>	<i>SF-PTSA</i>	<i>CF-PTSA</i>	<i>CS-PTSA</i>
<b><i>Morphology</i></b>				
<b><i>Average size</i></b>	≤20-30 nm	≤100-200 nm	30-300 nm	200-300 nm
<b><i>Shape</i></b>	Regular	Regular	Irregular	Regular
<b><i>Crystallinity</i></b>	<b>63%</b>	<b>77%</b>	<b>54%</b>	<b>70%</b>
<b><i>Conductivity</i></b>	Maximum	Minimum	Minimum	Moderate
<b><i>DC (S/cm)</i></b>	15.4 ± 0.6	1.6 ± 0.4	1.3 ± 0.3	4.5 ± 0.1
<b><i>Metallicity</i></b>	Maximum	Minimum	Minimum	Moderate
<b><i>EM Shielding</i></b>	Maximum	Minimum	Minimum	Moderate
<b><i>2-14 GHz</i></b>	73 ± 4 dB	16 ± 3 dB	17 ± 3 dB	37 ± 6 dB
<b><i>Charge delocalization</i></b>	Maximum	Minimum	Minimum	Moderate
<b><i>Conformation</i></b>	Expanded	Expanded	Expanded	Compact

The difference between solvent-free (SF) and solvent-limited (SL) syntheses, both unconventional approaches, was elucidated. SL synthesis in a slightly-wetted solid paste reaction provides substantial material property improvements over the unconventional SF and conventional solvent-rich oxidations with rate-limited addition or abundant oxidizer (CS and CF samples, respectively).

The enhancement of the DC conductivity of PTSA-PAN prepared with the SL approach (similar to the SF-HCl-PAN method in contrast of organic vs. aqueous inorganic acids,) indicates the importance of tuning the solvent amount in PAN polymerization medium as a powerful and promising tool to be utilized for further shielding enhancements. Collective data analysis demonstrates the importance of conductivity over crystallinity for enhancing SE for nanoPAN. The synthesis protocols that lead to maximizing crystallinity are not recommended, as there appears to be an intermediate optimum with respect to conductivity and EM shielding, just as there was for the inorganic acid dopant case with PAN nanopowders.

The results of XRD make it clear that the PTSA-PAN structures are very sensitive to synthesis conditions even when the same composition (in dopant to polymer ratios) nanopowder is produced. Furthermore, PAN polymorphism (ES-I and/or ES-II) was significantly affected by the synthesis conditions and thus may be controlled within a certain fine-tuning range for nanopowder products. It was found that the SL, SF and CS approaches lead to PAN emeraldine PTSA salts of type ES-II. On the other hand, the CF approach leads to mixed phases (ES-I/II), respectively. The impact of emeraldine PTSA salt type alone on electrical properties of PAN is therefore not the key concern for predicting or designing particular crystallinity or conductivity.

The superior shielding performance of SL within a broad frequency band (2-14 GHz) supports the suggestion that the SL approach leads to PTSA-doped PAN with relatively the most conjugated structure (as with SF-HCl-PAN—the closest equivalent method possible with concentrated HCl) and the (inferred) fastest polaron delocalization<sup>1</sup> with respect to CS, CF and SF. Also, it could be expected that SL-PAN has the faster and improved dielectric response at high frequency.<sup>1,23</sup>

This result supports the presence of a polaron lattice electronic structure (highly delocalized polarons) in SL-PAN products. Moreover, the proposed polaron lattice may be the key feature for enhancing high-frequency dielectric response due to a long-range displacement of electrons as the governing characteristic.

Thorough characterization with the current chemical details herein is expected to demonstrate the importance of tuning delocalized polaron electronic structure (viz., increasing their extreme) relative to bipolarons and/or localized polarons when attempting to enhance average response for EM applications using nanoPANs, and perhaps can be generally extended to other doping/polymerizing systems. Optimizing the SL approach for particular solvent-limited conditions (e.g., what is the optimum amount of solvent to maximize SE for a given dopant species in the polymer, as well as perhaps an optimum for local oxidant concentrations via both addition methods and concentration profiles over the synthesis process) toward well-defined polymer needs for conductivity and chemical/conformational structures shows great potential for further advancements. It is difficult to tell quantitatively the relative compactness or expandedness of PAN chains, but the impact of synthesis approach on electronic structures (through the well-developed polaron lattice) is clear and obvious for the observed electrical conductivity behavior of PTSA-doped samples especially.

It can now be concluded overall with strong experimental validation sets that the synthesis approach through solvent limited condition controls the polymerization reaction to some significant and highly efficacious degree for polyaniline with *in situ* acid doping, directing the reaction to form predominate electronic structures from which the bulk conductivity and EM shielding emerge.

To the best of our knowledge, this is the first time that the impact of limiting solvent was investigated as a critical parameter to the tuning of the key physicochemical properties in the preparation of a conducting polymer, doped polyaniline. Further focusing on this solvent-limited key factor should undergo deeper investigation for practical implementations to targeted application needs as well as to understand the synthesis-structure-property connections better.

Further enhancement the EM shielding efficiency from polyaniline nanoparticles doped with inorganic/organic sulphonic acids holds significant potential to address the long-term goal to develop new light-weight and affordable high-frequency EM shielding materials with an eco-friendly fabrication method.

## **7.2. Future Work**

Based on the conclusion details, future work should involve three major directions. Figure 7.1 shows a schematic diagram for different future work trends. The first (I) would involve the extreme fine-tuning to determine the further possibility of a true optimal enhancement of the EM shielding effectiveness (SE) for the precise relative amounts of solvent (i.e., water) with respect to the type of acid dopant whether inorganic or organic and continuing with our well-defined systems of HCl-PAN and PTSA-PAN nanopowders. The second direction (II) will utilize different inorganic and organic acid dopants toward the some fine-tuned synthesis approaches but through the broader comparative study for the promise of a more generalized and deep understanding of this emerging solvent-limited methodology for simultaneous polymerization and doping of conducting PANs, to be extended to other polymer systems.

Together, directions I and II move toward a robust and thorough approach for well-defined polymer design on the basis of conductivity and chemical/conformational structures, which shows inherent promise for various technological applications. Arena II could obvious take a substantial and perhaps ever-increasing allotment of time and personnel to address extensively.

Finally, the third direction (III) will incorporate at least two additional constituents to the formulations for further possible enhancements in the EM SE: transition metals<sup>24-27</sup> as co-dopant and magnetic ferrite<sup>11,28-31</sup>. Together, these are expected to further increase conductivities and contribute to EM absorption via magnetic eddy currents with the goal of producing the ultimate in light-weight and affordable broad band EM shielding materials and their generalized formulations for a comprehensive synthesis approach to prepare the best suited product for a given application need. Initial studies on metal co-dopant PAN nanopowders is already underway.

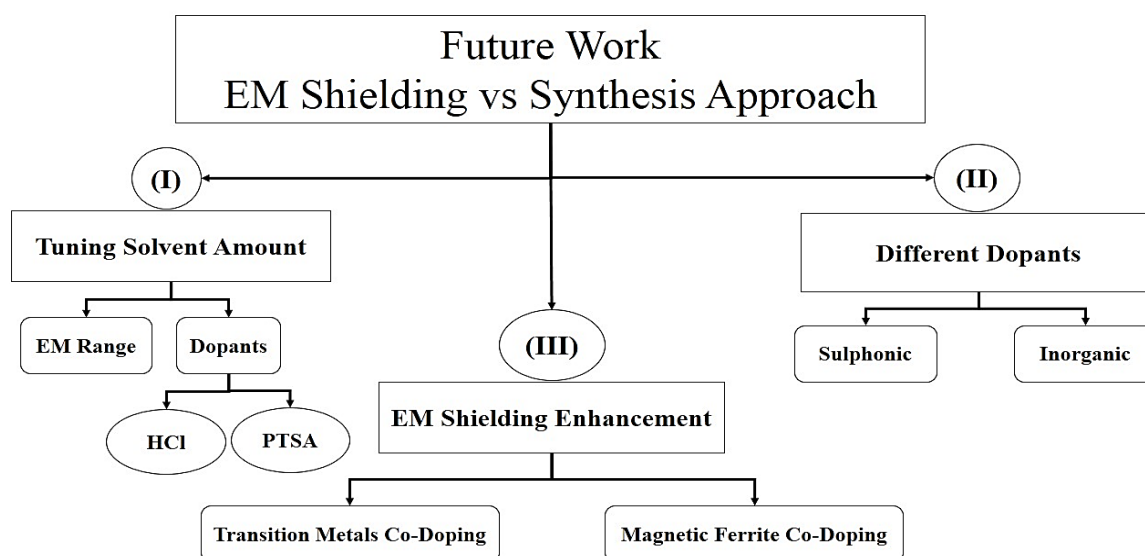


**Figure 7.1.** Schematic diagram for different future work trends.

### 7.3. References

- (1) Yan, X. Z.; Goodson, T. High Dielectric Hyperbranched Polyaniline Materials *J. Phys. Chem. B* **2006**, *110*, 14667-14672.
- (2) Stejskal, J.; Sapurina, I.; Trchova, M. Polyaniline Nanostructures and the Role of Aniline Oligomers in Their Formation *Prog. Polym. Sci.* **2010**, *35*, 1420-1481.
- (3) Pan, L. J.; Pu, L.; Shi, Y.; Sun, T.; Zhang, R.; Zheng, Y. O. Hydrothermal Synthesis of Polyaniline Mesostructures *Adv. Funct. Mater.* **2006**, *16*, 1279-1288.
- (4) Liu, H.; Hu, X. B.; Wang, J. Y.; Boughton, R. I. Structure, Conductivity, and Thermopower of Crystalline Polyaniline Synthesized by the Ultrasonic Irradiation Polymerization Method *Macromolecules* **2002**, *35*, 9414.
- (5) Zhang, K.; Li, Y. Electrical Conductivity Enhancement of Polyaniline by Refluxing *Polym. Adv. Technol.* **2011**, *22*, 2084-2090.
- (6) Nand, A. V.; Ray, S.; Gizdavic-Nikolaidis, M.; Travas-Sejdic, J.; Kilmartin, P. A. The Effects of Thermal Treatment on the Antioxidant Activity of Polyaniline *Polym. Degrad. Stab.* **2011**, *96*, 2159-2166.
- (7) Bhadra, S.; Khastgir, D. Extrinsic and Intrinsic Structural Change During Heat Treatment of Polyaniline *Polym. Degrad. Stab.* **2008**, *93*, 1094-1099.
- (8) Laslau, C.; Zujovic, Z.; Travas-Sejdic, J. Theories of Polyaniline Nanostructure Self-Assembly: Towards an Expanded, Comprehensive Multi-Layer Theory (Mlt) *Prog. Polym. Sci.* **2010**, *35*, 1403-1419.
- (9) Wan, M. *Conducting Polymers with Micro or Nanometer Structure*; Tsinghua University Press ; Springer: Beijing; Berlin, 2008.

- (10) Wang, Y.; Jing, X. Intrinsically Conducting Polymers for Electromagnetic Interference Shielding *Polym. Adv. Technol.* **2005**, *16*, 344–351.
- (11) Gairola, S. P.; Verma, V.; Kumar, L.; Dar, M. A.; Annapoorni, S.; Kotnala, R. K. Enhanced Microwave Absorption Properties in Polyaniline and Nano-Ferrite Composite in X-Band *Synt. Met.* **2010**, *160*, 2315-2318.
- (12) Moon, Y. E.; Yun, J.; Kim-II, H. Synergetic Improvement in Electromagnetic Interference Shielding Characteristics of Polyaniline-Coated Graphite Oxide/ $\Gamma$ - $\text{Fe}_2\text{O}_3$ / $\text{BaTiO}_3$  Nanocomposites *J. Ind. Eng. Chem.* **2012**.
- (13) Stejskal, J.; Sapurina, I.; Trchová, M.; Konyushenko, E. N.; Holler, P. The Genesis of Polyaniline Nanotubes *Polymer* **2006**, *47*, 8253-8262.
- (14) Li, Y.; Zheng, J. L.; Feng, J.; Jing, X. L. Polyaniline Micro-/Nanostructures: Morphology Control and Formation Mechanism Exploration *Chem. Pap.* **2013**, *67*, 876-890.
- (15) Šeděnková, I.; Trchová, M.; Blinova, N. V.; Stejskal, J. In-Situ Polymerized Polyaniline Films. Preparation in Solutions of Hydrochloric, Sulfuric, or Phosphoric Acid *Thin Solid Films* **2006**, *515*, 1640-1646.
- (16) Zhang, D. On the Conductivity Measurement of Polyaniline Pellets *Polym. Test.* **2007**, *26*, 9-13.
- (17) Chaudhari, H. K.; Kelkar, D. S. Investigation of Structure and Electrical Conductivity in Doped Polyaniline *Polym. Int.* **1997**, *42*, 380-384.
- (18) Bohli, N.; Gmati, F.; Mohamed, A. B.; Vigneras, V.; Miane, J. L. Conductivity Mechanism of Polyaniline Organic Films: The Effects of Solvent Type and Casting Temperature *J. Phys. D: Appl. Phys* **2009**, *42*, 205404.

- (19) Chaudhari, H. K.; Kelkar, D. S. X-Ray Diffraction Study of Doped Polyaniline *J. Appl. Polym. Sci.* **1996**, *62*, 15.
- (20) Bianchi, R. F.; Ferreira, G. F.; Lepienski, C. M.; Faria, R. M. Alternating Electrical Conductivity of Polyaniline *J. Chem. Phys.* **1999**, *110*, 4602.
- (21) Dutta, P.; Biswas, S.; De, S. Alternating-Current Conductivity and Dielectric Permittivity of Polyaniline Doped with B-Naphthalene Sulphonic Acid *J. Phys.: Condens. Matter* **2001**, *13*, 9187.
- (22) Han, M. G.; Im, S. S. Dielectric Spectroscopy of Conductive Polyaniline Salt Films *J. Appl. Polym. Sci.* **2001**, *82*, 2760-2769.
- (23) Guo, M.; Yan, X.; Kwon, Y.; Hayakawa, T.; Kakimoto, M. A.; Goodson, T. High Frequency Dielectric Response in a Branched Phthalocyanine *JACS* **2006**, *128*, 14820-14821.
- (24) Sedenkova, I.; Trchova, M.; Stejskal, J.; Prokes, J. Conformational Transition in Polyaniline Films - Spectroscopic and Conductivity Studies of Ageing *Polym. Degrad. Stab.* **2008**, *93*, 428-435.
- (25) Yang, C.; Chen, C.; Zeng, Y. Fourier Transform Infrared Spectra of Transition Metal Ion-Containing Polyanilines Synthesized in Different Reaction Conditions *Spectrochimica Acta Part A: Molecular and Biomolecular Spectroscopy* **2007**, *66*, 37-41.
- (26) Smertenko, P. S.; Dimitriev, O. P.; Schrader, S.; Brehmer, L. Doping of Polyaniline by Transition Metal Salts: Current-Voltage Characteristics of the Ito/Polymer Film/Metal Heterostructures *Synt. Met.* **2004**, *146*, 187-196.

- (27) Dimitriev, O. P. Doping of Polyaniline by Transition Metal Salts: Effect of Metal Cation on the Film Morphology *Synt. Met.* **2004**, *142*, 299-303.
- (28) Jiang, J.; Li, L.; Zhu, M. Polyaniline/Magnetic Ferrite Nanocomposites Obtained by in Situ Polymerization *Reactive and Functional Polymers* **2008**, *68*, 57-62.
- (29) Wang, W.; Gumfekar, S. P.; Jiao, Q.; Zhao, B. Ferrite-Grafted Polyaniline Nanofibers as Electromagnetic Shielding Materials *Journal of Materials Chemistry C* **2013**, *1*, 2851-2859.
- (30) Babayan, V.; Kazantseva, N. E.; Sapurina, I.; Moučka, R.; Stejskal, J.; Sába, P. Increasing the High-Frequency Magnetic Permeability of Mn<sub>2</sub>Zn Ferrite in Polyaniline Composites by Incorporating Silver *Journal of Magnetism and Magnetic Materials* **2013**, *333*, 30-38.
- (31) Selvakumar, N.; Jeyasubramanian, K. Pani-Magnetic Nanoparticles for EMI Shielding & Corrosion Resistance Application *Journal of NanoScience and NanoTechnology* **2014**, *2*, 29-33.

## Appendix A

### Copyright Letter Form the Journal of Applied Materials

## Appendix A

### Copyright Form for Paper Published from Chapter 2 of Dissertation in the Journal Applied Materials

3/26/2014

RightsLink® by Copyright Clearance Center



# RightsLink®

[Home](#)
[Create Account](#)
[Help](#)


**ACS Publications** Title:  
High quality. High impact.

Comparison of Electromagnetic Shielding with Polyaniline Nanopowders Produced in Solvent-Limited Conditions

**Author:** Hesham Ramzy Tantawy, D. Eric Aston, Jacob R. Smith, and Jeffrey L. Young

**Publication:** Applied Materials

**Publisher:** American Chemical Society

**Date:** Jun 1, 2013

Copyright © 2013, American Chemical Society

User ID

Password

Enable Auto Login

[Forgot Password/User ID?](#)

**If you're a copyright.com user,** you can login to RightsLink using your copyright.com credentials. **Already a RightsLink user or want to learn more?**

#### PERMISSION/LICENSE IS GRANTED FOR YOUR ORDER AT NO CHARGE

This type of permission/license, instead of the standard Terms & Conditions, is sent to you because no fee is being charged for your order. Please note the following:

- Permission is granted for your request in both print and electronic formats, and translations.
- If figures and/or tables were requested, they may be adapted or used in part.
- Please print this page for your records and send a copy of it to your publisher/graduate school.
- Appropriate credit for the requested material should be given as follows: "Reprinted (adapted) with permission from (COMPLETE REFERENCE CITATION). Copyright (YEAR) American Chemical Society." Insert appropriate information in place of the capitalized words.
- One-time permission is granted only for the use specified in your request. No additional uses are granted (such as derivative works or other editions). For any other uses, please submit a new request.



Copyright © 2014 [Copyright Clearance Center, Inc.](#) All Rights Reserved. [Privacy statement.](#)  
Comments? We would like to hear from you. E-mail us at [customer@copyright.com](mailto:customer@copyright.com)

## Appendix B

**Copyright Letter Form the Journal of Physical Chemistry C**

## Appendix B

### Copyright Form for Paper Published from Chapter 3 of Dissertation in the Journal of Physical Chemistry C

3/28/2014

RightsLink® by Copyright Clearance Center



# RightsLink®

[Home](#)
[Create Account](#)
[Help](#)

**ACS Publications** Title:

High quality. High impact.

Chemical Effects of a Solvent-Limited Approach to HCl-Doped Polyaniline Nanopowder Synthesis

**Author:** Hesham Ramzy Tantawy, Andrew T. Weakley, and D. Eric Aston

**Publication:** The Journal of Physical Chemistry C

**Publisher:** American Chemical Society

**Date:** Jan 1, 2014

Copyright © 2014, American Chemical Society

User ID	<input type="text"/>
Password	<input type="password"/>
<input type="checkbox"/> Enable Auto Login	
<a href="#">LOGIN</a>	
<a href="#">Forgot Password/User ID?</a>	
<p><b>If you're a copyright.com user,</b> you can login to RightsLink using your copyright.com credentials. <b>Already a RightsLink user</b> or want to <a href="#">learn more?</a></p>	

#### PERMISSION/LICENSE IS GRANTED FOR YOUR ORDER AT NO CHARGE

This type of permission/license, instead of the standard Terms & Conditions, is sent to you because no fee is being charged for your order. Please note the following:

- Permission is granted for your request in both print and electronic formats, and translations.
- If figures and/or tables were requested, they may be adapted or used in part.
- Please print this page for your records and send a copy of it to your publisher/graduate school.
- Appropriate credit for the requested material should be given as follows: "Reprinted (adapted) with permission from (COMPLETE REFERENCE CITATION). Copyright (YEAR) American Chemical Society." Insert appropriate information in place of the capitalized words.
- One-time permission is granted only for the use specified in your request. No additional uses are granted (such as derivative works or other editions). For any other uses, please submit a new request.

[BACK](#)
[CLOSE WINDOW](#)

Copyright © 2014 [Copyright Clearance Center, Inc.](#) All Rights Reserved. [Privacy statement.](#) Comments? We would like to hear from you. E-mail us at [customercare@copyright.com](mailto:customercare@copyright.com)